

**Scientific cruise report of  
Arctic Expedition ARK IV/3**

**Wissenschaftlicher Fahrtbericht der  
Arktis-Expedition ARK IV/3**

---

**Compiled by Jörn Thiede**

Ber. Polarforsch. 43 (1988)  
ISSN 0176-5027



**SCIENTIFIC REPORT ON THE ARK IV/3 EXPEDITION  
WITH PFVS POLARSTERN**

<u>Table of contents:</u>	<u>Page #</u>
1. Introduction: Oceanography, Biology and Geosciences of the Eastern Arctic Deep-Sea Basins	1
2. Bathymetric Surveys	7
3. Weather Conditions during the Expedition	11
4. Sea Ice Investigations of the Eurasian Basin	17
4. 1. Sea Ice Dynamics and Thermodynamics	17
4. 2. "Dirty" Sea Ice	25
4. 3. Biogenic Material in Sea Ice	33
4. 4. Proposed Future Research	36
5. The Oceanography Program: A Section across the Nansen Basin	39
5. 1. Introduction	39
5. 2. Scientific Goals and Objectives	46
5. 3. Sampling Groups	49
5. 3. 1. CTD, Continuous Profiling of Conductivity, Temperature, Pressure, and Transmissivity	49
5. 3. 2. Transmissometer and Suspended Sediments	49
5. 3. 3. Arctic Environmental Drifting Buoy (AEDB) Deployment	50
5. 3. 4. Small Volume Sampling	53
5. 3. 4. 1. Nutrients, Salinity, and Oxygen	53
5. 3. 4. 2. Total Carbonate, Total Alkalinity, Calcium	56
5. 3. 5. Trace Elements	56
5. 3. 6. Chlorofluoromethanes (Freons) and Halocarbons	57
5. 3. 7. H, He, Ne, O, AMS-C Studies	57
5. 3. 8. Nitrogen Isotopes	57
5. 3. 9. Large Volume Sampling	58
5. 3. 10. Artificial and Natural Radioisotopes in the Arctic: Large-Volume Pumping for Isotopes	59
5. 3. 11. Temperature and Velocity Structure	59
5. 3. 12. SOFAR Acoustic Ranging Experiment	61
5. 4. Oceanographic Preliminary Findings	68
5. 5. Conclusions for Future Work	76
6. Biological and Paleontological Observations	88
6. 1. Introduction	88
6. 2. Phytoplankton Studies	88
6. 3. Dinoflagellates, Pollen/Spore Assemblages and Related Studies	92
6. 4. Horizontal and Vertical Distribution of Planktonic Foraminifers and Pteropods on a Transect from the Barents Shelf to the Nansen-Gakkel Ridge	97
6. 5. Zooplankton: MULTINET Catches	101
6. 6. Production and Assemblages of the Calanoid Copepods in the Arctic Ocean	104
6. 7. Polar Cod Ecophysiology	105

	<u>Page #</u>
6. 8. Ecology, Biology and Paleoecology of Benthic Foraminifers	109
6. 9. Macrofauna Collections	113
6.10. Biological and Paleontological Observations: Short Summary and Reflection	113
7. Geophysical and Geological Properties of the Eurasian Basin of the Arctic Ocean and of Fram Strait	115
7. 1. Marine Gravity Profiling	117
7. 2. Heat Flow Measurements	121
7. 3. Distribution of Surface Sediments: 3.5 KHz Profiling	127
7. 4. Sediment Sampling: Instrumentation and Station Work	142
7. 5. Surface Sediments and Sediment Surfaces	148
7. 6. Surface Sediment Layers: Composition and Structure	151
7. 7. Long Sediment Cores: Composition and Structure	155
7. 7. 1. Sediment Features and Composition of Long Box Cores	155
7. 7. 2. Long Sediment Cores: Composition of the Sand Fraction of Cores 11/296, 340 and 372	158
7. 7. 3. Preliminary Discussion of KAL sediments from the eastern Arctic Ocean	168
7. 8. Biostratigraphy of Quaternary Deposits	171
7. 8. 1. Introduction	171
7. 8. 2. Abundance of Coccoliths in Sediments of the Eastern Arctic Ocean	171
7. 8. 3. Foraminiferal Content and Distribution in Eastern Arctic Sediments from selected KAL Cores: An Attempt at Stratigraphic Correlation	174
7. 8. 4. Palynomorphs	177
7. 8. 5. Conclusions	184
7. 9. Pore Water Content and Chemistry of Sediments	186
7. 9. 1. Sediment Samples for Measurement of Water Content	186
7. 9. 2. Pore Water Chemistry	189
7.10. Physical Properties: Thermal Conductivities	197
7.11. Physical Properties: Magnetic Susceptibility	202
7.12. Magnetostratigraphy of the Sediment Section	206
8. Synthesis and Summary of ARK IV/3 Scientific Investigations	213
8. 1. Ice Dynamics and Influence in the Eurasian Basin	213
8. 2. Oceanography of the Eurasian Basin Water Column	215
8. 3. The Arctic Marine Ecosystem	216
8. 4. Geophysical Properties of the Eurasian Basin and Fram Strait	217
8. 5. Geological History of the Eurasian Basin and Fram Strait	222
9. References	226
10. Alphabetical List of Scientific Participants	235
11. List of Acronyms used in the Text	236

## 1. INTRODUCTION: OCEANOGRAPHY, BIOLOGY AND GEOSCIENCES OF THE EASTERN ARCTIC DEEP-SEA BASINS

The eastern Arctic deep-sea basin between the Lomonosov Ridge and the Eurasian continental margin comprises one of the worlds least known oceans. After earlier, modest attempts its scientific exploration began with Fridtjof Nansen's famous expedition from 1893-96 on the reknown FRAM, the first research vessel especially constructed to withstand the dangers of the Arctic ice pack. This expedition whose men and ship returned safely home after a courageous, well-planned scientific enterprise, was the first one to prove: that the Arctic Sea had deep-sea basins with sea floors covered by fossiliferous pelagic and hemipelagic sediments; that the ice cover drifted in a predictable way; that water masses filling this basin had specific hydrographic properties; and that faunas and floras of the Arctic were adapted to their special and cold environments (Nansen 1902).

Except in its marginal areas (continental margins of the Barents Sea, Fram Strait) oceanographic research of this area lagged behind investigations of the central Arctic Ocean, where US-American, Canadian and Russian expeditions on floating ice-islands collected important data. It was not before the late seventies that state-of-the-art expeditions were organized to explore geological, oceanographic and biological properties of the eastern Arctic deep-sea basins (YMER-80, POLARSIRKEL, LANCE, FRAM ICE ISLAND expeditions; Kristoffersen 1979, Boström & Thiede 1984).

The Eurasian Basin of the Arctic Ocean (Fig.1) has a number of unique characteristics. It is an area where the mid-ocean ridge is anomalously deep compared to other mid-ocean ridges, and where spreading rates are the slowest of the entire world ocean. Its sediments can probably provide key data to solve the mystery of the initiation and variability of glacial ages during the Late Cenozoic. Its shallow and deep water masses are exchanged with those of the Norwegian-Greenland Sea resulting in relatively young deep waters in the Eurasian Basin and are linked to North Atlantic Deep Water formation which ventilates the entire world ocean. Its highly variable, seasonally persistent ice-cover is probably unstable, but seems to have existed for at least 2.5 million years with important impact on the composition and life cycles of the Arctic faunas and floras and sedimentation. Plankton tows as well as skeletal material in surface sediments seem to indicate that phytoplankton is a qualitatively important, but quantitatively rare element of the Arctic pelagic biota.

When planning for the Arctic expeditions of PFVS POLARSTERN for the late 80's heavy emphasis was placed on studies of the Fram-Straight area and of the northernmost parts of the Norwegian-Greenland Sea. Research interests of oceanographic and geoscientific working groups showed early a considerable regional overlap in the Eurasian Basin. The oceanographic group was interested in extending investigations begun in 1984 under the acronym ARCHY

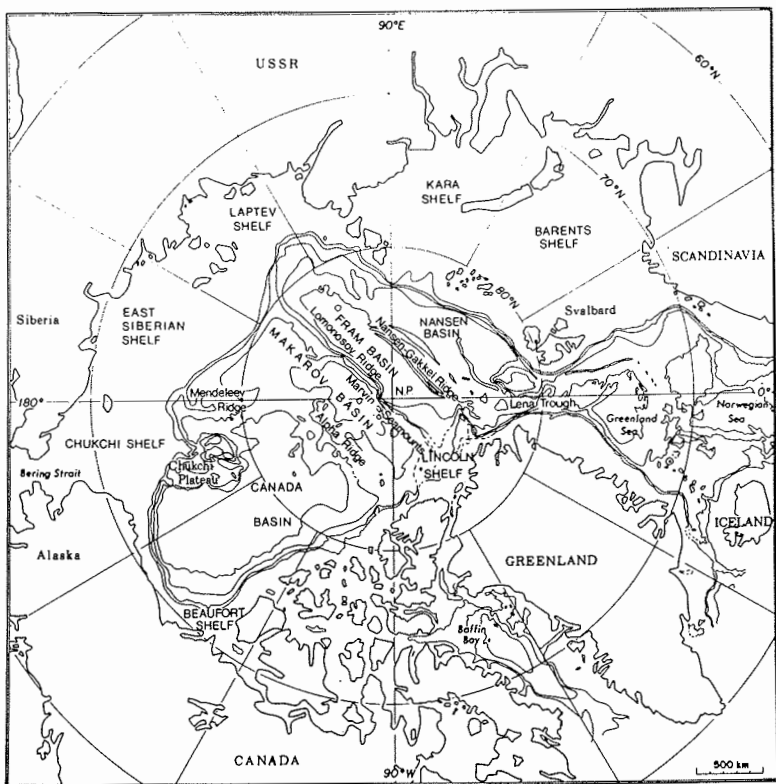


Fig.1 a) Arctic seafloor nomenclature and gross bathymetry. Contour interval is 1 km. Also shown is the 500 m contour. From Sweeney et al. 1982.

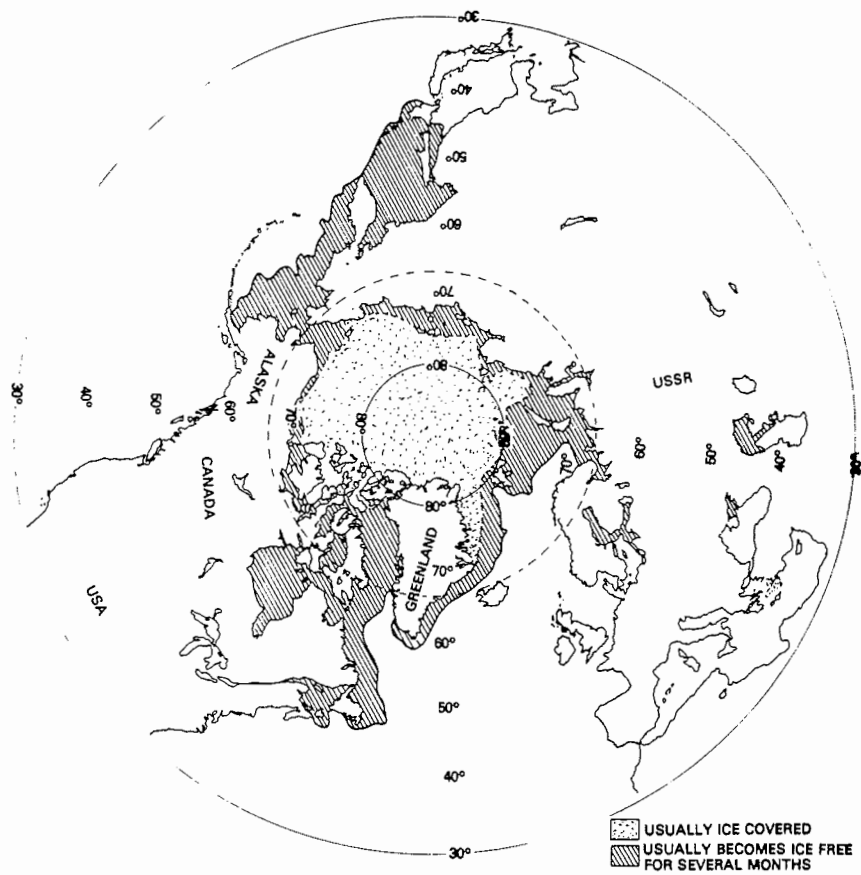


Fig.1 b) Mean maximum and minimum seasonal sea ice extent in the Arctic. From Slater 1969.

(ARctic Chemistry and HYdrography) north of Fram Strait. A combined effort resulted in this nine-week expedition, the 3rd leg of the ARKTIS IV program of PFVS POLARSTERN (ARK IV/3 and ARCHY87, Fig. 1).

The expedition began in Tromsö on July 4, 1987 and ended in Hamburg on September 2, 1987. Fifty-seven scientists and technicians from 19 institutions in 8 European and North American countries joined forces to carry out a complex program of oceanographic, meteorologic, biologic, and geoscientific studies. The POLARSTERN succeeded in penetrating the eastern Arctic ice pack as far north as 86° 11' N, further than any surface ship dedicated to a scientific research cruise before. It also represented the first modern, mobile, surface research platform with sophisticated equipment which reached a central Arctic area, and the first oceanographic transect into the basin interior (Fig. 2 a and b).

Beyond the successful execution of the expedition a set of unique scientific data on the properties of the Arctic Ocean was collected which will only be analyzed and published after a number of years. In this first report we present a description and first analysis of data and samples gathered during ARK IV/3. The report was written during the final days of the expedition before reaching Hamburg; data and interpretations presented are therefore preliminary. However, they offer a comprehensive account of scientific activities during the expedition. Documentation of the station locations and weekly reports can be found in the German expedition report, published by Krause et al. (1988) in a separate issue of the BERICHTE ZUR POLARFORSCHUNG. Detailed core descriptions, including thermal conductivities of cores and measurements of water content are published by the Geoscientific Working Party (1988) in BERICHTE 21: CAU/GIK.

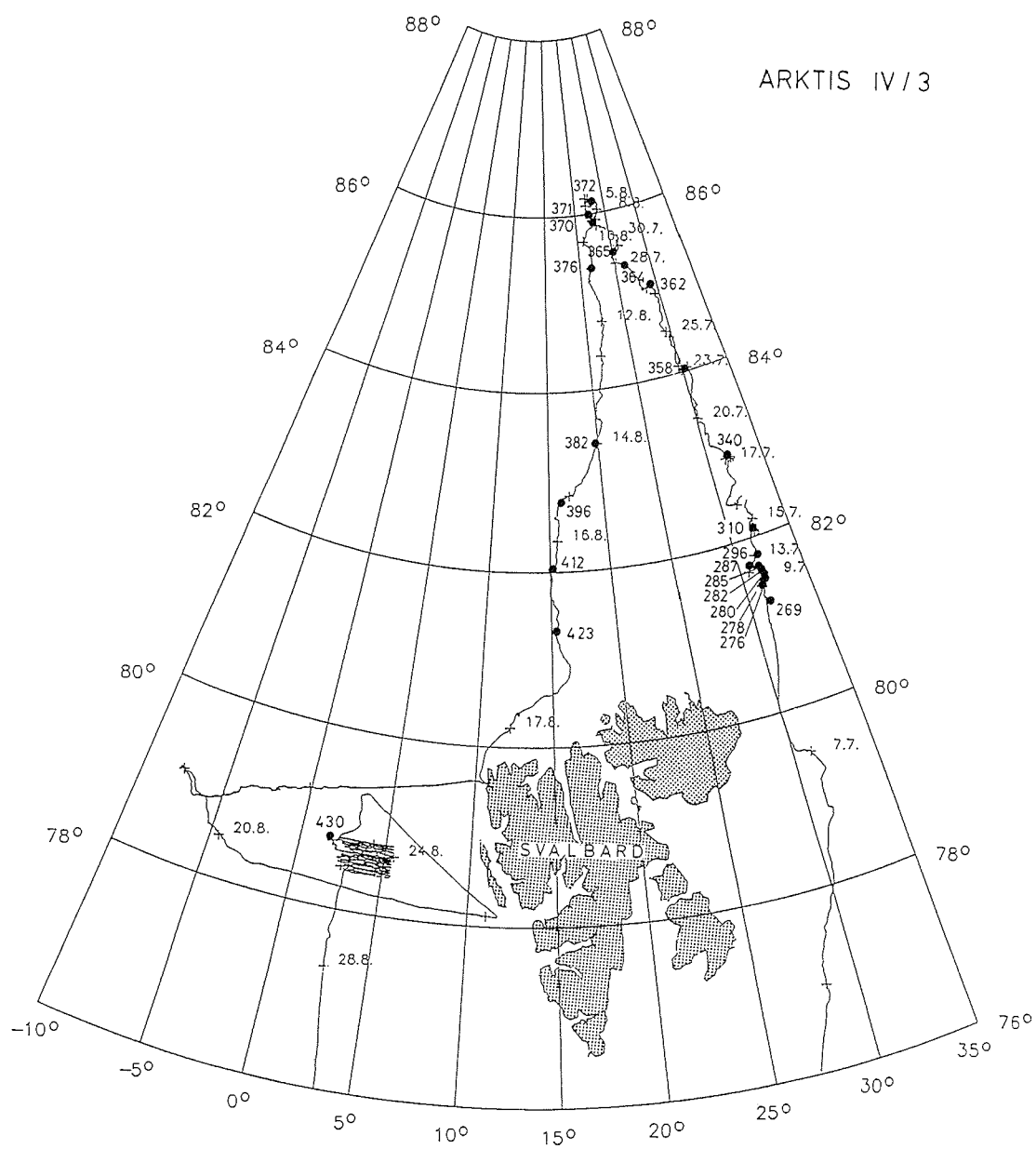


Fig.2 a) Track chart of ARKTIS IV/3.

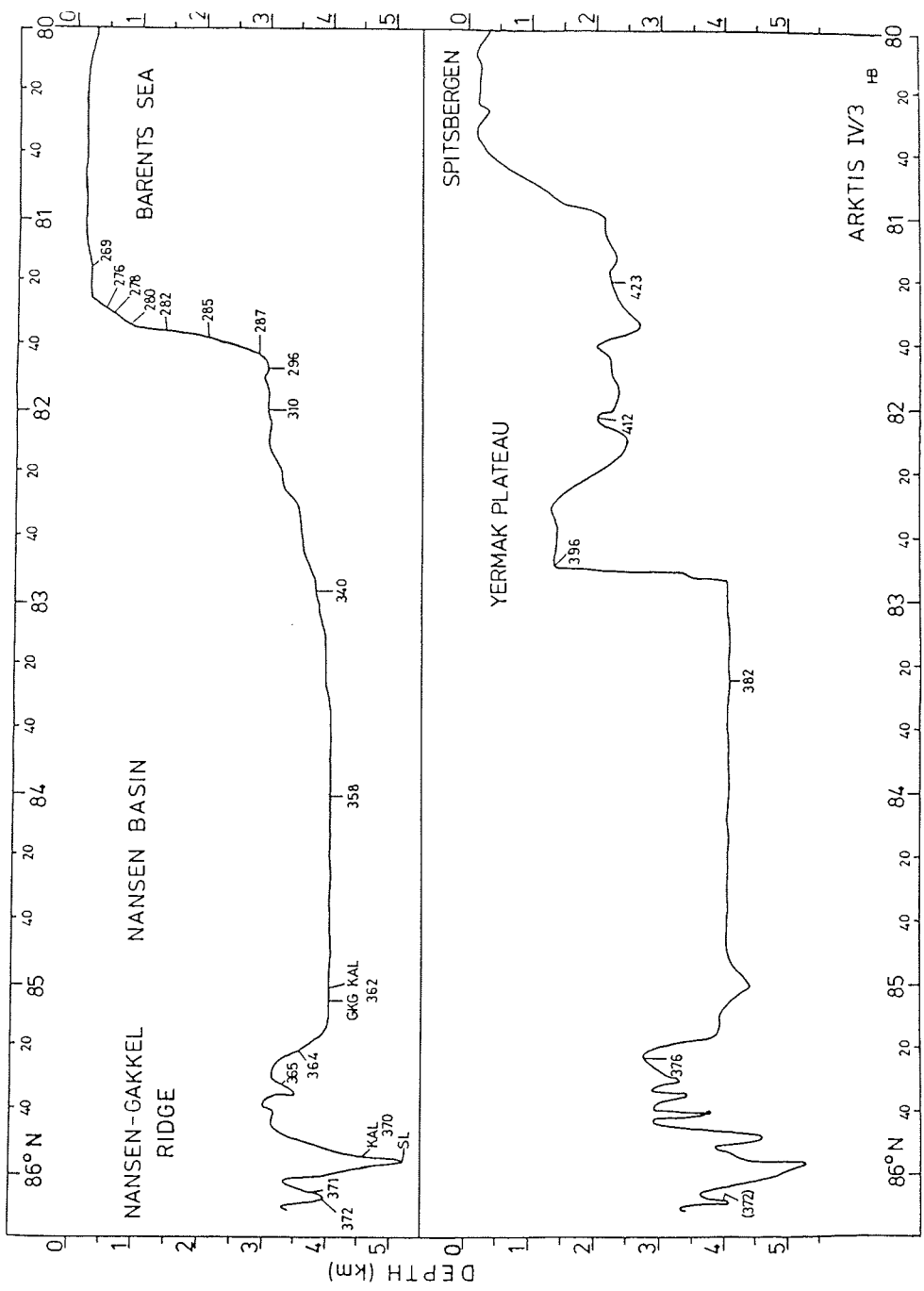


Fig. 2 b) Bathymetric profile (simplified) along the track line of ARKTIS IV/3. Station locations are marked c.f. Krause et al. in press

## 2. BATHYMETRIC SURVEYS (AWI, GIK)

The bathymetry of the Arctic Sea is known only in its main structures (Perry et al. 1986). This year the ARK IV/3 expedition showed that existing charts give a rather inaccurate bathymetric picture which makes planning of research programs and interpretation of scientific results difficult.

Two detailed profiles were obtained from the Svalbard margin to the Nansen-Gakkel Ridge. All systems ran continuously for depth measurements and the results were registered as analog signals and/or on magnetic tape.

At the end of the cruise a systematic survey of a large area in the Fram Strait was conducted as part of a long time commitment to compile an atlas of this important region. The ice situation in the northwestern region prevented continuation of profiles of POLARSTERN's former Arctic expeditions.

Depth measurements were carried out with the:

- NBS single narrow beam echo sounder, which supports ship navigation,
- SEABEAM, the multibeam bathymetric swath survey system, and
- the 3.5 kHz subbottom profiler.

On board POLARSTERN two systems independently receive positions:

- INDAS (Integrated Navigation and Data Acquisition System)

- GPS (Global Positioning System)

All positions were collected and stored on the onboard computer VAX 11/750.

### Measurements

Continuous depth-profiling ran in parallel to all other research activities on the two 600 km profiles in the eastern Arctic Basin. The northward profile started northeast of Spitsbergen and proceeded along 30-31° E over the Barents Abyssal Plain to the Nansen-Gakkel Ridge. The northernmost point at 86° 11' N and 22° 04' E was the beginning of the second profile heading southwestward to the Yermak Plateau (Fig. 3). Poor data quality on these transects due to extreme ice conditions was compensated by a high number of measurements as the ship moved very slowly.

SEABEAM, 3.5 kHz and a seagravimeter observations were continued in the Fram Strait as follows. The northern boundary of the survey area was between 78° 26' and 78° 48' N, the western boundary was between 2° and 3° E given by the natural limitation of the ice-cover, and the survey extended eastward to 5° 30' E (Fig. 4). The survey area, comprising 65 x 42 km, was covered by 23 longitudinal and two diagonal profiles which partly surveyed the Hovgaard Fracture Zone in the west. Average depth was 2500 m, requiring 1 nm spacing between survey lines.

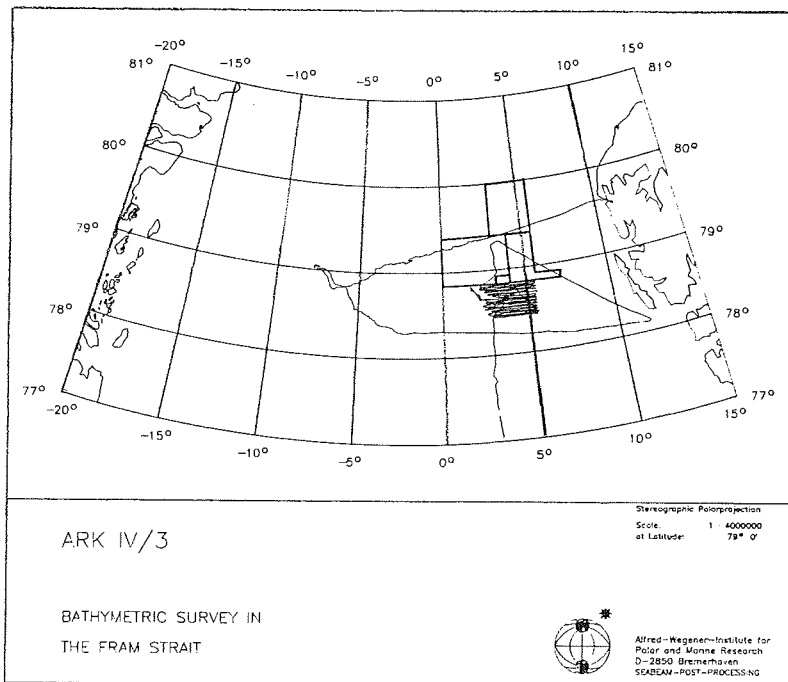


Fig.3 Bathymetric survey in Fram Strait. Boxes show previous surveys for Fram Strait atlas.

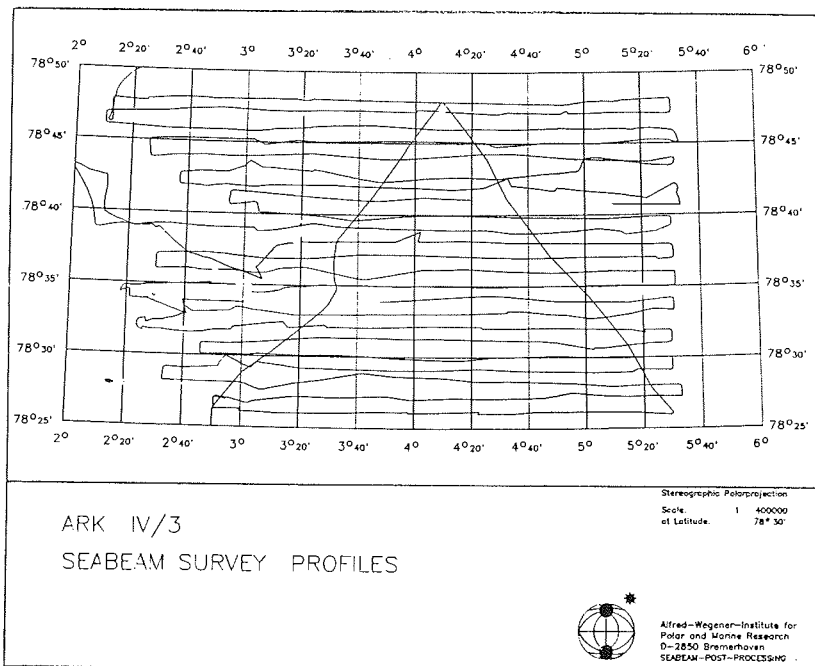


Fig.4 Seabeam survey profiles in Fram Strait ARK IV/3.

### System Performance

This cruise was POLARSTERN's first expedition with long lasting hard ice conditions. All systems installed on the ship received ship noise. Although the systems could not work normally we were successful in retrieving much new data in the poorly known eastern Arctic Basin.

- During the hard ice conditions the NBS received noisy signals. The analog registration showed the depth profile on a poor print. The analog/digital unit often functioned incorrectly and the system displayed wrong values.
- The 3.5 kHz subbottom profiler worked after some difficulties at the beginning of the cruise. In the ice, the system showed a noisy registration. Additionally the system is very sensitive to minor adjustments.
- At the beginning of the cruise the SEABEAM system did not function. After repair, the system worked continuously for eight weeks. Because of noise during hard ice breaking many measurements in the ice were wrong and the system often stored zero values. Also the system often was not able to react fast enough on depth changes. This effect had been observed also on earlier expeditions surveying steep slopes (Augstein et al. 1984). When this occurs, the program has to be set on stand-by mode and has to be restarted afterwards.
- Angles of the roll and pitch motion were measured on a gyro stabilized platform and were fed to the SEABEAM system for compensation of these systematic influences. During icebreaking the platform malfunctioned and the angle values became too large and unreliable. Therefore the consequence the platform could not be used. The roll and pitch angle was set to zero. The relatively stable position of the ship in the ice was used as a compromise. In the future a more reliable behavior of the platform has to be developed. During very difficult ice conditions a depth value could only be obtained by comparing all measuring systems.
- The INDAS system based on transit satellite fixes needs information about speed and heading for computation of the actual position. Sensors for measuring speed malfunctioned in the ice. The EM-log was destroyed by ice and the more slowly working Do-log malfunctioned during icebreaking because the ship moved back and forth. INDAS computed the actual position during the whole time in the ice with an estimated speed. Therefore the accuracy of the positions was poor.
- GPS was available during two timespans every day. In the Arctic, the windows with enough satellite coverage were the intervals between 6 am to 12 am and 6 pm to 12 pm. GPS is an independent navigation system and needs no information from other systems. The system worked very reliably with only one breakdown during the whole cruise.

#### Preliminary Results

- All position files are processed. GPS is the system with higher accuracy. Therefore GPS is the base of the data file, which is completed with positions of INDAS. The final result is a file with positions each 20 seconds.
- SEABEAM transmits depth, heading and time to the VAX computer. The depths were merged with the positions of GPS/INDAS and stored on magnetic tapes in a shorter format. During ARK IV/3 nearly 700,000 measurements were taken.
- The first results of the long depth profiles into the Arctic show that a lot of work is necessary to get the best depth after comparison and verification of all onboard systems. It is possible that some incorrect values are in the preliminary data files.

All measurements taken during the cruise are very important. The processed data will be sent to international data bases to improve the charts in the unknown regions of the Arctic Sea.

### 3. WEATHER CONDITIONS DURING THE EXPEDITION (SWA)

After leaving the harbor of Tromsö on 04.07.1987, depressions which developed in the polar frontal zone at the northern flank of a anticyclone over central Europe crossed the track of POLARSTERN. In prevailing southeasterly winds of force 3 to 4 and temporary rain, the ice edge was reached on 05.07.1987 at 76° N and 27° E.

During our northbound track, we came to the southern flank of an almost stationary cyclone north of Svalbard, so that the light wind veered from south to southwest. This cyclone filled and a anticyclone developed on 09.07.1987 over the Laptev Sea and Svalbard with light to moderate northeasterly winds and high probability of fog. This anticyclonic weather was ended by the frontal cloud band of a series of cyclones in the Svalbard region causing rain and northerly winds.

One of these depressions intensified north of the POLARSTERN area so that on 13.07.1987 the wind backed to westerly directions reaching force 7 and precipitation changed more and more to snow. At the same time, a high pressure zone over Scandinavia intensified. At its northern flank cyclones developed in the polar frontal zone and passed the operational area of POLARSTERN to the northeast (see Fig. 5). These cyclones circled the Pole counterclockwise and dominated the weather over our area until 25.07.1987. The wind came mainly from westerly directions at force 3 to 4 and the precipitation was partly snow or rain resulting in marginal values of ceiling and visibility and moderate icing conditions for the helicopter. The ship's progress in heavy ice on 23.07.1987 at 84° N and 30° E was seriously hindered by visibilities less than 1000 m. The forecast values of 300 ft ceiling and 2000 m visibility were critical, but sufficient for the supply flight of a Norwegian Lockheed P3-Orion on 24.07.1987.

On 29.07.1987 the operational area of POLARSTERN was temporarily under a high pressure influence. At the same time, an intense depression developed over northern Norway, moved northward to south of Svalbard with its frontal band crossing POLARSTERN the next day. Easterly winds of force 5 and freezing rain were encountered during the frontal passage.

Commencing on 31.07.1987, a fundamental change of the weather situation took place: The low south of Svalbard filled, while an anticyclone over the East Siberian Sea built up a wedge to the Barents Sea. This wedge intensified, resulting in a continuous veering of the wind from easterly to southerly directions. Simultaneous cyclonic activities over northern Scandinavia caused a high pressure gradient and, in combination with supergeostrophic effects due to anticyclonic curvature of the isobars, resulted in winds of force 6. During this situation, prevailing marginal values of ceiling and visibility as well as drizzle and rain, partly freezing, caused problems to the ship's and helicopter's operations. On 02./03.08.1987 at position 86° N and 22° E, ice

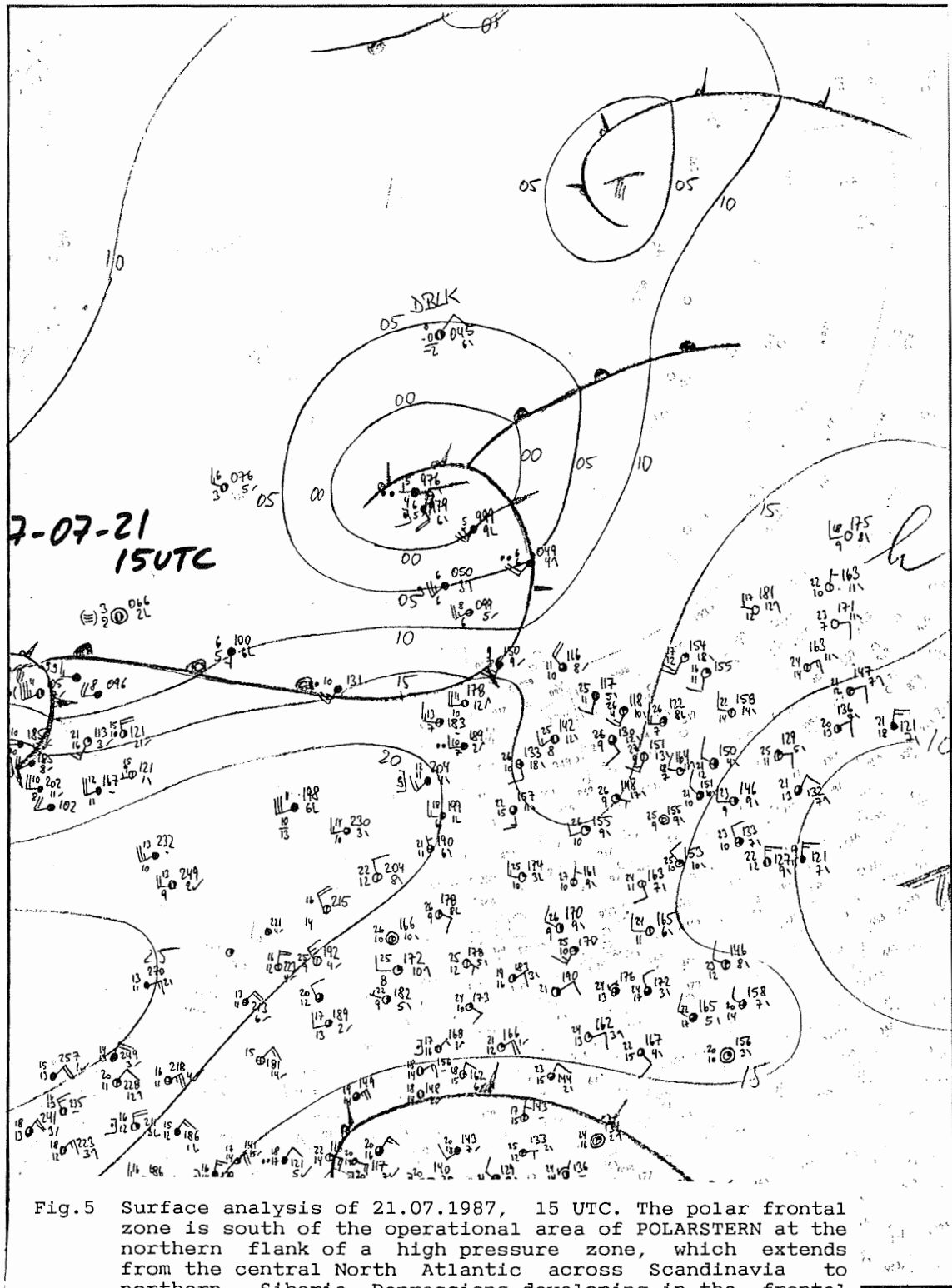


Fig.5 Surface analysis of 21.07.1987, 15 UTC. The polar frontal zone is south of the operational area of POLARSTERN at the northern flank of a high pressure zone, which extends from the central North Atlantic across Scandinavia to northern Siberia. Depressions developing in the frontal zone moved to the northeast. Prevailing weather conditions were good, but sometimes deteriorated due to lifting of warm and moist air masses before the warm front.

conditions again were heavy with ice thickness of 4 m and ridges up to 10 m. Reconnaissance flights with the helicopter, important for the ship's navigation in the ice, were made possible by short-range forecasts using actual radiosoundings (Fig. 6).

Preliminary evaluations make it likely that the weather situation described above caused an abnormal ice drift: Drifting buoys, deployed by LODYC (see Chapter 4.1) during this cruise and buoys which had been deployed earlier, showed trajectories following the change of wind direction. This ice drift was the reason that the attempt to return southward resulted in a northward drift to the farthest north position of 86.2° N and 22.1° E on 05.08.1987.

Later on, this anticyclone moved to the Barents Sea so that the operational area of POLARSTERN was at its western flank. While smaller secondary lows passed by, the force 6 wind veered to southwest, and after 08.08.1987 temporarily from east to southeast at force 3 to 4. Due to fog and drizzle both the helicopter and the ship operations were hindered.

After the high pressure zone had crossed Svalbard for Greenland, it intensified, causing the winds to veer to northwest to north. The wind speed was again higher than given by the pressure gradient due to the anticyclonic curvature of the isobars and reached force 4 to 5. This made the way back south less difficult and also decreased the frequency of reduced visibility due to fog. Snow flurries from time to time did not cause icing conditions for the helicopter.

This anticyclonic northwesterly flow was ended on 15.08.1987 by a depression moving from the Barents Sea to Svalbard. Its cold front crossed the area of POLARSTERN just north of Svalbard and again caused interference with operations due to fog and precipitation, together with low ceiling and visibilities less than 1000 m. Later on, a low at higher levels developed in the area between Svalbard and Franz Josef Land resulting in a stationary surface low. At its western flank, frontal cloud bands with embedded showers crossed the area of POLARSTERN. The conditions for a helicopter-flight to Longyearbyen were marginal at first due to these showers, but a radiosounding showed stabilizing upper level warm air advection. This confirmed actual weather observations which showed decreasing shower activity so that the flight could be performed without problems.

After this depression had almost filled, rising pressure from Greenland resulted in high pressure gradients with wind speeds up to force 7 on 22.08.1987. These high wind speeds lasted for a few hours only. At the northern flank of a mid-Atlantic high, a weak trough influenced the weather with light and variable winds during the last station on 24.08.1987.

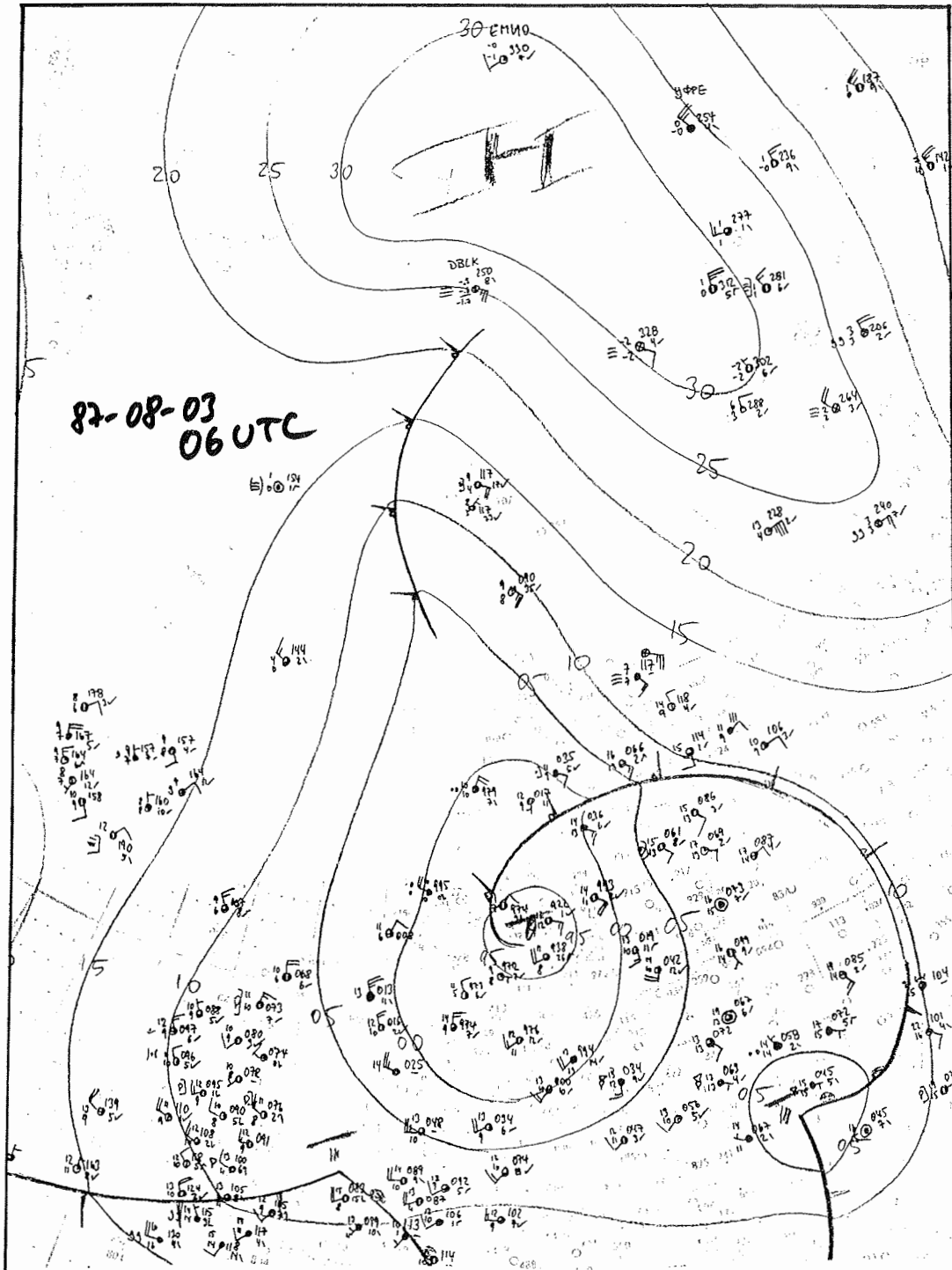


Fig.6 Surface analysis of 03.08.1987, 06 UTC. The operational area of POLARSTERN is at the southern flank of a high which extends from the polar region to northern Siberia. Anticyclonic curvature of the isobars resulted in supergeostrophic wind speeds. Due to embedded frontal bands, weather conditions were temporarily marginal for - 14 - helicopter operations.

TABLE 1: Statistics of weather elements during ARK IV/3 are listed below according to the observations of the German Weather Service. Total number of cases is 288.

Wind

Force	1	2	3	4	5	6	7	8
% of cases	7	11	31	27	15	7	2	0
Cummulative %	18	49	76	91	98	100	100	

Sea and Swell

Height	0 (ice covered)	1m	2m	3m	4m	Total: 102
% of cases	93	1	6	2	0	

Significant Weather

	Fog	Drizzle	Rain	Snow	Shower	not significant
% of cases	12	22	6	30	10	20

Visibility

	<200m	<500m	<1000m	<1nm	<2nm	<5nm	<10nm	>10nm
% of cases	1	2	13	9	6	21	38	10
Cumulative %	3	16	25	31	52	90	100	

Ceiling

	< 600ft	< 2000ft	> 2000ft
% of cases	55	37	8
Cumulative %		92	100

Cloud Cover

	< 3/8	< 6/8	> 7/8
% of cases	1	7	92

The statistics of weather elements (Table 1) show that marginal weather conditions have a high probability in the Arctic. This observation is supported by climatological data. High wind speeds and, of course, high sea and swell are less likely in the Arctic than in the mid-latitude oceans. Continuous weather analysis and forecasts help to reduce the interference of weather phenomena with ship and aircraft operations.

#### **4. SEA ICE INVESTIGATIONS OF THE EURASIAN BASIN**

Sea ice investigations were primarily concerned with understanding sea ice dynamics/thermodynamics and impact of ice on sedimentation and biologic productivity. The program was carried out by deploying an array of 12 satellite-tracked buoys for ice motion, ice temperatures and meteorological observations; ice coring and surface snow and ice sampling for biologic, sedimentologic, ice crystallographic, and chemical analysis; helicopter observations and photography of ice characteristics; and measurements of light transmission through and below the ice.

In addition, several investigators used the ice as a platform or made measurements to support major shipboard investigations. These studies are detailed in the following sections as follows: gravity measurements (7.1); launching of expendable current profilers (5.3.11); trace elements of meltwater, sea surface and shallow water samples (5.3.5); radioisotopes of 50-100 liter samples of surface meltwater at Stations 11/285 and 11/364 to assess whether the melted snow and ice might have imput from the 1986 fallout of Chernobyl radionuclides (5.3.10). At one station samples were obtained to study halocarbons in meltwater and surface seawater samples, freons in surface seawater, and tritium and helium of surface seawater (5.3).

##### **4.1 Sea-ice dynamics and thermodynamics (LODYC, WHOI, SWA)**

Sea ice is obviously one of the most characteristic features of the Arctic Ocean. Although we know the basic physics to explain why sea-ice grows, melts and moves, we are still trying to answer when, where, how much and how fast it does so. In the Arctic, sea ice goes from a nearly total coverage of the area in winter and early spring to about a 50% coverage in summer. That means 50% of the total coverage resists complete melting in summer, and explains why multi-year ice is a common Arctic sea-ice feature. This is a remarkable difference when compared with the Antarctic where nearly all sea-ice melts during summer.

Two major circulation patterns characterize Arctic sea-ice drift. One is the so-called "Beaufort Gyre" in the Amerasian Basin, and the other, called the "Transpolar Drift" extends over the entire Eurasian Basin (Fig. 7). The Transpolar Drift crosses the Nansen Basin and the main area of investigation of ARK IV/3. Most of this ice is exported out of the Arctic Ocean through Fram Strait and is replaced by relatively warm and salty waters carried from the south by the Norwegian Current. This water mass of Atlantic origin passes by the western coast of Spitsbergen and, after entering the Arctic Ocean by the northwest corner of Spitsbergen, heads east along the continental slope north of Svalbard. Another branch of the West Spitsbergen Current follows the Yermak Plateau on its western and northern flank, situated at about 83°N.

While a major part of the oceanographic program of the ARK IV/3 cruise concerned a detailed survey of the Atlantic layer flowing eastward along the continental slope of the Eurasian Basin, a

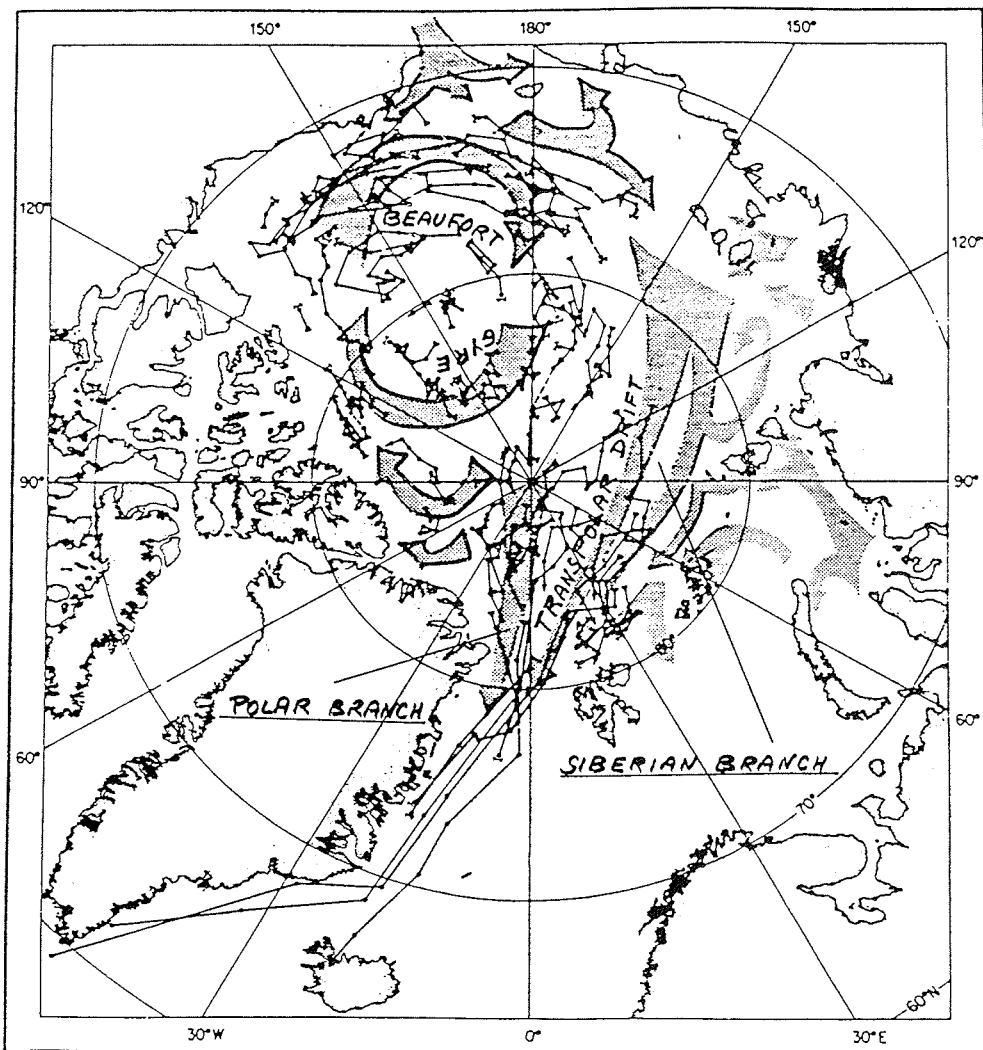


Fig. 7 Drift paths of 45 air-dropped data buoys between January 1979 and December 1981 (adapted from Untersteiner and Thorndike, 1982). The stippled arrows indicate an early estimate of the mean circulation of the upper several hundred meters of water in the Arctic basin (Gordienko, 1958).

detailed program to study sea-ice dynamics and thermodynamics over this area was also carried out. This program has major implications for the oceanographic, geologic, and biologic programs.

#### Methodology

In order to look at the dynamics and thermodynamics of sea-ice, one has to look not only at the ice itself, but also at the atmospheric boundary layer above and at the oceanic mixed layer beneath. From a dynamical point of view, in order to answer the question "How does sea-ice move?", it is necessary to observe simultaneously ice drift, surface winds and surface currents in order to estimate stresses at the two interfaces.

In terms of sea-ice motions, it is necessary to observe sea-ice thickness distribution, ridges and keels to get an estimate of roughness. It is also necessary to estimate ice compactness and, consequently, estimate of internal stresses transmitted into the ice pack. In summertime, it is usual to assume free ice drift, which results from loose pack ice because of numerous leads. Internal stresses are considered zero in this case.

Regarding the atmospheric boundary layer, the main dynamical component is the surface wind (speed and direction). It has been demonstrated in past experiments (AIDJEX) that geostrophic winds, which can be derived from surface air pressure measurements, allow a good estimate of the wind stress on pack ice. Regarding the oceanic mixed layer, it is necessary to know the geostrophic currents and the depth of the mixed layer as pointed out by Ekman in 1905, after the Fram expedition and Nansen's observations, in his famous theory about the so-called "Ekman spiral".

From a thermodynamical point of view, in order to answer the question "How does sea-ice melt and grow?" it is necessary to measure the heat fluxes at the two interfaces and conduction through the ice. As a first approach, the sensible and latent heat fluxes at surface can be estimated indirectly from climatological data (long and short wave radiation as a function of time and latitude) and meteorological data (cloud cover, inversion layers, wind forces, air versus ice surface temperatures, humidity). Oceanic heat flux at the lower interface  $F_w$  needs to be estimated directly by measuring ice thickness variations as a function of time  $dH/dt$  and temperature profiles (vertical) across the ice  $dT/dz$ .

$$F_w = K(dT/dz) - pq(dH/dt)$$

where K: thermal conductivity,

q: specific heat,

p: specific mass.

### Instruments Used and Scientific Investigations

In order to look at sea-ice dynamics and thermodynamics over the Nansen Basin following this methodology, an array of twelve buoys was deployed between 82° N and 86° N from July 15 until August 14 (see Table 2). All these buoys can be located several times a day via ARGOS on board NOAA satellites. These buoys give a prime estimate of ice motions (translation, rotation, convergence, divergence). Five out of the 12 buoys (1479, 5077, 5079, 9260, 9262) are equipped with meteorological sensors. They transmit information to the GTS for global weather forecasting. These "met-buoys" return data to estimate wind stress on the surface of the ice. Three out of the 12 buoys (1479, 5077, 8440/41) are equipped with a thermistor chain across the ice ("Met/Ice Buoy") to estimate ice thickness variations and ocean heat fluxes. One buoy (8440/41) is equipped with a thermistor chain in the mixed layer and with a vertical acoustic doppler profiler, giving currents relative to the ice in the first 300 meters (except the first 20 meters below the surface). This, combined with the ice motion, will give a good estimate of ice - ocean stresses at this location.

In order to map subsurface currents on a larger (basin) scale and to infer large scale ice-ocean stresses, we expect in the near future to make extensive use of neutrally buoyant floats drifting at constant depth (or pressure) beneath the ice. The floats will be tracked acoustically by autonomous listening stations, deployed on the ice and transmitting acoustic signals received from floats to satellite in near real time (see Chapter 5.3.12).

### Stations and Progress

Buoy deployment began on July 15 at 21:00 UTC and ended on August 14 at 20:00 UTC. Buoys were regularly deployed at about 50 km intervals for ice motion studies and at about 100 km intervals for meteorological observations (Fig. 8). At the northernmost point, 3 buoys were deployed with short spacing (a few kilometers) for detailed ice motion observations (translation, rotation) as well as oceanographic (current and temperature profiles in the first 100 m to 300 m beneath the ice), meteorologic, biologic observations (sediments, light transmission) and acoustic propagation (SOFARGOS). The whole array will operate for about one year, during which time positions as well as messages will be obtained via the ARGOS system. It is likely that most of the buoys north of 83° N will pass through the Fram Strait before the end of 1987. We expect to recover some of these buoys (at least the 3 northernmost ones) by spring 1988 in the Denmark Strait close to Iceland.

South of 83° N, most of the buoys will likely remain in an area east of the Yermak Plateau where their lifetime is expected to be only of the order of few months.

BUOYNBR	DATE	JULIAN	LAT(Dg-Mn) NORTH	LONG(Dg-Mn) EAST	H-LIT	FLOE THICKNESS
5095 Ice Temp	15/07/87	196	82° 25.7	31° 19.6	21.10	
5079 Met-Buoy	16/07/87	197	82° 59.4	31° 55.6	11.00	
5094 Ice Temp	20/07/87	201	83° 24.47	30° 07.62	00.00	3 m
9260 (*)	22/07/87	203	83° 58.1	29° 53.4	14.00	
4996	23/07/87	204	84° 27.3	30° 01.2	24.00	4.5 m
5077 Met/Ice Buoy	27/07/87	208	85° 02.5	28° 33.9	01.35	2.8 m
4992	28/07/87	209	85° 31.1	25° 17.0	14.20	2.8 m
3491 Sofargos	31/07/87	212	85° 54.4	22° 40.2	22.00	> 3 m
8440 (**) 8441	04/08/87	216	86° 07.3	22° 02.4	10.30	3.5-4 m
9262 (*)	04/08/87	216	86° 08.8	22° 02.1	17.30	3 m
4994 acoustic source	11/08/87	223	85° 22.1	21° 28.3	05.44	
1479 Met/Ice Buoy	14/08/87	226	83° 22.5	19° 50.3	19.50	2.5 m

(\*) Dr. Hoeber Meteorological Institute, Hamburg, RFA  
 (\*\*) R Krishfield, Woods Hole Oceanographic Institution, Woods Hole, USA  
 ( ) Dr Gascard, LODYC, Paris, FRANCE

Table 2: Argos buoy deployments on ARK IV/3.

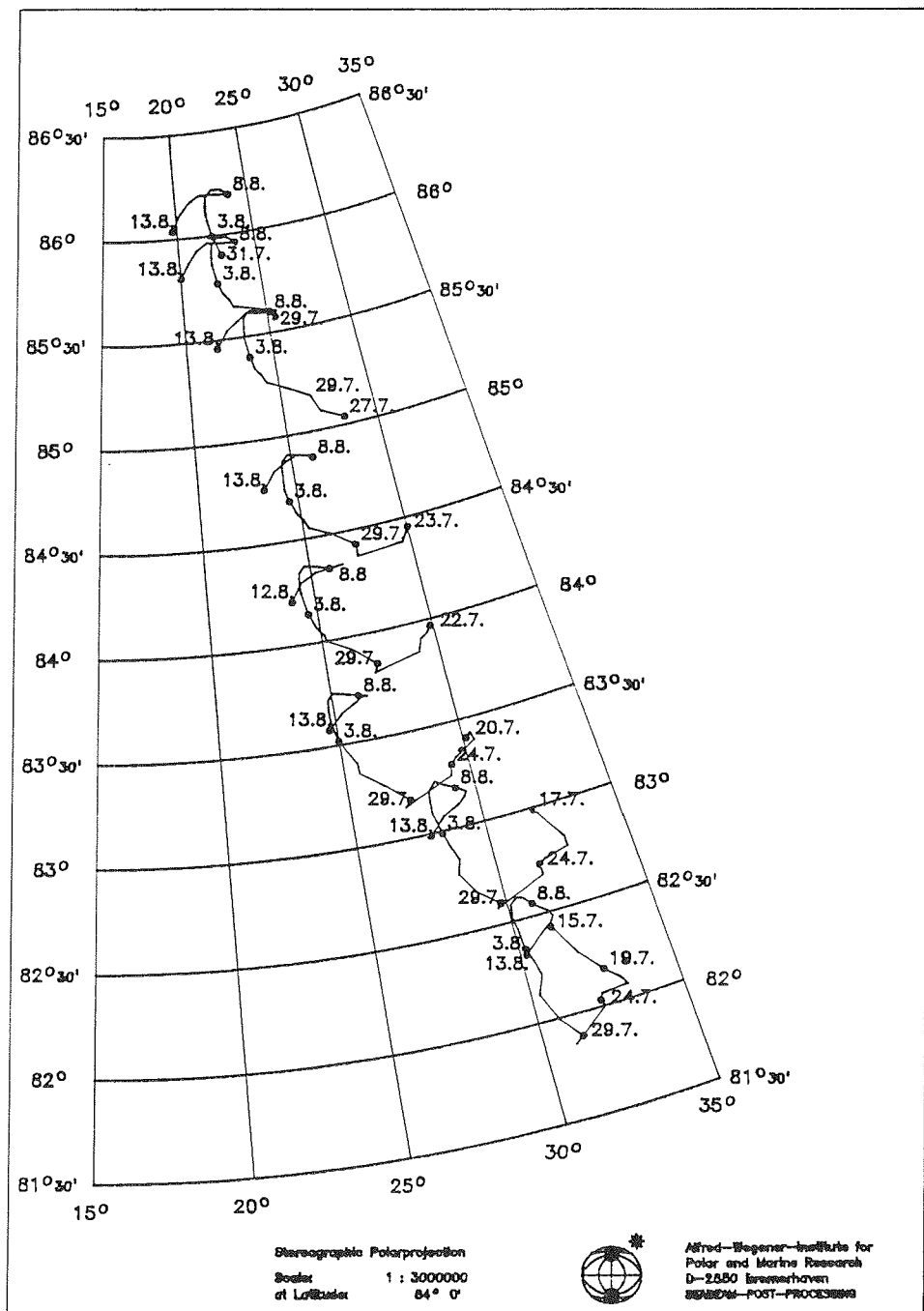


Fig.8 Drift paths of 12 satellite tracked buoys deployed during ARK IV/3 as observed for the 40 days following the deployment. The trajectories of 3 buoys deployed in fall 1986, 1000 km upstream, are also shown from January 1, 1987 up to now.

### Preliminary Findings

Mean sea-ice drift observations made during the cruise (Fig. 8) agree with a circulation pattern first identified by Gordienko (1958), and more recently, by Untersteiner & Thorndike (1982), Vinje (1982), Colony & Thorndike (1983) and Gascard and Jeannin (1986).

The area north of Svalbard can now be divided into four parts (Fig. 7):

- the near continental slope area, up to  $83^{\circ}$  N, which is mainly influenced by topography including the Yermak Plateau and its northern boundary at about  $83^{\circ}$  N, and by the circulation of Atlantic water masses carried by the West Spitsbergen Current. This area is characterized in summertime by loose pack ice and high melting rates due to an active ocean-ice heat flux which weakens the ice cover drastically. Most of the ice entering the area is trapped eastward of the Yermak Plateau and is not likely to reach Fram Strait before melting entirely.
- the area located north of  $83^{\circ}$  N and south of the Nansen-Gakkel-Ridge. This area is characterized by one of the major branches of the Transpolar Ice Drift, the "Siberian Branch". Most of this ice originates from the Siberian shelves in the Laptev Sea. In this area, we typically observe a convergence zone, where most of the drifters deployed on the ice in the past tend to concentrate. The Siberian Branch was first documented by the famous historical FRAM Expedition. Most of the ice located in this region is likely to cross Fram Strait 3 to 4 months later where it will join the East Greenland Current (Fig. 7).
- the area located above the Nansen-Gakkel Ridge, characterized by a divergence zone from which drifters deployed upstream on the ice are very seldom encountered.
- the area located around the North Pole, characterized by the second major branch of the Transpolar Drift, the "Polar Branch". This branch, oriented north-south, joins the East Greenland Current in Fram Strait together with the Siberian Branch between  $80^{\circ}$  to  $79^{\circ}$  N and  $0^{\circ}$  to  $5^{\circ}$  W.

In terms of variability, the observations made in July and August 1987 (Fig. 8) confirmed a typical summertime drift pattern in this area (ARCTEMIZ 86). This variability is mainly due to typical wind variability in summer. A sequence of southerly winds alternating with easterlies and westerlies is often observed during the summer season (Fig. 9). Northerlies, which are the predominant winds in other seasons, are much weaker during summer. During the ARK IV/3 cruise, the northward sea-ice drift, observed from July 31 (day 212) until August 6 (day 218) is markedly correlated with a period of southerlies. This event occurred at the same time POLARSTERN was reaching her northernmost position and it induced some navigational problems since, at the same time, most of the open waters (leads) closed off.

## WIND OBSERVATIONS ON BOARD POLARSTERN

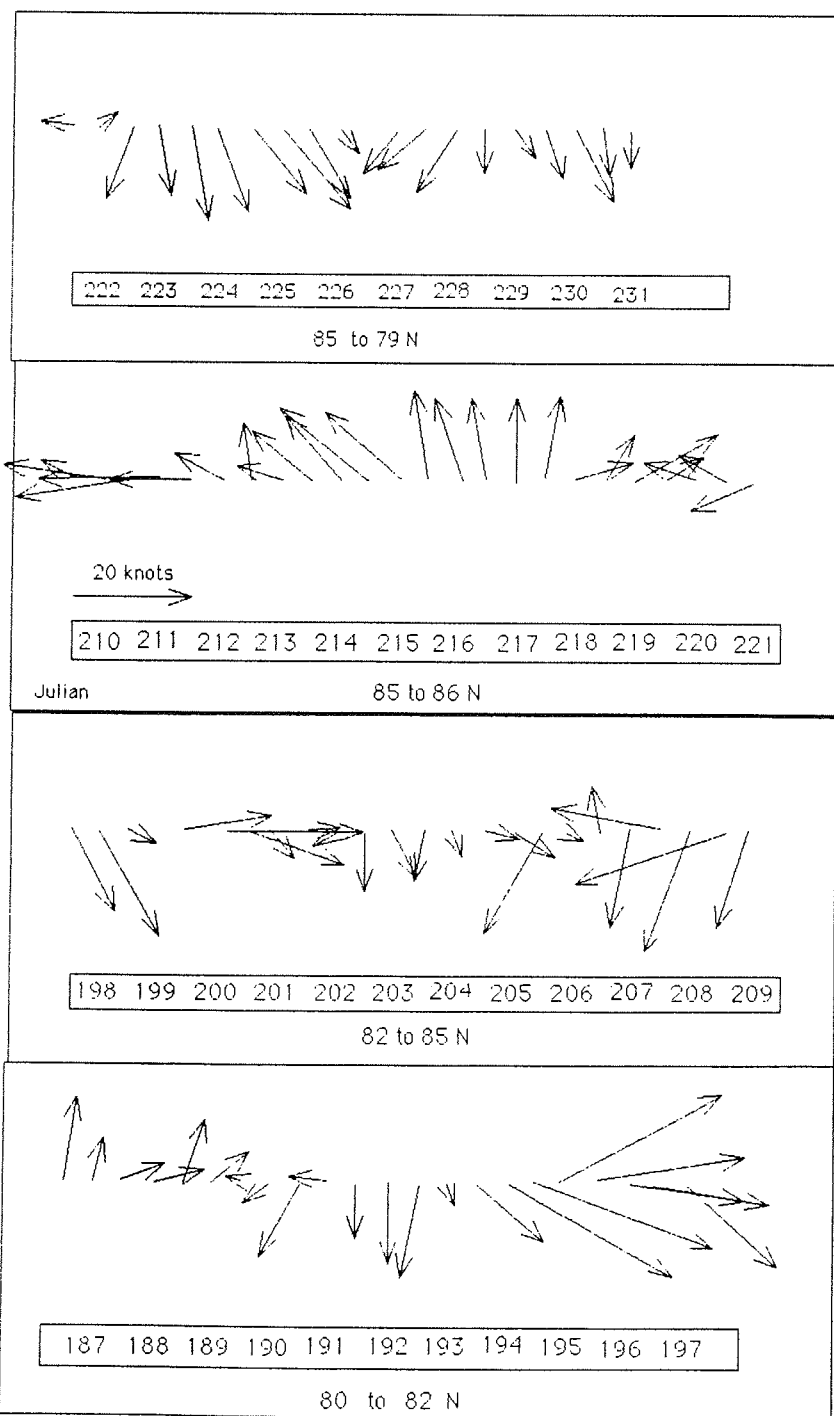


Fig.9 Daily wind observations (06.00 and 18.00) made by the meteorological station on board POLARSTERN during ARK IV/3 cruise.

The five buoys equipped with meteorological sensors deployed during the cruise, in addition to three other buoys deployed last year farther east (upstream), gave the missing information to investigate the weather patterns developing over the area (Fig. 10).

#### Plans for Future Work

This experiment will continue after completion of the cruise. In the future, the entire array is going to move southwestward and most of the buoys will cross Fram Strait in the early part of the coming winter. By springtime of 1988 they are expected to be located north of Iceland and most of them will be picked up when passing by Denmark Strait in late spring 1988. Most of the data will then be collected, processed and analysed jointly by the various institutions participating in this program.

In September 1987, other buoys will be air dropped in the Nansen Basin by the Norsk Polarinstitutt (Norway) and APL to sample the seasonal variability of the Transpolar Drift. Next year (August 1988), ten SOFAR floats will be launched in Fram Strait by the LODYC to monitor circulation of Atlantic Water masses in the Greenland Sea and the Nansen Basin. This program is part of the on-going Greenland Sea Project.

#### **4.2 "Dirty" Sea Ice (GIK, AWI, RWTH)**

Today the Nansen Basin is covered by year-round pack ice. Previous observations of the ice surface in the Nansen Basin north of Svalbard indicated that as much as 10% of the ice surface may be affected by material accumulation (Drewry 1986, p. 229). Sediments transported by sea ice are considered as the principal source for the sediments accumulating in the central Arctic during interglacial times when ice conditions were similar to the present (Clark & Hanson 1983).

Sediment can be incorporated in sea ice by a variety of mechanisms, almost all of which occur on the continental shelves or in the near-shore environment. These different origins can be distinguished to some extent by the composition of biogenic and lithogenous material together with crystallographic and chemical analysis of the sea ice itself. Drewry (1986) summarized the most important sources as follows:

Rivers: fluvial sediments can be included in river ice which is discharged to the sea, or may flood over and under the ice when the river ice breaks up in spring.

Beaches: beach material may be incorporated in the ice foot of shorefast ice which grows in early winter and usually breaks up and melts in place in spring.

Coastal cliffs: cliff sediments can avalanche, slump or slide on to sea ice along the shore.

Sea floor sediment: sea floor sediments from shallow continental shelves can be incorporated in sea ice in a variety of ways. Anchor ice forms when supercooled water encounters the sea bed

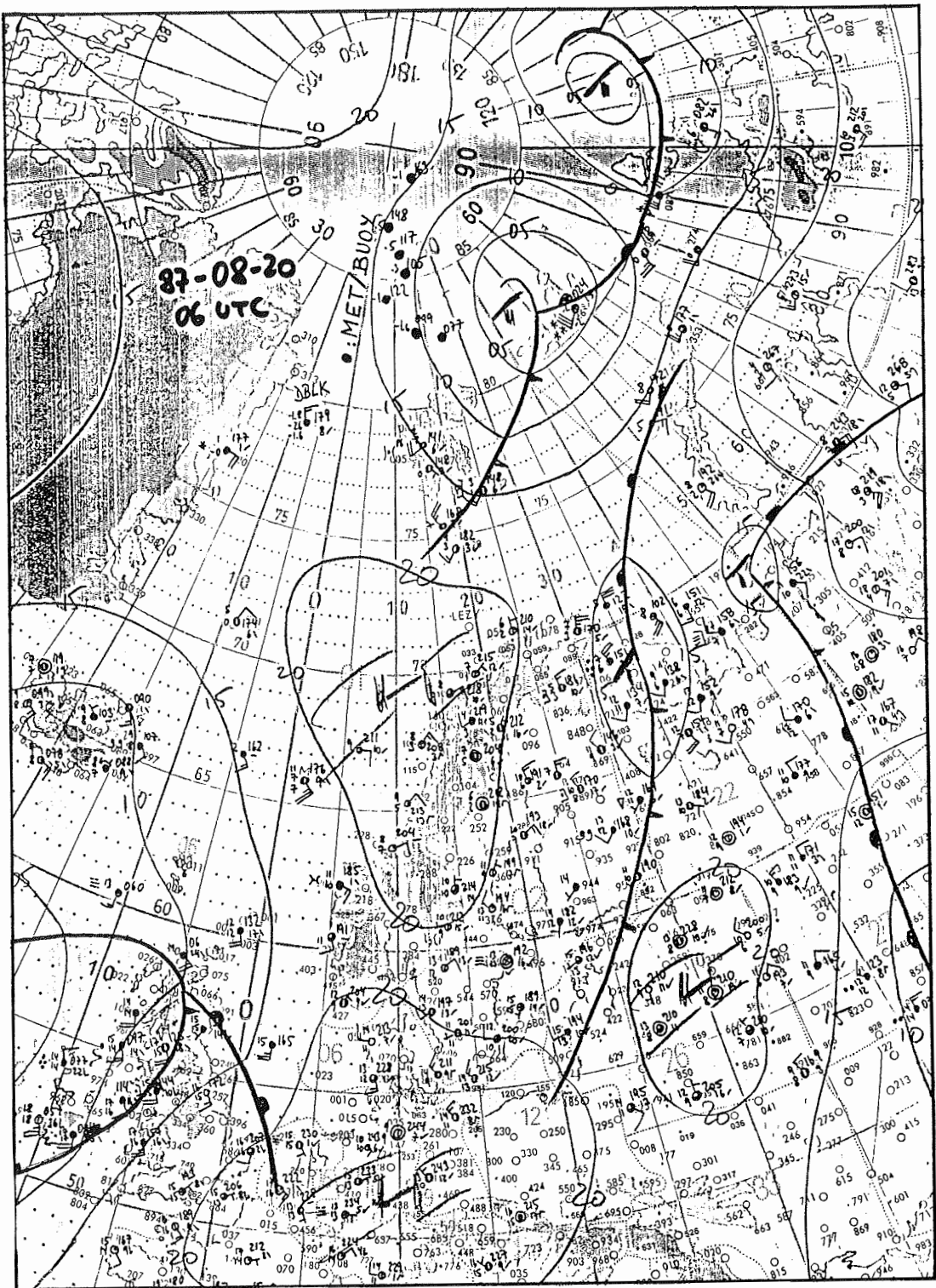


Fig.10 Daily weather observation map showing surface pressure front locations, including data from Met-Buoys deployed during ARK IV/3.

forming ice which can raft bottom sediments and organics to the sea surface. Frazil ice formation can freeze in sediment which is suspended in the water column. Sediment could be in suspension due to storms, tidal current activity, ice scour, and perhaps convection caused by brine rejection during sea ice formation. Sediments were recently observed by Vinje (1987) to accumulate on the underside of the ice during March on Spitsbergenbanken when the water column contained a lot of suspended sediment. Ice gouging of the sea floor by pressure ridges can also result in material accumulation on the underside of ice.

Aerial transport: sediments can be transported from snow and ice free terraine onto near shore ice, or be redistributed from regions of very dirty ice surfaces on the polar ice pack. Long distance transport can also contribute to the surface material accumulation.

Once material is included in ice, surface melting and freezing of new ice at the base may accumulate material at the ice surface in multiyear floes. Each year approximately 40 cm of surface ice plus snow melts while an additional 40 cm is added to the base, eventually resulting in a relatively stable ice thickness of 3-4 m (Untersteiner 1986).

An important source for sea ice in the Nansen Basin is the Siberian shelf. This continental shelf is shallow, broad, is influenced by river input, and therefore has the potential of including sediment in ice by many of the processes listed above. Shelf or shorefast sea ice which escapes from the Laptev and East Siberian Sea and is included in the polar ice pack will generally be transported with the Transpolar Drift westward across the Eurasian Basin. Most of this ice exits through Fram Strait after undergoing several years of melting and freezing, and deformation (see Chapter 4.1).

The primary objectives of the "dirty" ice project of the ARK IV/3 cruise are to:

- 1) document the regional distribution and variability of material-laden ice,
- 2) identify the amount and type of material contained in the pack ice,
- 3) evaluate possible processes by which material may be initially incorporated and how sensitive these processes are to environmental factors,
- 4) determine how material in sea ice may be redistributed during melting and refreezing,
- 5) identify transport paths,
- 6) understand depositional processes and identify possible depositional locations, and
- 7) determine the contribution of sea-ice rafted material to the sea-floor sediments of the Eurasian Basin.

### Sampling

On the transect from the Svalbard margin to the Nansen-Gakkel Ridge, ice sampling was carried out both from the ship and with helicopter support (Fig. 11). Sampling equipment and materials were kindly provided by AWI, LODYC and WHOI. Cores were obtained primarily in or near dirty ice locations. One to six ice cores were obtained at each sampling site with 4" diameter corers. In the field, cores were photographed, described and the temperature measured every 50 cm downcore. A total of 69 ice cores were obtained on 31 stations amounting to about 173 m of ice. The average length of ice cores is 3 m; the shortest core is 38 cm, the longest one is 455 cm. Cores were placed in a -27°C freezer as soon as possible and will be transported to AWI on return of the POLARSTERN to Germany.

At selected locations, light transmission was measured through the holes left by ice coring (see Section 6.2). These measurements will provide an indication of the effect of material accumulation on biologic productivity (Fig. 12). Chemical analysis for nutrients were carried out on board on two cores, and further chemical analysis will be conducted on shore.

In addition to the ice cores, 102 samples of surface snow and/or surface sediment were taken, and observations were made of the surface characteristics of the ice floes, including grain size and temperature, for correlation with satellite images in conjunction with other investigators (DHI; YU).

Observations of the distribution of dirty patches on the sea ice, percentage of ice cover, ridges and meltwater ponds, were obtained during 36 flights with the helicopter aboard the POLARSTERN. More detailed mapping of ice characteristics were carried out 6 times by flying over an 8 mile grid (Fig. 13).

On shore, the ice cores will be examined by M. Lange at AWI for analysis of structure and textural parameters, in order to understand the growth processes of the sampled floe and the relationship of material accumulation to ice classification (Lange 1987). Following this investigation, examinations of the material distribution will be conducted as follows: 1) determination of sediment concentrations in ice cores and surface samples, 2) analyses of composition, grain sizes, mineralogy and surface microtextures of lithogenous particles, 3) comparison of the ice data with sediment cores obtained on this cruise, in the Fram Strait and in the Barents Sea in order to determine the contribution of sea ice rafted material to sedimentation.

This research will be supported by cooperation with other investigators as follows: AGC/BIO (see below) for analysis of the biogenic material; the transport of dirty ice and possible deposition locations of ice rafted debris will be determined in

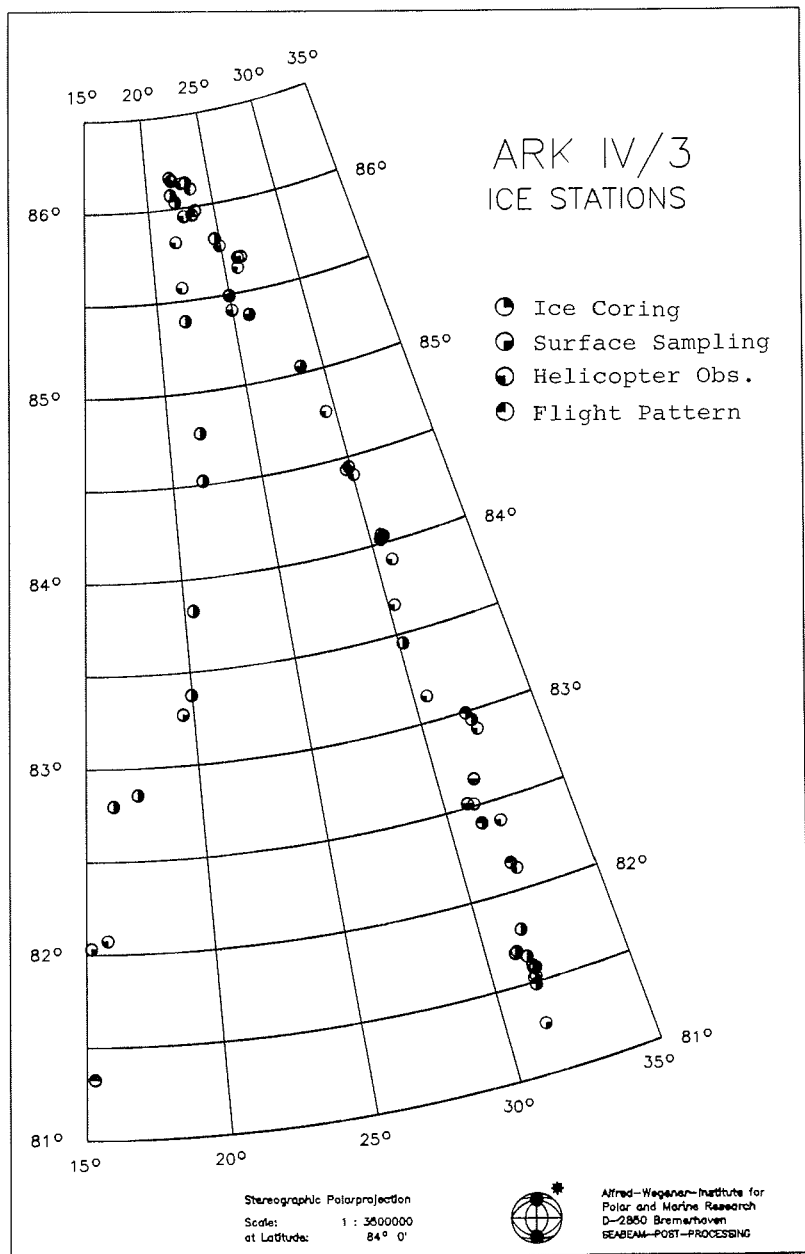


Fig.11 Map of ice stations and helicopter observations.

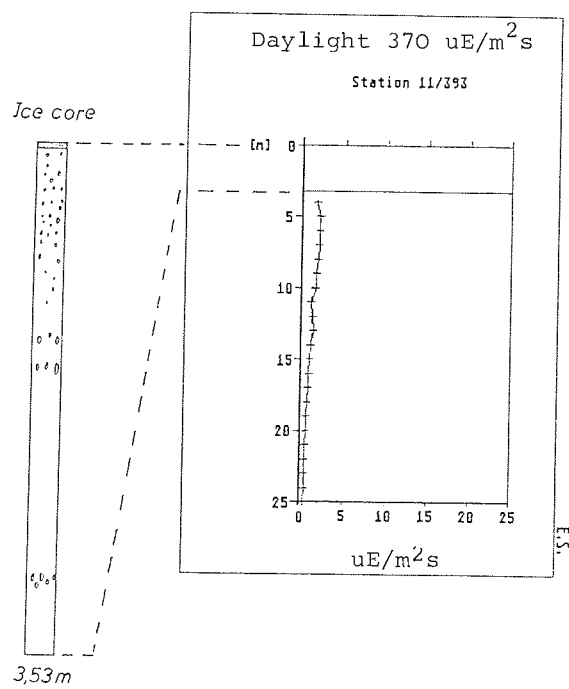
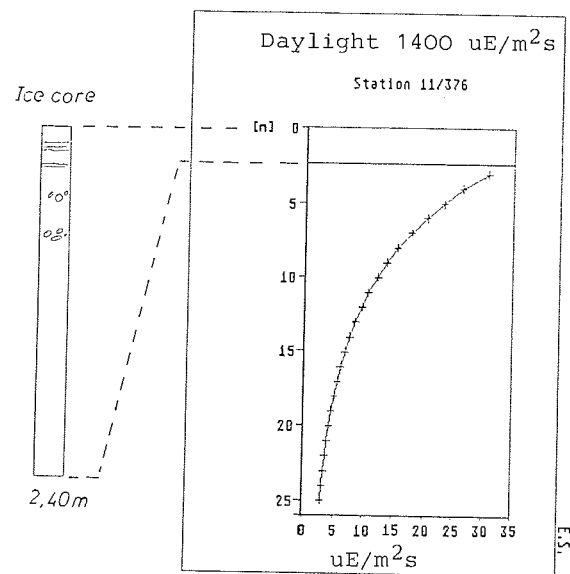


Fig.12 Examples of two ice cores showing regions with material accumulation and light attenuation profiles under the ice.

## Flight pattern

Position of the ship: N 85 55, E 22 46

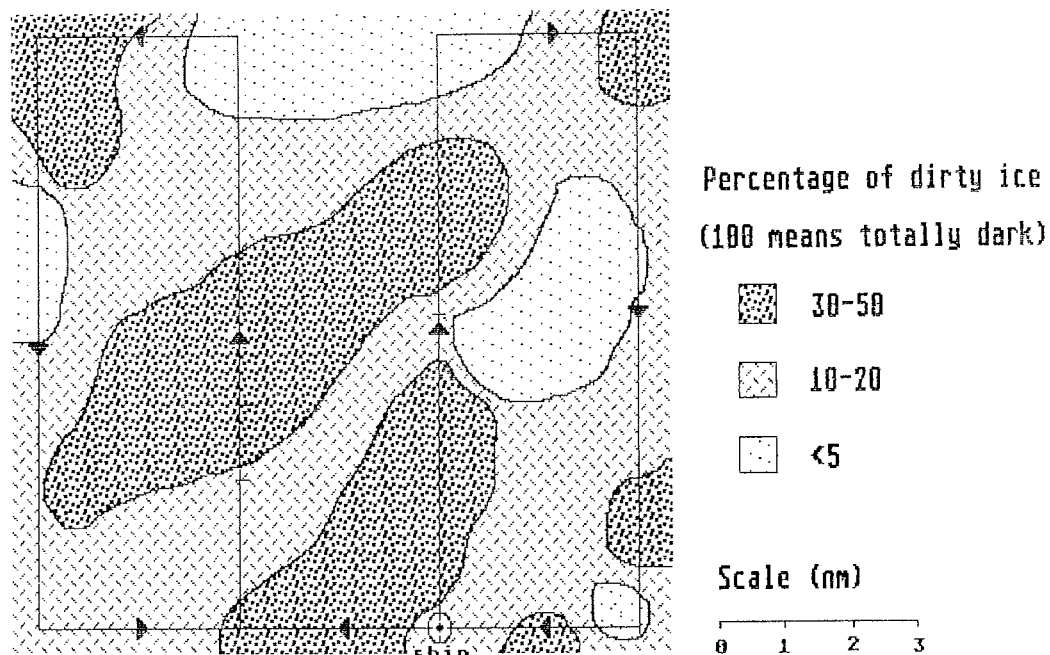


Fig.13 Example of special flight pattern used for aerial observation of the sea ice (arrows show flight directions).

cooperation with LODYC and the deployment of Argos buoys on this cruise (see Chapter 4.1);  $\delta^{18}\text{O}$  of ice cores to determine the meteoric influence with IUPH; and data exchange and discussion with chemical oceanographers from the cruise, UGö and BIO, on the chemistry and origin of surface waters.

#### Preliminary Findings

The primary result of the "dirty" ice investigation is that the sea ice in the Nansen Basin contains a considerable amount of sediment, much more than expected. Although only one transect through the Nansen Basin provides limited opportunity for areal mapping, it appears that the highest concentrations of dirty ice occur along the southern margin of the Nansen Basin from  $83^{\circ} 27'$  N to  $85^{\circ} 02'$  N and near the Nansen-Gakkel Ridge in the region of the Transpolar Drift  $85^{\circ} 40'$  N to  $86^{\circ} 10'$  N. Chemical analysis of surface waters conducted on the cruise (see Chapter 5.4) showed that in the southern region, the surface water chemistry appears to reflect sea ice meltwater input. At northern stations, the chemistry of the surface waters changed markedly with high alkalinity reflecting a river source (perhaps the Lena?) for surface waters of the Transpolar Drift stream.

Most cores obtained from dirty ice locations appeared to sample multiyear ice. Extreme material accumulation at the surface was associated with regions where surface melting was extensive, covering 15-40% of the ice surface. Although most samples were frozen for analysis on shore, a few samples were examined on board. The grain size of the sampled sediment is mainly silt and clay. As seen in smear slides the bulk of the silt fraction is quartz. The minor part consists of feldspar, carbonates, amphibolites and plagioclases. Some diatoms and benthic foraminifera have also been found.

Seven possibilities of sediment/sea-ice relationships can be distinguished:

1. a clear, white surface without sediment underneath;
2. a clear, white surface with one or more sediment layers underneath;
3. a dirty surface layer, mostly between 3 and 15 cm thick, without sediment down core;
4. a dirty surface with one or more sediment layers or patches underneath;
5. meltwater ponds, which contain sediment in small holes often 9-20 cm deep, 3-5 cm in diameter and with dirty surface surrounding the pond. Underneath, cases 3. and 4. occurred;
6. frozen, dirty meltwater ponds with an surrounding higher ring of dirty ice (they looked like "atolls");
7. ridges with surface material accumulations, mostly only on one side of the ridges and apparently associated with recent wind transport. Coring through the ridges sometimes revealed sediment layers or lenses underneath. In one case a 1 m block of ice was cut through a ridge and revealed deformed layers of material at depth.

#### Special features of surface material:

At almost all sites of dirty ice material was observed to form small aggregates. These aggregates sometimes accumulated in up to 1 cm thick black layers at the surface. In some cases round to elongate cohesive sediment accumulations, so called "mudballs", were found in holes in meltwater ponds and on the ice surface similar to those described by Nansen (1902). These mudballs were 1-3 cm in diameter and consisted mainly of clay and silt-sized mineral grains and biogenic material. Similar features were also observed in sea-floor sediment samples, both in surface sediments and accumulated in deeper layers (see Chapter 7.7).

The sea ice sometimes had a patchy, reddish appearance, which was found to be red ice algae (tentatively identified as Chlammydomonas nivalis) living on the ice surface (see below).

#### 4.3 Biogenic Material in Sea Ice (AGC/BIO, GIK)

The extent and thickness of Arctic sea ice cover are primary factors controlling the climate and ocean circulation of the northern hemisphere. Many studies have tried to interpret the history of this ice cover from analysis of ice rafted clastic material in Arctic sediment cores (e.g. Clark & Hanson 1983). Few studies, however, have attempted to relate the ice biota (i.e. cryophilic floras and faunas) to the microfossil record of these sediments. On ARK IV/3, therefore, sea ice and the overlying snow cover were systematically sampled in order to search for ice biota that may characterize different types of sea ice and leave a fossil record in the sediments. For example, diatoms, silicoflagellates and dinoflagellates have been found in sea ice of the circum-Arctic region (Horner 1985), but their in-situ occurrence has not been established for the ice over the Arctic Ocean. Studies were also made for the following purposes: 1) to estimate the annual influx of pollen and terrigenous spores to the Arctic Ocean, 2) to evaluate the importance of ice rafted debris as a source of reworked palynomorphs in Arctic Ocean sediments, and 3) to investigate the relation between cryophilic motile-stage dinoflagellates (which do not survive as fossils) and the occurrence of fossil resting-stage cyst forms in the Arctic Ocean (see sections 6.3 and 7.8 for details).

#### Sampling

A total of 53 samples were obtained from 20 stations (Fig. 11). Most of these stations were sampled in July on a transect along the 31° E meridian from the outer Barents Shelf (81° 20' N) to the northern flank of the Nansen-Gakkel Ridge (86° N). Four stations were also sampled in early August on a subparallel transect about 20-100 km west of the July line. At most sites, the samples were collected from holes drilled by auger for expendable current profiles (XCPs, Chapter 5.3.11). These holes were usually located in flat areas of clean ice about 200 m from the ship positions (Fig. 11). Routine sampling involved collection of the snow layer from an area of ca. 0.25 m<sup>2</sup>.

followed by collection of the ice chips accumulated at the surface of the 12 cm-wide auger hole after each 1 m-long drilling interval. At Stations 11/340, 358 and 384, clean snow was also sampled over a 1 m<sup>2</sup> grid in order to obtain replicate samples of 0.25 m<sup>2</sup> areas for evaluation of possible large spatial variation in pollen content as observed in circum-Arctic snowfields (Burgeois et al. 1985). Areas of snow or ice containing large amounts of visible clastic sediment were sampled by bulk collection (ca. 2 kg wet weight) of the "dirty" snow or slush ice and by scooping sediment from shallow meltwater drainage basins.

All samples were sealed in clean plastic bags and left to melt at 18° C. The meltwater volume was then measured and each sample was gravity filtered through a nylon mesh sieve. A sieve pore-size of 5 µm was used for all except the ice sediment samples for which a pore-size of 20 µm was used. The filtration was carried out in a small laboratory where periodic control samples showed that contamination by shipboard dust was insignificant but included cloth fibers, human hair and small amounts of fine to medium silt. The filtered sample was then washed with distilled water, followed by methanol. The samples were finally stored in methanol.

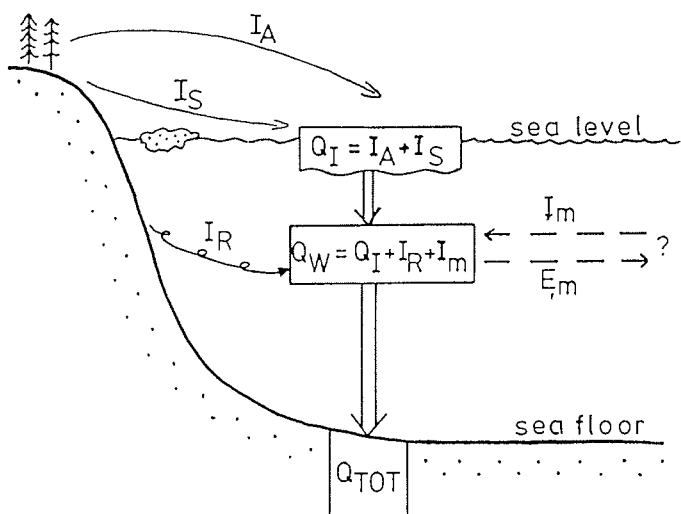
Analysis of these samples will be carried out at Bedford Institute of Oceanography and will include:

1. taxonomic studies (where necessary, in conjunction with other specialists, e.g. Lichti-Federovich and Rao for Arctic diatoms and archaeomonads, Paranjape for Tintinnids);
2. quantitative estimates (see Burgeois et al. 1985) of palynomorphs, siliceous and organic-walled biota before and after acid digestion with HCL and HF;
3. palynological analysis of the ice rafted sediment after acid digestion; and
4. in conjunction with the water sample data (see Chapter 6.3) and surface sediment data (see Chapter 7.8), the quantitative palynological data will be used in a box model study of pollen influx to Arctic Ocean sediments (Fig. 14).

#### Preliminary Findings

Qualitative shipboard studies were made of 20 subsamples from sites at the southern, central and northern parts of the transect. The salient findings are summarized below.

All ice samples contain large numbers of a small (20-30 µm) unicellular algae tentatively referred to as Archaeomonad sp., and a larger (30-50 µm) cyst form with a thin organic wall and morphology resembling that of dinocyst Cyclopsiella. These algae are also present in the surface and some subsurface samples, and they may prove to be useful guide fossils for perennial sea ice conditions. A similar Archaeomonad has recently been reported for the Canadian polar margin (Lichti-Federovich, pers. comm. 1987).



Inputs are:  $I_A$  = aerial

$I_S$  = ice rafted sediment

$I_R$  = resuspended sediment

$I_m$  = water-mass advection

Storage is:  $Q_I$  = quantity in annual snow/ice

$Q_W$  = quantity in surface water  
layer

$Q_{TOT}$  = quantity deposited on seafloor

and  $E_m$  = possible export, excluding  
residual ice

Fig.14 Box model for Arctic pollen influx study

Most of the ice samples contained a limited diatom flora dominated by Nitzschia frigida, Thalassionema nitzchioides, Chae-  
toceros sp. and/or Melosira cf. arctica. These diatoms have thin walls and, although they are present in the surface sediment, they were not found in subsurface samples, suggesting that conditions for diatom preservation are poor in the Eurasian Basin.

Very low quantities of recent pollen and spores in snow and ice samples have a boreal forest or tundra origin which is consistent with their composition in the sediment samples from the sea floor surface.

Samples of ice rafted sediment from Stations 11/370, 371 and 377 all contained abundant cylindric and pennate diatoms. A primary objective of the post cruise studies will be to try and determine whether the diatom flora is of continental or marine origin or a unique freshwater ice pond form. An unicellular organism containing bright red pigment bodies was also found. This organism is tentatively identified as Chlamydomonas nivalis which lives in snow at 0-14° C and metabolizes lipids with a bright red protein pigment. This red organism was also common in surface and subsurface sediment at these sites. The sediment samples also contained numerous wood fragments, moss leaves and moss spores which suggest a primary origin from an onshore region. No reworked (pre-Quaternary) palynomorphs were found in the ice-rafted sediments.

#### The Large Diameter Ice Core

At Station 11/371, the Arctic Environmental Drifting Buoy (AEDB) was deployed by WHOI (see Chapter 5.3.3). The bottom 7 cm were cut off of a large ice plug (diameter 84 cm, 3.69 m long) obtained during deployment. Most of the ice was melted and subsampled for organic carbon, chlorophyll A and a portion was frozen for tomographic and sedimentologic analysis on shore. The nutrient content was determined by on board:

(μmole)	Phosphate	Ammonia	Nitrate	Silica
Ice sample	0.55	14.83	1.46	<0.1
Water sample (5m depth)	0.42	<0.1	2.86	2.7

The pH value became acidic (5.3) during melting. About 10% of the material in the ice was greater than 20 μm and 90% was greater than 63 μm. In addition to fathom algae and fine mucus, two amphipods and one small polychete were found. The material were conserved with methanol/bengal red for further analysis in Kiel.

#### **4.4 Proposed Future Research**

Interest in future work on sea ice in the Nansen Basin by cruise participants appears to fall into two categories: first to examine the origin for sea ice and its material content,

requiring an expedition to the Laptev and East Siberian Seas; and secondly to understand the transition between ice and water formed on the shelves and the ice and water structure of the Transpolar Drift across the Nansen Basin.

The Siberian Shelf project should be multidisciplinary. These shelves are markedly different from the Alaskan or Barents and Kara shelves because they are broad, shallow, have large river input and ice escaping from the shelves is transported with the Transpolar Drift. In contrast, ice formed on the narrow Alaskan shelves, although it may contain a lot of sediment, either melts in place or enters the Beaufort Gyre. Ice formed in the Barents and Kara Seas has more limited export into the Nansen Basin, and appears to have less potential for material accumulation.

Investigation on the Siberian Shelf should take place in September, when the ice is forming, and in May when the ice is breaking up on the shelf and in the rivers. At this time, approximately 1/2 of the annual river discharge occurs during a 2 week period (Drewry 1986), possibly contributing large amounts of terrestrial material onto and under the ice.

Research should focus on the influence of rivers on sea ice formation, material inclusion and export to the Arctic Ocean. In particular, one aspect of interest is to compare the Lena and McKenzie Rivers which drain markedly different hinterlands and discharge into different near-shore environments. Much of the Canadian margin is composed of granitic rocks, while the Siberian margin is composed low-lying sedimentary rocks.

The second project, tracking the Transpolar Drift, also has multidisciplinary support. The main objectives are to determine: how, when, and where sea ice formed on the shelves gets into the Transpolar Drift; what currents drive the drift; how sea ice is altered and material released or incorporated along the transport path; and where and when it finally disintegrates, depositing its material load.

Some specific questions arising from the Nansen Basin transect conducted on this cruise are summarized below.

- Although buoy deployments across the Transpolar Drift have now yielded a picture of the transport direction and velocity, next to nothing is known about the absolute velocities of the ocean currents. Underwater floats could be deployed at various depths in the deep basin to understand the general circulation and its relationship to ice dynamics and thermodynamics. In addition, floats should be deployed along the continental margins to track waters moving from the shelf into the basin interior.
- The flora associated with sea ice is most abundant in dirty ice samples. Does the flora grow in response to special conditions provided by the dirty ice, e.g. nutrients, low predation? Or is the flora incorporated at the same time as the clastic material? Diatoms are found in sea ice, but are not found in sea-floor sediments of the Arctic Ocean Basins. Other fine-grained materials occurring in ice, such as organic walled spores are deposited

on the sea-floor. Is there something about the chemistry of the ice which dissolves the silica tests?

- The large amount of material observed on this cruise to be included in sea ice of the Nansen Basin must deposit when the ice finally melts. How has the material altered during the transport with the Transpolar Drift? Where and in what form will it finally reach the sea-floor? Many questions about the material flux can be addressed through time series sediment traps. Sediment traps could be either deployed on the ice floe as was done on this cruise, but in dirty ice locations, deployed along the basin margins or deployed under the polar ice pack.

## 5. THE OCEANOGRAPHY PROGRAM: A SECTION ACROSS THE NANSEN BASIN

### 5.1 Introduction

The Arctic Ocean is unusual compared to other oceans in several respects. Most obvious is the extensive year round ice cover over much of its surface. This tends to inhibit heat exchange with the atmosphere and mixing by winds and, together with considerable freshwater runoff, results in a shallow mixed layer. Thus, the Arctic Ocean is a comparably low energy regime, with a stratified, stable surface region characterized by a pronounced halocline. Underneath the halocline is the Atlantic layer, water of Atlantic origin that is thought to have been cooled by the surface layer. Under the Atlantic layer is cold water whose exact origin is not yet well determined, but which is generally thought to have a major component of Norwegian Sea Deep Water. While a limited amount of information is available for some of the Arctic Ocean basins, there have been essentially no modern measurements made in the Nansen Basin. ARK IV/3 offered the opportunity for obtaining the first extensive set of measurements in the Nansen Basin and the first ever oceanographic section in the central Arctic Ocean.

Oceanographic data for this area were obtained only from icecamps near the periphery and from air-borne surveys with CTD - casts to depths of about 1500 m. These data are augmented by few but high quality chemical data. The present perception of the internal circulation of the Nansen Basin, how it is tied into the general circulation of the Arctic Ocean and its role in the formation of the intermediate and deep water masses is based on very sparse and often inadequate data. Thus an attempt to penetrate into the basin and possibly reach its northern limit with a well equipped research vessel warranted careful preparation to make optimal use of this opportunity.

Earlier work strongly suggests that the Arctic Ocean halocline is maintained by the flow of cold, relatively saline water from the continental shelves produced as a result of brine rejection during the formation of sea ice (Aagaard et al. 1981; Mellings & Lewis 1982). More recent work proposed in addition that the upper halocline water in the Canada Basin, which has a pronounced nutrient maximum, was formed from water enriched in nutrients from the Chukchi and East Siberian Seas, whereas the lower halocline water was formed from water of Atlantic origin considerably modified in the Barents Sea before flowing out into the main Arctic Ocean basins (Jones & Anderson 1986). This lower halocline water differs from the upper halocline water by its lower nutrient concentrations and slightly higher salinity. It can also be clearly identified by the parameter "NO" (Jones & Anderson 1986), a conservative water mass tracer defined from the nitrate and oxygen concentrations in the water. A goal of this cruise therefore was to measure the water mass characteristics near the surface in Nansen Basin close to where the lower

halocline water is believed to have obtained its characteristics to check the hypothesis regarding the area of origin of the lower halocline water.

The Atlantic layer underlies the halocline water at depths roughly between 300m and 600m. It is formed from North Atlantic Water that enters the Arctic Ocean through Fram Strait where at its core, the salinity is over 34.9 and the temperature is near 3.5°C. In the central Arctic Ocean the salinity is lower and the temperature at the core of the Atlantic layer has been reduced to about 0.5°C. Much of this cooling likely occurs within the Nansen Basin (Coachman & Barnes 1962). Our measurements should help to show whether the cooling is a result of a vertical heat flux into the cold halocline from the Atlantic layer or whether other processes might be involved. These will be studied by both the more conventional approaches using salinity and temperature measurements as well as by looking at changes in chemical parameters.

The deep water of the Arctic Ocean is formed in part from Norwegian Sea Deep Water that has entered through Fram Strait. What other water masses contribute to it is not yet very clear. Norwegian Sea Deep Water itself has a component of outflowing Arctic Ocean Deep Water that has mixed with Greenland Sea Deep Water before flowing into the Norwegian Sea (Koltermann 1987, Swift & Koltermann 1987). A probable significant contributor to the Arctic Ocean Deep Water is some of the same type of dense, cold shelf water that is involved in maintaining the halocline. This water would flow from the shelves down the slopes of the Nansen Basin, cooling and adding salt to the inflowing deep water. Previous studies have been almost entirely confined to the periphery of Nansen Basin just north of Fram Strait, so that the nature of the deep water could be inferred only from samples that might have contained mostly Amundsen Basin water or a mixture of deep water from the Amundsen and Nansen Basins.

The oceanography programme was designed to determine the surface-to-bottom distributions of the physical and chemical characteristics of Nansen Basin waters and the variation of these characteristics at each level both within and away from boundary regions, thus determining the physical and chemical structure across the Barents shelf, slope and in the deep Nansen Basin. It was hoped that the measurements would identify principal boundary currents and determine their structure. No reference-quality data of similar scope and completeness existed from this domain prior to this expedition, and so this cruise extended existing Greenland, Iceland, and Norwegian Sea, Fram Strait, and limited Arctic Ocean ice camp data north and east, thus enabling improved estimates of the characteristics, origin, and circulation of the various water masses. Recent studies of high latitude basins have revealed the existence of deep, narrow boundary currents as an important and effective means of advectively transporting water of very specific characteristics over long distances (Koltermann 1985, 1987). For these reasons a well defined boundary current at mid-depth, that is at the appropriate density level, is expected to be

responsible for transporting deep water from south of Fram Strait into the Arctic Ocean (Aagaard et al. 1985). This implies for the deep circulation of the Arctic basins that deep boundary currents follow the rim of the basins, fed by water coming over or through the separating ridges. By diffusive mixing and isopycnal spreading these water masses are transported into the basin interior.

Other specific problems to be addressed on ARK IV/3 are related to the origin of the water of the lower halocline, the evolution of the water of Atlantic origin as it flows through the Arctic Ocean, and the characterization of the deep Arctic Ocean water, particularly with respect to the residence time of the deep water and the transport of some anthropogenic materials to it. A general question related to these is by what processes and at what rate does ventilation of the Arctic Ocean occur?

The total carbonate and total alkalinity in the surface layer in regions of the Arctic Ocean have been related to river input from Siberian rivers (Jones & Anderson 1986; Anderson & Dyrssen 1981). Measurements of these quantities should be useful in tracing the paths of this river input in the Nansen Basin and thereby trace the near-surface currents from their source off the Siberian shelves.

The questions regarding the ventilation of the Arctic Ocean focus on circulation patterns, mixing, and mixing rates at all depths. Several tracers in addition to salinity and temperature can be employed to address these questions. Particularly revealing for the halocline and Atlantic layer have been measurements of nutrients, total carbonate, alkalinity and oxygen. These have been used to distinguish clearly between the upper and lower halocline water in the Canada Basin (Jones & Anderson 1986) and to show as well that there must be some intrusion of brine-enriched shelf water intruding directly into the Atlantic layer (Anderson et al. 1987). The age and rate of formation of water masses can be determined from models that employ transient tracers. Particularly useful in the Arctic Ocean are chlorofluoromethanes (CFM, Freons F-11, F-12), in large part because of the large range of concentrations found there gives a high signal-to-noise ratio. Chlorofluoromethane measurements made in the central Arctic Ocean (Canada Basin) have been used to discern structure and to constrain models for mixing and residence times within the halocline and Atlantic layer (Wallace & Moore 1985; Wallace et al. 1987). The deep water contained little or no chlorofluoromethane, indicating the residence time to be long. This was confirmed by carbon-14 measurements (Östlund et al. 1987). Chlorofluoromethane measurements made during ARK II/3 indicated water thought to be from the Nansen Basin to be much younger (Smethie et al. 1987). Because these data were obtained on the periphery of the Nansen Basin, they may not represent conditions more typical of the major portion of the basin. Results from the deep basin were needed to clarify the significance of the earlier measurements.

One of the main reasons why the ventilation of the Arctic Ocean needs to be investigated is related to the build-up of fossil fuel carbon dioxide in the atmosphere. A recent assessment of the role of the Arctic Ocean in the global carbon budget concluded that although the Arctic Ocean was relatively active in the short term storage of carbon dioxide from the atmosphere, little of this carbon dioxide is transported to the deep water where it would have to go if the Arctic Ocean were to be a significant sink for atmospheric carbon dioxide in the context of the global climate (Anderson et al. 1987). In this assessment, no account could be made of the possible role played by the Nansen Basin because no data were available. Data from this region are clearly desirable. Measurements of total carbonate provide the information required to address this question. These measurements might also be used in an inverse way. The fossil fuel carbon dioxide component of the total carbonate can be used together with nutrient and oxygen measurements as a transient tracer to help assign ages to water masses. Such determinations will be useful as an adjunct to chlorofluoromethane and halocarbon measurements as well as to the radionuclide measurements being made by other groups during ARK IV/3.

ARK IV/3 is the first oceanographic cruise on which an extensive suite of anthropogenic and natural halocarbons has been measured. In addition to chlorofluoromethanes, analyses have been performed for carbon tetrachloride, methyl chloroform, perchlorethylene, and bromoform. The simultaneous measurement of these compounds in the Nansen Basin allows the assessment of several important questions concerning transient tracers and environmental chemistry pollution studies. First, the various anthropogenic compounds each have a different input function describing their history in oceanic surface waters. For example, carbon tetrachloride has been released into the environment by man for a considerably longer period than the chlorofluoromethanes. Currently, however, it has a slower rate of increase in the atmosphere (and hence in surface waters) than the chlorofluoromethanes. The different input functions should provide additional constraints for models of water mass ventilation. Second, there is some uncertainty about whether there are any natural sources for carbon tetrachloride, i.e., whether any background concentrations existed during the pre-industrial era. Correlation of chlorofluoromethanes with carbon tetrachloride, especially in deepwaters with low or zero chlorofluoromethane concentrations should allow useful limits to be placed on pre-industrial concentrations of carbon tetrachloride. Third, correlation of the depth of penetration of the carbon tetrachloride, methyl chloroform and chlorofluoromethane signals will allow assessment of the importance of the oceans as a sink for atmospheric carbon tetrachloride and methyl chloroform. Fourth, bromoform, being the only biogenic halocarbon determined during this cruise, has a different input function compared to the anthropogenic compounds. It is mainly formed in belts of certain algae, e.g., Asparagopsis taxiformis (Burreson et al. 1975) close to the surface, and will therefore provide additional information regarding the near surface structure of the ocean.

During the past decades measurements of natural and anthropogenic tracers have developed into an important tool in studies of deep water formation and circulation. Having specific time-dependent histories of the input to the ocean and characteristic sources and sinks in the ocean, tracer measurements can give information on the direction and the velocity of water movement and mixing processes even in cases where this information cannot be derived from the temperature and salinity fields. Additionally, tracer measurements can be used in studies of ocean/atmosphere exchange and water/ice interaction.

In the system Greenland Sea, Norwegian Sea and Eurasian Basin which is the source of the North Atlantic Deep Water, tracer studies so far have been concentrated on the Greenland/Norwegian Seas while from the Eurasian Basin only few tracer data have been obtained on stations located at the southern end of the basin. The main focus of the first tracer studies has been the determination of the deep water renewal of the Greenland/Norwegian Seas using  $H$ ,  $^{14}C$ , and chlorofluoromethanes as tracers. In these studies the ultimate source of the Greenland Sea Deep Water (GSDW) and the Norwegian Sea Deep Water (NSDW) has been assumed to be the Greenland Sea surface layer (Peterson & Rooth 1976; Bullister & Weiss 1983) or a mixture of surface and intermediate waters within the Greenland Sea (Schlosser 1985). Recent hydrographic surveys revealed a second different source water mass for NSDW. Salinity data give evidence for the production of deep water in the Arctic Ocean which flows southward through Fram Strait and mixes along the Greenland continental slope with GSDW to form new NSDW (Koltermann 1985; Aagaard et al. 1985). The exchange of deep waters through Fram Strait has been taken into account by Smethie et al. (1986, 1987) and Heinze et al. (1987) who coupled the Eurasian Basin to the Greenland/Norwegian Seas in tracer data evaluations on the basis of time dependent box models. A critical point in these studies, however, is the fact that all stations available from the Eurasian Basin are located at the southern boundary which might not be representative for the deep water of the central basin. The samples collected during ARK IV/3 should be very helpful in improving the estimates of the deep water renewal rates of the Greenland/Norwegian Seas and the Eurasian Basin.

From the few tracer data available from the Eurasian Basin it is evident that isotope measurements can contribute considerably to the understanding of the oceanography of this region. As shown by Östlund et al. (1982) and Schlosser (1985)  $H/He$  measurements can be used to estimate the mean residence times of the halocline waters.  $^{14}C$ -data are of particular interest in studies of the bottom water which shows  $H$  concentrations close to or below the detection limit (Östlund et al. 1982). Additionally,  $^{14}C$  measurements can be used to estimate the uptake of anthropogenic  $CO_2$  in the Eurasian Basin.  $O$  is a sensitive tracer for shelf water contributions to the deep water of the Arctic Ocean as has been shown by Östlund et al. (1987). The samples now available

therefore should help to develop a more detailed picture of the mixing processes and circulation in the Eurasian Basin.

Radionuclides with different half-lives, source functions (transient vs. steady state) and reactivities can be used to resolve vertical and horizontal transport processes in the Arctic Ocean. We intend to measure the water column distribution of the Th, Am, Pu, Ra, Cs and Sr isotopes to address questions of partitioning of tracers between particles and solution and the effects of advective transport on the profiles. This work builds in part upon previous studies which have used the radionuclides released from nuclear fuel reprocessing at Sellafield, U.K. (<sup>137</sup>Cs and Sr) to study ventilation and circulation processes in the Arctic (Livingston 1987).

A comparison of the radionuclide distribution between the central Nansen Basin (Station 11/358) and the basin margin (Station 11/287) and the Nansen-Gakkel Ridge (Station 11/370) will reveal effects of horizontal transport and scavenging near the ocean boundaries. Data from the more soluble Cs and Sr isotopes will be used, along with the CTD and other tracer data collected on this cruise, to better understand water mass circulation processes in the Nansen basin. Our data will be compared to a similar study in the Northwest Atlantic Basin (Cochran et al. 1987) to reveal differences in the Arctic particle scavenging regime due to quantitative and qualitative differences in the suspended and sinking particulate matter beneath the ice.

Many trace elements are transported to the Arctic Ocean by precipitation and by airborne particles. They include anthropogenic metals such as lead as well as many others which enter the atmosphere through normal terrigenous erosion. These elements typically accumulate on the ice during the winter season. During the summer when the ice starts to melt they are released into the surface water of the ocean. As almost all of the lead in the oceans is of anthropogenic origin, it is a possible inorganic tracer that may complement the organic tracers such as the chlorofluoromethanes. Unlike chlorofluoromethanes, however, trace elements in general are highly reactive, some forming insoluble inorganic complexes and others becoming incorporated into biota. The particles formed by either of these processes sink into deeper water where they might redissolve or become part of the sediment, depending on their individual nature.

Trace element distributions in the Arctic Ocean are almost completely unknown. The distributions of bioactive trace elements such as cadmium and zinc in the Pacific Ocean show a large accumulation in the deep water. Elements such as iron show the opposite behaviour, with depleted values in the deep water. In the Pacific, the deep water likely differs from that in the Arctic Ocean in ways which may affect trace element distributions, the Pacific water being older, for example. One goal of this work is to compare distributions of trace metals in the Arctic Ocean to those in other oceans to try to sort out the processes controlling the trace element distributions.

Knowledge about the distribution of water masses is important for the understanding of Arctic oceanic dynamics as well as of air-sea-ice interactions (heat - momentum - buoyancy) in this area. Knowledge about the general oceanic circulation is also an important prerequisite in this respect and, in particular, for the very active and complex area north of Svalbard. Direct monitoring of the circulation of:

1. surface polar waters transporting ice out of the Arctic through the Fram Strait,
2. Atlantic waters bringing heat and salt to the Nansen Basin, and
3. deep layers which ventilate the interior,

is an absolute necessity.

For this reason, during MIZEX 84, we investigated the surface and subsurface circulation in Fram Strait using a lagrangian current monitoring method. Why such a choice? Direct monitoring of the general ocean circulation in the Arctic is a challenging undertaking. Indeed, most of the actual operational methods used up to now for open ocean circulation studies as well as for the Arctic Ocean are mostly indirect methods, and most of them give only partial answers to the basic problem. Geostrophic current calculations from water mass density distributions can only resolve the vertical shear of the horizontal currents in the absence of an objective absolute velocity reference surface. Tracer studies integrate many processes including isopycnal and diapycnal mixing, and mesoscale and large scale dynamics. Still a critical point remains, that is to estimate the pseudo-lagrangian behavior of each tracer; unfortunately, this is not an easy task. These are wellknown problems in physical oceanography. Indeed, a real opportunity in the near future to make progress on the subject, will be remote sensing monitoring of the sea surface topography by subdecimetric satellite altimetry in addition to an increased effort in eulerian and lagrangian in situ current observations. However, of these technologies, only lagrangian methods are applicable to the Arctic.

The circulation pattern in the Nansen Basin, though it is not well known, defines to a large degree the sedimentary environment. The present-day distribution of suspended particulate material (SPM) gives a snapshot view of sources and dynamics of particle flux. Elevated levels of SPM generally occur in surface waters as a result of biological production but much of the material is recycled and does not settle to the sea floor. Bottom current activity along the basin boundaries may erode, resuspend and transport bottom sediments and can be observed as regions of high near-bottom SPM. The fine-grained component of sediments in suspension forms a background which settles very slowly (McCave 1975). This background level can be used as a tracer for water masses and is observed to be advected along isopycnal surfaces

(e.g. Brewer et al. 1976) and to mix by diffusion into the basin interior. Understanding of the processes controlling particle flux provides a bridge between oceanographical and geological investigations.

## 5.2 Scientific Goals and Objectives

The main objectives of the oceanography programme for this cruise are to:

- describe the main features of the halocline, intermediate and deep circulation of the Nansen Basin using classical hydrographic arguments supported by transient and natural tracers,
- try to understand the role of the Nansen Basin in its relation to the Barents Sea and its shelf to the south and the Amundsen Basin to the north
- try to describe the fate of the surface, intermediate and deep waters that come north through Fram Strait or the origin or source of surface, intermediate and deep waters of the Arctic Ocean that move south towards Fram Strait,
- support existing data and ideas that explain the formation and spreading of upper and lower halocline waters in the Arctic Ocean.
- to understand the effect of circulation patterns in the Nansen Basin on the present sedimentary environment,
- to measure concentrations and to establish pathways for several anthropogenic materials.

To meet these objectives, a sampling programme was drawn up that, (Fig. 15,16) meeting the quality standards set for such a programme, could be accommodated on the vessel in terms of logistical and personnel constraints. Groups were approached that could contribute to these objectives under above requirements and constraints. The field party of the cruise ARK IV/3 was gathered to:

- collect a high quality temperature, salinity, nutrients and tracer data set at a great number of levels and possibly adequate horizontal spacing across the Nansen Basin,
- complement the small-volume sampling with large-volume sampling for tracers deemed necessary to understand the large-scale or time-dependent processes of the basin,
- augment this data set with temperature and velocity information of the surface layer and lagrangian information of the large and meso-scale motion of the ice cover and the underlying current system.

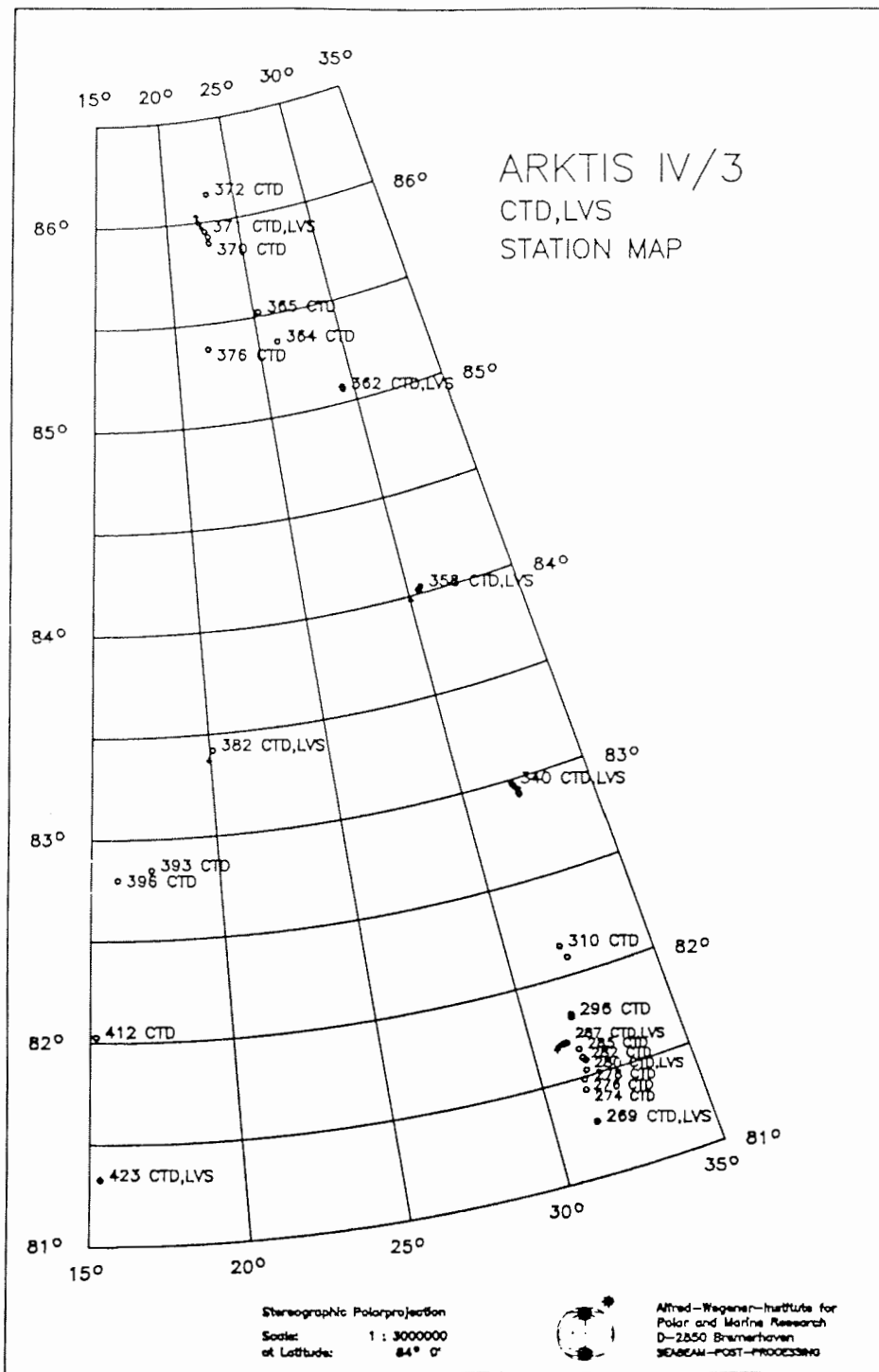


Fig.15 Map of station locations of CTD and LVS casts obtained on ARK IV/3. For station locations see Krause et al. (in press),

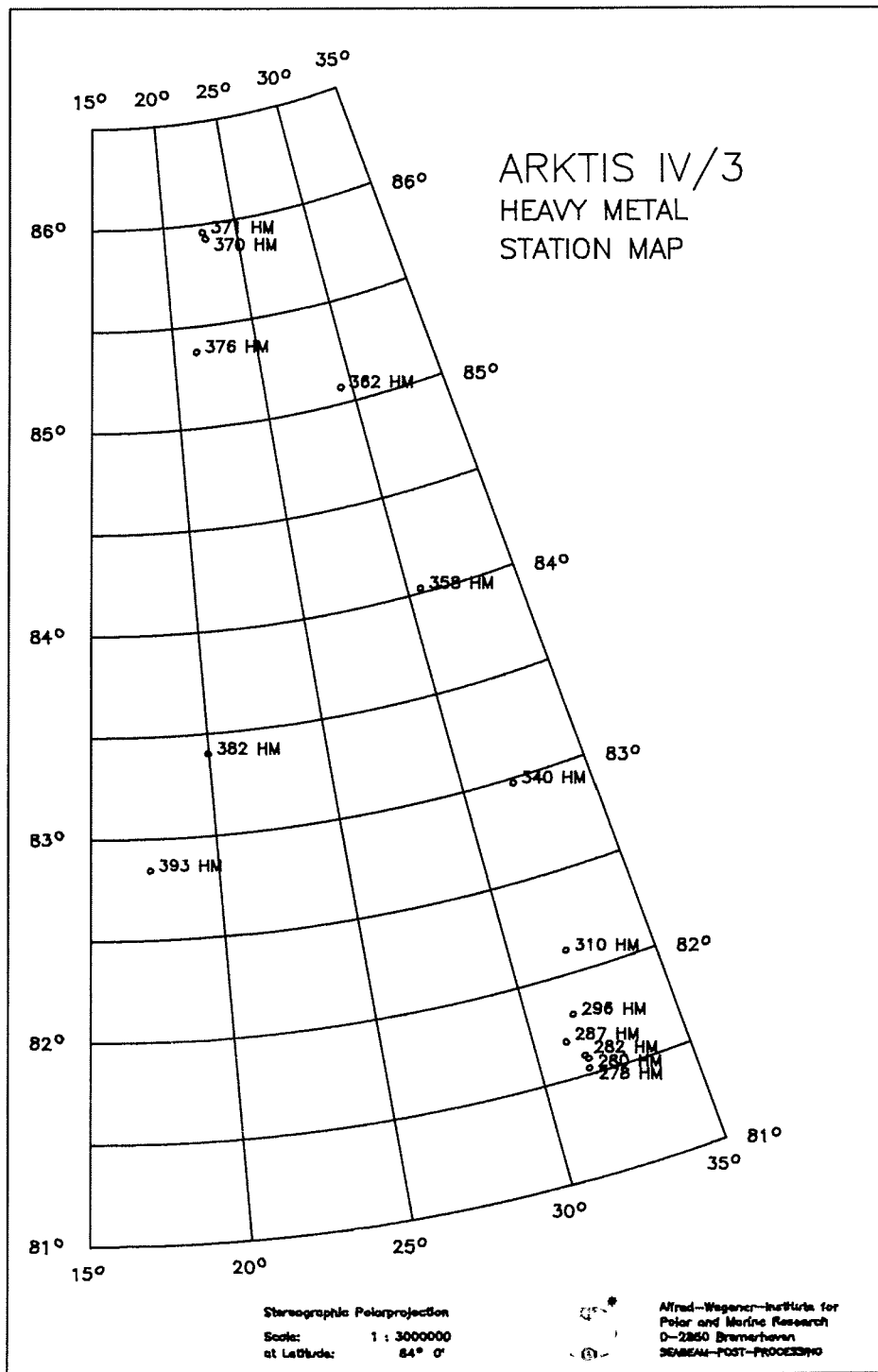


Fig.16 Map of station locations of heavy metal sampling casts obtained on ARK IV/3. For station locations see Krause et al. (in press).

The subsequent report details on the sampling programme, summarizing the group activities. At the end a first assessment of the data already available and some first synthesis are presented. This is concluded by an outlook on other scientific questions in the oceanography of the Arctic Basins that can be tackled with considerable hope for success using an adequately equipped research vessel and experience gained from this cruise.

### 5.3 Sampling Groups

#### 5.3.1 CTD, Continuous Profiling of Conductivity, Temperature, Pressure and Transmissivity (DHI)

During the ARK IV/3 leg of POLARSTERN 35 CTD casts on 25 stations (Fig. 15), mostly full depth, were carried out in the Nansen Basin. No instrument problems occurred. For calibration purposes more than 625 salinity data points from bottle samples are available. The CTD unit had, prior to the cruise, been calibrated in p,T,C at SIO/PACODF. The CTD was matched with a WHOI-transmissometer and a 24 x 10 l rosette from SIO without problems. Accuracy and precision of the instrument are as stated by the manufacturer, taking utmost care and providing calibration points for all parameters. The precision is taken to be 0.002 °C for temperature, 1 dbar for p and 0.002 PSS78 in calculated salinity.

The data will be processed, using profile by profile calibration to ensure a high quality. The averaged 1-dbar- data will be used to calculate the geostrophic flow across the section. Using nutrient and tracer data as additional constraints, inverse methods will be employed to derive the total baroclinic/barotropic transports across the Nansen Basin section.

#### 5.3.2 Transmissometer and Suspended Sediments (GIK, WHOI)

The scientific program for analysis of suspended particulate material (SPM) consists of four components: 1) determination of the distribution and composition of SPM, 2) correlation with water mass and circulation information in cooperation with DHI and SIO in order to identify possible sources and transport paths for SPM, 3) comparison with particle flux information determined from sediment traps deployed previously in the Norwegian-Greenland Sea (Honjo et al. 1987) and the sediment trap deployed under the ice on this cruise (see Chapter 5.3.3), and 4) comparison with sea-floor characteristics and paleoceanographic analysis of the sedimentary record to assess variability of the modern pattern through geologic time.

On all CTD casts a profiling transmissometer attached to the DHI CTD provided continuous output of beam transmission with depth. The transmissometer is manufactured by Sea Tech, Inc., has a 25 cm path length and the light source is a collimated light emitting diode with a beam diameter of 15 mm. The wavelength is 660 NM, designed to eliminate attenuation due to dissolved humic acids and therefore light attenuation is primarily caused by

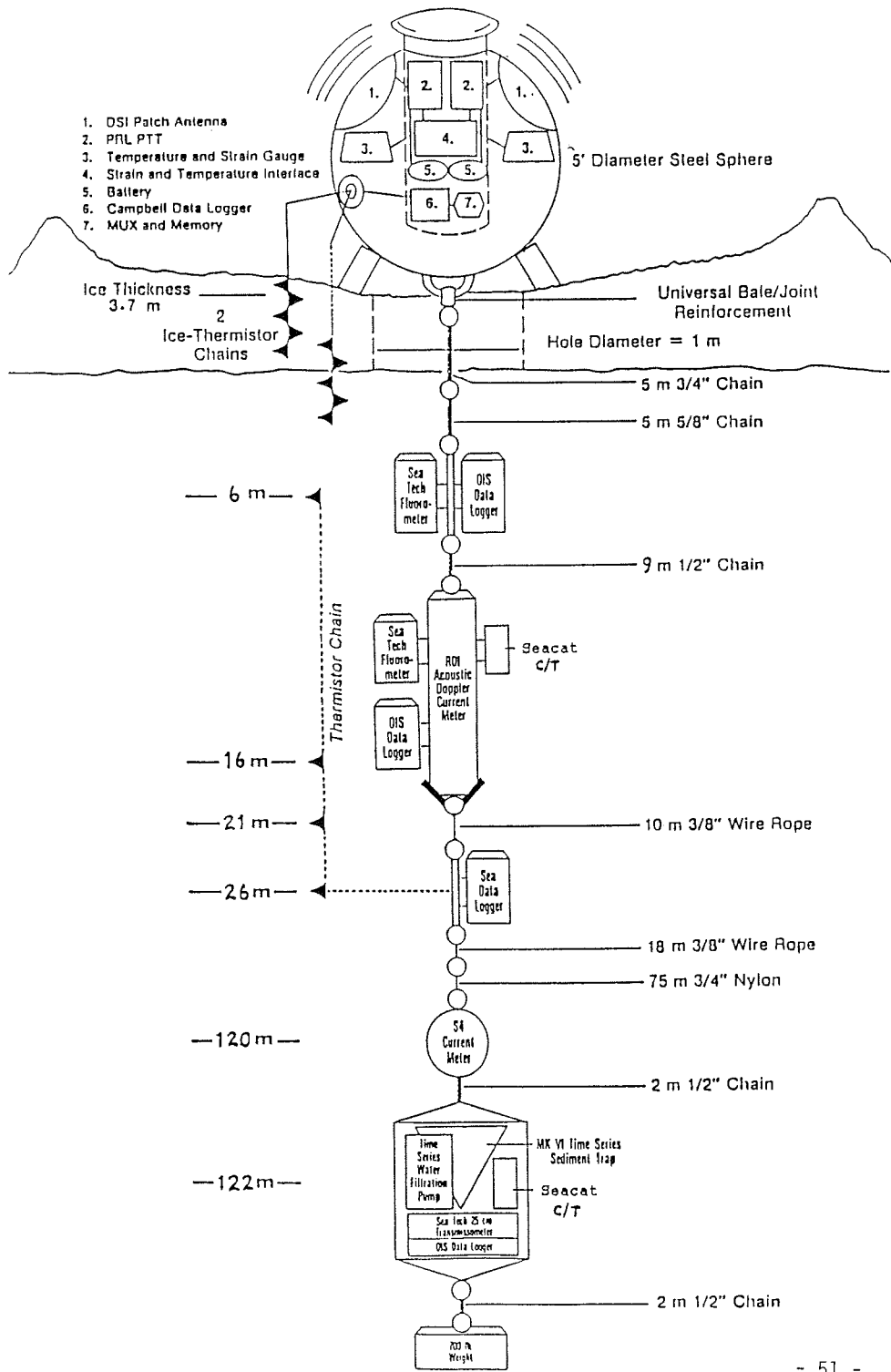
particles in suspension (Bartz et al. 1978). Based on the transmissometer profile and hydrographic analysis provided by DHI, SIO, BIO and UGÖ, water samples from the SIO rosette were selected and obtained at 4 to 10 depths per station. In total, samples were obtained from 183 water depths. These samples were then filtered on preweighed 0.45 um Nucleopore filters.

Future work will focus on analysis of the SPM samples to determine composition and concentration, and correlation of these results with the transmissometer profiles obtained on this cruise and previous profiles in the Norwegian-Greenland Sea. Data will be exchanged and discussed with other investigators from the cruise in order to understand the relationship of modern SPM distribution with the oceanographic and geologic regime.

### 5.3.3 Arctic Environmental Drifting Buoy (WHOI)

The primary objective of the Arctic Environmental Drifting Buoy (AEDB, Fig. 17) is to measure particle fluxes under the Arctic sea ice over a period of time along a drift path. The secondary purpose is to gather essential and associated data to understand the vertical and advective sediment transport mechanisms in the Arctic Ocean and Greenland Sea by deploying a set of telemetered and self recording instruments. It is expected(Fig. 18) that this instrument package will be transported by the sea ice out of the eastern Arctic Basin, through Fram Strait, and along the east coast of Greenland over a track of approximately 2000 km. Between March and May of 1988, the system should reach open waters north of Iceland, where a prompt recovery is planned with the RV Bjarni Saemundsson. The AEDB consists of several components and instrument packages. A 5-foot diameter foam-filled steel sphere supports the mooring on the ice and while it floats in the sea. It contains a positioning system that transmits positions via the ARGOS satellite system to Woods Hole. Attached to the AEDB is a taut-line fed through the ice on which are mounted several instrument packages. Except for positions and some engineering information regarding the sphere, all information gathered is stored in the instrument packages to be read upon retrieval. Two high-sensitivity fluorometers with data storage modules will provide information on the variability of phytoplankton pigments under and near the sea ice and should provide a key to understanding the productivity of polar and high latitude ocean environments. The shallower fluorometer is mounted at 10 m below the sphere, or approximately 6 m below the bottom of the ice floe. The second is mounted 16 m below the ice where a chlorophyll maximum is usually observed. This boundary will change in time as the buoy drifts. Several thermistors are mounted along the mooring line to monitor the relative position of this boundary. An Acoustic Doppler Current Profiler (ADCP) is mounted alongside the lower fluorometer together with a conductivity-temperature recorder. These will monitor the sub-ice horizontal velocity field as a function of depth and horizontal position as the AEDB drifts south.

WII01/ONR Arctic Environmental  
Drifting Buoy



- 51 -

Fig.17 Schematics of the Arctic Ocean Environmental Buoy (AEDB).

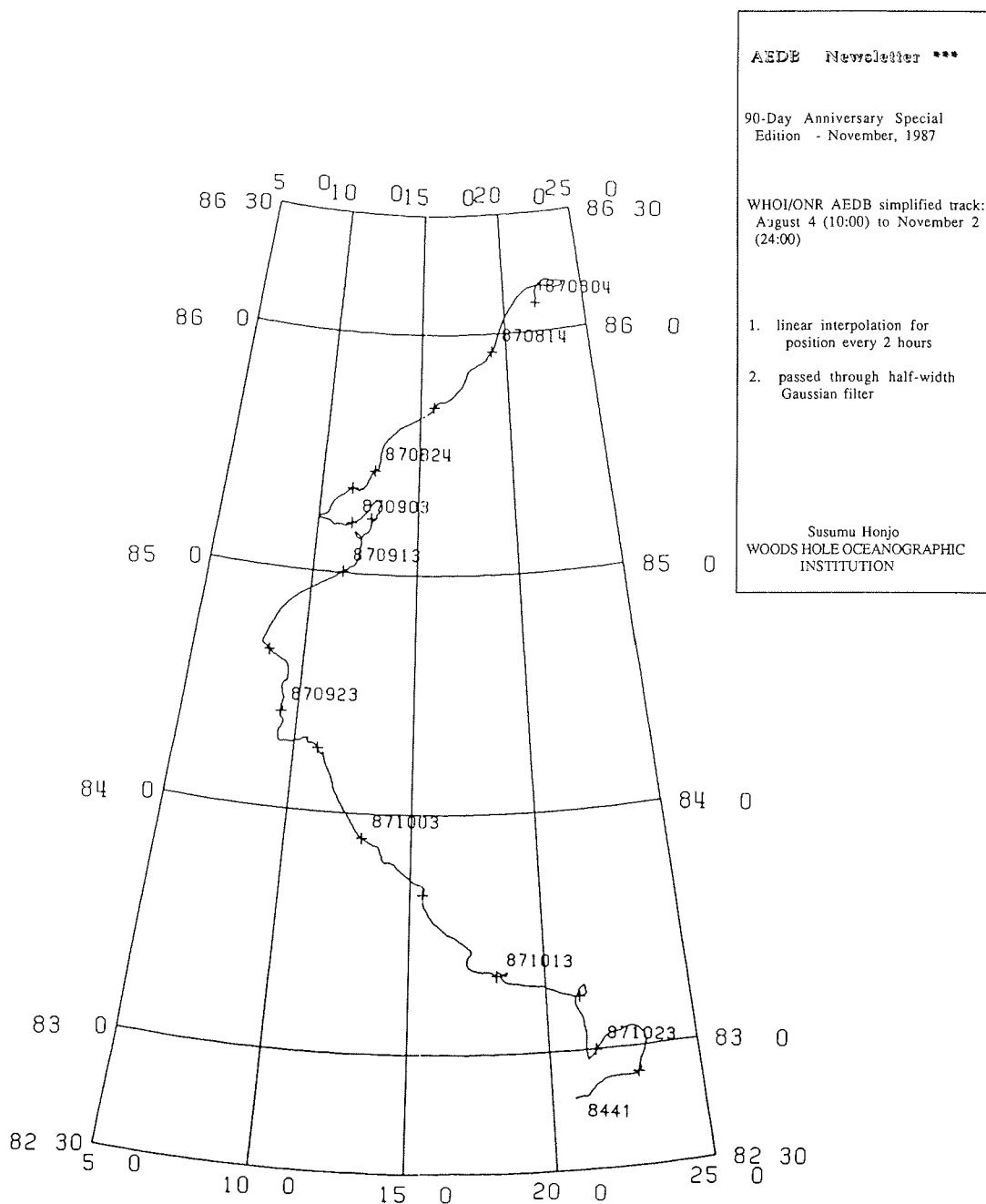


Fig.18 Drift of AEDB during the first 3 months after deployment.

The primary purpose of the AEDB is served by a sediment trap package suspended 129 m below the bottom of the ice. This package consists of a time series oceanic sediment trap, a time series micro-filter pump, and a precision light transmissometer, all designed to provide comprehensive particle data along the track of the buoy. A second conductivity-temperature recorder is mounted inside the sediment trap frame. With an hourly sampling interval synchronous with the shallower conductivity-temperature recorder, a two-point salinity curve may be obtained. The freshening effects of the sea ice on seawater may then be monitored.

For deployment, a site was chosen to protect the buoy as well as possible from the effects of shearing and ridging. The buoy was positioned on a large multi-year ice floe in 3.7 m thick ice. Surrounding the site, the ice was found to be greater than 6 m thick. On three sides large ridges already had been formed, attesting to the strength of the ice floe. The buoy rests on four wooden posts to prevent it from absorbing heat and melting through the ice. A heavy 3/4 inch chain attached the sphere to the rest of the mooring line. This chain will freeze into the ice. The system should then be locked into the ice floe and drift southward without the shifting dynamics encountered in the open ocean until it leaves the ice in about 7 to 10 months. Results of the AEDB rely on retrieving the buoy when it floats out of the sea ice, as all the pertinent oceanographic data are internally recorded or collected in the individual instruments. During the 7 to 10 months that the buoy travels through the Arctic, only positions and physical effects on the sphere may be monitored. Future projects in the field may include telemetering of more of the data during the track of the buoy, however results from this project need to be analyzed before detailed plans can be made.

#### 5.3.4 Small-Volume Sampling

##### 5.3.4.1 Nutrients, Salinity and Oxygen (SIO, BIO)

Special attention was given to the hydrographic measurements (temperature, salinity, oxygen, and nutrients) partly because the interpretation of other data, such as those from geochemical tracer measurements, is enhanced when combined with this background information. This is especially true for the parameters which need to be related to density, and to make comparisons with other regions. Density is closely tied to salinity at the extremely cold temperatures typical of the Nansen Basin domain. A rosette water sampler with a capacity of  $24 \times 10\text{ l}$  Niskin type sample bottles was used for water sampling (Fig. 15). The rosette was mated without problems with a conductivity/temperature/pressure (CTD) probe by Neil Brown Instrument Systems (NBIS). Essentially all small-volume sampling was done from the rosette sampler. The 10-liter sample bottles were thus heavily utilized, and many of the bottles were fully drained. A blank sample log sheet (Fig. 19) shows the typical order and sample-plus-rinse water volumes required.

Fig.19 Rosette sample log sheet used on ARK IV/3, displaying sample order.

Arktis IV/3 Rosette Sample Log Sheet		Date	Station	Cast	Page
		Oxygen Box No.	Salt Box No.	Nutrients Box	
NISKIN	1 2 3 4 5 6 7 8 9 10 11 12 13 14 15 16 17 18 19 20 21 22 23 24				REMARKS
DEPTH					
BIO NUMBER					
FREON	0.6				
HALOCARBON	0.5				
BIO OXYGEN	0.4				
SIO OXYGEN	0.4				
HELIUM	1.5				
TCO <sub>2</sub> /ALK	0.6/0.6				
NUTRIENT	0.1				
SALINITY	0.6				
CALCIUM	0.1				
TRITIUM	1.1				
AMS C-14	1.4				
BIOLOGY	0.1/0.2/all				
SEDIMENTS	all				
REMARKS					

Three or four racks of deep-sea reversing thermometers - two protected and one unprotected thermometers - were mounted on the rosette bottles. For all Nansen Basin work the protected thermometers were special low range (-2 to +2° C) instruments. Thermometric temperatures were used to check the CTD platinum resistance thermometer temperatures and pressure sensor, and to monitor rosette tripping sequence. Rosette bottles were closed on up casts by the CTD operator, at depths chosen after consideration of the down cast profiles. Samples were collected in the order shown in Fig. 19 from each rosette bottle. Salinity samples were usually collected in 250 ml aged citrate bottles. Salinity samples from large-volume and heavy-metal casts, from rosette casts as duplicates for salinometer comparisons were collected in 200 ml glass bottles. Salinities were analyzed on a Guildline Autosal four-electrode salinometer. Replicate salinities on several casts were run on an AGE Mini-sal salinometer as part of an instrument comparison test. All Autosal samples were run at sea, after equilibrating to laboratory temperature, but within approximately 48 hours. All salinities were standardized against Wormley P105 standard seawater, with fresh vials opened before and after the analyses for each cast. The standard deviation of Autosal laboratory measurements of standard seawater is about 0.0004 Practical Salinity Units (PSU). Examination of the deep salinity values from ARK IV/3 suggests that the salinities are usable to about 0.002 PSU. Dissolved oxygen was determined using titration following the Winkler method as modified by Carpenter (1965) (equipment and procedure outlined by Anderson (1971)). Examination of the deep oxygen profiles across the Nansen Basin section reveals subtle features in dissolved oxygen consistent from station to station, with extrema as small as 0.02 or 0.03 ml/l different than adjacent layers, indicating a precision possibly somewhat smaller than this value. Despite this internal consistency, comparison with dissolved oxygen data from the same rosette bottles carried out during ARK IV/3 by SIO and BIO showed that one or two of the least well resolved features are open to question, and the group-to-group oxygen differences suggest absolute accuracies are not quite as good as the single-set, intra-cruise precision. Silicate, phosphate, nitrate, and nitrite were determined using a Technicon autoanalyzer, with the output read from pen recorders. The procedures used were basically those described by Atlas et al. (1971). All samples were refrigerated after collection and run within one day. The instrument was located in an amid-ship chemical analysis laboratory with no doors or surfaces to the outside. There were very few problems with the analyses, although on certain casts, or portions of casts, nitrate and phosphate showed higher values than at similar levels at adjacent stations. In some instances, these nitrate-phosphate 'highs' persisted slightly from one station to the next. We have no ready explanation for these features.

Hydrographic data were collected from 35 rosette casts at 25 stations. In all but 2 cases, at least one of the casts at each station was deployed to within approximately 10 meters of the

bottom. At many stations, approximately six levels were sampled with two rosette bottles in order to obtain a full 10-liter water sample for suspended sediment studies. The resulting typical 42 hydrographic sampling levels for the deep basin stations allowed 150-200 meter spacing in the deep water together with high-resolution (10-20 meter) sampling of the halocline (about upper 200 meters). Salinity and nutrient check samples from large-volume and trace-metal casts were also run.

#### 5.3.4.2 Total Carbonate, Total Alkalinity, Calcium (BIO, UGÖ)

Total carbonate was determined on board ship by a coulometric titration of carbon dioxide degassed from acidified seawater (Johnson et al. 1985). The precision of the analysis was better than 0.1%. Total alkalinity was also measured on board ship using a standard potentiometric titration in a closed cell. The titration curve will be evaluated by a curve fitting procedure (Johansson & Wedborg 1982) giving both the total alkalinity and total carbonate with a precision of near 0.1%. Samples were collected for the determination of calcium concentrations and stored for later analysis in the laboratory in Goteborg using an automated titration method with a precision of better than 0.1% (Anderson & Graneli 1982).

#### 5.3.5 Trace Elements (UGÖ, MIT)

During this cruise, samples for trace element analysis (Fig. 16) were collected in a transect across the Nansen Basin. They were taken from the very surface, including surface water and ice samples, to the bottom of the water column. The elements included in the study are copper, cadmium, cobalt, iron, nickel, lead and zinc in both dissolved and particulate forms. Ice-melt samples will be analyzed for additional elements to determine if they could be of interest in future arctic work.

The samples for trace elements from 50m and deeper were obtained using 12 l or 2.5 l teflon-coated Go-Flo sampling bottles hung on a plastic coated hydrowire. The shallower samples, above 50m, were collected from ice floes. For the collection of surface and ice-melt samples, arm-length polyethylene gloves were used in immersing sample bottles which were opened, filled and closed under water. Sampling down to 20m was done with plastic Ruttner samplers hung on a polyester line. All samples were drawn from the sampling bottles in transportable clean room laboratory on board ship where they underwent pre-analysis treatment. Two samples from every cast were filtered through 0.4 um Nucleopore filters to collect particulate matter for analysis of suspended trace elements. The filtrate from these samples and all other unfiltered samples were acidified with nitric acid to a pH of 2.0. Surface water and one deeper water sample at every station was processed through a colloids catching column for later speciation studies of the trace elements. Final analyses will be done at the University of Göteborg. Aliquots of all samples were taken for analysis of salinity and nutrients on board.

Some samples were collected into acid-cleaned polypropylene bottles for later trace element analysis at MIT for aluminum, beryllium, bismuth and selenium. Some additional samples were also collected from the rosette samples for MIT.

#### **5.3.6 Chlorofluoromethanes (Freons) and Halocarbons (BIO, UGÖ)**

Chlorofluoromethanes and halocarbons were measured using gas chromatography with electron capture detection. The chlorofluoromethanes were determined using a purge and trap technique whereas the halocarbon analyses employed liquid-liquid extraction into purified pentane. Samples were collected from the rosette sampler equipped with 10 l sampling bottles with O-rings specially prepared to give very low background concentrations of chlorofluoromethanes. All analyses were completed within 12 (chlorofluoromethanes) to 24 (halocarbons) hours after sampling. On two occasions, several bottles were triggered at the same depth and sampled from 1- 6 hrs after being brought on deck. No significant bottle contamination was observed over this time period for any of the halocarbons.

#### **5.3.7 $^3\text{H}$ , $^3\text{He}$ , Ne, $^{18}\text{O}$ , AMS- $^{14}\text{C}$ (IUPH)**

On 18 stations (26 casts) a total of 524 samples have been collected for the analysis of tritium,  $^{18}\text{O}$ , helium/neon and  $^{14}\text{C}$ . The samples for measurement of tritium and  $^{18}\text{O}$  have been stored in 1 l glass bottles, the noble gas samples ( $^3\text{He}$ ,  $^4\text{He}$ , neon) have been stored in pinched-off copper tubes. The tritium samples will be analyzed either by conventional low level counting techniques (Weiss et al. 1976) or mass spectrometrically via  $^3\text{He}$  ingrowth using a special helium isotope mass spectrometer (Lynch & Kay 1982). The helium and neon isotopes are measured with the same mass spectrometer.  $^{18}\text{O}$  samples are measured mass spectrometrically with a commercial stable isotope mass spectrometer. 48 small volume samples for  $^{14}\text{C}$  measurement by AMS have been collected at 7 stations. The samples are stored in preevacuated 1 l glass bulbs and are poisoned by addition of  $\text{HgCl}_2$ . The procedures of  $\text{CO}_2$  extraction and target preparation are described in Schlosser et al. (1987) and Kromer et al. (1987). Measurement of the samples is done at the ETH/SIN AMS facility (Zürich) as described by Bonani et al. (1986).

#### **5.3.8 Nitrogen Isotopes (WHOI)**

The ratio of stable 15-Nitrogen to 14-Nitrogen can be a valuable tool in studies of biological productivity and large particle removal in the oceans. On an opportunistic basis, it was felt worthwhile to attempt to examine the  $^{15}\text{N}/^{14}\text{N}$  ratio of dissolved and particulate samples from the Arctic seas, where no data of this kind exist. The data will be compared to more complete studies throughout the world's oceans, and in particular at a site near Bermuda in the Atlantic.

The samples collected were either water remaining in the CTD after the major programs were completed, or a subsample of water obtained with the 30 l Niskin bottles on casts taken for biological studies. Below 100m, the samples were one liter in volume and generally unfiltered. In the samples above 100m, when there was sufficient water available (>5 l), the water would be filtered through precombusted GF/F filters, and the filters and one liter of the filtrate saved.

### 5.3.9 Large-Volume Sampling

On 9 stations (18 casts) large volume samples have been obtained from 126 depth levels using 270 l - stainless steel Gerard-Ewing samplers. Sample depth has been checked by unprotected thermometers and by comparison of the salinity and nutrient concentrations of the large volume samples with the bottle data obtained from the rosette samples.

#### $^{14}\text{C}$ (IUPH)

A total of 129 large volume  $^{14}\text{C}$  samples have been collected on 9 stations with a maximum of 20 depth levels per station. The water has been processed on board by extraction of the dissolved gases, pumping the water through one of two vacuum extraction units operated at a flow rate of 6-8 l/min. The  $\text{CO}_2$  has been absorbed by passing the extracted gases through NaOH. The  $^{14}\text{C}$  samples will be measured at the Heidelberg low-level counting  $^{14}\text{C}$  laboratory (Schoch & Münnich 1981)

#### $^{85}\text{Kr}$ and $^{39}\text{Ar}$ (PHYBE, LDGO)

After the absorption of the  $\text{CO}_2$  for  $^{14}\text{C}$  analysis the extracted gases have been compressed into steel containers for measurement of  $^{85}\text{Kr}$  (LDGO and PHYBE) and  $^{39}\text{Ar}$  (PHYBE). For  $^{85}\text{Kr}$  analysis a total of 24 samples have been collected (2 profiles plus 1 surface sample from the Barents Sea). As for one  $^{39}\text{Ar}$  sample 1-1.5 m of water are required dedicated  $^{39}\text{Ar}$  casts were run on 4 stations using 4-5 Gerards per  $^{39}\text{Ar}$  sample. The spacing between the Gerards was 15 m. All together 8  $^{39}\text{Ar}$  samples were collected in this way including 2 surface samples taken from the ship's special sea water intake. The samples will be measured at LDGO and PHYBE using low-level counting techniques (Loosli 1983, Smethie & Mathieu 1986).

#### $^{226}/^{228}\text{Ra}$ (PU)

On 4 stations samples were obtained for measurement of the  $^{226}\text{Ra}$  concentration (32 samples) and the  $^{226}\text{Ra}/^{228}\text{Ra}$  ratio (54 samples). The samples will be measured at PU.

#### $^{90}\text{Sr}$ and $^{137}\text{Cs}$ (WHOI/SUNY)

In support of the studies of anthropogenic and naturally occurring radionuclides (WHOI/SUNY), the LVS samples were subsampled

after  $^{14}\text{C}$  extraction. Subsamples for  $^{90}\text{Sr}$  were collected in 55 l deldrums (52 samples from 5 stations), and subsamples for  $^{210}\text{Pb}$  were collected in 4 l plastic containers (21 samples from 2 stations).

#### 5.3.10 Artificial and natural radioisotopes in the Arctic: Large-Volume Pumping for Isotopes (WHOI)

On the ARK IV/3 cruise, samples were obtained via an in-situ pumped extraction system which collects particulate and dissolved radionuclide activities from large (approximately 1000 liter) volumes of seawater. Each pump is lowered to depth, and passes seawater first through a 0.5  $\mu\text{m}$  polypropylene filter cartridge, then through two identical cartridges coated with  $\text{MnO}_2$ , and finally through two additional cartridges which are coated with cupricferrocyanide. The  $\text{MnO}_2$  cartridges are used to collect the particle reactive isotopes (such as the isotopes of Th, Pu & Am), and the cupric ferrocyanide cartridges are very efficient at collecting the Cs isotopes.  $\text{Sr}$  and  $^{210}\text{Pb}$  will be analyzed from separate water samples taken from the Gerard bottles after  $^{14}\text{C}$  extraction.

Analysis of the cartridge samples will be at both WHOI and SUNY, by wet chemical digestion followed by low level alpha, beta and gamma counting techniques.

#### 5.3.11 Temperature and Velocity Structure (APL)

Expendable Bathythermographs (XBTs) and Expendable Current Profilers (XCPs) were deployed during ARK IV/3. The goals of the XBT deployments were to make one detailed section of temperature versus depth in the upper 800 meters across the warm Atlantic water flowing eastward along the Barents slope, and a less detailed section north of the boundary current to measure the levels of temperature fine structure between the CTD/rosette stations. The goals of the XCP deployments were to make a relative velocity section across the boundary current along with the XBT section, and to measure the levels of internal wave shear and mesoscale eddy activity away from the boundary current. Another goal was to test the operation of XCPs in the weak magnetic fields north of 84° N. The XBT deployments follow temperature measurements across this domain carried out by Perkin & Lewis (1984), from which it was deduced that the Atlantic layer is likely carried in separate in shore and off shore cores, with the northernmost edge at about 82°30' N. Very few current meter records exist from this domain, and no detailed section of velocity measurements against depth had ever been attempted.

The XBT and XCP electronics were mounted in the CTD room overlooking the fantail. XBTs were to be dropped from the fantail. The plan was to launch XCPs at every CTD station. Because XCPs should be deployed at least 200m from the POLARSTERN in order to minimize data contamination by the ship's electric

field, at most stations the XCPs were deployed from the ice nearby the ship: during a CTD cast a small party would disembark, drill a hole, alert a person standing by in the lab, call for radio silence, then drop the XCP probe. An alternate procedure was to use the timed-released flotation collar and deploy the probe from the fantail, trying to time the release with 200m or greater forward progress by the ship during the release time delay, yet remain within radio reception distance of the probe.

108 XBT probes were deployed from the ship at 99 locations during ARK IV/3. Of these 50 yielded temperature profiles to less than 200 meters, 22 between 200 and 400 meters, 19 between 400 and 600 meters, and 22 to full wire depth. Preliminary examination of temperature profiles from successful deployments near CTD stations showed that the XBT profiles contained similar features and strength of extrema as compared to the CTD temperature profiles. Deployment from the fantail when the ship was in the ice (as it was throughout the period of XBT deployments) was a difficult operation because the fast-moving, chaotic chunks of ice in the strong wake usually cut the XBT wire at two or three hundred meters depth. Attempts to deploy the probes as the ship crossed leads were often thwarted by ice carried along with the ship, or by unpredictable course changes.

46 XCP probes were deployed at 42 locations during ARK IV/3 (there were 4 probe failures followed by redeployment). Of these, 29 were considered good, 9 marginal, and 8 gave no data. During the northward transect of the cruise, XCPs were deployed only at CTD stations, usually during one of the CTD casts at the station. Shear at various scales was evident, and the measurements seemed successful. The XCP probes also yield high-quality temperature profiles, which showed strong agreement with the accompanying CTD temperature profiles. As the ship headed south toward the Yermak Plateau and Spitsbergen, the remaining XCP and XBT probes were deployed in a survey mode, alternating XBTs and XCPs every three miles (i.e. one of each type every six miles) from approximately 83.3° N until the probe supply was exhausted. Probes were deployed from the fantail. 14 XCPs and 5 XBTs were successfully deployed during this transect, which extended from the Nansen Basin abyssal plain, over and across the Yermak Plateau, and up to the continental shelf north of Spitsbergen.

The XBT and XCP probe data will be processed at APL, and a final set of profiles will be produced. Interpretation of the probe data will be carried out together with the CTD data. One result will be two sets of velocity and temperature sections - one at approximately 31° E and the other near 20° E, across the Barents Sea slope to the deep Nansen Basin, with the 31° E section extending to the mid-ocean ridge. An intense study using XBT and XCP probes is planned for the Yermak Plateau region for early 1989 as part of the Arctic Oceanography Initiative (AOI) program sponsored by the U.S. Office of Naval Research. The ARK IV/3 data will help identify signal strengths, instrument problems, and key measurement scales for that project.

### 5.3.12 SOFAR FLOAT Acoustic Ranging Experiment (LODYC)

#### Monitoring Arctic Ocean Currents by SOFAR Float Techniques

Commonly SOFAR technology makes use of the so-called "Swallow Float" which is a neutrally buoyant drifting float at constant level (like a constant level balloon). In the simplest version, the Swallow Float is a structure less compressible than sea water. Ballasted at the surface in order to sink, the float will gain buoyancy with increasing pressure. According to a preselected surface ballasting, the float can possibly find an equilibrium at a depth where it is neutrally buoyant. The float would then be passively advected by the horizontal current at this depth. Monitoring this current is equivalent to tracking the float with time. One way of accomplishing this is by acoustic localisation using listening stations at known locations (like for radionavigation systems) to listen to the floats equipped with acoustic sources. The only waves which propagate freely over long enough distances in the ocean are sound pressure waves. Lower frequencies result in less sound propagation attenuation and thus longer ranges. Typically ranges of hundreds to thousands of km can be reached in the ocean with frequencies in the hundreds to thousands Hertz range. Unfortunately, there are critical limitations in designing high efficiency, very low frequency transducers. This is primarily due to an increase in transducer size as frequency decreases and the subsequent increase of electrical power required for the same amount of sound pressure transmitted into the fluid. Actually frequencies commonly used depend upon the objectives. For example:

-for small scale applications, like internal waves, upwelling and deep convection studies, 5 Khz has been commonly used in the past (for instance during MEDOC cruises in the Northwest Mediterranean (1969-75), during Labrador 76 and 78 cruises and during Mediterranean Outflow studies in the Straits of Gibraltar in 1981).

-for mesoscale applications, like ocean eddies studies, 1.5 Khz has been selected in several instances, for example in the TOURBILLON Experiment (1979) and, more recently during MIZEX 84.

-for large scale applications (basin wide, gyre circulation) 260 Hz has been commonly used during the past 10 years like in the MODE and POLYMODE experiments conducted in the North American Basin. In this case, ranges of 1000 kM and more have been obtained taking advantage of a deep sound channel at mid depth (1500 m) due to the presence of a temperature inversion at the level of the Mediterranean water layer.

-In the case of the Arctic, no such favorable conditions exist. Due to the presence of ice, the problem is even worse, since not only water induces sound attenuation, but also sea-ice which drastically affects sound propagation by absorption, refraction, multiple reflection effects on ice keels in particular.

Extrapolating the results obtained during MIZEX (120 km maximum range at 1.5 KHz beneath ice-covered areas) and considering actual data related to Arctic sound propagation, it is expected that 260 Hz will give a range of approximately 300 to 500 kms and 80 Hz will give a range of 500 to 800 km, with the assumption that transducer efficiency will be equivalent at both frequencies, which might be far from being the case. So, during ARK IV/3 cruise, it was proposed to test the sound propagation range at both frequencies (80 and 260 Hz) in actual field conditions, to prepare for future extensive SOFAR floats experiments in the Arctic as well as in the Antarctic (Fig. 20).

#### Instrumentation and Scientific Investigation

A dual frequency (80 Hz - 260 Hz) source has been designed by Webb Research Corporation in Falmouth (USA). This source uses the classical SOFAR signal which is a long pulse (80 s) during which the nominal frequency changes linearly with time by approximately 1 % (that is, 1 or 2 Hz). The 260 Hz transducer is the type commonly used in the North Atlantic during past and actual experiments. It is a tube (about 1.8 m high and 30 cm in diameter) closed at one end where it is excited to its natural frequency by a mosaic of piezoelectric elements. The 80 Hz transducer is a prototype using the Helmholtz resonance principle. In this case, the excitation is applied at both ends of a tube 1.6 m long and 30 cm in diameter.

The source has been programmed via a microprocessor to operate in two different modes:

1. a fast cycle mode during which each pulse at 80 sec is sent at 30 min intervals. Both frequencies alternate regularly and each are then transmitted every hour during 256 h (10 d + 16 h)
2. following the fast cycle mode, a slow cycle mode during which each pulse is sent at 12 h intervals, one pulse at 4:00 UTC and the second one at 16:00 UTC, during 256 d. The 4:00 UTC pulse called the "main pulse" is followed a few minutes later by a telemetry signal which indicates the water temperature at the float depth. During odd days (julian days) the main pulse is transmitted at 260 Hz and a telemetry pulse follows on at the same frequency. On these days, the 16:00 UTC pulse occurs at 80 Hz and vice versa during even days.

The listening equipment is composed of an underwater unit called "Autonomous Listening Station" (ALS) equipped with an hydrophone array. The array has significant directivity in the horizontal plane and it is critical to maintain it as vertical as possible to insure good reception. Briefly the ALS uses a correlator which compares, every 1/10 second, acoustic noise received by the array over 80 sec time duration with a standard SOFAR signal identical to the one programmed into the source. The 4 highest levels of correlation found during 10 minutes intervals are stored on an internal tape recorder, together with their corresponding accur-

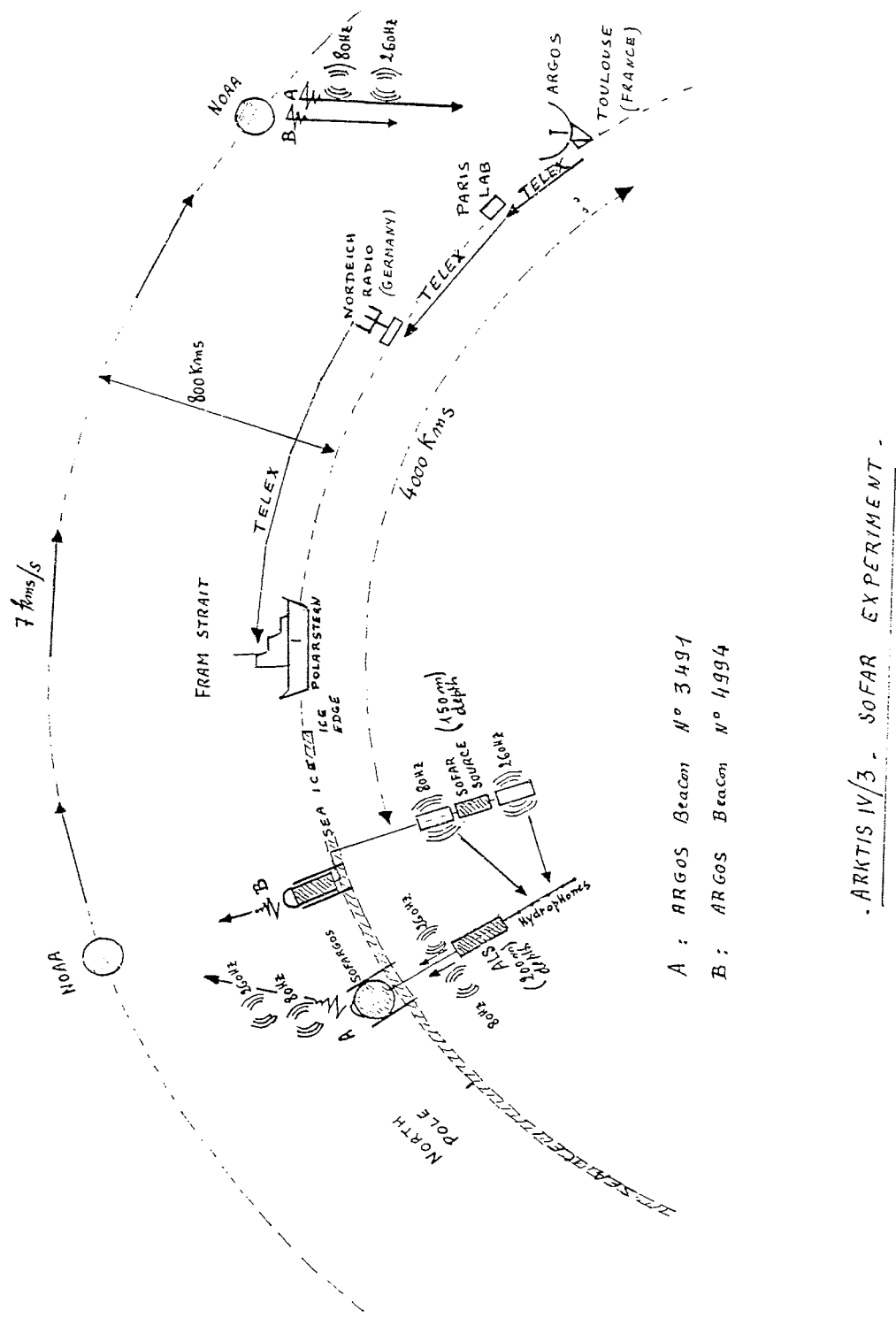


Fig.20 Field configuration of the SOFARGOS system.

ate timings. A correlation level of around 30 (arbitrary units) indicates noise, and, around 100 indicates that a strong SOFAR signal either at 80 Hz or 260 Hz has been received by the ALS unit. This correlation technique greatly improves the signal to noise ratio.

These data are not only recorded internally by the ALS, but also transmitted via an electrical cable to a surface unit called "SOFARGOS" which transmits at minute intervals ALS correlation signals to the ARGOS receivers on board NOAA satellites. This information is then transferred from the satellites to a receiving ground station in Toulouse (France). We know the departure time of the SOFAR signal from the source. So we have to measure precisely the arrival time at the ALS of any significant correlation level in order to range the SOFAR signal sent by the source (significant means well above the noise level). To accomplish this, the internal clock in the ALS is compared with a very stable clock in the ARGOS satellite. This comparison allows us to eliminate any possible clock drift problem in the ALS.

In addition, the ARGOS system locates the SOFARGOS unit like with a normal ARGOS buoy. The schematic shows the field configuration of the whole system (Fig. 20).

#### Stations - Progress During Expedition

During the ARK IV/3 cruise, the SOFARGOS ( $N^{\circ} 3491$ ) was deployed at the northernmost position ( $85^{\circ} 54.4' N$   $22^{\circ} 40.2' E$ ) on July 31 at 22:00 UTC, on a 3 m thick ice floe close to a melt pond surrounded by a lot of ridges. The underwater unit (ALS) was placed at about 200 m depth and electrically connected to the SOFARGOS unit. The source was deployed at 150 m depth at  $85^{\circ} 22' N$   $21^{\circ} 28' E$  on August 11 at 06:00 UTC. The source was tethered to an ice floe marked by an ARGOS beacon ( $N^{\circ} 4994$ ) located by satellite several times per day.

On August 11 at 3:40 UTC, the SOFARGOS was located at  $86^{\circ} 10.2' N$   $20^{\circ} 57' E$ . This position was approximately 89 km north of the SOFAR sound source as estimated from satellite fixes of the two ARGOS beacons. The fast cycle mode initialised on August 11 (Julian Day 223) at about 06:00 UTC on the source, ended on August 22 at 22:00. Then the slow cycle mode began on August 22 (day 234) at 4H00 and will last until May 4, 1988. At this time it is expected that both SOFAR and SOFARGOS units will be located close to Iceland, where we will try to recover them.

#### First Results

Fig. 8 shows the drifts of the SOFAR source and SOFARGOS receiver since their deployment. Since August 11, they have drifted about 80 km during the first 10 days (fast cycle period) in a southwest direction towards Fram Strait. The distance between the two buoys has stayed within 2-3 km of 90 km. According to past observations of sea-ice drift in this region, speeds as well as the distance

between SOFAR and SOFARGOS should progressively increase when approaching Fram Strait. The first data received at the Space Center in Toulouse and transmitted daily by telex to POLARSTERN, indicate that the two frequencies are being received by the SOFARGOS and properly transmitted to the satellite. The travel time of the SOFAR signal between the source and the ALS is close to 1 minute which, for a sound speed of about 1500 m/s, corresponds to 90 km/h. This is in quite good agreement with the distance calculated from the ARGOS positioning.

Fig. 21 shows a one-day example (August 16) of the signal level (correlation level) at both frequencies, as it is received at the ARGOS Space Center in Toulouse and transmitted daily back to us via Telex. Some discrepancies have already appeared which we cannot yet interpret. The signal level fluctuates quite significantly on a daily basis although it remains well above the noise. Most of the time, it seems that the signal level is stronger at 260 Hz than at 80 Hz for this range. On Fig. 21, we present results obtained during the 256 h fast cycle test. Obviously, more irregularities appear in the 80 Hz transmission than in the 260 Hz one.

In all 246 out of 256 signals at 260 Hz were received and most of the missing information is due to ARGOS gaps. The average signal correlation level is 92.7 with a RMS of 28.9. 85 out of 256 signals at 80 Hz were received for which the average signal correlation is 69.2 with a RMS of 22.1.

We received the first data for the slow cycle mode on August 23 (Julian day 235) and following days. The results are quite encouraging. Both frequencies seem to work properly and correlation levels are now quite comparable. This experiment will last until May 4, 1988, thus it is much too early to draw more conclusions. Slow cycle mode data for the period beginning on August 23 (Julian day 235) and following days are summarized in the Table 2.

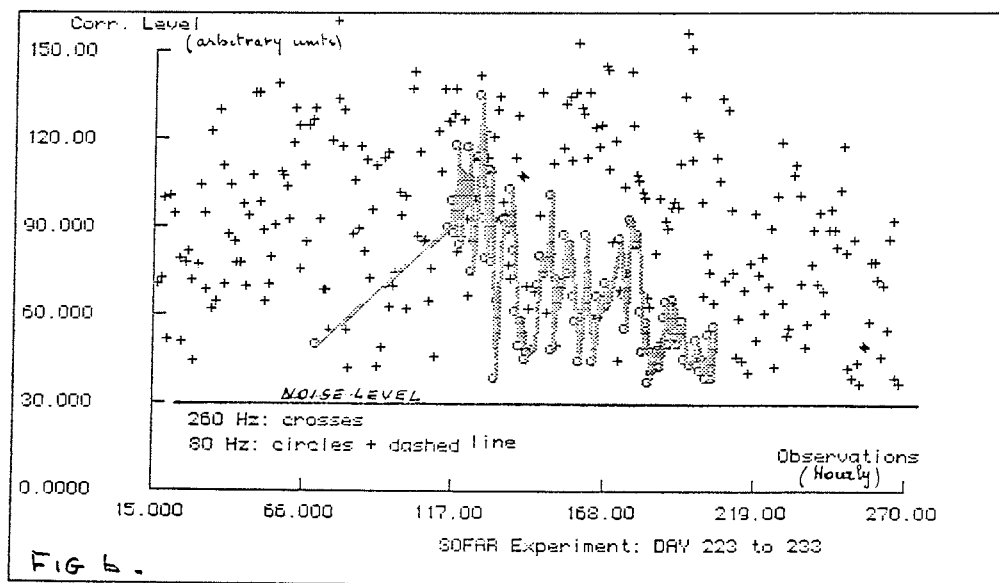
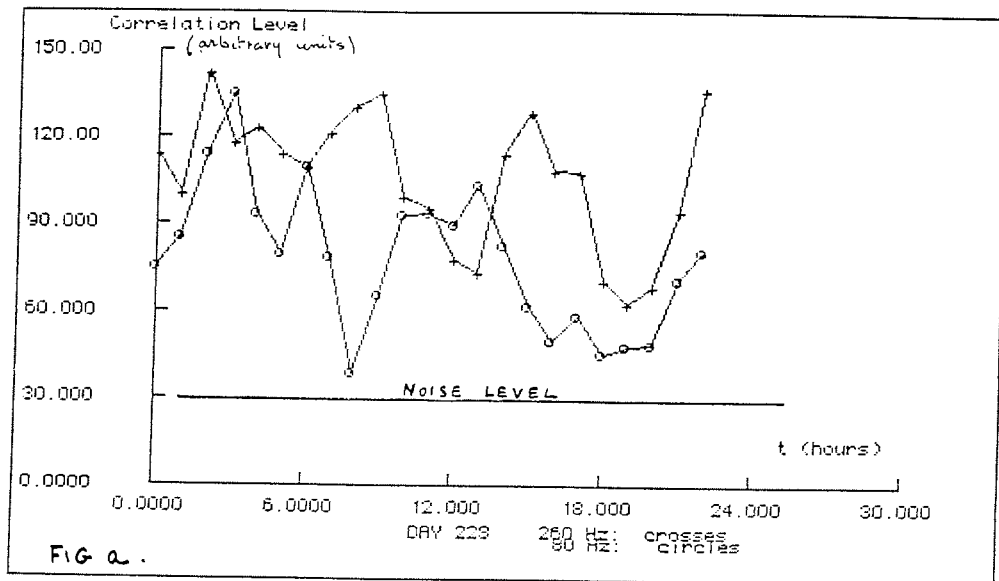


Fig.21 Signal correlation level for SOFAR experiment.

TABLE 2: Cycle Mode Date of SOFAR Experiment

Day	80 Hz			260 Hz		
	Time	Corr.	Level	Time	Corr.	Level
235				04h02m22s		97
235	16h02m24s	81		04h11m55s		107
236	04h02m24s	112				
236	04h12m00s	107		16h02m22s		117
237				04h02m22s		127
237	16h02m24s	138		04h11m57s		109

From the times indicated in the above table, we have to subtract the 80 sec pulse duration to get the travel time of the SOFAR signal from the source to the SOFARGOS. So this time is 62 sec according to the 260 Hz and 64 sec according to the 80 Hz.

#### Plans for Future Work

During summer 1988, 10 SOFAR floats (260 Hz) will be deployed west of Spitsbergen to investigate the circulation and recirculation of Atlantic waters in Fram Strait. These floats will be tracked by an array of 4 autonomous listening stations ALS moored on the bottom and not transmitting to satellites. This program is adjacent to a tomography experiment planned at the same time in the same region. Both are part of the Greenland Sea Project. In Spring 1989, we will complement the 1988 float deployment with a few more floats launched around the Yermak Plateau area. We will also increase the bottom moored ALS array with a few SOFARGOS stations put on the ice. This program will be developed in cooperation with WHOI and LDGO. In 1990, and in conjunction with the ERS1 mission, we are planning to deploy several SOFARGOS stations along the axis of the Transpolar Drift, in order to be able to track SOFAR floats as far north as possible, year around. Our first objective is to map the subsurface geostrophic current, just below the Ekman layer. Then the investigations will be extended to the Atlantic layer at intermediate levels and, finally, to the deep layers later on.

Depending upon the quality of the SOFAR acoustic transmission at long ranges, we are also planning to connect inverted echosounders to SOFAR floats to measure ice thickness at float locations and along their drift trajectories. Ice thickness data will then be telemetered to SOFARGOS just like temperatures and pressures are telemetered in the actual floats.

#### 5.4 Oceanographic Preliminary Findings

In a first assessment of the available data, the Nansen Basin section reveals an extremely variable zone close to the boundaries of the basin. Both at the Barents shelf slope and near the Nansen-Gakkel Ridge the hydrographic data reveal, supported by a full suite of nutrient data, narrow and well confined boundary currents, closely following the depth contours.

Despite the coarse station spacing of about 100 km (Fig. 15) the basin interior shows distinct changes also for the intermediate and deep layers. Extrema in the nutrient data may indicate patchiness in the deep waters especially. A thin oxygen minimum separates the lower part of the Atlantic layer from deeper ones.

The CTD-data show for the top and intermediate layers the expected distribution of cold and fresh polar surface layers, increasing in thickness towards the north to about 200 m (Fig. 22). The warm and salty Atlantic signal is reduced from 1.9° C north of the Barents shelf break to about 1.2° C over the Nansen-

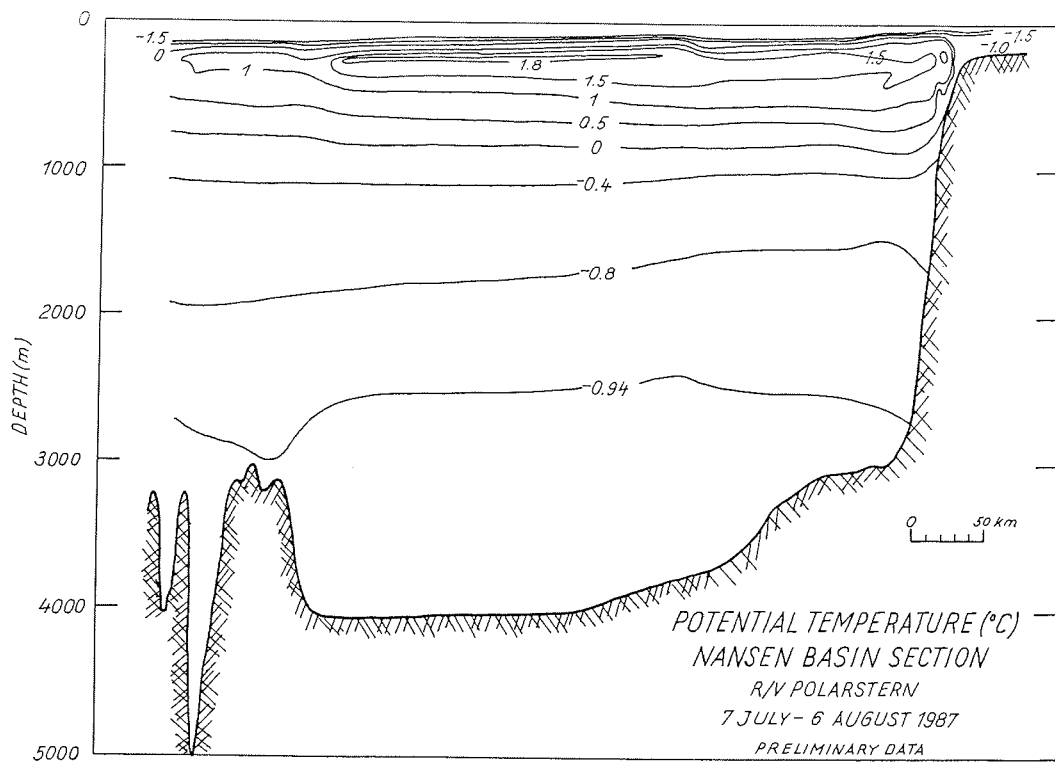


Fig.22 Nansen Basin section of potential temperature (prelim. data)

Gakkel Ridge. Multiple temperature maxima occur between 200 m and 500 m. They cannot be traced individually due to the coarse station spacing. Over the Nansen-Gakkel Ridge the form of the Atlantic layer approaches that found in the Canada Basin. It is characterized by a broad, smooth temperature profile. The 0° C isotherm along this section lies between 750 and 950 m depth. Near 83° N subtle changes in T and S, supported by changes in the nutrients, document the transition from the southern half of the Nansen Basin, where it is more typical of the Fram Strait and northern Greenland Sea, to the northern half, where it resembles more the one typical for the central Arctic Ocean. These changes are also clearly seen in biological and geological data.

Beneath the Atlantic layer, we found at most sites clear indications of double diffusion, again decreasing in amplitude and frequency with latitude. Deep and bottom potential temperatures are around -0.94° C, salinities between 34.936 and 34.943 ppt.

On the rim, the intermediate and deep layers show an interleaving of narrow, well concentrated boundary currents with saltier and warmer water with Greenland and Norwegian Sea Deep Water characteristics at different depths (Fig. 23). Within the abyssal plain, an otherwise smooth transition from the boundary current regime to that of the plain is strongly marked by horizontal gradients particularly at Station 11/340. The temperature distribution on the southern ridge of the Nansen-Gakkel Ridge is disturbed at Station 11/365 below 1500 m by a warmer, slightly fresher intrusion. The northernmost stations at about 86° 8' N show at greater depth the first signs of a spillover of deep waters from the Amundsen Basin. Near and over the Nansen-Gakkel Ridge at 86° N several layers with noticeable gradients in hydrographic properties indicate a very variable region. The analyses of additional samples from this cruise has to clarify the origin and history of these water masses.

XBTs and XCPs helped resolve smaller scales on an otherwise basin-wide study of the general circulation and water masses.

The total carbonate data from the Nansen Basin are typified by a profile near the southern end of the section across the Basin and one near the northern end. Because there is such a large background concentration of total carbonate ( $C_t$ ) in the ocean that is proportional to salinity, it is useful to consider total carbonate values normalized to a reference salinity,  $S = 35$  ppt, or  $C_t(35) = 35C_t/S$ . These values are plotted vs depth in Fig. 24. The profiles show considerable structure in the upper regions of the water column with smaller variation in the deep water. In addition to the effect of salinity on  $C_t$ , there are contributions from the addition or removal of dissolved calcium carbonate to seawater and from the fixing and decay of biogenic matter. Both of these processes give signals in  $C_t$  distributions that must be extracted in order to exploit the measurements. The addition to  $C_t$  from the decay of biogenic matter can be accounted for by calculating the amount of carbon added from

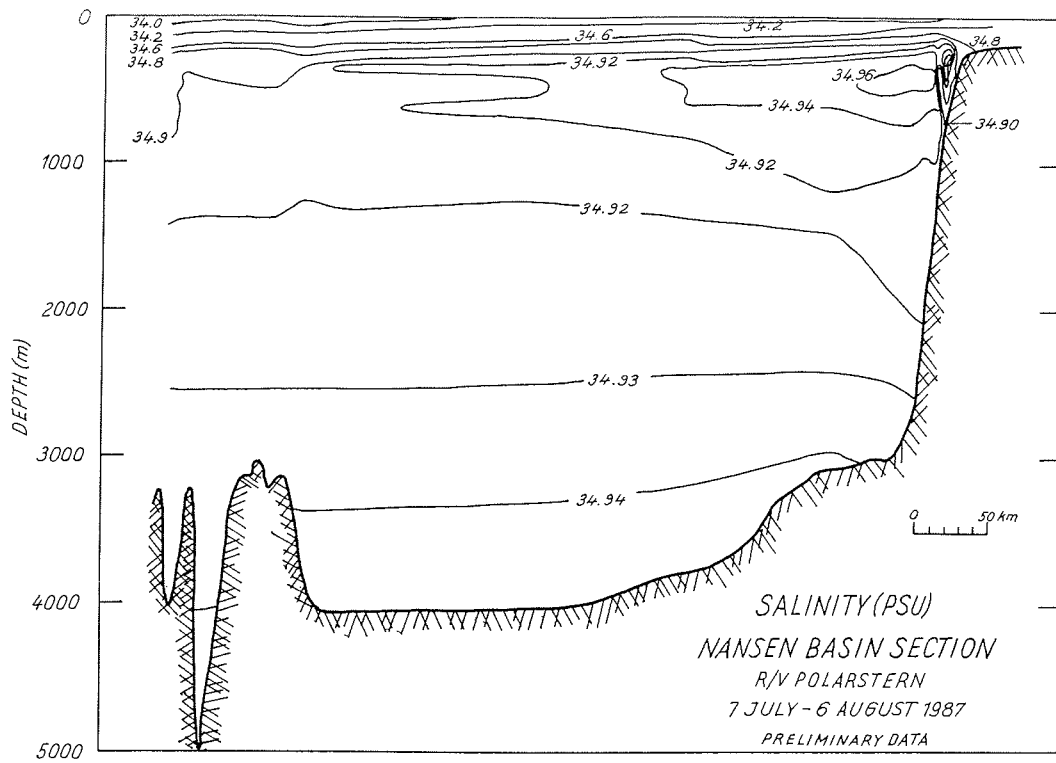
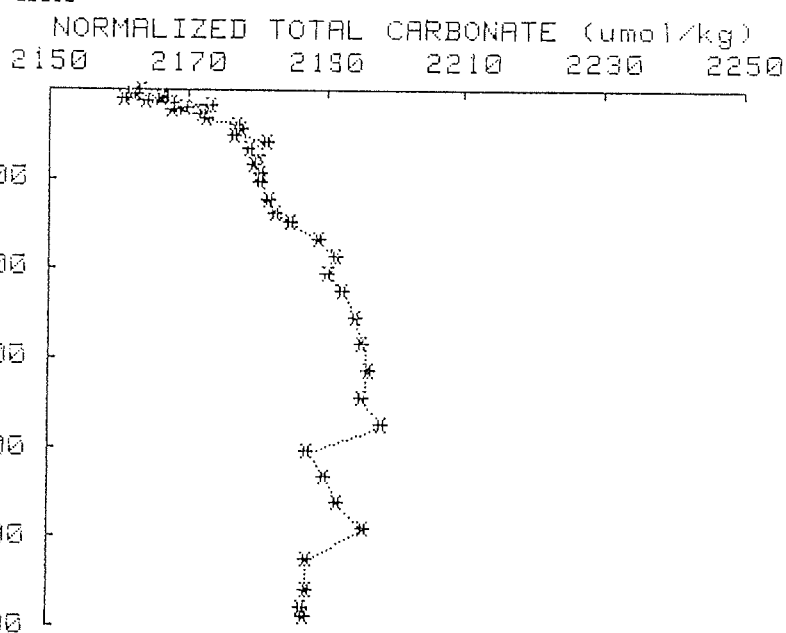


Fig.23 Nansen Basin section of salinity (prelm. data).

STATION 29612



STATION 371

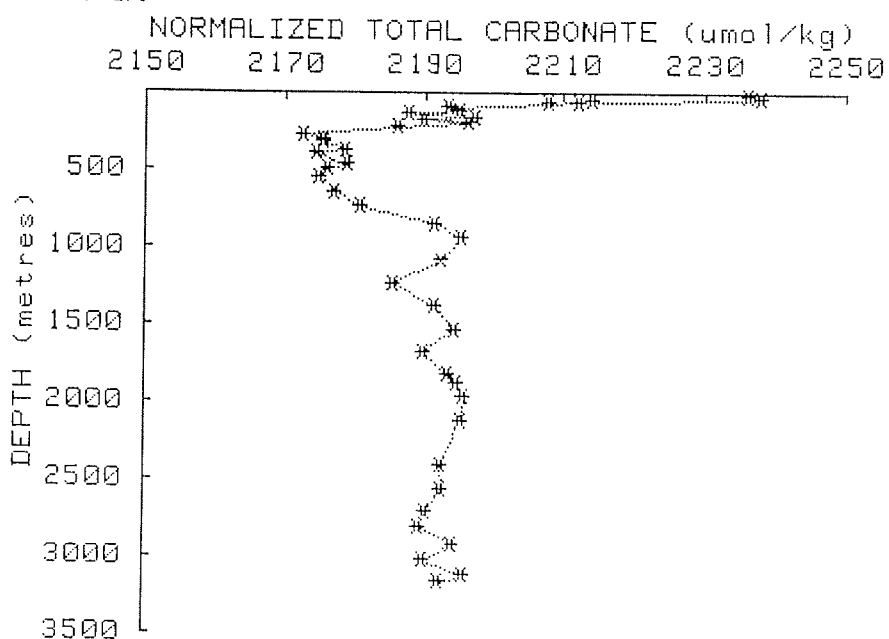


Fig.24 Profiles of total carbonate. Station 296 and 371

the amount of oxygen depleted in the water during decay using the Redfield-Ketchum-Richards model for the composition of biogenic material (Redfield et al. 1963). The "corrected" normalized total carbonate,  $C_t(35)\text{corr}$ , is then essentially a conservative tracer.

The most immediately obtainable result from this data is a description of some of the surface region water masses in Nansen Basin together with indications of their sources. More detailed interpretations involving the deeper data and addressing the fossil fuel  $\text{CO}_2$  question the possibility of using  $\text{CO}_2$  as a transient tracer will require further work incorporating results from other investigations.

As mentioned in the introduction, river runoff from Siberian rivers contributes calcium carbonate to the surface waters in the Canada Basin of the Arctic Ocean (Jones and Anderson 1986; Anderson et al. 1987). Thus, the lower salinity waters in the surface will show higher values of  $C_t(35)\text{corr}$  if river runoff is present than they will if the salinity is lowered by sea ice meltwater. A map of surface  $C_t(35)\text{corr}$  values for the Arctic Ocean surface waters should be able to trace the river input as it moves across the Arctic Ocean. Following this argument, we see in a plot of  $C_t(35)\text{corr}$  vs. salinity (Fig. 25) that the surface values clearly show that the source of the fresh water in the northern profile is mostly river-runoff, whereas in the southern profile the source is mainly sea ice meltwater.

A plot of NO vs. salinity for the northern station (Fig. 26) shows two distinct water masses: at  $S = 34.5 \text{ ppt}$  and at a depth of near 250m and the second at lower salinities at a depth near 50m. (NO is a conservative tracer based on the Redfield-Ketchum-Richards model expressing the fact that as biogenic material decays, oxygen is consumed and nitrate released in a fixed ratio.) In the southern station, no such clear distinction of near-surface waters exists. The value of NO at the core of the  $S = 34.5 \text{ ppt}$  water is just above 400 umol/kg. Water with a salinity near  $S = 34.2 \text{ ppt}$  and near-freezing temperatures in the Canada Basin is at the core of the lower halocline water whose source was speculated to be in the Barents-Kara Sea region (Jones and Anderson 1986). The lower halocline water is also characterized in the Canada Basin by a low "NO" value, about 400 umol/kg compared to values near 420 umol/kg for underlying water and 440 umol/kg for water closer to the surface. The similarity of the characteristics of the northern station to those of the lower halocline in the Canada Basin gives a strong indication that the speculation regarding the source of the lower halocline water is correct. The different values at the southern station indicate that the water that eventually finds its way into the lower halocline in the Canada Basin must be fed into the Eurasian Basin further to the east than the stations of the Nansen Basin section.

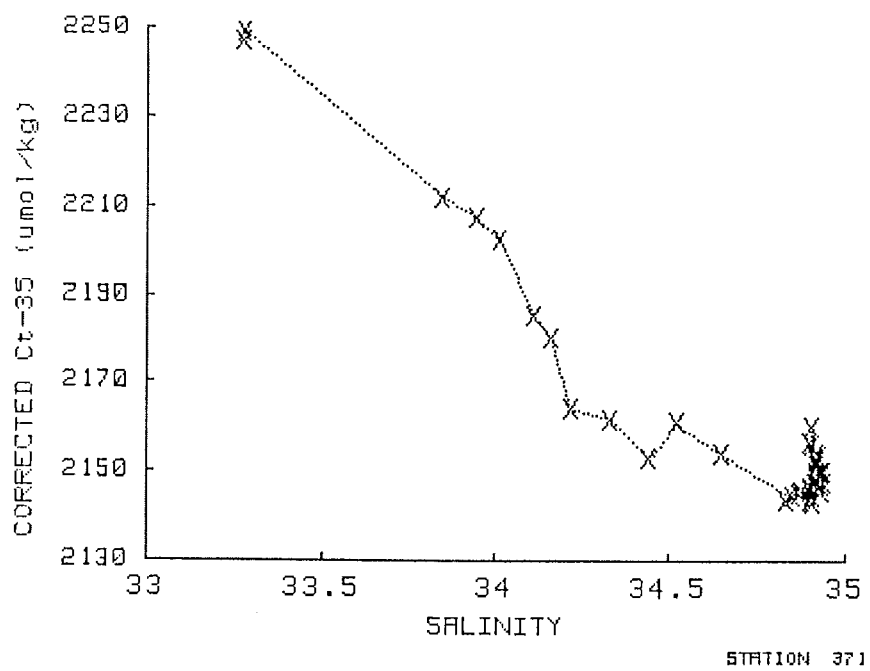
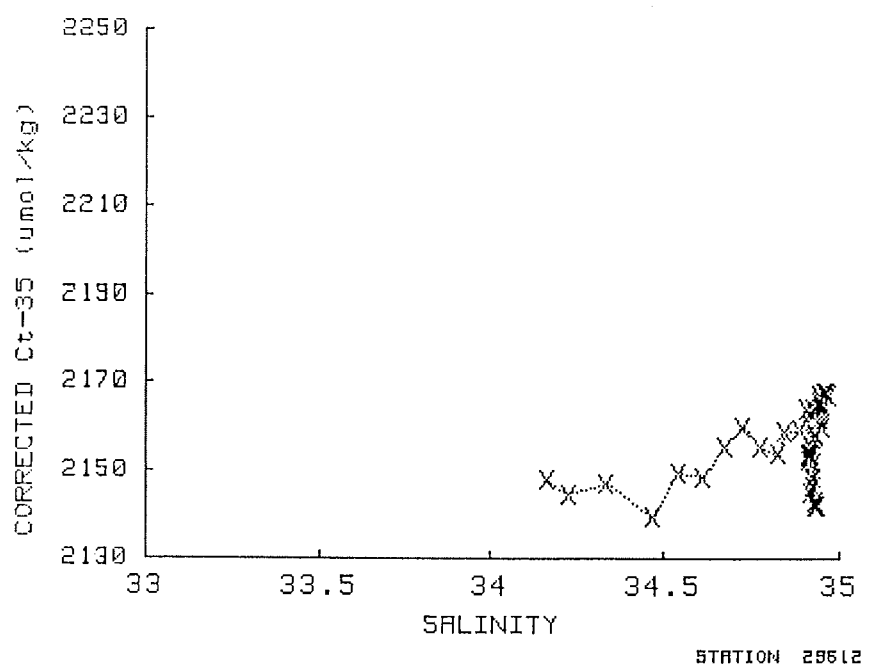


Fig.25 Correlation between  $Ct(35)\text{corr}$  and salinity for two stations on the Nansen Basin section. Station 296 and 371

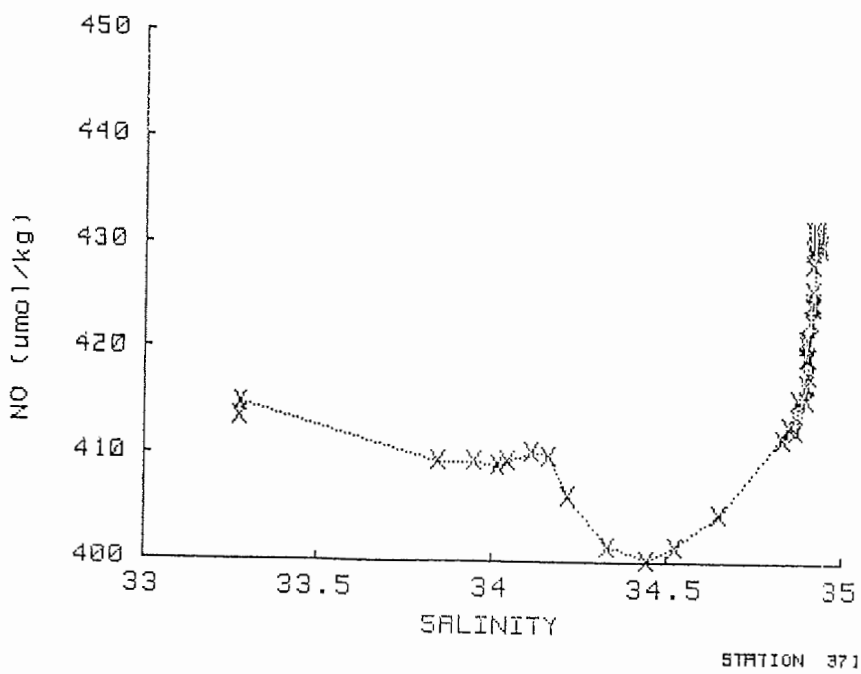
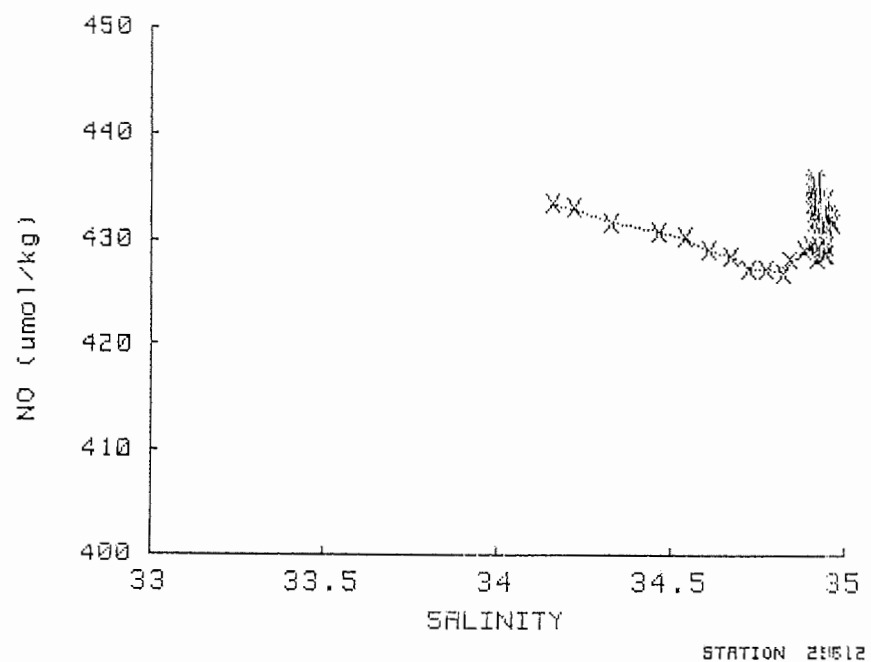


Fig.26 Correlation between NO and salinity for two stations on the Nansen Basin section. Station 296 and 371

On the basis of the only previous study of chlorofluoromethanes in the Nansen Basin (sampling confined to the southern periphery of the basin, Smethie et al. 1987) there was a clear indication of significant levels of chlorofluoromethane. Perhaps the single most unexpected finding of the ARK IV/3 section was the presence of a large pool of water in the centre of the Nansen Basin (below 3000m) with undetectable levels of chlorofluoromethanes F-11, F-12 and methyl chloroform. This indicates that the age of the Deep Water is at least several decades. On the other hand, preliminary results indicate that carbon tetrachloride was present in detectable amounts in this water. There are two possible reasons for this: (1) either the carbon tetrachloride has some unknown natural source (e.g. biogenic) and hence had some preindustrial background concentration; or (2) the deep-water signal reflects anthropogenic releases prior to the extensive usage of chlorofluoromethanes and methyl chloroform. It is expected that a detailed examination of the data and historical input functions will allow one of these hypotheses to be rejected.

The chlorofluoromethanes were found to be significantly above the detection limit both at the southern boundary of the Nansen Basin and in the vicinity of the Nansen-Gakkel Ridge, presumably the signature of a boundary current.

The intermediate-depth and near-surface waters were characterised by much higher concentrations of all halocarbons, with significant amounts of interleaving and structure observed at many stations. The inventory of chlorofluoromethane in the Nansen Basin water column is much larger than was observed in the central Canada Basin (Wallace & Moore 1985), indicative of more rapid ventilation of the water masses. The various halocarbons (with the exception of biogenic bromoform) showed many similarities in their depth distributions (Figs. 27-30). The origin and age of the various water masses are clearly reflected in these halocarbon depth profiles. Bromoform, on the other hand, has been present in the ocean for a very long time, and is found to be fairly well-mixed throughout the water column.

In some marine environments, the discharge of halocarbons can create a significant pollution problem. Levels in the central Arctic Ocean are, however, far too low to pose an environmental threat.

##### 5.5 Conclusions for Future Work

Close co-operation between the participating scientists will guarantee an extensive evaluation of this unique data set. The investigators collaborating in the oceanography program plan to join in preparation of papers aimed at scientific questions such as: What are the characteristics of the waters in the Nansen Basin? How are the intermediate and deep waters of the Nansen Basin ventilated? Can we detect a significant signal traceable to the Barents Sea in the intermediate or abyssal interior Nansen Basin? What happens to the Atlantic Water entering the Arctic

SATION 358

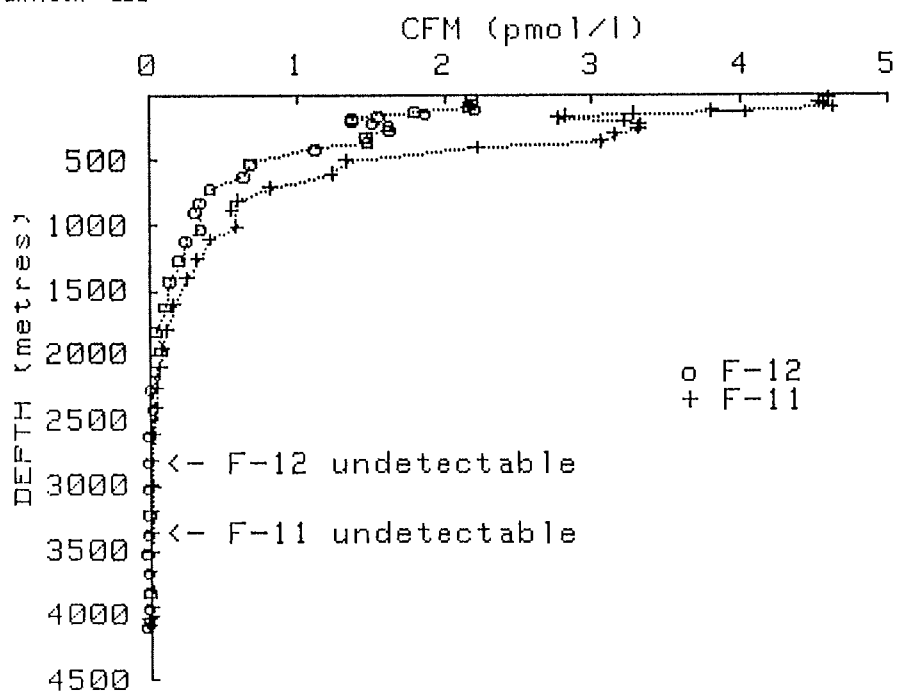


Fig.27 Vertical profiles of chlorofluoromethane measured at station 358 in the central Nansen Basin.

STATION 358

Methyl Chloroform

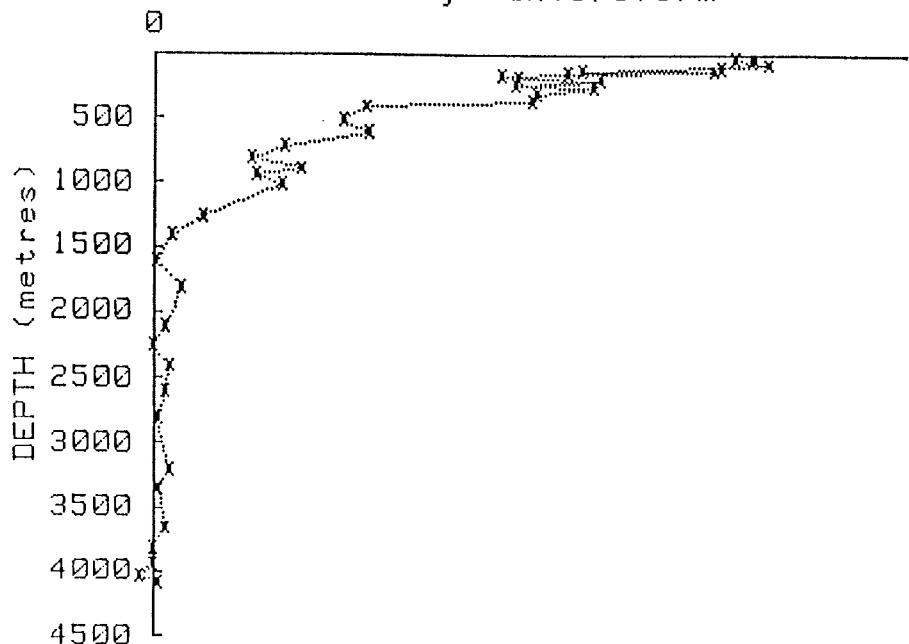


Fig.28 Vertical profile of methyl chloroform at station 358 in the central Nansen Basin.  
(Concentrations are subject to final calibrations, but lie in the range of 0 to  $4.5 \times 10^{-9} \text{ g/l}$ ).

STATION 358

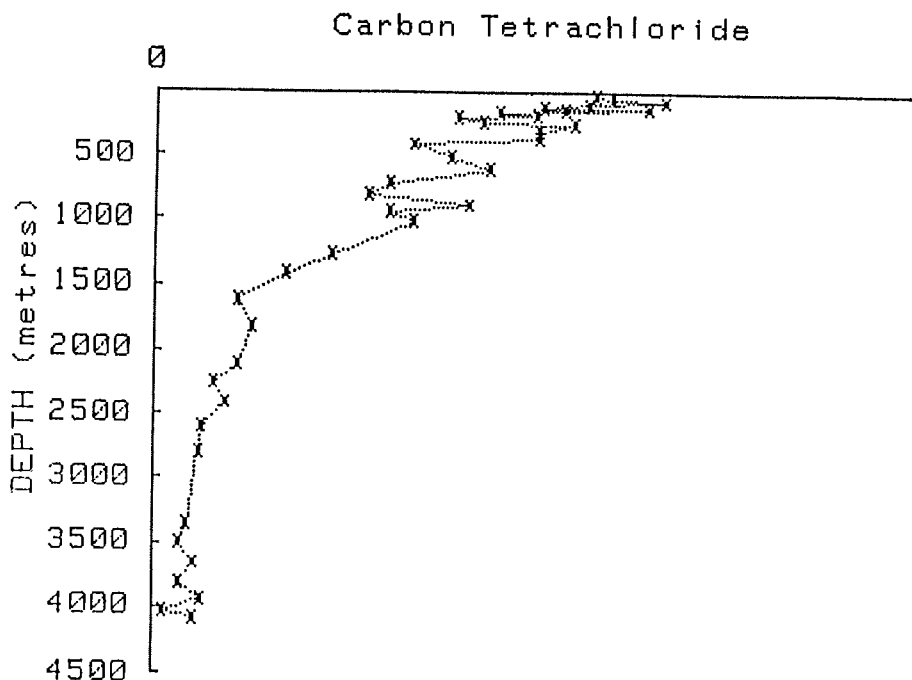


Fig.29 Vertical profile of carbon tetrachloride at station 358  
in the central Nansen Basin.  
(Concentrations are subject to final calibrations, but  
lie in the range of 0 to  $1,6 \times 10^{-9}$  g/l).

STATION 358

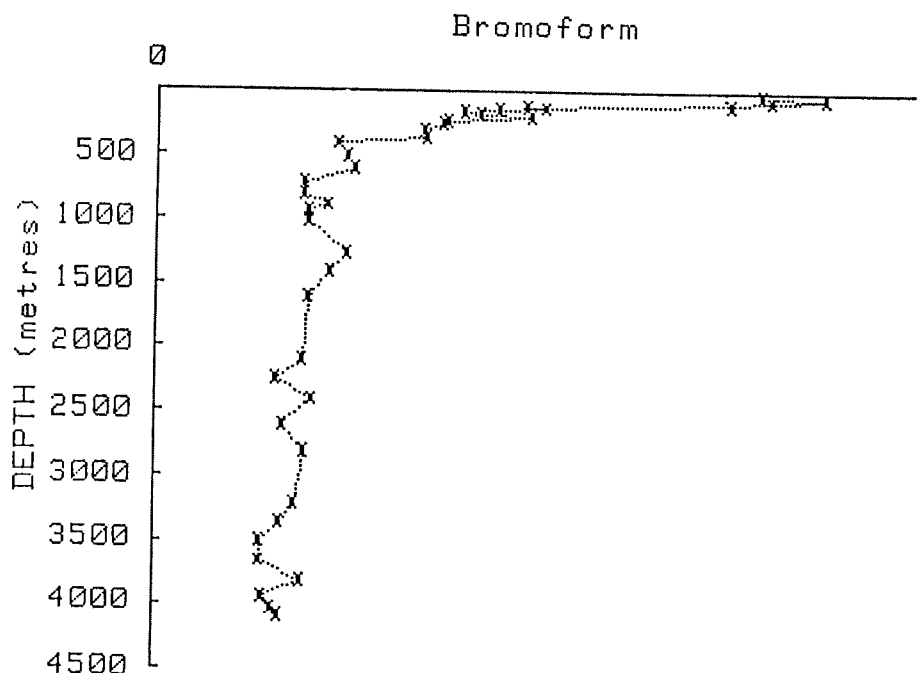


Fig.30 Vertical profile of bromoform at station 358 in the central Nansen Basin.  
(Concentrations are subject to final calibration, but lie in the range of 0 to  $4.0 \times 10^{-9}$  g/l).

Ocean? Are the characteristics of the intermediate and deep waters at the boundaries significantly different from those in the basin interior? Data reports will be made available on different levels of data verification soon after the cruise, focussed on the requirements of the participants. A final data report will make all oceanographic data available in due course.

The questions stemming from this cruise fall into two categories. The first concerns the technical and logistical feasibility, the second deals with the scientific justification. After the first ideas for running such a programme on POLARSTERN in November 1982 and a 'practice run' during ARK II/3 in 1984, it was felt that such a programme could succeed. After this cruise, since all scientific objectives have been met, in great part even surpassed, very few remaining technical and logistical questions need to be resolved before a similar task in the future. A basin-wide section was the ultimate goal, but seemed almost out of reach. The advantage of a mobile, well equipped platform with an adequate endurance allows scientific investigations with the necessary resolution that ice camps cannot provide.

The scientific questions asked before the cruise have now already in part been answered. For example there is a strong interaction between the shelf and Fram Strait with the Nansen Basin proper at almost all depths. New and barely touched is the question of the inter-basin exchange between the Amundsen and the Nansen Basin or even the Makarov Basin. Again unknown is a quantitative assessment of the importance of the Siberian shelves to the circulation of the Arctic basins in general and the Nansen Basin in particular. The existing data and potentially available models cannot explain a detailed circulation for the entire, very long Nansen Basin. In view of the strong contribution from the shelves, the part of the East Siberian shelves remains an unresolved question.

In planning details of the oceanographic programme on the basis of a 30-60 km station spacing, a full hydrographic station every 1-2 days, depending on the ship's progress, was envisaged. This would put an even work load on the groups analysing the samples on board. The size of the oceanographic complement proved to be completely satisfactory. An increase in analysis capacity would not necessarily increase data quality or throughput on a cruise lasting over two months.

Teaming up with a geology programme thus was sensible and of considerable benefit to both groups. Besides having similar concepts on station strategy and spacing and general work routine, the two groups paced out the work-load over the length of the cruise to maintain even work quality. More groups with inevitably conflicting strategies are thought likely to dissipate efforts from achieving the main goals of a cruise, fewer could hardly maintain heavy work for periods in excess of two months. The co-operation with geology in the end led to a very effective

symbiosis to the advantage of both programmes, both in terms of workplans and, most satisfactorily, in terms of an overlap of scientific ideas and results.

Regarding future field work, top priority must be given to investigations dealing with the circulation in the Nansen Basin and the interaction with the Amundsen Basin. This requires a crossing of the Amundsen Basin, i.e. from the mid-ocean ridge to the Lomonosov Ridge, with a program similar in scope and quality to that of ARK IV/3. There are, however, at present no firm plans to carry out that work. Detailed ideas for such work will emerge in evaluating and interpreting the present data set (Tables 3-7).

TABLE 3: List of Small-Volume Sampling for ARK IV/3, ARCHY87

Sta. No.	Date	Sound. depth (uncorr. Cast m)	Lat. °N	Long. °E	F	H	O	H	T	N	S	C	T	A	S	T
269	070787	199	81	16.3	31	24.2	x	x	x	x	x	x	x	x	x	x
274	080787	251	81	26.2	31	20.5	x	x	x	x	x	x	x	x	x	x
276	080787	571	81	31.4	31	27.4	x	x	x	x	x	x	x	x	x	x
278	080787	749	81	32.1	31	32.9	x	x	x	x	x	x	x	x	x	x
280	080787	1028	81	34.5	31	32.6	x	x	x	x	x	x	x	x	x	x
282	090787	1393	81	34.9	31	36.9	x	x	x	x	x	x	x	x	x	x
285	090787	1927	81	38.7	31	30.1	x	x	x	x	x	x	x	x	x	x
2871	100787	2795	81	41.0	31	10.2	x	x	x	x	x	x	x	x	x	x
2872	100787	2724	81	41.0	30	59.9	x	x	x	x	x	x	x	x	x	x
2961	120787	3014	81	49.2	31	35.1	x	x	x	x	x	x	x	x	x	x
2962	120787	3007	81	48.2	31	35.1	x	x	x	x	x	x	x	x	x	x
3101	130787	3056	82	09.5	31	52.8	x	x	x	x	x	x	x	x	x	x
3102	130787	3012	82	05.4	32	02.2	x	x	x	x	x	x	x	x	x	x
3401	170787	3784	82	59.3	31	58.9	x	x	x	x	x	x	x	x	x	x
3402	170787	3775	82	58.8	32	00.4	x	x	x	x	x	x	x	x	x	x
3403	180787	3743	82	56.5	32	09.4	x	x	x	x	x	x	x	x	x	x
3404	190787	3726	82	55.4	32	08.6	x	x	x	x	x	x	x	x	x	x
3581	200787	4044	84	01.6	30	37.2	x	x	x	x	x	x	x	x	x	x
3582	210787	4044	84	01.5	30	30.1	x	x	x	x	x	x	x	x	x	x
3621	260787	4037	85	04.2	29	17.8	x	x	x	x	x	x	x	x	x	x
3622	260787	4037	85	05.0	29	19.8	x	x	x	x	x	x	x	x	x	x
364	270787	3667	85	22.1	26	08.5	x	x	x	x	x	x	x	x	x	x
365	280787	3177	85	31.4	25	17.5	x	x	x	x	x	x	x	x	x	x
3701	310787	4536	85	53.8	22	45.8	x	x	x	x	x	x	x	x	x	x
3702	010887	5142	85	55.7	22	46.3	x	x	x	x	x	x	x	x	x	x
3711	030887	3324	86	03.4	21	56.7	x	x	x	x	x	x	x	x	x	x
3712	040887	3769	86	06.5	22	01.6	x	x	x	x	x	x	x	x	x	x
372	060887	3986	86	08.3	23	01.4	x	x	x	x	x	x	x	x	x	x
376	100887	2874	85	22.9	21	53.9	x	x	x	x	x	x	x	x	x	x
382	130887	4064	83	25.4	20	01.6	x	x	x	x	x	x	x	x	x	x
393	140887	3411	82	51.0	17	15.8	x	x	x	x	x	x	x	x	x	x
396	150887	1387	82	48.1	15	59.9	x	x	x	x	x	x	x	x	x	x
412	160887	2043	82	01.6	15	11.4	x	x	x	x	x	x	x	x	x	x
423	160887	2299	81	19.6	15	20.7	x	x	x	x	x	x	x	x	x	x
430	240887	2555	78	47.6	01	41.2	x	x	x	x	x	x	x	x	x	x

TABLE 4: Large-Volume Sampling for ARK IV/3, ARCHY87

ARK IV/3 Pump Casts				Station 11/287			
Cast # 1	07/10/87	Cast # 2	07/11/87				
Lat. 81° 40.85' N		Lat. 81° 38' N					
Long. 30° 53.42' N		Long. 30° 43' E					
Depth 2850m		Depth 2250m (+/- 100m)					
(deep pump ?? -100m)							
<hr/>							
Pump z (m)	Sample (liters)	Cast #	Pump #	Flow (l/min)	Start (gal.)	End (gal.)	Pump t (min.)
6	1459.7	0	ship	3.6	56.3	441.9	403
50	1305.6	1	4	4.4	130.4	475.3	300
100	1243.1	1	2	4.1	6614.1	6942.5	300
350	1106.5	1	3	3.7	2507.7	2800.0	300
400	1681.5	2	7	4.7	14910.0	15354.2	360+100m
500	1606.1	1	6	4.5	28231.6	28655.9	360
800	1605.0	1	7	4.5	14486.0	14910.0	360
1050	1588.7	2	6	4.4	28656.1	29075.8	360+100m
1450	873.7	2	8	2.4	6665.9	6896.7	360+100m
1650	1034.5	2	5	2.9	307.2	580.5	360+100m
1850	1174.2	2	4	3.3	475.3	785.5	360+100m
2050	684.0	2	3	1.9	2799.9	2980.6	360+100m
2150	769.2	2	2	2.1	6942.6	7145.8	360+100m
<hr/>							
ARK IV/3 Pump Casts				Station 11/358			
Cast # 1	07/21/87	Cast # 2	07/22/87				
Lat. 84° 01.74' N		Lat. 83° 58.14' N					
Long. 30° 38.80' E		Long. 29° 54.80' E					
Depth 4045m		Depth 4047m					
<hr/>							
Pump z (m)	Sample (liters)	Cast #	Pump #	Flow (l/min)	Start (gal.)	End (gal.)	Pump t (min.)
6	1802.2	0	ship	3.7	442.0	918.1	490
50	1427.9	2	4	4.3	817.2	1194.4	330
270	1656.5	2	8	5.0	7214.4	7652.0	330
400	1914.3	2	7	5.6	15712.8	16218.5	340
570	1646.6	2	6	5.0	29404.4	29839.4	330
870	117.0	2	5	0.4	822.4	853.3	330
1500	1193.2	1	8	4.0	6899.2	7214.4	300
2000	983.1	2	2	3.0	7339.6	7599.3	330
2500	1343.4	1	7	4.5	15358.0	15712.9	300
3100	1236.3	1	6	4.1	29077.8	29404.4	300
3400	908.5	1	5	3.0	582.6	822.6	300
3850	101.4	1	4	0.3	787.3	814.1	300
3950	687.1	1	3	2.3	2983.0	3164.5	300
4000	732.1	1	2	2.4	7146.2	7339.6	300
<hr/>							

## ARK IV/3 Pump Casts

Station 11/370

Cast # 1 08/01/87  
 Lat. 85 54.89' N  
 Long. 22 44.11' E

Depth 4810m (bottom varied + 130m, but wire out was fixed)

Pump z (m)	Sample (liters)	Cast #	Pump #	Flow (l/min)	Start (gal.)	End (gal.)	Pump t (min.)
6	1349.5	0	ship	3.1	918.5	1275.0	435
150	1056.1	1	3	3.2	3164.5	3443.5	330
275	1013.4	1	2	3.1	7600.9	7868.6	330
550	1496.0	1	8	4.5	7653.5	8048.7	330
1500	1363.5	1	7	4.1	16221.3	16581.5	330
2500	1373.0	1	6	4.2	29842.0	30204.7	330
3500	1117.1	1	5	3.4	853.4	1148.5	330
4500	985.3	1	4	3.0	1195.2	1455.5	

## ARK IV/3 Pump Casts

Station 11/423

Cast # 1 08/17/87  
 Lat. 81 19.85' N  
 Long. 15 18.89' E  
 Depth 2245m (bottom varied + 25m, but wire out fixed)

Pump z (m)	Sample (liters)	Cast #	Pump #	Flow (l/min)	Start (gal.)	End (gal.)	Pump t (min.)
6	863.4	0	ship	3.1	1276.9	1505.0	279
250	1200.7	1	8	4.0	8048.7	8365.9	300
750	1728.0	1	7	5.8	16581.5	17038.0	300
1400	1609.6	1	6	5.4	30204.7	30629.9	300
1650	1143.9	1	5	3.8	1149.0	1451.2	300
1900	1041.0	1	4	3.5	1455.3	1730.3	300

TABLE 5: List of Large-Volume Sampling for ARK IV/3, ARCHY87

Station: 11/269  
 cast 14C 85Kr 226Ra 228/226Ra 39Ar 90Sr 210Pb  
 1 x x

---

Station: 11/280  
 cast 14C 85Kr 226Ra 228/226Ra 39Ar 90Sr 210Pb  
 1 x x

---

Station: 11/289  
 cast 14C 85Kr 226Ra 228/226Ra 39Ar 90Sr 210Pb  
 1 x x x x x  
 2 x x x x x  
 3 x x x x x

---

Station: 11/340  
 cast 14C 85Kr 226Ra 228/226Ra 39Ar 90Sr 210Pb  
 1 x x x x x  
 2 x x x x x  
 3 x x x x x  
 4 x x x x x

---

Station: 11/358  
 cast 14C 85Kr 226Ra 228/226Ra 39Ar 90Sr 210Pb  
 1 x x x x x  
 2 x x x x x  
 3 x x x x x

---

Station: 11/362  
 cast 14C 85Kr 226Ra 228/226Ra 39Ar 90Sr 210Pb  
 1 x x x x x  
 2 x x x x x

---

Station: 11/371  
 cast 14C 85Kr 226Ra 228/226Ra 39Ar 90Sr 210Pb  
 1 x x x x x x  
 2 x x x x x x

---

Station: 11/382  
 cast 14C 85Kr 226Ra 228/226Ra 39Ar 90Sr 210Pb  
 1 x x x x x

---

Station: 11/423  
 cast 14C 85Kr 226Ra 228/226Ra 39Ar 90Sr 210Pb  
 1 1 x

---

TABLE 6: Nitrogen Isotopes Sampling (WHOI)

Stations and depths:

-----  
Sta. 310 40,88,118,220,550,1000,1450,2050,2575,3060m

Sta. 340 10m

Sta. 370 16,30,39,60,90,135,260,500,1500,3200,4510m  
-----

TABLE 7: Trace Metal Stations (UG)

Station numbers and number of samples levels

-----  
260:6 310:11 371:10  
278:9 340:25 376:10  
280:9 358:11 382:11  
282:7 362:11 393:11  
285:4 364:4 423:3  
287:9 365:4  
296:10 370:28  
-----

Trace Elements Samples taken for MIT

-----  
280:7 310:1  
282:7 340:15  
285:1 358:8  
287:1 362:6  
296:1  
-----

N.B. Samples at Stations 11/340 and 11/365 have been taken from  
the CTD-Rosette

## 6. BIOLOGICAL AND PALEONTOLOGICAL OBSERVATIONS

### 6.1 Introduction

Because of perennial ice cover, very low nutrients, the existence of two benthic communities (attached to the bottom of the ice and to the sea floor), and extreme seasonality, the Arctic basin is different from all other deep sea environments of the earth. Food chains are based on production of single-celled algae which grow only during the short Arctic summer. However, this food source is the basis for the entire system -- leading up to fish, seals, seabirds and polar bears, which have been observed several times during the cruise. How these different plants and animals are adapted physiologically to this very special environment to get maximum efficiencies and survival capability is not clear in all cases. The unique opportunity to penetrate the deep Arctic basin with the POLARSTERN was used by phytoplanktologists, zooplanktologists, fishery researchers, paleontologists and benthos biologists to look at discrete links of the food chain.

### 6.2 Phytoplankton Studies (RWTH)

During the POLARSTERN expedition of ARK IV/3 biological studies concentrated on measurements of primary production in the euphotic zone under well controlled temperature and light conditions and the preserving of duplicate samples for later microscopic analysis of phytoplankton distribution. Additional chemical analyses concerning protein and carbohydrate contents of the several phytoplankton populations with respect to their value as food supply for herbivores were performed. This work continues studies from previous POLARSTERN cruises in the Fram Strait area, going north into the Nansen Basin of the Arctic Ocean. The data are of critical importance not only for understanding the present day food chain but also in evaluating palaeoceanographic and paleoclimatic patterns.

#### Sampling

The following devices were used:

1. a handnet 10  $\mu\text{m}$  (0 - 30m)
2. a large rosette water sampler (6 x 30 liters)
3. a Secchi - disc for determining respective light depths (100%, 50%, 30%, 16%, 5%, 1%). These depths corresponded to rosette samples.
4. an underwater quantum-meter was used for making several measurements on light attenuation in water under changing ice conditions.

The goals of the sampling were:

1. determination of the qualitative and quantitative phytoplankton distribution.
2. estimation of primary production of natural phytoplankton populations using the  $^{14}\text{C}$  method under standardized light and temperature conditions. Light intensities provided ranged from 4.4 to 415  $\mu\text{E}/\text{cm}^2 \times \text{s}$ . Temperature was 0°C.

3. determination of the biochemical composition of the natural plankton population (chlorophyll, protein, carbohydrate, contents).
4. measurement of particulate organic carbon and particulate organic nitrogen.
5. cultivation of important algae species, autecological experiments and first determinations of their nutritional values for the zooplankton, especially Calanus hyperboreus female.

#### Station Work

Figure 31a gives an overview about the stations undertaken during the cruise and the kind of work done. The numbers indicate the depths in meters from where the samples were obtained. Additionally, light measurements were carried out under the ice and in the open water. Supplementary experiments were done on the productivity of a Melosira cf. arctica assemblage and of other algal populations in a meltpond, the underside of the sea ice, and on the sea ice surface.

#### First Statements on Primary Production

Figure 31b shows the results of the primary production estimations. As expected, production was mostly performed by phytoplankton smaller than 20 µm. This is due to the phytoplankton distribution: in the pack ice mostly small flagellates occur, whereas the occurrence of diatoms is mostly restricted to the bottom of the ice floes (Melosira cf. arctica) and polynyas (e.g. station 340). Production values are fairly high. Of course, the measurements only reflect the possible production as it would be in the natural water column without ice coverage. Based on the results of the autecological investigations and the "in situ" light measurements, one can say that the real production in the natural environment is about 1 to 10% of the values given here.

Additional results from selected samples:

1. The bottom of a meltpond on the sea ice: a society of algae with Melosira cf. arctica as its most dominant species had a productivity of 475 mg C/m<sup>2</sup> x d at 350 uE/m<sup>2</sup> x s. The salinity was only 0.09 ppt.
2. A red-colored patch on the sea ice surface: after melting its productivity was 87 mg C/m<sup>2</sup> x d at 350 uE/m<sup>2</sup> x s. These reddish-colored patches can be observed on snow in high mountains where they are mostly caused by Chlamydomonas nivalis, a volvocal chlorophyte.
3. The bottom of an ice core, (2 cm of 221 cm): after melting and, incubating at 56 uE/m<sup>2</sup> x s the production was 30.45 mg C/m<sup>2</sup> x d.

Future work will include: chemical analyses; a close study of the plankton populations (by light and electron microscope) and their individual physiological characteristics.

station	station- type	ice- cover	surface temp.	secchi- depth	primary production measurement	phytoplankton dis- tribution	POC PON	chem. anal.
269	ice	10/10	-1,5	22	0, 16, 25, 39, 60	0, 16, 25, 39, 60	0, 16	0, 16
274	ice	10/10	-1,4	22	-	0, 20	-	-
276	ice	10/10	-1,6	-	-	8, 20, 40, 60, 80,	-	-
280	ice	10/10	-1,3	27	0, 7, 10, 15, 25, 50	0, 7, 10, 15, 25, 50	0, 7	0, 7
282	ice	10/10	-1,7	30	-	0, 20, 40, 60, 80	-	-
285	ice	10/10	-1,7	30	0, 12, 21, 34, 53, 80	0, 12, 21, 34, 53, 80	0, 12	0, 12
287	ice	10/10	-1,6	30	0, 12, 40, 53, 80	0, 12, 40, 53, 80	0, 12	0, 12
296	ice	10/10	-1,2	28	0, 11, 20, 31, 49, 75	0, 11, 20, 31, 49, 75	0, 11	0, 11
310	ice	10/10	-1,1	18	-	0, 20, 32, 49	-	-
340	polynya	3/10	-0,7	24	0, 10, 27, 42, 65	0, 10, 27, 42, 65	0, 10	0, 10
358	ice	10/10	-1,6	20	0, 8, 14, 22, 35, 54	0, 8, 14, 22, 35, 54	0, 8	0, 8
362	ice	10/10	-0,6	19	0, 8, 14, 21, 34, 52	0, 8, 14, 21, 34, 52	0, 8	0, 8
364	ice	10/10	-1,3	19	-	10, 20, 30, 40, 50, 60	-	-
365	ice	10/10	-0,8	27	-	25, 50, 75, 100	-	-
370	ice	10/10	-0,8	22	0, 9, 16, 25, 39, 60	0, 9, 16, 25, 39, 60	0, 9	0, 9
371	ice	10/10	-0,8	18	0, 7, 13, 20, 32	0, 7, 13, 20, 32	0, 7	0, 7
372	ice	10/10	-0,7	22	0, 9, 16, 25, 39, 60	0, 60, 51, 55, 77, 100	0, 9	0, 9
376	ice	10/10	-0,6	19	0, 8, 14, 21, 34, 52	0, 8, 14, 21, 34, 52	0, 8	0, 8
393	ice	8/10	-1,0	17	0, 7, 12, 19, 30, 46	0, 7, 12, 19, 30, 46	0, 7	0, 7
396	ice	8/10	-	-	-	35, 50, 70, 90	-	-
412	ice	8/10	-1,6	19	-	6 standard- depths	-	-
423	ice	8/10	-1,5	20	-	6 standard- depths	-	-
430	ice	5/10	-0,7	16	-	6 standard- depths	-	-

Fig.31 a)Station list RWTH Aachen.

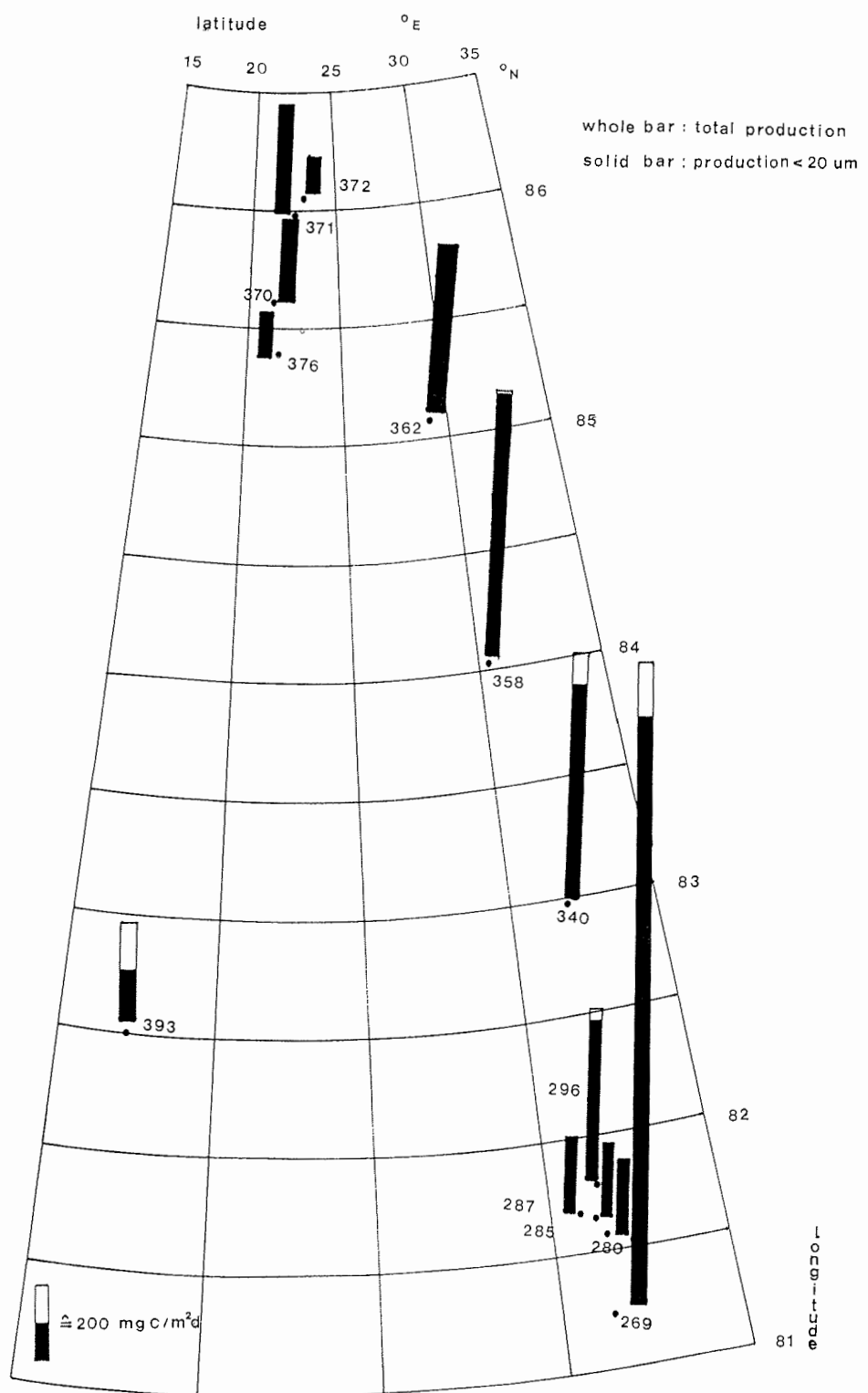


Fig.31 b) Primary production ARK IV/3 integrated over the euphotic zone.

### Scientific Plans for Future Expeditions

This expedition gave us the chance to investigate plankton occurrences in a region of almost total year round ice cover in waters with a low nutrient level. For future expeditions, special attention should be given to the phytoplankton smaller than 20 um and the importance of ice algae and their contribution to primary production. Very little is known about the survival strategies of the algae and their life and development cycles in the Arctic. Investigations should be carried out on the availability of the phytoplankton as food for the zooplankton as this also would contribute to the explanation for the high productivity of the polar regions.

### **6.3 Dinoflagellates, Pollen/Spore Assemblages and Related Studies (AGC/BIO, GIK, AWI)**

#### Introduction

Previous studies suggest that dinoflagellate cysts and pollen-spore assemblages are useful microfossils for dating and paleo-ecological analyses of Arctic Ocean sediments in the Alpha Ridge (Mudie 1985; Aksu & Mudie 1985) and Fram Strait areas (Robertsson 1984). Organic-walled dinocysts, pollen and spores are very resistant to dissolution and they are often the main microfossils in siliciclastic sediments of the Arctic region. In Alpha Ridge cores, dinocysts show cyclical variations between "Atlantic" assemblages dominated by gonyaulacoid cysts (mainly Operculodinium centrocarpum, Spiniferites elongatus) and high arctic assemblages dominated by peridinioid cysts (mainly Multispinula minutula, Brigantedinium simplex). These cycles broadly correspond to glacial-interglacial cycles as determined by oxygen isotopic data (Mudie 1985). Pollen-spore assemblages also show similar cycles of increased boreal tree pollen influx (Picea, Abies) during interglacial stages and dominance of subarctic shrub (Betula, Alnus) and tundra species (Gramineae, Polytrichum) during glacial stages.

The apparent paleoenvironmental value of the palynomorphs, however, is presently limited by uncertainties about their origin and mode of transport in the Arctic Ocean. Thecate-stage (i.e. planktonic-stage) dinoflagellates are known to live in Arctic waters and ice (Horner 1985) but these organisms have cellulose walls which do not survive as fossils in the sediments. The fossilizable resting-stage cysts of these thecate dinoflagellates have rarely been found in Arctic plankton tows, and some palynologists (Dale, pers. comm. 1986) argue that all dinocysts in Arctic sediments are the result of advection in water masses from Subarctic regions. It has also been suggested that all pollen-spore assemblages in deep water Arctic Ocean sediments are the result of reworking from ice rafted or shelf sediments. In contrast, studies of pollen distributions in snow/ice samples strongly suggest that these palynomorphs are unique tracers of paleowind directions in the high Arctic (Bуржоис et al. 1985).

A primary purpose of the biological studies on the ARK IV/3 cruise therefore was to obtain data which address the following questions.

1. What species of dinoflagellates live in the surface water layer of the eastern Arctic Ocean and do these species form cysts in this environment?
2. What is the relation between dinoflagellates in Arctic Ocean surface waters and recent dinocyst assemblages on the seabed?
3. What is the relation between the pollen-spore composition of the annual snow/ice cover, surface water layer und surface seabed assemblages?

#### Methods

Samples of snow, ice, surface water and seabed surface sediment were obtained at 20 stations on two transects across Nansen Basin (Fig. 32) and at a few sites in Fram Strait. Details of the methods used for the snow/ice studies are reported in Chapter 4.3. Methods used for sediment sampling and processing are described in Chapter 7.8. The surface water samples were obtained with the membrane pump system located in the bow of the POLARSTERN, with the intake at 6.5 m below the water-line. The membrane pump operates by movement of a rubber gasket that pumps water directly through PVC pipes into a wet lab on E deck. The pump delivers a maximum volume of >7.0 l/min, the outflow rate of which can be regulated in the lab by a faucet valve. Prior to sediment sampling at each station on the ARK IV/3 cruise, the membrane pump was used at a flow rate of ca. 1 l/min. to obtain 60-450 l samples which were filtered directly through a nylon sieve with mesh openings of 20  $\mu\text{m}$ . This filtrate was then preserved in methanol for study of dinoflagellates, pollen and spores. At each oceanographic (CTD) station, a second larger water sample (4 l/min. flow rate for 1-2 h) was filtered through a nylon sieve with 40  $\mu\text{m}$  mesh openings, after which the filter was stored in methanol and kept in cold storage ( $1^\circ\text{C}$ ) for post-cruise studies of siliceous plankton (radiolarians, silicoflagellates and diatoms).

During the ARK IV/3 cruise, subsamples of the preserved >20  $\mu\text{m}$  phytoplankton samples from selected stations at the ends and centre of the transect lines were washed with distilled water concentrated by centrifuging at 5000 rpm for 5 min. The concentrated samples were then mounted in glycerine gelatin for preliminary shipboard studies of dinoflagellate and pollen-spore numbers and species composition. The slides were examined by light microscopy at magnifications of x320 to x1600.

#### Initial Results

1. Surface Water Samples. Thecate-stage dinoflagellate populations ranging from 33 - >2000 individuals/m<sup>3</sup> were observed, with numbers first increasing seawards over the continental slope to

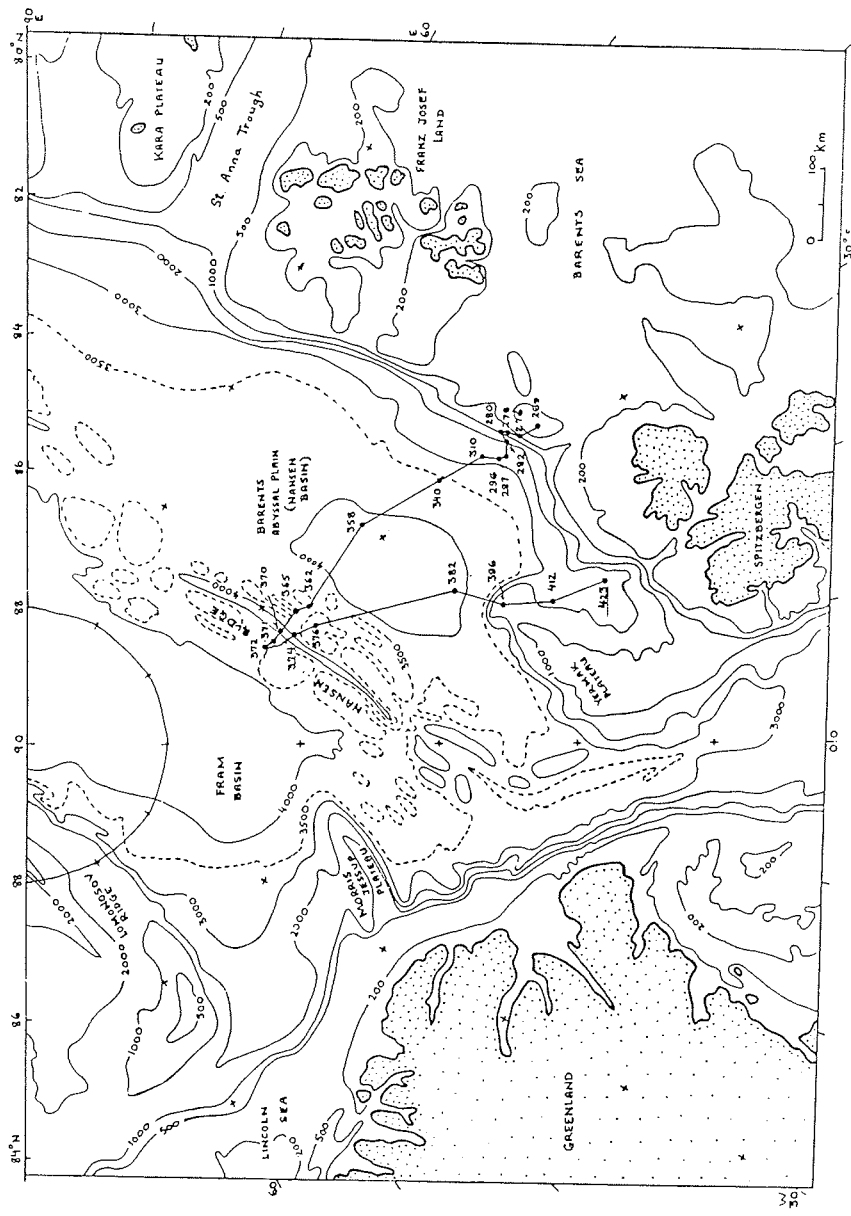


Fig.32 Bathymetric map showing locations of sample stations

reach maximum values at Stations 11/358-362, followed by a decline in numbers to a minimum at Stations 11/371-376 (Fig. 32). Postcruise studies, using special techniques to clear the cell walls, SEM and TEM microscopy, are necessary to make accurate taxonomic investigations of these phytoplankton. Shipboard studies, however, showed that the living dinoflagellate flora is clearly dominated by Protoperidinium species, including the cyst-forming taxa, P. conicum, P. faeroense and P. pallidum, of which only cysts of P. faeroense were found in the samples examined. Thecate and cyst-forms of Diplopsalis lenticulata were found at the continental margin sites, and small numbers of Gonyaulax species were found at Stations 11/269, 358 and 412, together with rare cysts of O. centrocarpum. At Stations 11/371-376, large numbers of a small unicellular alga tentatively identified as an Archeomonas species were found together with a bright-red alga (cf. Chlamydomonas nivalis) and a non-pigmented organic-walled alga resembling the dinocyst genus Cyclopsiella. The biota is abundant in the ice cover at these sites and it appears to constitute a unique multiyear ice flora (see Chapter 4.3 for details).

2. Surface Sediment Samples. Numbers of dinoflagellate cysts and archeomonads in the surface samples of GKG box cores range from ca. 6-90 specimens/cm<sup>2</sup> wet sediment, with maxima occurring at the continental slope sites on both the eastern (Stations 11/276-280) and western (Stations 11/396-423) transects of the Nansen Basin. Based on the known distributions of recent dinocysts in the North Atlantic and western Arctic (Mudie & Short 1985; Mudie 1985), together with the new ice flora data, three ecological cyst groups were distinguished, as shown in Fig. 33 and defined below.

- A. "Atlantic" flora, characterised by the gonyaulacoid cysts O. centrocarpum, S. elongatus (including S. frigidus & intergrades) and Nematosphaeropsis labyrinthaea;
- B. Circum-Arctic flora, characterised by the peridinioid cysts M. minuta, Brigantedinium species and a glenodinioid cyst form, Dinocyst sp. R;
- C. Multi-year ice flora, characterised by archeomonads, cf. Cyclopsiella and cf. Chlamydomonas nivalis.

The relative abundance of these ecological indicators shows a systematic change along the transects, with "Atlantic" species tending to prevail in the continental margin sites and with the ice flora prevailing north of 83° N, becoming totally dominant at ca. 86° N. Further studies are required to confirm these shipboard observations (see Chapter 7.8); however, the apparent similarity between the distributions of the "Atlantic" dinocysts and subpolar foraminifera suggests that similar oceanographic parameters control the distributions of the two plankton groups.

3. Pollen-spore Assemblages. Very low numbers of pollen and spores were found in both the surface water samples (6-30 grains/m<sup>3</sup>) and surface sediment samples (1-7 grains/cm<sup>3</sup>). This observation is consistent with previous studies (Mudie 1985; Burgeois et al. 1985) which indicate that the annual influx to

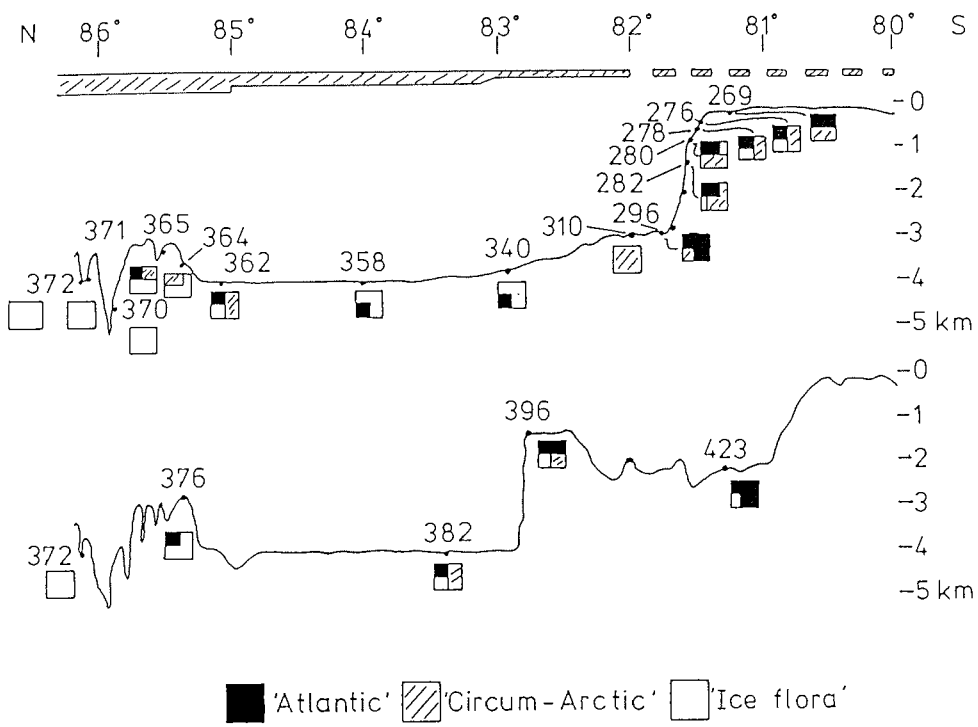


Fig.33 Profiles of the western (top) and eastern (bottom) transects across Nansen Basin, showing the changes in dinocyst assemblage composition of the seabed surface sediments in relation to bottom topography and sea ice cover (hatched lines at top of diagram).

Arctic sea ice is on the order of 200-1000 grains/m<sup>2</sup>/yr. Furthermore, the pollen flora in the ARK IV/3 surface water samples is composed entirely of boreal bisaccates (*Pinus*, *Picea*) and typical Subarctic/tundra indicators, e.g. *Betula nana*, *Gramineae*, *Rumex*, and *Sphagnum*. The composition of the pollen flora thus resembles that of the circum-Arctic region and there is no indication of large influxes of temperate climate species from either aeolian or subsurface water mass transport.

#### Conclusions

1. Preliminary shipboard results of the ARK IV/3 cruise show that living peridiniod and gonyaulacoid dinoflagellates occur in the eastern Arctic Ocean and that some of their cyst-stages occur in the surface water layer formed within the ocean basin. The area of largest populations broadly corresponds to that of the diatom maximum in the central Fram Basin, while the area of highest primary productivity in the multi-year ice at the northern end of the transect corresponds to the area with maximum numbers of archeomonads and red snow algae.
2. Dinocyst assemblages in the surface sediment layer show a predominance of "Atlantic" species below the saline wedge of Atlantic water on the basin margin which also corresponds to the area of thinner sea ice and more open water in summer. A unique multi-year ice flora characterises the region from ca. 83°-86° N.
3. Pollen-spore numbers and composition in the surface water and seabed sediments indicate a primary aeolian source, with the flora circum-Arctic boreal-tundra vegetation.

#### **6.4. Horizontal and Vertical Distribution of Planktonic Foraminifers and Pteropods on a Transect from the Barents Shelf to the Nansen-Gakkel Ridge (FG/UB)**

While the distribution of planktonic foraminifers in the world ocean is quite well known and described from various authors, very little information exists on living Arctic planktonic foraminifers (Be' 1960), especially from the area north of Svalbard. As planktonic foraminifers are important in micropaleontology, understanding their life cycle is necessary for deciphering the sediment record.

#### Methods

Investigations on the distribution of planktonic foraminifers were carried out using a "Kiel-Multinet", opening 0.25 m<sup>2</sup>, 63 µm mesh. Plankton hauls were done at the following stations (Fig. 34):

11/269	282	340	376
274	285	358	382
276	287	362	393
278	296	370	412
280	310	371	

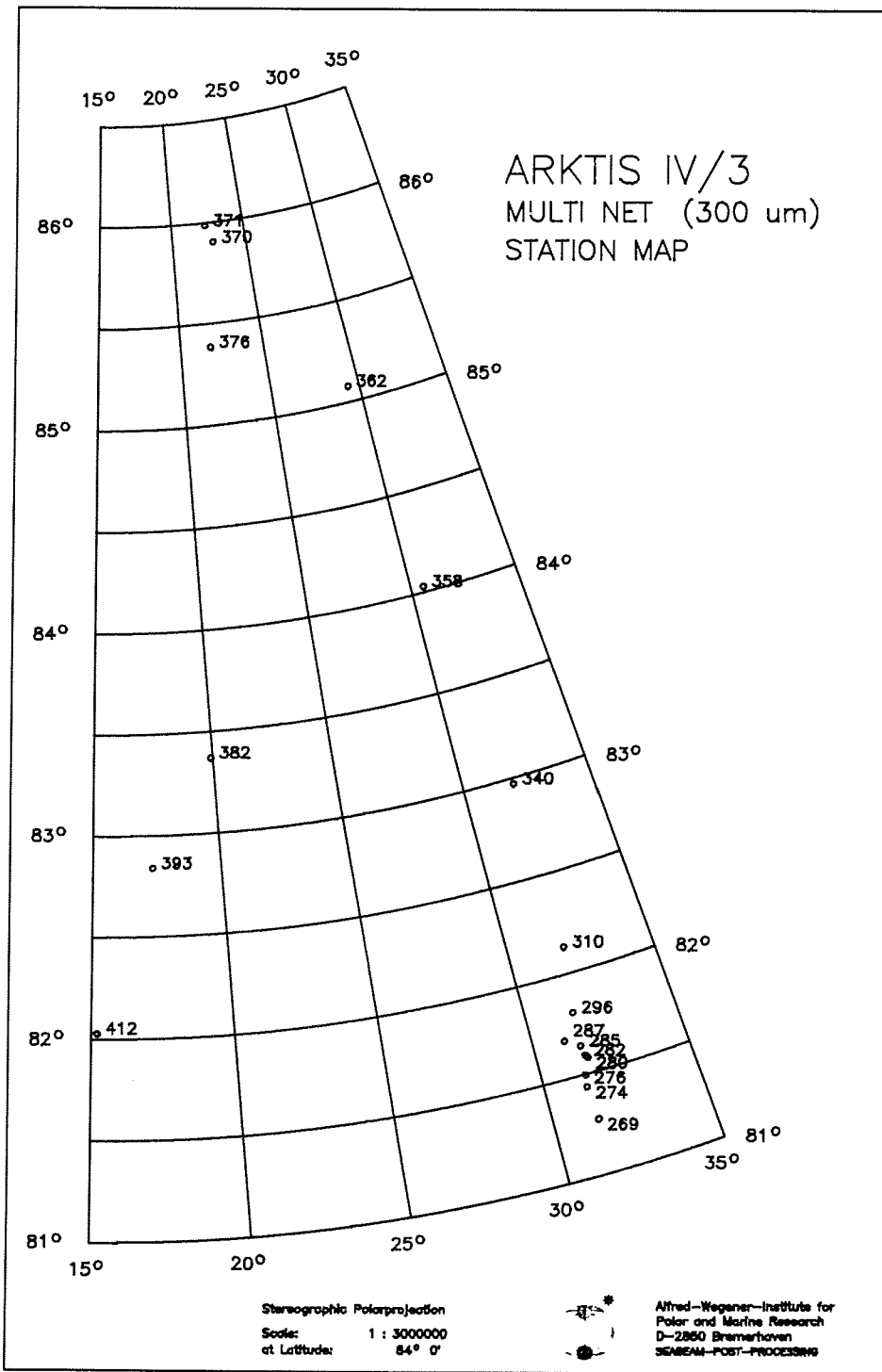


Fig.34 Map of station locations of Multi Net (300  $\mu\text{m}$ ) width deployments on ARK IV/3. For station locations see Krause et al. (in press).

Generally the following depth intervals were sampled:

0 - 50 m  
50 - 100 m  
100 - 200 m  
200 - 300 m  
300 - 500 m

For the Stations 11/296 and 11/274 the following intervals were sampled:

0 - 25 m  
25 - 50 m  
50 - 100 m  
100 - 150 m  
150 - bottom

Station 117282 had the same intervals, but with a maximum depth of 200m.

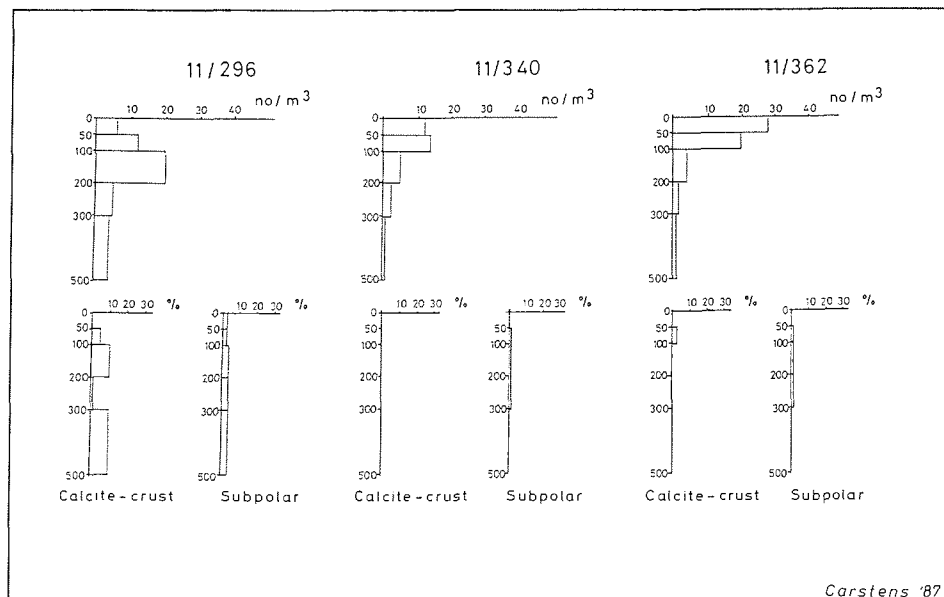
Samples were preserved in a 4%-formalin-seawater solution and stored at sampling temperature. A few samples were prepared on board. The specimens were picked out individually under a binocular microscope at 63x magnification. They were counted, the polar/subpolar and the dead/living ratios were calculated and the proportion of heavy encrusted specimens estimated.

#### Preliminary Results

Samples are always dominated by Neogloboquadrina pachyderma. Globigerina quinqueloba was also observed with co-occurring individual specimens of Globigerina bulloides and Globigerinita. The latter is always smaller than 125 um. Subpolar forms never exceed 10% of the sample. Stations situated at the shelf and upper slope contained a few benthic foraminifers. They are very small in size, translucent and well preserved. It is as yet uncertain if they are reworked from bottom currents or if they have come from the ice. The distribution of pteropods is patchy, and living ones are only found in the upper 50 m of the water column. In general they seem to be more abundant south of 83° N.

The maximum abundance of planktonic foraminifers (Fig. 35) is 28 specimen/m<sup>3</sup> at station 362 in the upper 25m, the mean from other stations is 15 specimen/m<sup>3</sup>. The portion of dead individuals is lower than 5% in all samples. Heavy encrustation is only observed in the southern stations. The size of planktonic foraminifers decreases north of Station 11/296 to smaller than 125 µm and they prefer a shallower life habit. Parallel, the amount of subpolar species is diminished by 1%.

A general change in species composition and life cycle of planktonic foraminifers takes place at a distinct boundary near 83° N. Other investigations on zooplankton showed a similar change, most likely reflecting a change in the water regime (c.f. Chapter 5.). A major faunal change is also observed in the benthic assemblage, and it may also be observed in the sediment record. Understanding the reasons for the boundary will aid in



*Carstens '87*

Fig.35 Distribution of planktonic foraminifers in Arctic plankton net of ARK IV/3.

interpretation and dating the cores. For example, as the southern fauna seems to be influenced by Atlantic waters, we should expect faunal variations through time similar to those observed in the North Atlantic sediment cores.

#### Future Work

Detailed work will be carried out to identify species composition and morphotypes. Of high priority is determination of stable isotope composition of these species. The influence of the faunal change on the sediment record will be calculated.

#### Consequences for new expeditions

As plankton tows show only a short time segment of the assemblage, detailed time-series sampling is required to fully understand the living populations. The strong seasonality which occurs at such high latitudes makes time-series sampling especially important. Time-series sediment traps, used successfully before in the Fram Strait and the Norwegian-Greenland Sea, would provide much information on this little-known region. In particular, a detailed study should be undertaken on the faunal shift at 83° N, including a comparison with the sediment record.

A continuation of the profile, northward over the Nansen-Gakkel Ridge and into the Canada Basin, would give further information on the distribution of the living population.

#### **6.5 Zooplankton: MULTINET Catches (IPō)**

Biological research in the Arctic dates back to the mid-1890's. With their vessel FRAM frozen in the pack ice, F. Nansen and his crew discovered the Transpolar Drift on a three year voyage across the eastern Arctic Ocean. Extensive hydrologic and biologic sampling were carried out from the drifting ship. Since then, large moving ice floes have been used as natural research platforms.

Long term observations from Canadian, North American and Soviet Union drifting ice stations provide information on zooplankton species composition and on seasonal and diurnal vertical distribution patterns of the most abundant metazoans of the polar seas: copepods. Confined to the drifting routes, this research mainly covered the American and Asian part of the Arctic Ocean. Thus, very little is known about the area north and northeast of Fram Strait. The transect from the Barents Sea shelf up to 86° N during ARK IV/3 provided a unique opportunity for a zooplankton survey in this transition zone. Changes in water mass distribution, increase in thickness and duration of ice cover and, as a consequence, marked shortening of the pelagic primary production season are considered to be major factors influencing species composition and physiological state of zooplankton.

### Methodology

Vertical hauls with a multiple closing net ('KIEL MULTINETZ', 0.25 m<sup>2</sup> net opening, 300 µm mesh size, approximately 0.5 m/s hauling speed) were carried out during geologic and oceanographic station work (Fig. 34). Maximum hauling depth was 500m, and samples were obtained at five standardized depth intervals on all stations deeper than 500m (Table 8). The contents of each net was fixed with buffered 4% formaldehyde-seawater solution immediately after the haul.

In total, 19 hauls on 18 stations from 07/07 to 15/08/87 between 81° 16' N and 86° 09' N yielded 90 zooplankton samples.

### Preliminary Findings

Only crude observations made during processing of the catch can be reported at this time. Zooplankton standing stocks in the permanently ice covered area were generally low, decreasing towards the northernmost stations. Highest abundances were mainly encountered in the upper two nets (50-25-0m) within the Arctic surface water whereas species diversity seemed to be higher at greater depths in water of Atlantic origin. Preliminary examination showed that copepods were the predominating metazooplankton organisms, followed by chaetognaths (arrow worms) and occasionally ostracods.

A faunistic boundary between 83° N and 84° N was noticeable in the upper 100m for copepods (Calanoidea). To the south, high numbers of copepod developmental stages (despite coarse mesh size) and adult females of the Atlantic species C.finmarchicus dominated the catches. North of approximately 84° N C.glaucis became the most conspicuous copepod, accompanied by C. hyperboreus and Metridia longa.

A similar boundary phenomenon was observed for the deeper living single cellular foraminifers (Chapter 6.4). Besides copepods, additional species from MULTINET catches will be screened for analogous patterns.

Euphausiaceans (genus Thysanoessa) and hyperiid amphipoda (e.g. genus Themisto) were caught in small numbers in the deepest nets (500-100m). Amphipods (Gammaridae) of the sympagic ("with ice") fauna which had been seen frequently in surface waters close to ice floes did not occur in the samples. Net avoidance might explain the absence of these relatively large crustaceans from MULTINET catches.

Detailed information on species composition, abundances and depth distribution in relation to water masses will be available after taxonomic examination of samples following this cruise.

TABLE 8: MULTINET stations and fishing depths

#	Station	Fishing depth (m)	Water depth (m)
01	269	200-100-50-25-10-0	200
02	274	230-150-50-25-10-0	246
03	275	500-200-100-50-25-0	575
04	280	"	897
05	282	"	1392
06	285	"	1905
07	287	"	2700
08	296	"	3008
09	310	"	3039
10	340	"	3788
11	"	200-100-50-25-10-0	3730
12	358	500-200-100-50-25-0	4045
13	362	"	4038
14	370	"	4611
15	371*	2500-2000-1500-1000-500-0	3611
16	376	500-200-100-50-25-0	2898
17	382	"	4065
18	393	"	3230
19	412	"	2043

\* :nets did not open, no samples

## **6.6. Production and Assemblages of Calanoid Copepods in the Arctic Ocean (IfMK)**

Herbivore calanoid copepods are important members of the Arctic food-chain. Egg production rates in non-growing copepod females may be used as a direct measure of net production, and are therefore important in understanding productivity. Egg production and diversity also reflect environmental quality by responds to food- and physico-chemical variables. During pre-MIZEX '83, MIZEX '84 and ARK IV/1,2 '87 egg production rates of *Calanus finmarchicus*, *Calanus hyperboreus*, *Calanus glacialis* and *Mitridia longa* were measured in the pack-ice zone of the east Greenland shelf, the Greenland Sea and the Yermak Plateau. During ARK IV/3 egg production-rates of calanoid copepods were measured using methods modified for the thick pack-ice and low food concentrations of the Arctic basin.

### Methods

Live copepods were caught with a bongo-net (300- and 500 µm mesh-size). The net was lowered to 80m depth and hauled at a rate of 0.5 m sec<sup>-1</sup>. While the 300 µm catch was obtained for biomass determination the 500µm catch was diluted with surface water. Sampling procedure did usually not last more than 10 min. For egg production measurements, 30 to 100 copepod females of the dominant species were identified under the microscope from the 500 µm net sample. The female copepods were transferred into a seawater filled 2 l plexiglass cylinder with a 330 µm mesh at the bottom, permitting the eggs to sink out and escape predation by the females. After 24h of incubation in the cold-room, the females were removed, preserved in 4% buffered formalin and eggs were counted. When egg production occurred due to bad food conditions, 20 females of each species were introduced to high food levels for experiments.

Other analyses were as follows: for gut-fluorescence measurements 2x10 *Calanus hyperboreus* females and *Calanus hyperboreus* CV were stored deep frozen (-66°C); long-term feeding and starving experiments were also made during the cruise; in-situ chlorophyll fluorescence was measured with a fluorescence-probe connected to the bongo-net during the haul, and profiles were registered on a chart-recorder, and seawater of the upper water-layers was filtered and filters were kept frozen for phaeopigment analysis.

### Stations

11/269, 274, 276, 280, 285, 287, 296, 310, 340, 358, 362, 370, 371, 372, 376, 382, 393, 432 (for locations, see Fig. 2a).

### Preliminary Findings

In the field, eggs were only observed to spawn on Station 11/382, obtained in an area of open water. A small *Chaetoceros*-bloom was measured at this station, while on all other stations no eggs were laid because of low food-conditions. Egg production was

induced in the dominant species of each station by feeding the females in the laboratory, but it took 4 to 11 days to attain egg production.

Fluorescence rapidly decreased on the way into the dense pack-ice: values were under 1000 while Fram Strait is around 18000. Biomass was low. On the transect from the shelf to the Nansen-Gakkel Ridge and on the way back, a Subarctic-Arctic faunistic boundary between 83° and 84° N could be detected. The Subarctic fauna on the shelf regions are from an under-ice Atlantic water-influenced environment and 90% of the catch were developing stages with a few Calanus hyperboreus, Calanus finmarchicus and Mitridia longa females. In the real Arctic water regions to the north, Calanus glacialis, Mitridia longa and Calanus hyperboreus females dominated. Calanus finmarchicus and developing stages were missing or rare on the northernmost stations.

#### Future Work

Gut-fluorescence, lipids and phaeopigment analysis will show under what circumstances and food variables these northernmost species live in the Arctic water. New expeditions to this area should focus on determining when and how copepod females reproduce and how developing stages overwinter in these areas of extreme food shortage.

#### **6.7 Polar Cod Ecophysiology (IPō)**

The benthic fauna of the Arctic Ocean is very poor in comparison to adjacent shelf areas. The generally great depths mean that little food is available to bottom living fish species. Surface waters, enriched by syagic ("with ice") fauna (mainly crustaceans), offer a concentrated food supply even under permanent ice cover.

The Polar Cod (Boreogadus saida), a relative of the boreal gadoid fish species, is a very successful inhabitant of this environment. Living in channels and crevices of the high Arctic pack ice, it is the only fish to occur in large numbers in the Polar Basin. During summer, Polar Cod constitutes the staple food of seals and sea birds in this region. Spawning and development of the larval stages take place during winter in the shallow coastal waters of Siberia and Alaska.

Contact with ice during summer and exposure to harsh environmental changes between spawning places and feeding grounds suggest unique adaptations although physiological aspects of the cryopelagic life of Polar Cod are hardly known.

During ARK IV/3 it was planned to catch specimens for shipboard experiments, for analysis of stomach samples and for histological and biochemical examinations.

### Fishing Methods

Long stations for geologic and oceanographic sampling ( $\geq 12\text{h}$ ) provided excellent opportunities to set out fishing rods and fish traps. Fishing rods were launched through drill holes and small cracks within the sea ice. Artificial copepod decoys attached to the fishing seine were used to try to attract Polar Cod optically. Hooks were moved up and down during fishing either manually or by means of surface-mounted swimmers. Fishing depth varied between 2m and 20m.

Fish traps were either attached to a swimmer for deployment from the ship or were launched into small leads directly from the sea ice. Depth was adjusted between 3m and 6m, depending on ice thickness.

Attempting to attract living prey organisms of Polar Cod, fish traps and occasionally fishing rods were baited with dead shrimp, fish gut and fish filet.

Two double-oblique hauls (0m-50m-0m) were carried out with a BONGO net in open water on the northwestern coast of Svalbard. Another horizontal BONGO haul was done in open pack ice in the Fram Strait area (fishing depth approximately 0m-10m).

### Shipboard Observations

During daily observations Polar Cod was seen frequently. It was either washed onto ice floes by the moving ship or picked up by seabirds from open water behind the ship. In open pack ice and leads Polar Cod could be observed close to individual floes when leaving or entering channels/crevices.

Estimated length of sighted specimens varied between 8cm and 15cm. Small Polar Cod ('young-of-the-year'?) tended to be light-yellowish whereas larger specimens were much darker, almost black. High numbers were encountered at the ice edge when the ship entered and left the pack ice. Besides these observations, no clear distributional pattern emerged along the cruise track (Table 9).

Although Polar Cod seemed to be present at nearly every station not a single fish was caught. The only sample obtained during the whole cruise were the bones of one specimen which obviously had been eaten by a seabird. A seagull or fulmar probably spit out the undigestible skeleton.

Despite reports from coastal areas of Canada and Greenland on successful Polar Cod capture with fishing rods, this method does not seem to be appropriate in the high Arctic pack ice. Horizontal hauls close to the surface with a bigger net might catch sufficient numbers of Polar Cod in open pack ice. Living fish from net hauls often have a damaged mucus layer and will suffer from infections if kept in aquaria, however. If station time allows, fine-meshed drifting nets possibly could provide

Polar Cod in good condition. Scuba diving with hand nets could yield healthy specimens offering the additional advantage of direct under-ice observation.

TABLE 9: Polar Cod Observations

Date	Lat. (°,')	Long. (°,')	Station	Observations	Remarks
06/07	77.48 N	029.42 E	-	*	
07/07	81.16 N	031.25 E	269	+	
08/07	81.32 N	031.29 E	-	+	
09/07	81.35 N	031.38 E	280	-	
10/07	81.36 N	031.32 E	282	-	
10/07	81.39 N	031.30 E	285	+	
10/07	81.41 N	031.07 E	287	+	
12/07	81.50 N	031.40 E	-	*	YOY
13/07	82.08 N	031.56 E	310	+	
17/07	82.58 N	031.59 E	340	-	
19/07	83.30 N	031.10 E	-	+	
21/07	84.01 N	030.36 E	358	+	
23/07	84.25 N	030.00 E	-	+	
24/07	84.30 N	030.00 E	-	-	
28/07	85.27 N	024.57 E	-	-	
30/07	85.49 N	024.24 E	-	+	bones recovered
31/07	85.54 N	022.43 E	370	+	
06/08	86.08 N	022.48 E	-	-	
07/08	86.06 N	023.12 E	-	-	
08/08	85.59 N	023.41 E	-	-	
09/08	85.51 N	023.08 E	-	-	
10/08	85.34 N	021.49 E	-	-	
10/08	85.25 N	021.53 E	-	*	YOY
11/08	84.55 N	022.10 E	-	+	
12/08	84.40 N	022.09 E	-	-	
13/08	84.01 N	020.53 E	-	+	
15/08	82.40 N	015.43 E	-	+	
16/08	81.20 N	015.24 E	-	+	
16/08	81.20 N	015.20 E	423	+	
17/08	81.00 N	015.57 E	-	*	YOY, ice edge
18/08	79.33 N	010.57 E	-	+	Magdalena-Fjord
19/08	79.07 N	002.16 W	-	+	Fram Strait
20/08	79.03 N	007.35 W	-	+	Fram Strait

- : none observed

+ : present

\* : abundant

YOY: 'young-of-the-year' ?

## **6.8 Ecology, Biology and Paleoecology of Benthic Foraminifers (GIK, UTÜ, IfMK)**

Recent investigations of deep sea benthic foraminifers of the North Atlantic (NOSOFO-Project/GIK; Sonderforschungsbereich 313; BIOTRANS/UTÜ) provided much new information on the ecology and biology of distinct species of foraminifers. Unfortunately, information on Arctic deep sea foraminifers is very restricted. For paleontologists, foraminifer species are useful which are found in deep sea sediment cores to reflect environmental fluctuations during glacial/interglacial periods. Therefore, investigations in the high Arctic Ocean environment, with permanent ice cover, low productivity and extreme seasonality, should increase knowledge on the biology and structure of Arctic populations and provide basic information for interpretation of faunal fluctuations in fossil assemblages.

### Methods

Samples of the sediment surface (Fig. 36) were taken with giant box grabs (GKG, 50x50x60cm). The biocontainer of the Sonderforschungsbereich 313 (Kiel University) was used for scanning the surface for living foraminifers and possible food particles with a binocular microscope, and video documentation of *in situ* observations of live positions. Living forams were isolated and fixed (glutaraldehyd/osmiumtetroxyde) for TEM-observations on protoplasm and food vacuoles. Small amounts of surface sediments (1 to 20 cm) were used for onboard studies of taxonomy and protoplasm activity, measurement of organic carbon and detection of bacterial biomass in the microhabitats of benthic foraminifers. For the investigation of assemblages and abundances, 400 cm surface samples were treated with methanol/bengalrose for fixation and staining of living individuals. One centimeter slices of deeper parts of the sediment (down to 10cm) were stained for observations of the depth settlement of infaunal species. X-ray photographs were made for the depth location of single individuals in undisturbed vertical sediment slices.

### Stations

The full program described above was conducted at Stations 11/269, 276, 278, 280, 282, 285, 287, 296, 310, 340, 362, 371, 376 and 396. Sediments for X-ray photographs and bacterial/microfaunal biomass were sampled at Stations 11/358, 362, 370, 371, 376 and 392 only. Due to time constraints, only one methanol/bengalrose sample was recovered from geologic-purpose GKG sediments at Stations 11/358, 364, 365, 370, 372, 382, 423 and 430.

### Preliminary Observations

First results indicate that the foraminiferal fauna is very rich and comprises at least 150 to 170 different species. Based only on the observation of living foraminifers, the assemblages on the

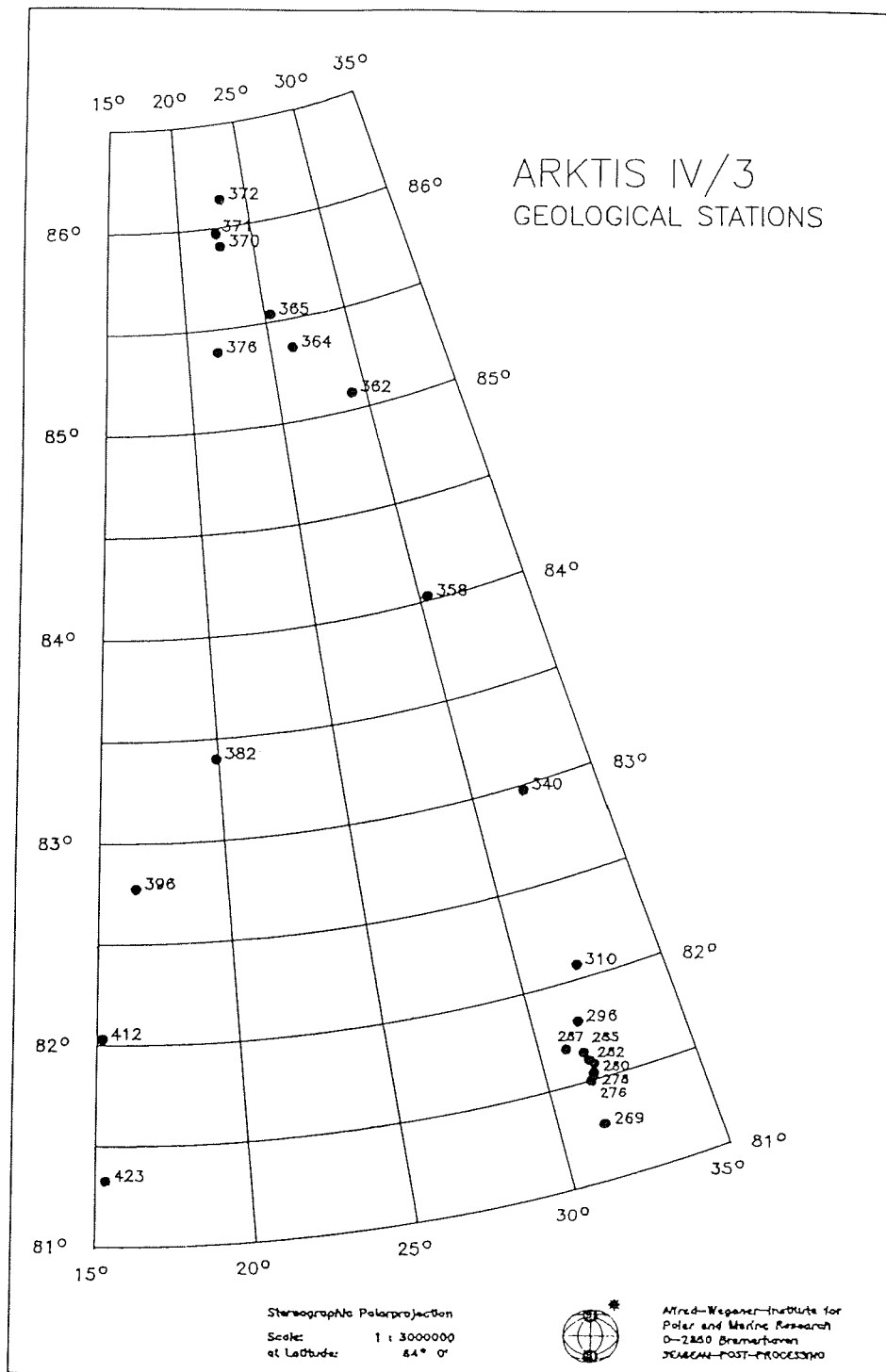


Fig.36 Map of geological station locations obtained on ARK IV/3. For station locations see Krause et al. (in press)

Svalbard/Nansen-Gakkel Ridge transect can be subdivided into 3 major groups, called Facies 1 to 3 in Fig. 37. Facies 1 is located along the continental shelf and slope (stations 11/269-310). The main species are well known from the Norwegian slope and continental margin, and no major differences were visible in foraminifers, other benthos or sediments. Rupertina stabilis populations indicate high and turbulent bottom currents at 700 m waterdepth and Cibicidoides wuellerstorfi was observed as epizoic, in biofacies similar to those of the Norwegian sea (see also cruise report ARK III/5).

A relative increase in Oridorsalis sp. and Epistominella sp. is detectable in Facies 2. Total abundances decrease rapidly, especially in the fraction greater 250 µm, and most common species from Facies 1 disappear.

Facies 3 appears similar to Facies 2, but, as far as is detectable at such low numbers of living individuals, contents of rare species are different. High numbers of sediment-filled and iron-hydroxyde-covered foraminiferal tests indicate resuspension in Facies 3.

Compared with results from plankton investigations during ARK IV/3, the main change from Facies 1 to Facies 2 coincides with the main boundaries of faunal and floral patterns in the euphotic zone. North Atlantic planktonic assemblages with high standing stocks, but low productivity, extend under the ice cover up to 83°N, while stations further north show Arctic plankton assemblages, with low, but active standing stocks.

Large arenaceous foraminifers and miliolids (e.g. Rhabdammina abyssorum, Reophax scorpiurus, Planispirnoides bucculentus, Pyrgo williamsoni, P. rotalaria and P. vespertilio, Triloculina trihedra and other species) were associated with large amounts of phytoplankton aggregates. These aggregates were used by the foraminifers as food sources. Similar observations were made from other areas of the deep Atlantic ocean where pronounced seasons occur.

#### Planned laboratory analysis

The distribution of living and dead assemblages, abundances and biomass will be counted and measured. This will give basic information for correlation with other investigations in biomass and productivity during ARK IV/3. These data will also assist in correlation of recent and fossil assemblages. TEM-investigations will provide detailed information on cell organelles and contents of food vacuoles.

Nucleomagnetic- and Computer-Tomographic investigations are planned as a first attempt to 3-dimensional structural analyses of microhabitats of benthic foraminifers. Detection of micro- and meiofaunal biomass will be included in this tomographic analysis.

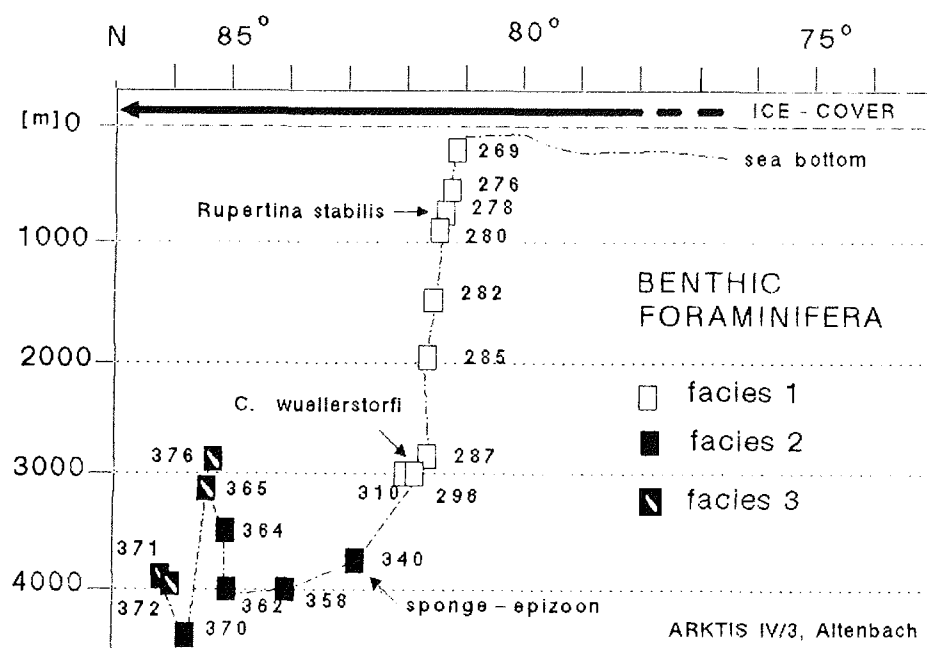


Fig.37 Distribution of benthic foraminiferal facies along the ARKTIS IV/3 transect.

### Perspective

This transect was unique in the history of Arctic foraminiferal deep sea research, and showed that it is important to evaluate distribution patterns in other parts of the Arctic Ocean. Due to the observed correlation of planktic and benthic patterns, further studies always should include biological observations on plankton biomass and productivity.

### **6.9 Macrofauna Collections (GIK)**

Before sampling the GKG surface sediments (Fig. 36), macrofauna specimens were sampled and fixed in methanol/bengalrose solution by paleontologists and geologists during ARK IV/3. As reported before (Boström and Thiede 1984), diversity and abundances in the Eurasian Arctic Ocean are low.

Polychaets, crustaceans, panthopods, crinoids and sponges were found on the continental slope, while sea cucumbers (*Elpidia glacialis*), hydrozoans and sponges seem to dominate in the Nansen Basin. On the Nansen-Gakkel-Ridge high amounts of empty shells of lamellibranchiats and gastropods appeared at some stations (11/365, 371, 372, 376). Some of these shells were manganese-covered on unburried parts or showed patchy dissolution structures. On the Yermak Plateau polychaets, crustaceans, porifera, sea cucumbers (*E. glacialis*) and echinoderms were sampled.

High numbers of meio-epizoon (in first benthic foraminifera) were found on sponges, crinoids, panthopods, polychaet worm tubes and shell fragments, and these samples will be sent to GIK for further micropaleontological investigations.

### **6.10 Biological and Paleontological Observations: Short Summary and Reflection**

Beginning at the start of the food chain, a productivity of 1 to 30 mg org. C/m<sup>2</sup> x d was measured for pelagic algae under lab conditions. It is important to point out potential productivity of algae recovered from the ice, which was up to two orders of magnitude higher. *Melosira* layers were sampled from the bottom of the ice, which were up to 1.5 cm thick. Computation of mean primary production, however, is not reasonable due to extreme seasonality and different light intensities, depending on season, thickness and density of ice cover. The AEDB sediment trap (see Chapter 5.3.3), deployed on drifting ice at 86°N, should add new information on the seasonality and production.

Zooplankton hauls provided data on abundance, species composition and depth distribution of copepods and planktonic foraminifers. Predominantly chaetognaths, ostracods and pteropods were caught. Active and sufficient nutrition can be expected for the planktonic foraminifers, as visible from the intensive reddish color of the protoplasm. The calanoid copepods only started egg production during experiments on board at food concentrations which exceed available concentrations in the Arctic Ocean waters.

A faunal boundary was observed between 83° and 84° N. Further north polar assemblages dominate the composition of calanoid copepods and planktonic foraminifers. South of 83° N., subpolar North Atlantic species dominate. This is obvious even in the benthic fauna. From the continental slope to 83° N main species compositions of benthic foraminifers are similar to those of the Norwegian Sea, while structure and composition of the assemblages significantly changes towards north.

An oceanographic frontier coincides with this faunal boundary, as shown by measurements during this cruise. The inflow of warm water masses of Atlantic origin, from the West Spitsbergen Current, along the Yermak Plateau to the east, up to 83° N, was described previously.

From geochemical measurements on board it might be expected that flux rates of organic material at the continental slope are much higher than those at the Nansen Basin. Reduction of nitrate, accompanied by an increase of ammonia in sediment pore water, is located in between the uppermost 20 cm of the shelf sediments, while it occurs at 80 cm to 100 cm depth in the deep sea sediments of the Nansen Basin. In contrast, oxygen contents are slightly lower in bottom waters of the Nansen Basin.

Variations in major water masses seem to be most important for the main faunal patterns from the Svalbard slope to the Nansen Basin for both planktonic and benthic communities.

These results are very valuable for paleontological interpretations. Subpolar assemblages are now known to be well established in Arctic environments, and analyses of the isotopic composition of tests and shell fragments between 83° and 84° N may show large changes in a region of perennial ice cover.

## 7. GEOPHYSICAL AND GEOLOGICAL PROPERTIES OF THE EURASIAN BASIN OF THE ARCTIC OCEAN AND OF FRAM STRAIT

The Eurasian Basin of the Arctic Ocean (Fig. 1) has a number of unique geological and geophysical properties compared to other young basins of the world ocean. For example, the morphology and structure of the Nansen-Gakkel Ridge are highly anomalous because of its spreading rate which is the slowest of the entire global mid-ocean ridge system (Fig. 38).

The paleoclimatic evolution of the earth, especially Late Cenozoic cooling and Pleistocene glaciation of the northern hemisphere, is intimately linked to the tectonic evolution of the Arctic Ocean. We know, based on a few samples from the central Arctic Alpha-Mendelyev Ridge, that the cold environment which today is typical for the polar Arctic Ocean has not existed for a very long geological interval (Jackson et al. 1985, Thiede et al. 1987 in press). Today, the cold Arctic environment has a controlling influence on the climatic, oceanographic and biologic properties of the Arctic Basin. In addition, many aspects of the northwest European and North American climates are influenced by the Arctic Ocean and its immediate surroundings; an in-depth understanding of the natural properties of this vast and poorly known ocean basin is not only of academic interest, but is of relevance for modern societies on the adjacent land regions, as well as in different parts of the earth.

Data on the geophysical and geological properties and history of the Eurasian Basin are sparse because of the persistent pack ice cover which has only been penetrated by few research vessels. Nansen (1902) during his famous expedition on FRAM made a number of important discoveries related to the geological properties of the Eastern Arctic. He found out that the Arctic Sea was comprised of deep-sea basins and he also developed a good grasp of the nature and importance of Fram Strait's morphology for the oceanography of the area. His men also succeeded in collecting the first deep-sea sediment samples (Böggild 1904), which led to first descriptions of benthic foraminiferal faunas (Kiär 1904), and sediment composition.

Later limited data on the geological and geophysical properties have been collected through a number of expeditions. Most bathymetric data have been collected by navy ships (Perry et al. 1986). Only in the area of the Yermak Plateau (Sundvor et al. 1982) and the Fram Strait (Thiede et al. in prep.) have detailed public bathymetric surveys been carried out. Geophysical properties of the Nansen Basin and the adjacent ocean regions, have been studied by means of airborne surveys by US and Soviet research institutions, and were recently compiled into magnetic anomaly maps of the entire deep-sea area (Vogt 1986) of the Eurasian Basin.



Fig.38 Plate boundary through the Nordic Seas in relation to the adjoining plates and their motions with respect to the deeper mantle. Spreading occurs along some plate boundaries, and slipping or closing occurs along others. The plate boundary between the Azores triple junction and Siberia is the boundary between the Eurasian and North American plates and is the active plate boundary in the Nordic Basin and the Eurasia Basin shown in Fig.2. This figure is redrawn from Minster and Jordan (1980).

Other geophysical and geological data and samples from the continental margin regions of the eastern Arctic deep-sea basins have only been collected during the past 8 years, through the FRAM-I and -IV ice drift stations (Kristoffersen, 1979), the POLARSIRKEL expedition of 1979 and the Swedish YMER-80 expedition (Boström and Thiede 1984). The ARK IV/3 expedition was the first voyage of a modern, well equipped research vessel to reach central parts of the Nansen Basin. This is particularly important for the geoscientific part of the program: no one had successfully sampled the basement of the eastern Arctic deep-sea region; most sediment cores collected from the ice islands were very short and of small diameter not providing sufficient sediment for detailed stratigraphic analyses; and regional variability of many geophysical parameters, was unknown. Therefore, much was to be gained by a comprehensive effort to carry out geophysical and geological station work during this expedition.

The results of the geoscientific research program ARK IV/3 of POLARSTERN will provide an important contribution to the understanding of the geophysical properties and the geology of the Nansen Basin and of the Nansen-Gakkel Ridge. Preliminary observations, based upon transects from the northeastern Barents Shelf across the Barents Abyssal Plain and the Nansen-Gakkel Ridge, and back to the Yermak Plateau are presented in the following chapters (Fig. 1).

#### 5.6.1. Marine Gravity Profiling (FG/UB)

The geologic origin and history of the Arctic is in most every respect less well known and understood than that of the other major world ocean basins. Due to the permanent ice cover, difficult logistics and working conditions, a very limited set of data from geophysical studies and direct geologic sampling is presently available. At least for the southern part of the Eurasian Basin and including the Nansen-Gakkel Ridge, the results obtained on ARK IV/3 of POLARSTERN represent a breakthrough after collection of the first geophysical data by Russian colleagues and the FRAM I-IV ice island stations (Kristoffersen 1979).

Seismicity data from previous geophysical work in the area suggest that the Nansen-Gakkel Ridge is an active spreading center. Interpretation of an aeromagnetic survey in the Nansen Basin and the Fram Basin concluded that the spreading (half-) rate was, on average, about 0.5 cm/y. during the last about 45 m.y., which is remarkably low. There is limited evidence that spreading has been asymmetric, with a slightly higher rate towards the south, and that the spreading rate was roughly twice as high during the early opening phase (Vogt et al. 1979). No reasonably precise timing for the onset of spreading could be defined, however. No data are available (at least not in the open literature) from seismic and gravity lines or heat flow profiles in the Eurasian Basin. Even bathymetric charts appear to have low regional resolution and precision.

As heavy ice conditions for most of the ARK IV/3 expedition made it absolutely impossible to use any towed or deep-towed geophysical equipment, only a seagravimeter system (on loan from DHI) was run during the cruise (thanks to Prof. D. Voppel, DHI Hamburg, for making available the seagravimeter equipment and Prof. H. Miller, AWI Bremerhaven, for help with the installation of the data acquisition system). It consists of two Askania GSS-3 gravimeters (No. 1 and No. 55; Bodenseewerk Gerätetechnik, Überlingen) mounted on a computer stabilized gyro table platform (Anschütz, Kiel). The output signals of the gravimeters are measured by digital voltmeters (DVM's, display accuracy: 1 mgal = 2mV = 20 digits). Their analog output (last three digits) is continuously fed onto a stripchart recorder. The DVMs further output to a sequential PDP-11 computer which writes the data at a sampling rate equivalent to about 20 m ship track intervals on a 1600 bpi tape together with a corresponding set of POLARSTERN INDAS navigation information.

No attempt was made on board to process the data or to apply standard reductions. From the analog recordings it is quite obvious that complex ship motions in the ice produce an extreme degree of noise. Collisions with ice floes result in short wavelength 'anomalies' with 50 mgal or higher amplitudes. Shore-based data evaluation, therefore, is expected to be a very time consuming, laborious task.

Connection to the gravity base net on land is achieved by measurements at reference points in Bremerhaven, Tromsö, Longyearbyen and Hamburg with a LaCoste & Romberg (LCR) Model G Land Gravimeter. Additional port connecting readings obtained at the piers in Tromsö and Hamburg will be used to quantify the drift of the seagravimeters.

With the main aim to independently document sudden instrument jumps in the seagravimeter system anticipated to occur when manoeuvring the ship in heavy ice, a series of 26 gravity measurements was done with the LCR gravimeter on the ice. The location map is shown in Fig. 39. These data are perhaps not of prime quality due to vibrations of the ice floes, but the typical problems in obtaining reproducible and reliable readings were much less severe than encountered on the Antarctic shelf-ice (Eckstaller et al. 1984).

For the computing a free-air anomaly profile, only the Tromsö base point reading is presently taken as a reference. The resultant gravity differences were then further reduced on the basis of the actual international gravity formula. Plotting these preliminary data as a function of the minimum distance of the individual observation points from the Nansen-Gakkel Ridge, reveals a number of interesting features (Fig. 40):

- a pronounced negative anomaly near the base of the continental slope;
- low amplitude, long wavelength anomalies over the abyssal plain;

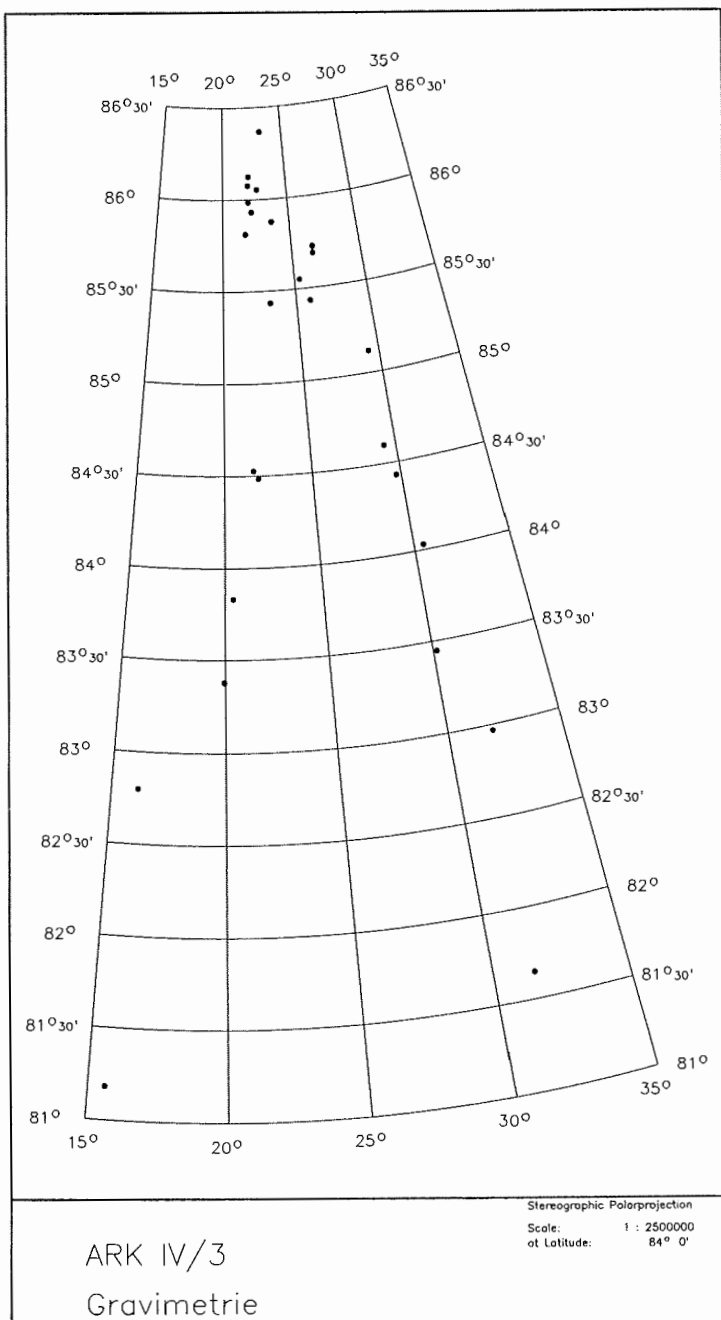


**Fig.39** Location map of gravity observation stations on ice floes during ARK IV/3. A LaCoste & Romber Model G Land Gravimeter was used for the measurements.

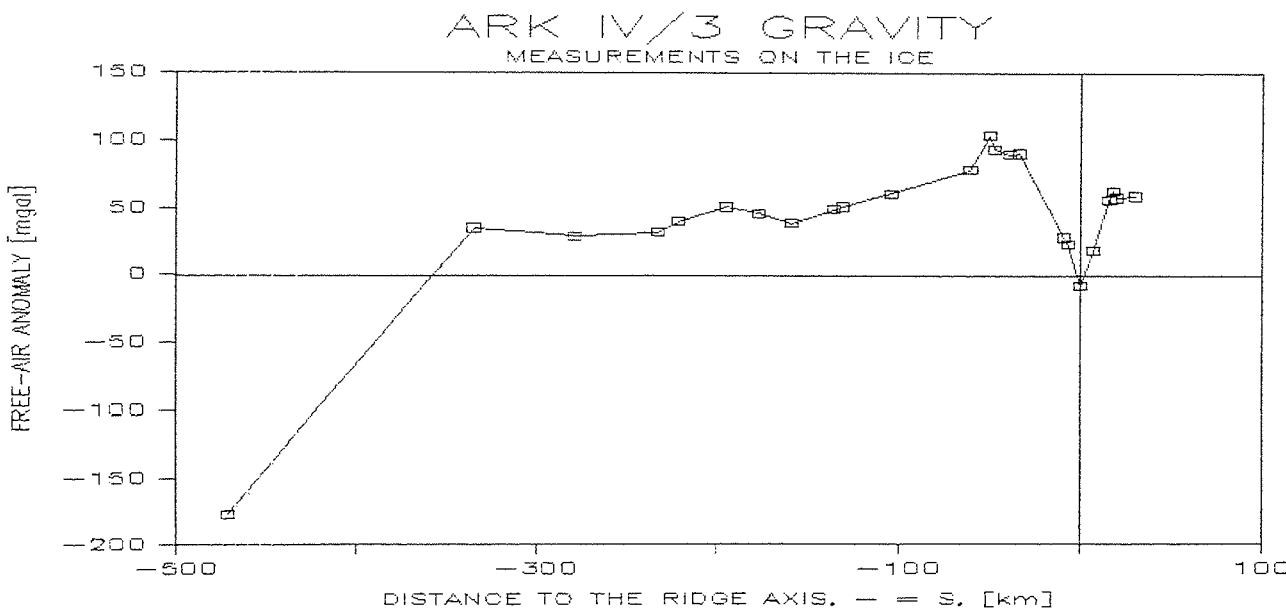


Fig.40 Free-air anomaly profile over the Nansen Basin and the Nansen-Gakkel Ridge. Note that the two western-most observation stations at the foot and on top of the Yermak Plateau have not been included in this graph.

- a gentle increase towards the ridge axis and positive anomalies associated with the topographically high flanking crests of the median valley for which a small negative anomaly is observed.

As a general pattern, this limited data set suggests that the Eurasian Basin of the Arctic Ocean has similar overall gravity characteristics as reported for other world oceans (Dehlinger 1978). Mostly the free-air anomaly trends appear to be in close conformance with topography. For example it is interesting to note that the asymmetric bathymetry of the northern and southern flanks of the ridge crest has an exact equivalent in the gravity data. A remarkable but yet unexplained feature is the unusually high positive level of gravity values over the Nansen Basin. It cannot be excluded at present that it results from an undetected problem in data reduction. On the other hand, near-zero average free-air gravity values over the abyssal plain would in turn further accent the already atypically high, negative anomaly amplitudes over the continental slope and the median valley. A full discussion of these and other questions crucial for the present state and the geologic evolution of the Eurasian Basin has to await extensive shore-based processing of the seagravimeter data.

## 7.2 Heat Flow Measurements (JSS)

The Nansen Basin is produced by sea-floor spreading at the Arctic mid-ocean ridge (Nansen-Gakkel Ridge) which is the northern extension of the Atlantic mid-ocean ridge system. Plate kinematics require a very slow spreading rate of 5 mm per year which is consistent with correlation of magnetic anomalies in the basin (Feden et al. 1979).

The westernmost part of the Nansen Basin is bounded by the shallow Yermak Plateau. Here extensive multichannel seismic surveys have carried out as far north as 82° N (Sundvor et al. 1982). Together with heat flow, gravimetric and seismic refraction data from the Fram III ice station, these data suggest that the northern part of the plateau and its counterpart in the northwestern part of the basin, the Morris Jesup Rise, are paired aseismic ridges formed at a triple junction before anomaly 13 when the three plates -- North-American, Greenland and Eurasian -- moved independently (Jackson et al. 1984).

Besides airborne magnetic surveys and sparse bathymetric data, no other geophysical measurements have been previously carried out in the main part of the Nansen Basin. Therefore, the purpose of the heat flow transect from the northern Svalbard margin to the Nansen-Gakkel Ridge were to clarify the age and extent of the oceanic crust.

A total of 22 measurements (Fig. 41) of the thermal gradient in the upper sedimentary layer were undertaken onboard POLARSTERN during ARK IV/3. Temperature is measured *in situ* using Model #2 of the Lamont-Doherty type digital heat flow equipment. Thermal probes are fixed along a lance at regular intervals. The lance is

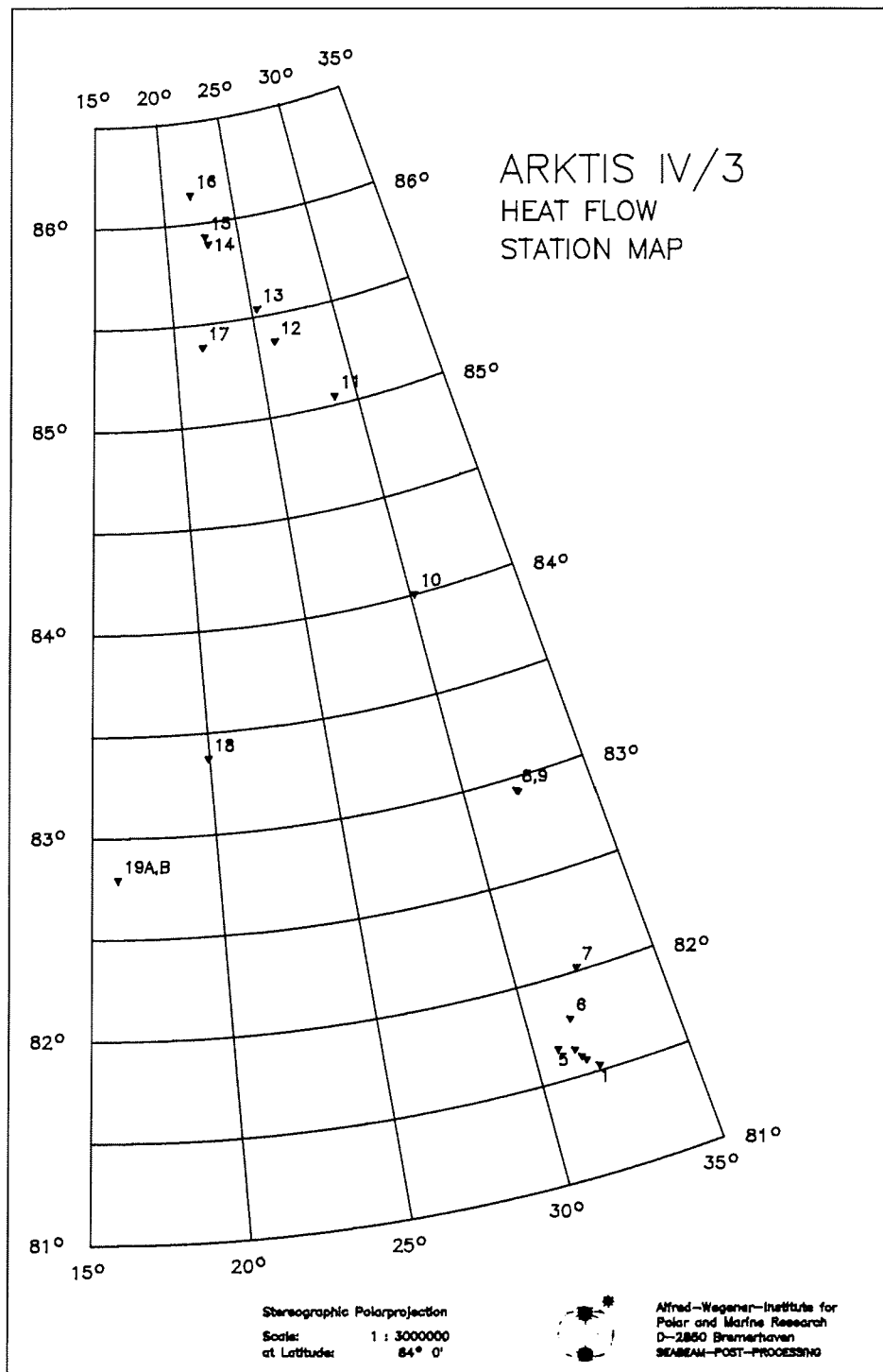


Fig. 41 Heat flow stations of ARK IV/3.

attached below a 900 kilogram metal weight. Penetration of the sea bottom lasts for 5-10 minutes. Before and after temperature measurements within the sediments, the lance is maintained 50 m above the sea floor in order to stabilize its temperature and to check validity of the temperature record in the sediments. Inside the digital recording system placed in the weight head of the equipment is also an acoustic pinger. Usually it is not difficult to receive the 12 kHz signal which permits both an immediate control of the penetration depth and also a preliminary heat flow gradient calculation. However, POLARSTERN is a very noisy ship and it was impossible to obtain reliable readings from water depths greater than 1000 meters.

The digital cassette reading system did not reach Norway in time for the cruise, due to a very long delivery time. The tape reader was later picked up in Longyearbyen at the very end of the cruise, but lacked documentation. Therefore, it was impossible to interface with the onboard HP-Integral 9807 which has the programs for a complete reduction of the data, within the few days left in the cruise. However, we were able to dump the tape readings on a Brother EPAA printer which permitted preliminary calculation of gradients. The results are presented in Table 10. Examples of plots of the change in temperature versus depth are given in Fig. 42.

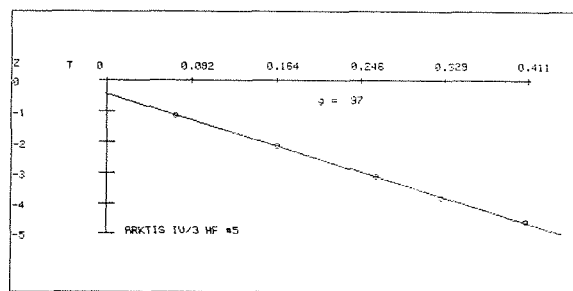
Of the 22 attempts to measure heat flow, 3 gave no penetration. These three stations were all located at the abyssal plain of the Nansen Basin where strange sediments prevented penetration of all long probes. Two readings showed nonlinear gradients. Due to an extremely high temperature regime in the Nansen-Gakkel rift valley (heat flow stations #14 and #15) the lower four of the five thermistors were off scale. On the basis of bottom water temperature measurements and the increase in temperature of the shallowest thermistor, gradient values are estimated at 770 and 1012  $\mu\text{K}/\text{m}$ . This is far higher than observed at the Knipovich Ridge where values from 245-291  $\mu\text{K}/\text{m}$  have been reported (Sundvor 1987). An exceptionally low heat flow value is recorded on heat flow station #17 (Fig. 41). The fact that this station was located on a seamount 1000 m shallower than the surrounding sea floor can explain this very low heat flow. A comparison of the measured heat flow in the Nansen Basin with suggested age and spreading rates is not possible at present. The measured heat flow values along the Nansen Basin transect are shown in Fig. 43.

ARKTIS IV/3 HF #5

$T(z=0) = -.042 \pm/- .004$   
 Gradient =  $97.1 \pm/- 1.2 \text{mK/m}$

Z	T	dT
1.15	.070	.000
2.15	.167	.001
3.15	.264	.000
3.87	.329	-.005
4.64	.411	.003

$\Sigma = 2.895763E-003$



ARKTIS IV/3 - HF #17

$T(z=0) = .075 \pm/- .002$   
 Gradient =  $13.4 \pm/- .5 \text{mK/m}$

Z	T	dT
1.15	.091	.001
3.15	.116	-.001
3.87	.127	0.000
4.64	.138	.001

$\Sigma = 9.745127E-004$

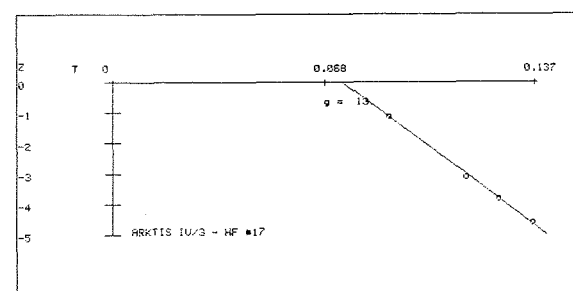
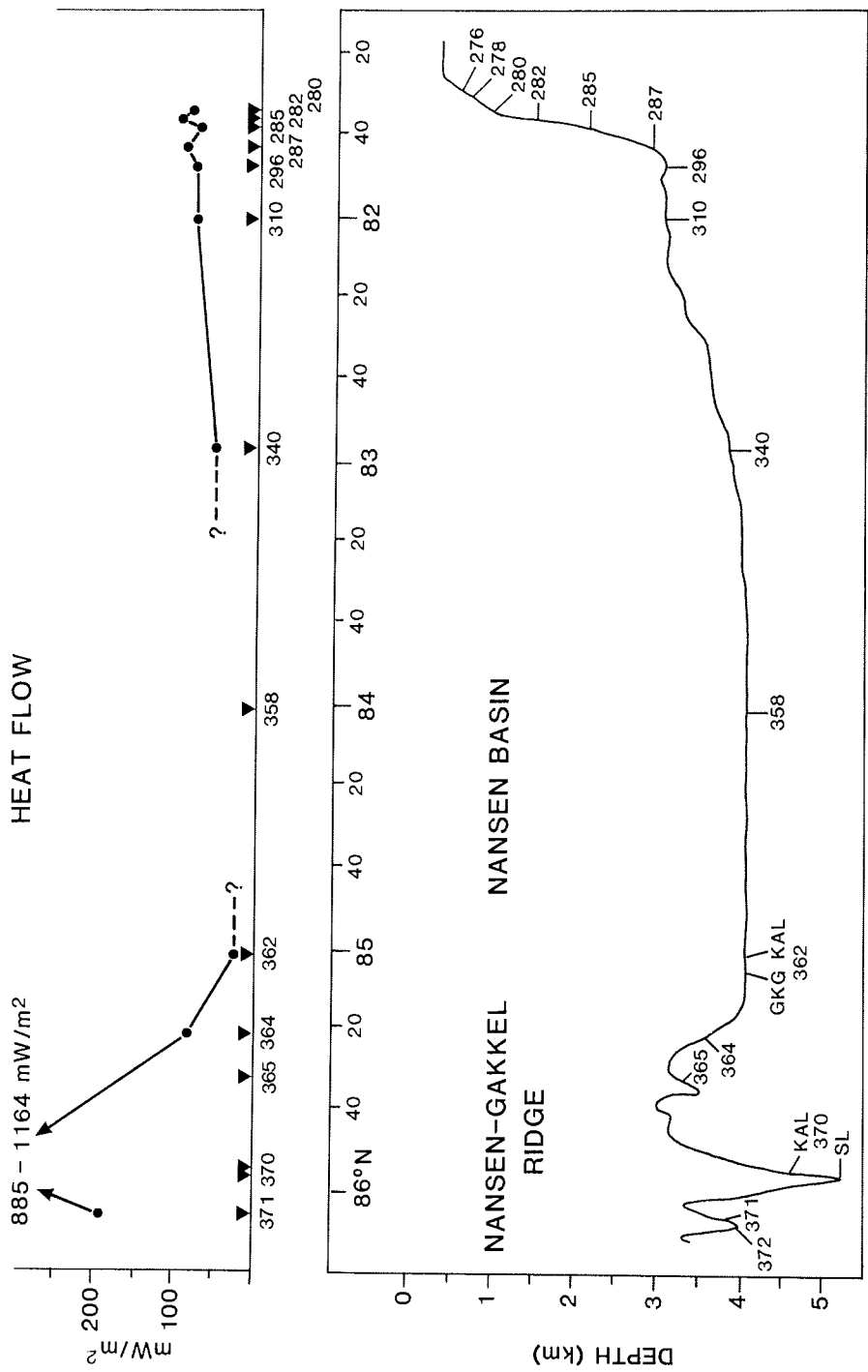


Fig.42 Heat flow measurements #5 and #7 (c.f. Table 10) of ARK IV/3.



**Fig. 43** Regional variability of heat flow along the track line (c.f. Fig. 41).

TABLE 10: Listing of heat flow stations during ARK IV/3.

NL = non linear gradient.

Station nos. HF POLARSTERN	Position		Water depth (m)	Penetr. depth (m)	No of therm.	Grad. (mK/m)	Cond. (W/ m/k)	H.F. (mW/ m+m)
	Lat. °N	Long. °E						
1	11/278	81°31.82	31°35.42	703	6.0	5	NL	
2	11/280	81°34.46	31°38.47	886	6.0	4	88± 4	0.93 82± 4
3	11/282	81°35.82	31°31.13	1437	4.8	4	105± 5	0.93 98± 5
4	11/285	81°38.09	31°21.45	2313	4.8	4	77± 6	0.94 73± 5
5	11/287	81°39.64	30°48.73	2698	4.8	5	97± 1	0.94 91± 1
6	11/296	81°47.34	31°30.14	2991	4.8	5	65± 4	1.18 77± 4
7	11/310	82°01.34	32°13.39	2925	4.0	3	79±12	1.01 80±12
8	11/340	82°56.58	32°04.18	3751	Fell over			
9	11/340	82°56.04	32°08.19	3735	3.5	4	46±11	1.15 53±12
10	11/358	84°00.44	30°13.01	3996	Fell over			
11	11/362	85°03.00	28°47.14	4024	4.8	4	27± 2	0.95 26± 2
12	11/364	85°22.30	26°02.75	3580	4.8	5	64± 3	1.34 86± 4
13	11/365	85°32.82	25°21.04	3366	4.8	3	NL	
14	11/370	85°53.84	22°50.19	4390	4.8	2	> 770	1.15 > 885
15	11/370	85°56.23	22°41.35	5100	6.0	2	>1012	1.15 >1164
16	11/371	86°09.09	22°09.92	3556	4.8	3	134±15	1.43 192±21
17	11/376	85°23.68	21°39.06	2892	4.8	4	13± 1	1.55 21± 1
18	11/382	83°22.82	19°55.89	4011	Fell over			
19	A11/396	82°48.05	16°00.91	1354	5.5	5	62± 4	1.21 75± 5
19	B11/396	82°48.10	16°00.96	1354	5.5	5	65± 2	1.21 79± 3
20	11/423	81°19.51	15°17.06	2219	4.8	5	63± 5	1.02 64± 5
21	11/430	78°45.11	01°51.17	2506	4.8	5	120± 4	1.15 138± 4

### **7.3 Distribution of Surface Sediments - 3.5 kHz Profiling (IBG,JSS).**

#### ARK IV/3 Track lines in the Nansen Basin

To date, most the eastern Arctic Basin has been inaccessible to seismic surveys to date because of its permanent ice cover. Data collected with the 3.5 kHz echosounder during the ARK IV/3 with POLARSTERN represent the first subbottom record from the Nansen Basin and the midoceanic Nansen-Gakkel Ridge. On this cruise, two profiles were run. The first is from the eastern part of the Svalbard continental margin at  $80^{\circ} 40' N$  -  $31^{\circ} 00' E$  northwards crossing the Nansen-Gakkel Ridge to  $86^{\circ} 11' N$  -  $22^{\circ} 00' E$ , and the second is from the latter location southwards to the western part of the Svalbard continental margin at  $80^{\circ} 10' N$  -  $11^{\circ} 40' E$ . Total distance is more than 1400 km (Fig. 44). Besides providing general information about the bathymetry, the 3.5 kHz has been very useful in the detection and interpretation of good locations for geological stations. The 3.5 kHz was run continuously together with the SEABEAM during the entire cruise.

The echosounder system onboard POLARSTERN consists of an ORE (Ocean Research Equipment) model No. 140 Transceiver. The transceiver was connected with an EPC crystal delay unit, an EPC Key/TVG unit, a Phillips PM 5171 amplifier/logarithmic converter and an EPC model 3200S printer. The pulse length used under the survey has varied between 0.5 to 4 ms. The equipment worked well the first two days, but problems started on the third when one key in the EPC Key/Gate-TVG unit (used for delaying the signal) was out of order. Because of this problem, which could not be repaired onboard, the second and third rolls were of poor quality, and the depth range setting at certain depths became more complicated, especially in areas where the water depth varied over short distances.

Most of the cruise has been in the sea ice covered area. Data quality varies according to the thickness of the sea ice. Ice breaking and ice ramming disturbed the data in two ways: 1. The ice breaking process creates a lot of noise in the 3.5 kHz band, and therefore adds noise to the registration. 2. When POLARSTERN rams ice, she moves back and forth, often in short intervals. If this occurs over for example the shelf edge or in other lines that can give side reflections the seafloor will look like a series of troughs and ridges. This effect is clearly shown in Fig.45.

The following is a brief description of each of the 19 rolls of the EPC records. Locations are shown in Fig. 44. For simplifying judgment of data quality we defined a 4-part scale as follows:

- Good data quality, i.e. the whole roll contains a readable record.
- Relatively good data quality, i.e. most of the roll contains a readable record.

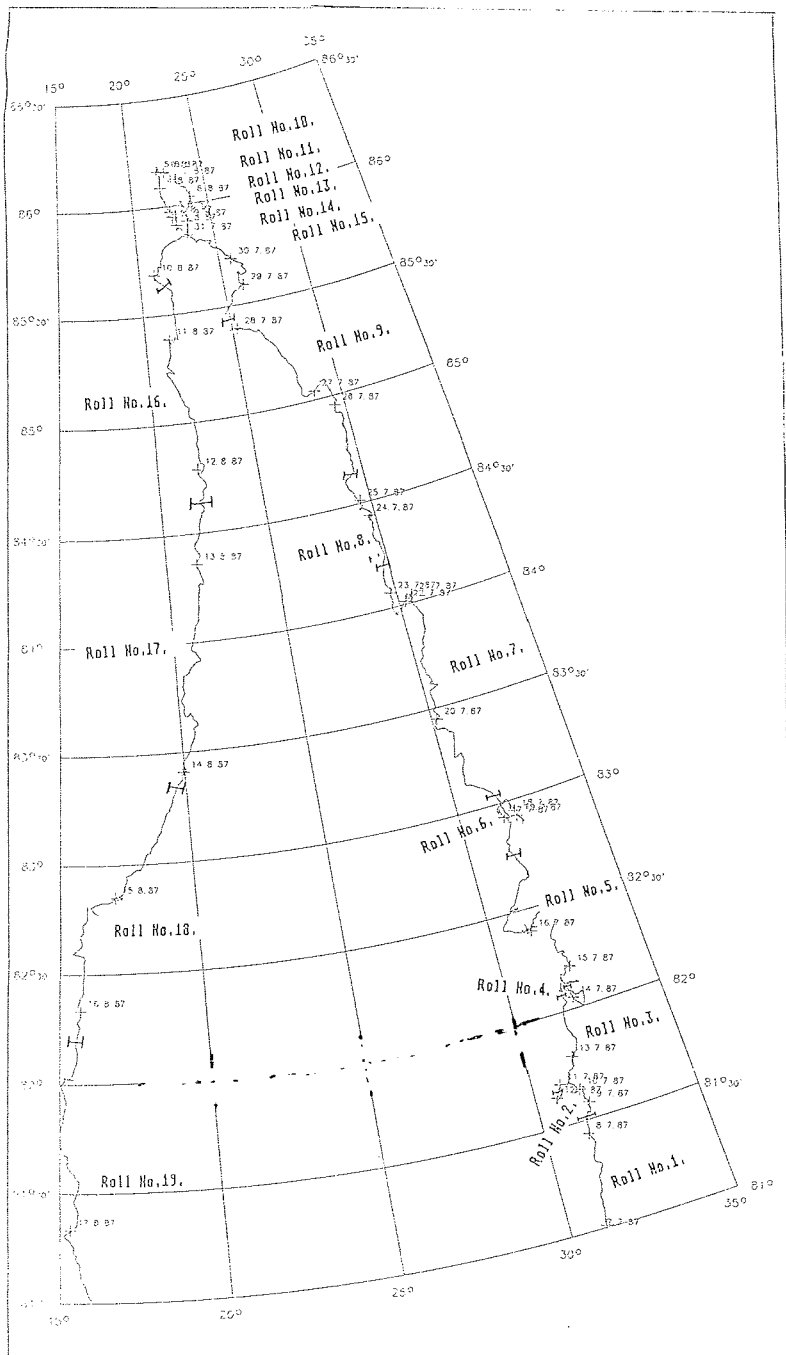


Fig.44 Map showing the ship track of POLARSTERN during ARK IV/3. Locations of different (1-19), 3,5 kHz rolls are indicated.

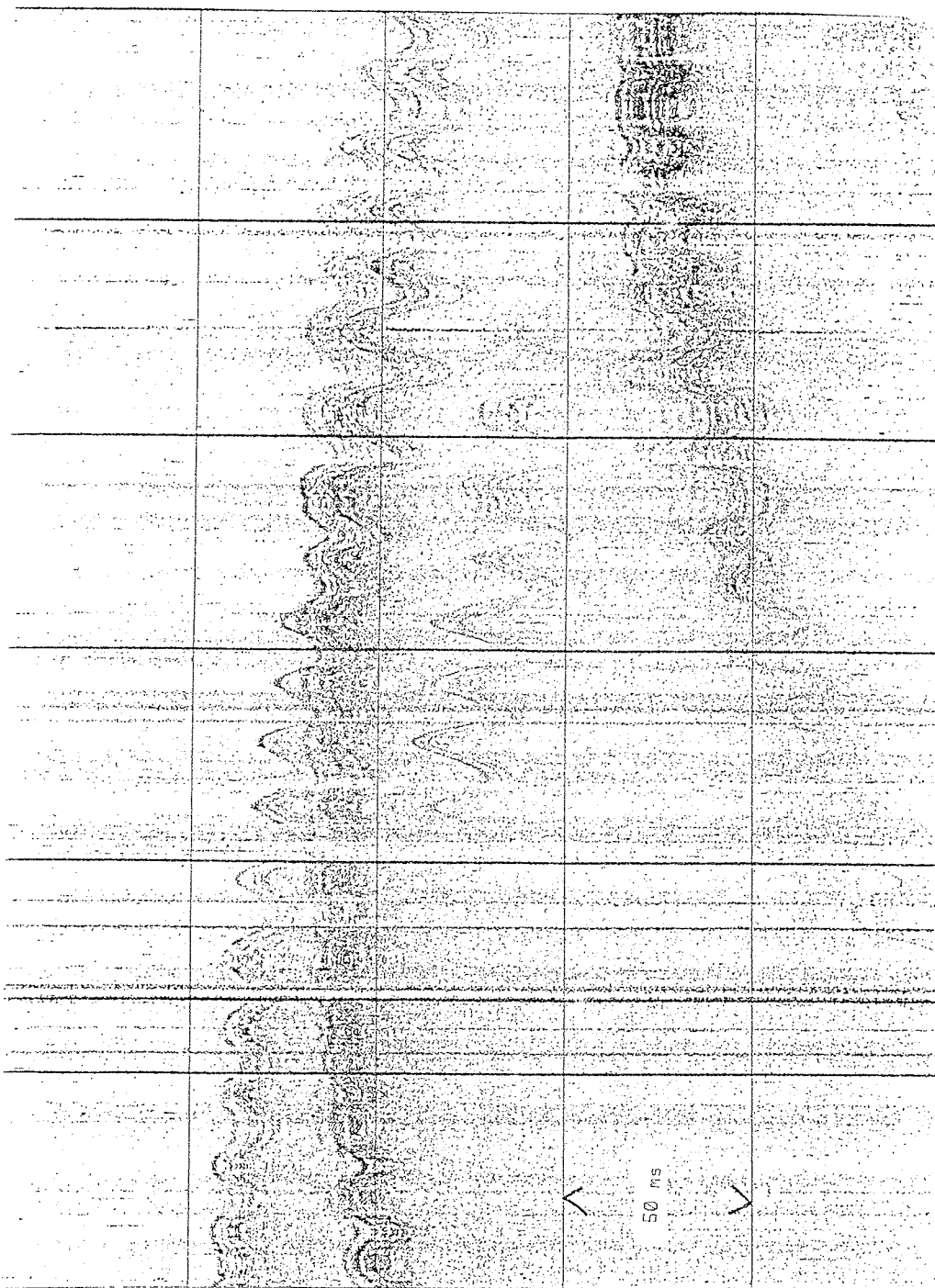


Fig.45 Example of a record showing several side-sweeps and the typical ice ramming pattern.

- Acceptable data quality, i.e. parts of the roll contains a readable record.
- Poor data quality, i.e most of the record is unreadable.

NB! All the time measurements (in milliseconds) are in two way travel time.

Roll No.1. Start:  $80^{\circ} 47' N - 31^{\circ} 03' E$  (07.07.87, 09:40)  
 ----- End :  $81^{\circ} 31' N - 31^{\circ} 33' E$  (08.07.87, 14:00)

Relatively good data quality. The line between  $81^{\circ} 11' N 31^{\circ} 16' E$  and  $81^{\circ} 15' N 31^{\circ} 22' E$ , (Fig. 46) shows continental shelf features with erosion channels/troughs, iceberg plough marks. An upper infill unit about 5 ms in thickness can be seen in the troughs. The bottom reflector is relatively strong, and penetration is less than 20 ms.

The line between  $81^{\circ} 25' N 31^{\circ} 21' E$  and  $81^{\circ} 27' N 31^{\circ} 23' E$  (Fig. 47) shows slump structures on the shelf break and down slope.

Roll No.2. Start:  $81^{\circ} 31' N - 31^{\circ} 33' E$  (08.07.87, 14:00)  
 ----- End :  $81^{\circ} 40' N - 30^{\circ} 52' E$  (11.07.87, 06:30)

Roll No.3. Start:  $81^{\circ} 40' N - 30^{\circ} 52' E$  (11.07.87, 06:30)  
 ----- End :  $82^{\circ} 05' N - 32^{\circ} 01' E$  (13.07.87, 19:00)

Poor data quality in Rolls 2 and 3 because of problems with the EPC Key/Gate-TVG unit.

Roll No.4. Start:  $82^{\circ} 04' N - 32^{\circ} 02' E$  (13.07.87, 20:40)  
 ----- End :  $82^{\circ} 07' N - 32^{\circ} 15' N$  (14.07.87, 19:00)

Poor data quality because of ice ramming.

Roll No.5. Start:  $82^{\circ} 07' N - 32^{\circ} 16' E$  (14.07.87, 19:00)  
 ----- End :  $82^{\circ} 44' N - 31^{\circ} 37' E$  (16.07.87, 19:30)

Acceptable data quality. The line between  $82^{\circ} 31' N 31^{\circ} 04' E$  and  $82^{\circ} 42' N 31^{\circ} 45' E$  (Fig. 48) shows lens to wedge-shaped units on the continental slope and rise. The units have an inner transparent character and the penetration is about 30 ms.

Roll No.6. Start:  $82^{\circ} 44' N - 31^{\circ} 37' E$  (16.07.87, 19:30)  
 ----- End :  $83^{\circ} 03' N - 31^{\circ} 33' E$  (19.07.87, 13:10)

Acceptable data quality. The beginning looks like the end of Roll 5. At the end of the roll there are signs of slump structures and further north some horizontal subbottom reflectors occur.

Roll No.7. Start:  $83^{\circ} 03' N - 31^{\circ} 28' E$  (19.07.87, 13:40)  
 ----- End :  $84^{\circ} 21' N - 29^{\circ} 48' E$  (23.07.87, 06:50)

Relatively good data quality. The line between  $83^{\circ} 03' N 31^{\circ} 28' E$  and  $83^{\circ} 28' N 29^{\circ} 54' E$  shows an undulating strong bottom reflector and the penetration is approximately 20 ms (Fig. 49).

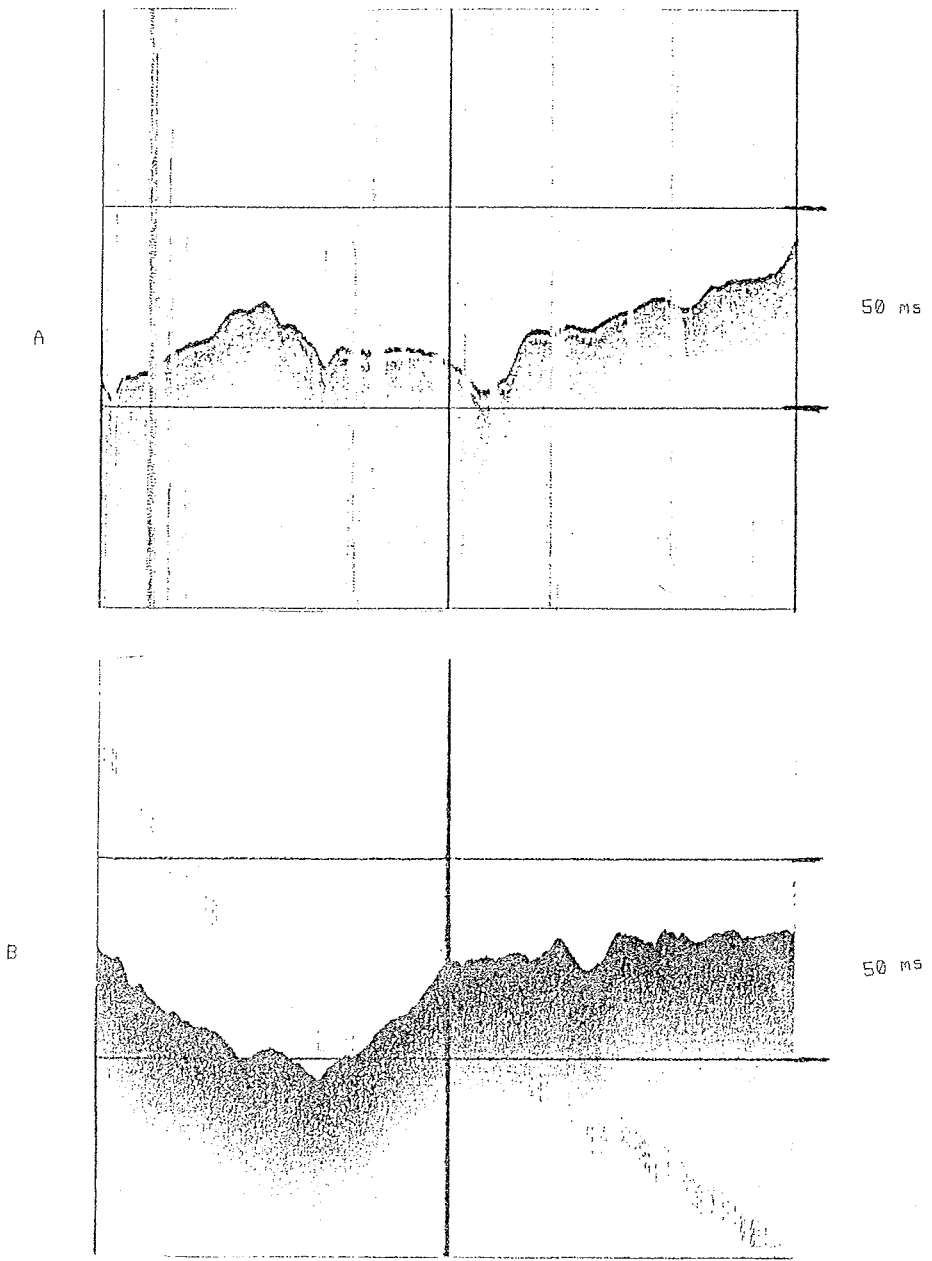


Fig.46 Continental shelf of the northeastern Svalbard margin (3A), compared to the northwestern Svalbard margin (3B). In contrast to the northeastern margin, the northwestern margin exhibits stronger sea bottom reflections and no interfaces can be seen under the sea floor. On both margins there are indications of erosion by ice.

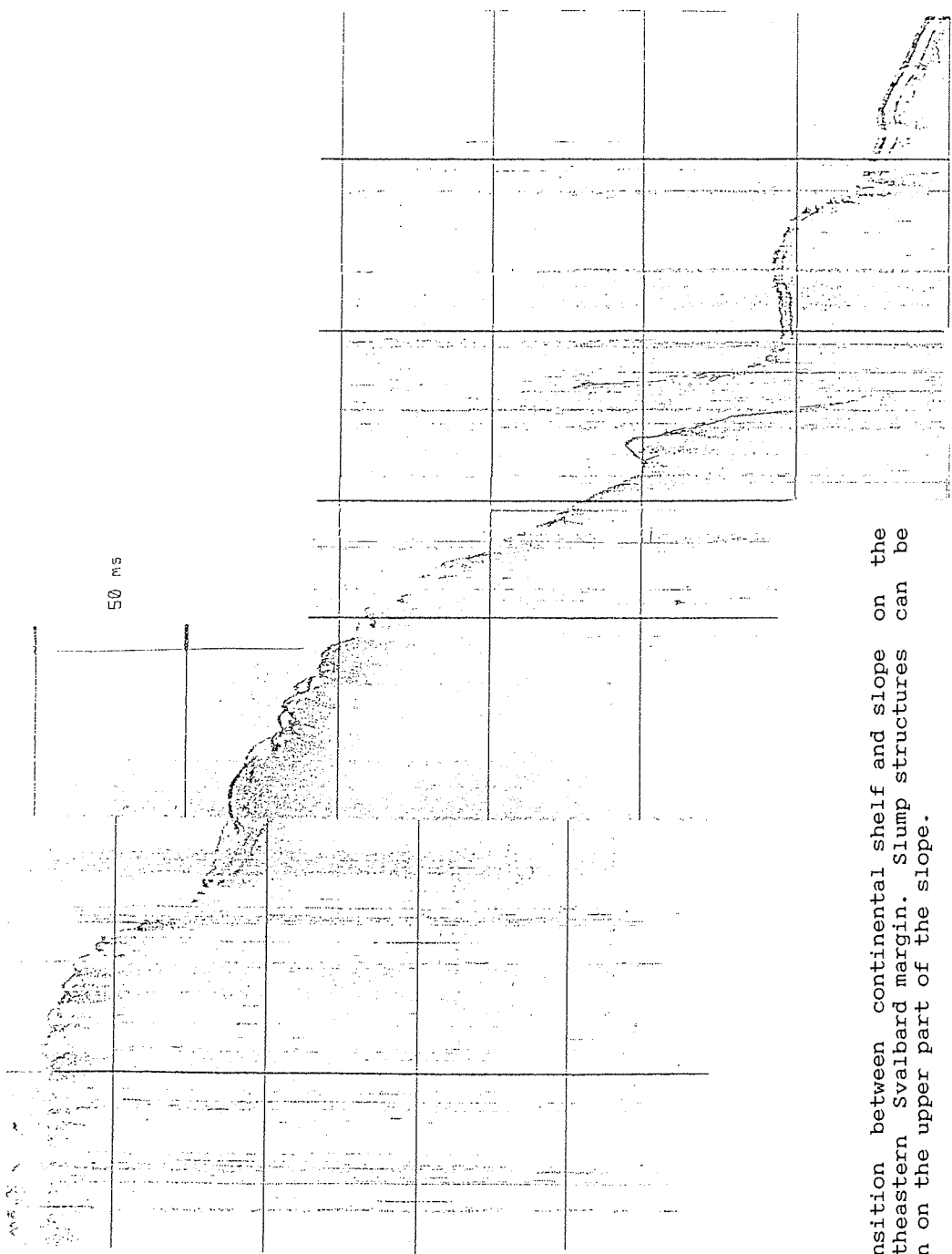


Fig. 47 Transition between continental shelf and slope on the northeastern Svalbard margin. Slump structures can be seen on the upper part of the slope.

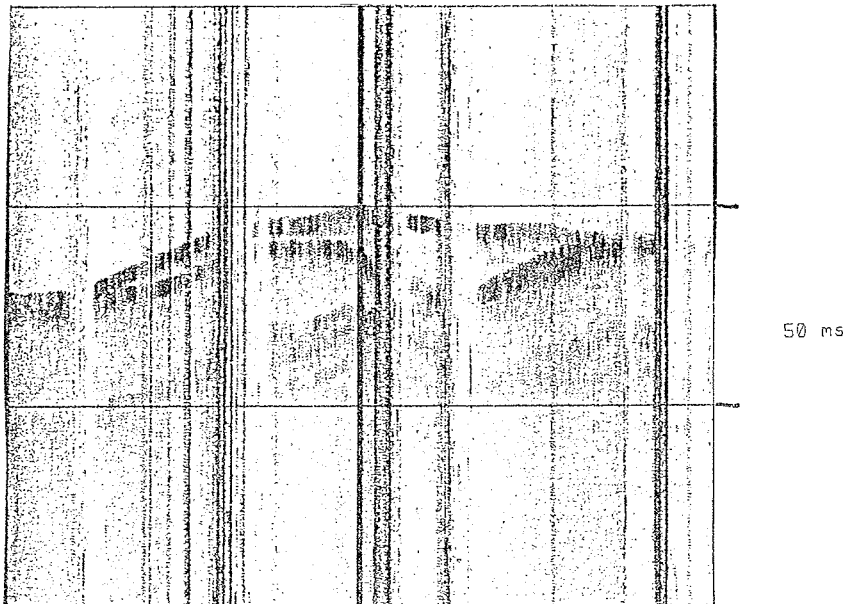


Fig.48 Lens-shaped, transparent units on the continental rise of the northeastern Svalbard margin.

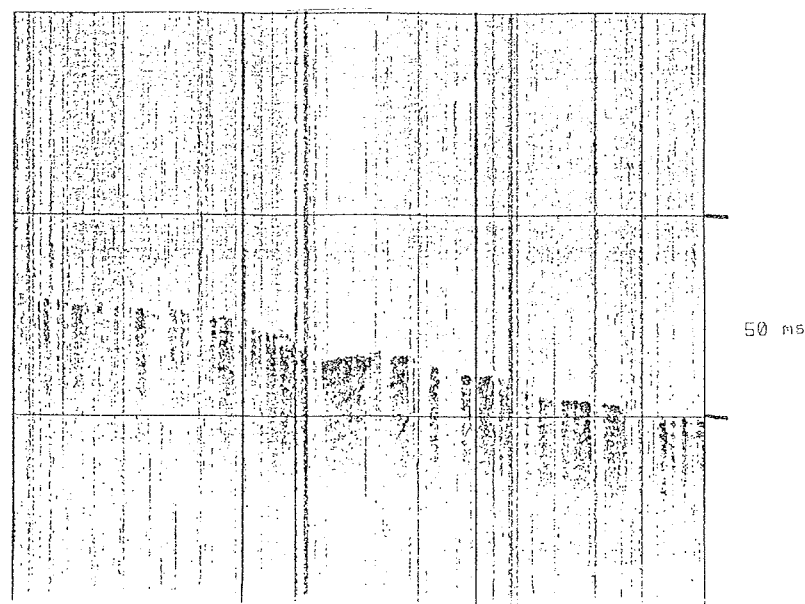


Fig.49 An undulating, strong sea bottom reflector indicating slumping on the outer part of the northeastern Svalbard continental rise.

The line between  $83^{\circ} 57' N$   $29^{\circ} 46' E$  and the end of the roll shows parallel reflectors. Two strong continuous reflectors at 5 ms and 15 ms separate a transparent layer (Fig. 50). Below 15 ms the reflection pattern are more diffuse, but down to approximately 50 ms parallel reflectors can be seen.

Roll No.8. Start:  $84^{\circ} 20' N$  -  $29^{\circ} 48' E$  (23.07.87, 07:00)  
----- End :  $84^{\circ} 38' N$  -  $29^{\circ} 03' E$  (25.07.87, 03:10)

Relatively good data quality. The reflection pattern is like the end of Roll no.7.

Roll No.9. Start:  $84^{\circ} 38' N$  -  $29^{\circ} 03' E$  (25.07.87, 03:40)  
----- End :  $85^{\circ} 25' N$  -  $24^{\circ} 47' E$  (28.07.87, 03:55)

Relatively good data quality. North of  $84^{\circ} 43' N$  the reflection pattern changes. The subbottom reflectors are spaced closer and the strong reflector at 5 ms disappears. A subbottom seamount can be seen at approximately  $84^{\circ} 48' N$   $29^{\circ} 41' E$ . The first seamount above seabottom is located at approximately  $84^{\circ} 49' N$   $29^{\circ} 41' E$  and rises 150 ms above the bottom. The second seamount is located at approximately  $84^{\circ} 52' N$   $29^{\circ} 43' E$  and rises 75 ms above seabottom (Fig. 51). The third seamount is located at approximately  $85^{\circ} 07' N$   $27^{\circ} 54' E$  and rises less than 50 ms above seabottom. The first seamount complex is located between  $85^{\circ} 09' N$   $27^{\circ} 56' E$  and  $85^{\circ} 14' N$   $27^{\circ} 37' E$ . The higest seamount rises about 150 ms above the seabottom. The seabottom between this complex and the next one is about 75 ms deeper than on the abyssal plain. The second seamount complex is located between  $85^{\circ} 15' N$   $27^{\circ} 21' E$  and  $85^{\circ} 20' N$   $27^{\circ} 02' E$ . From approximately  $85^{\circ} 20' N$  to the end of the roll data quality is very poor because of ice ramming.

Roll No.10. Start:  $85^{\circ} 25' N$  -  $24^{\circ} 47' E$  (28.07.87, 04:05)  
----- End :  $85^{\circ} 44' N$  -  $25^{\circ} 41' E$  (30.07.87, 01:45)

Roll No.11. Start:  $85^{\circ} 44' N$  -  $25^{\circ} 41' E$  (30.07.87, 01:45)  
----- End :  $85^{\circ} 55' N$  -  $22^{\circ} 46' E$  (01-08.87, 06:55)

Roll No.12. Start:  $85^{\circ} 55' N$  -  $22^{\circ} 46' E$  (01.08.87, 06:55)  
----- End :  $86^{\circ} 03' N$  -  $22^{\circ} 03' E$  (03.08.87, 14:00)

Roll No.13. Start:  $86^{\circ} 03' N$  -  $22^{\circ} 03' E$  (03.08.87, 14:00)  
----- End :  $86^{\circ} 11' N$  -  $22^{\circ} 03' E$  (05.08.87, 17:00)

Roll No.14: Start:  $86^{\circ} 11' N$  -  $22^{\circ} 03' E$  (05.08.87, 17:00)  
----- End :  $86^{\circ} 01' N$  -  $23^{\circ} 54' E$  (08.08.87, 02:30)

Roll No.15: Start:  $86^{\circ} 01' N$  -  $23^{\circ} 54' E$  (08.08.87, 02:30)  
----- End :  $85^{\circ} 34' N$  -  $21^{\circ} 49' E$  (10.08.87, 09:00)

All these rolls are of poor quality because of disturbance caused by ice ramming and side reflections from the uneven seafloor.

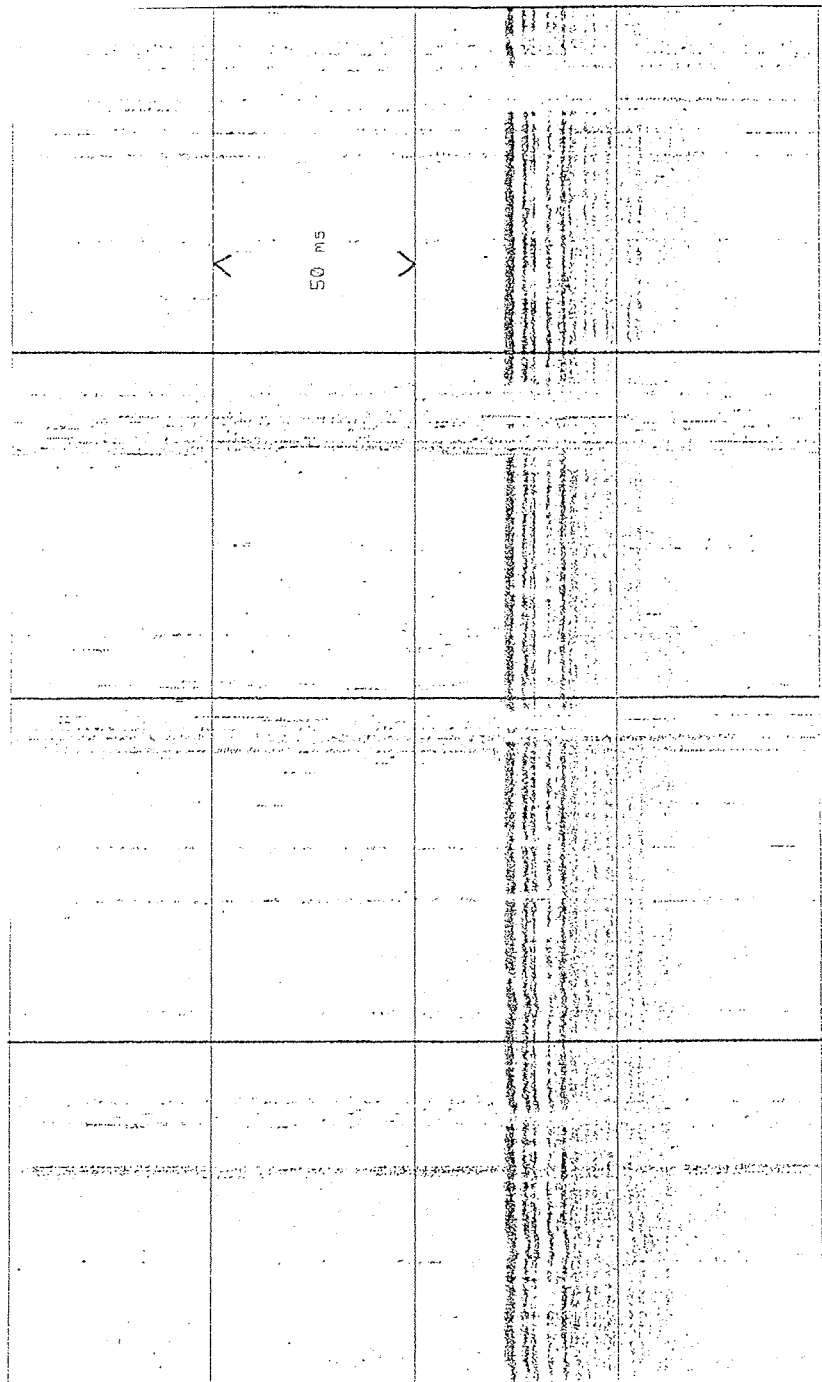


Fig. 50 Typical section from the abyssal plain in the Nansen Basin. Two strong reflectors at approximately 5 and 15 ms are separated by a transparent layer. Below 15 ms, the reflection pattern is more diffuse.

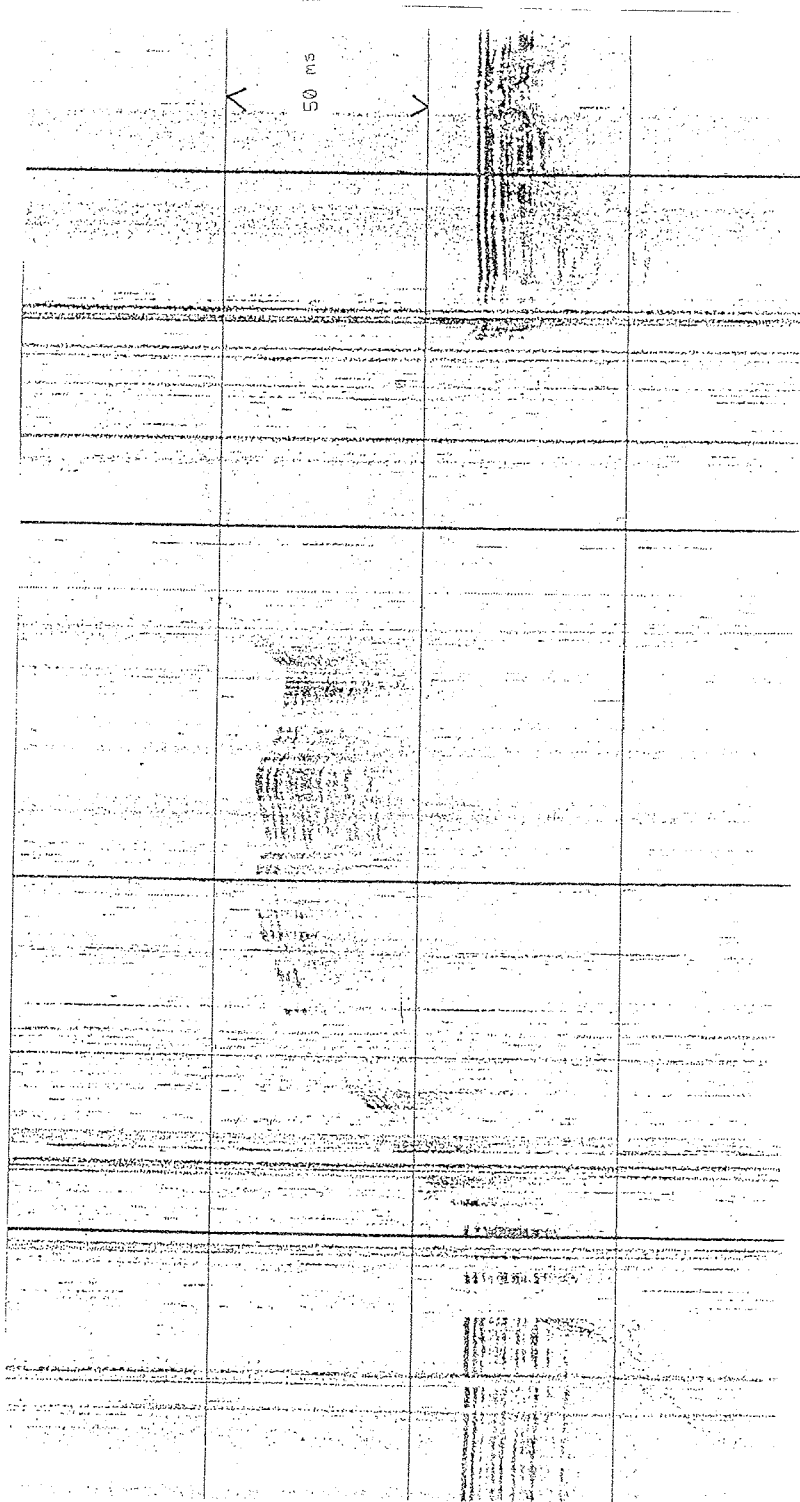


Fig.51 Seamount at position 8452'N-2941'E. The seamount can be traced to approximately 50 ms below sea floor.

Roll No.16: Start:  $85^{\circ} 34' N$  -  $21^{\circ} 49' E$  (10.08.87, 09:00)  
----- End :  $84^{\circ} 38' N$  -  $21^{\circ} 59' E$  (12.08.87, 07:45)

Relatively good data quality. The seamount complexes end at approximately  $84^{\circ} 48' N$   $22^{\circ} 10' N$ , but a single seamount can be seen further south at approximately  $84^{\circ} 44' N$   $22^{\circ} 02' E$ . The rest of the profile consists of discontinuous parallel reflectors. Penetration is about 75 ms.

Roll No.17: Start:  $84^{\circ} 38' N$  -  $21^{\circ} 59' E$  (12.08.87, 09:00)  
----- End :  $83^{\circ} 24' N$  -  $19^{\circ} 50' E$  (14.08.87, 04:20)

Good data quality. Penetration is more than 50 ms. A change in reflection pattern from parallel discontinuous reflectors to very continuous reflectors is seen at approximately  $84^{\circ} 32' N$   $21^{\circ} 45' E$ . In the line between  $84^{\circ} 30' N$   $21^{\circ} 42' E$  and  $84^{\circ} 27' N$   $21^{\circ} 32' E$  one can see subbottom reflectors bent over a structure while the seafloor is horizontal.

Roll No.18: Start:  $83^{\circ} 24' N$  -  $19^{\circ} 50' E$  (14.08.87, 04:20)  
----- End :  $82^{\circ} 11' N$  -  $15^{\circ} 35' E$  (16.08.87, 01:50)

Good data quality. The line between  $83^{\circ} 22' N$   $19^{\circ} 50' E$  and  $82^{\circ} 55' N$   $17^{\circ} 30' E$  shows a continuous parallel reflection pattern with occasional bent subbottom reflectors. The line between  $82^{\circ} 50' N$   $16^{\circ} 54' E$  and  $82^{\circ} 47' N$   $16^{\circ} 12' E$  climbs up Yermak Plateau from 2600 m water depth in the Nansen Basin to 1390 m water depth on the Plateau (Fig. 52). The line from  $82^{\circ} 46' N$   $15^{\circ} 58' E$  to  $82^{\circ} 21' N$   $15^{\circ} 40' E$  shows the reflection pattern on the Yermak Plateau (Fig. 53). The reflection pattern is parallel draped reflectors thicker in the troughs and thinner on the ridges. Penetration varies from 10 to > 50 ms, and the seafloor is irregular. The end of the roll is from the basin between the northeastern flank of Yermak Plateau (Sofia Basin) and the western Svalbard continental margin.

Roll No.19: Start:  $82^{\circ} 11' N$  -  $15^{\circ} 35' E$  (16.08.87, 01:50)  
----- End :  $80^{\circ} 09' N$  -  $11^{\circ} 41' E$  (18.08.87, 01:10)

Good data quality. From the start of the roll to  $81^{\circ} 00' N$   $15^{\circ} 57' E$  the record shows Sofia Basin (Fig. 54). The record shows continuous parallel reflectors along the entire line. The line between  $81^{\circ} 00' N$   $15^{\circ} 57' E$  and  $80^{\circ} 40' N$   $15^{\circ} 35' E$  shows the steplike pattern when climbing up from 2141 m water depth in Sofia Basin to 330 meter water depth on the Svalbard continental margin (Fig. 55). The seafloor is characterized by flat ramps and steep hills. From  $80^{\circ} 40' N$   $13^{\circ} 35' E$  to the end of profile the record shows the western Svalbard continental shelf. A hard, topographically irregular seafloor and with subbottom reflectors is characteristic for the Svalbard shelf (Fig. 46).

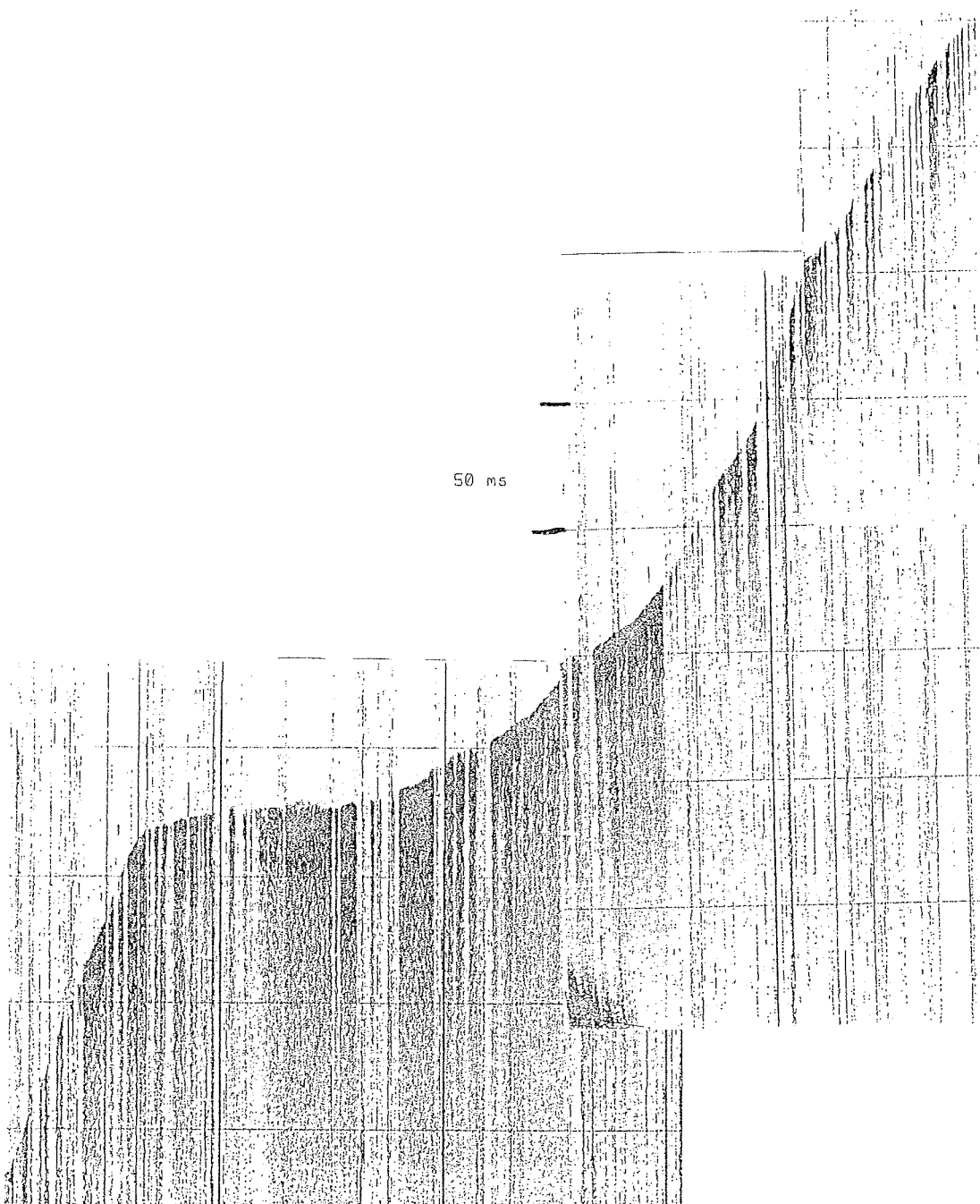


Fig.52 The continental slope from the Nansen Basin onto the northeastern part of the Yermak Plateau. Notice the steep slope and the absence of sea bottom reflections.

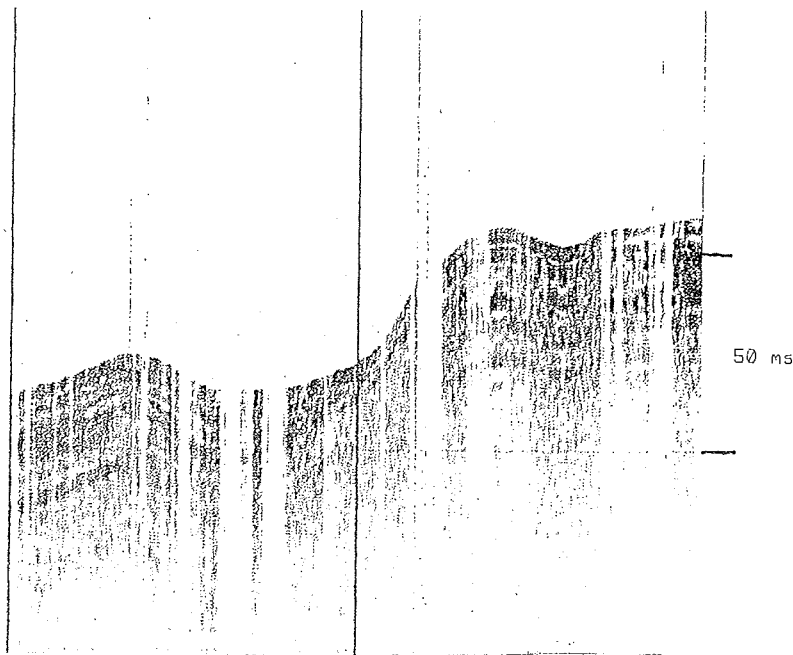


Fig.53 Section from the northeastern part of the Yermak Plateau.  
Parallel draped reflectors are thick in the troughs and  
thinner on the ridges.

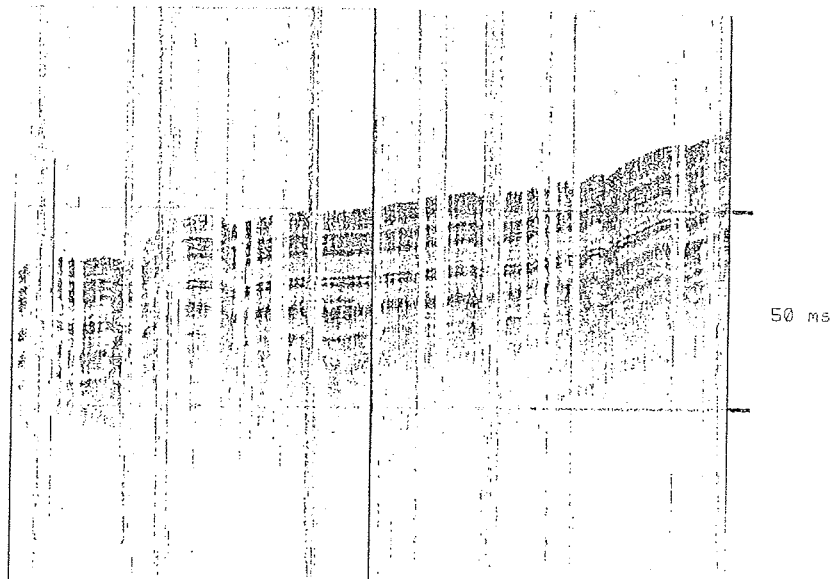


Fig.54 Section from the Sofia Basin, showing continuous parallel  
reflections.

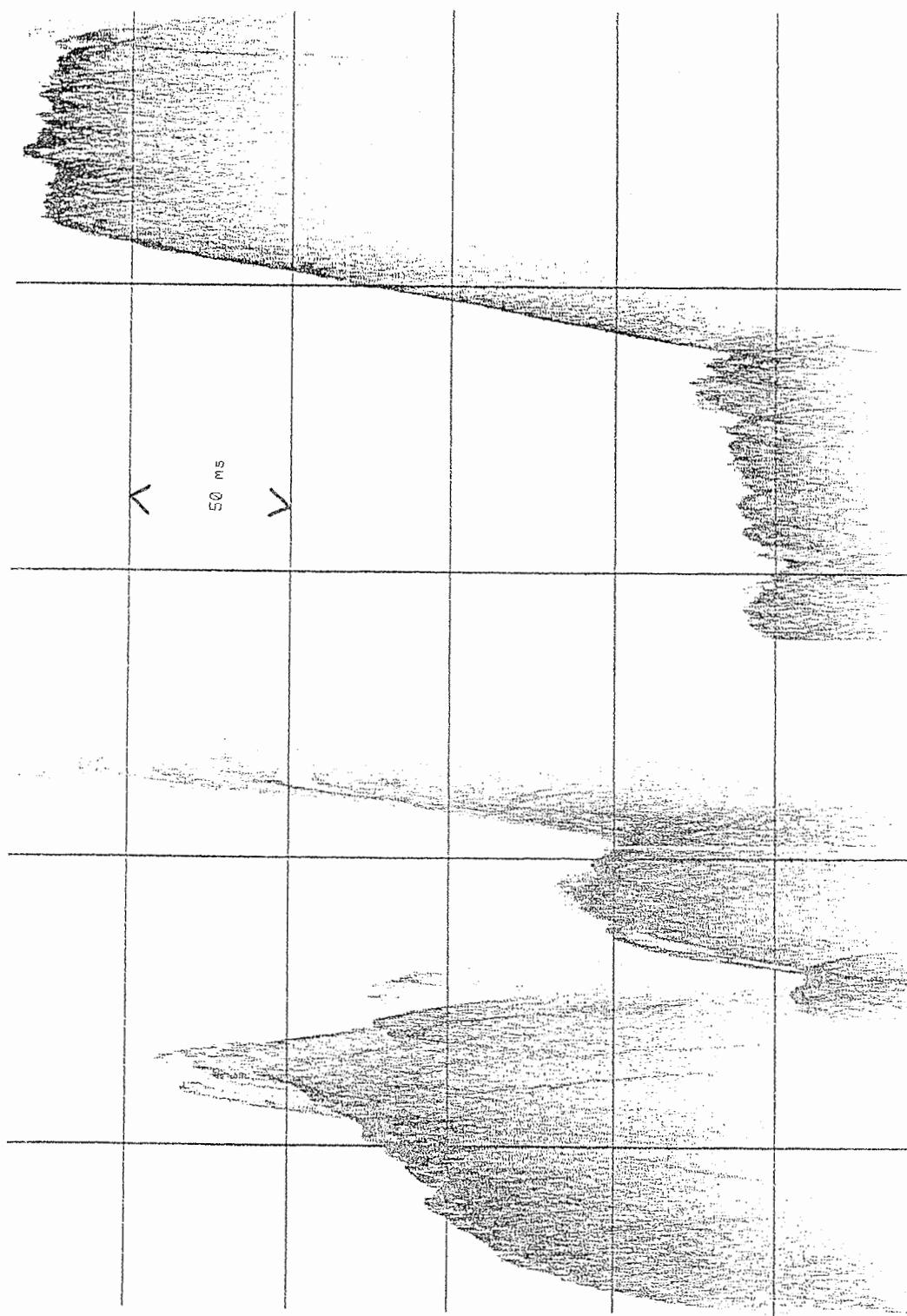


Fig.55 The continental slope between the Sofia Basin and the northwestern Svalbard continental shelf. The steplike pattern is probably caused by normal faulting.

### Summary

Several different discrete types of bottom and subbottom echoes have been detected in the eastern Arctic Basin and on the continental margin line south of the Basin. According to Damuth (1978,1980) different echo types are distinguished on the basis of the presence (or absence) and character of subbottom echoes. Other criteria for categorizing echoes include bottom roughness and whether the echoes are sharp (distinct) or indistinct.

On the continental shelf we have detected two different echo types. On the Barents Sea shelf the echoes are sharp, continuous and organized into a hummocky relief. An infill unit in the troughs can be seen. This corresponds to Damuth's type IA-2 which he interprets to be of glaciogenic origin, probably till. The infill unit could be either of glaciomarine or normal marine origin. It is most likely glaciomarine in this high latitude line. On the Svalbard continental margin a similar pattern occurs but with no infill unit in the troughs. This might correspond to Damuth's (1978) IA-1 echo type, interpreted to be caused late glacial and post glacial winnowing of glaciogenic sediments.

On the abyssal plain some very sharp, distinct and parallel subbottom reflectors grade into semiprolonged echoes with less distinct subbottom reflectors. These echo characteristics correspond to Damuth's (1978,1980) type IB and IIA and are associated with abyssal plains and continental rises. In the lower continental slope - upper continental rise line sharp continuous returns occur with one or more unconformable wedging subbottom reflectors. Damuth (1978) calls these echoes type IC, probably of turbidity and/or other gravity driven origin. On the Yermak Plateau and in the Sofia Basin regular conformable subbottom echoes are formed by sediments draped over topographically uneven seafloor. Along the midoceanic ridge line (The Nansen-Gakkel Ridge) very hard ice conditions disturbed the record. Bent subbottom reflectors along the seamount line indicate thin sediment cover or late pull up of oceanic basement. In the same line seafloor is deeper between the seamount complexes than on the abyssal plain, suggesting faster subsidence and/or slower sedimentation rate between the seamount complexes than on the abyssal plain. The first solution is the most likely.

Coring did not succeed on the abyssal plain, even though penetration was good on the 3.5 kHz, and we expected soft, easy-to-penetrate sediments. On the echo sounding profile, two strong subbottom reflectors at 5 and 15 ms could be seen. In the Norwegian/Greenland Sea and elsewhere (Damuth 1978, 1980) the echo types IB to IIA is associated with relatively coarse beds (silt, sand and occasionally gravel) in the subbottom. This might be the situation in the Nansen Basin too. Coarse sediments make core sampling very difficult (Damuth 1978,1980). On the other stations where the 3.5 kHz record was readable its reflection character and the seafloor morphology did assist in deciding where to core.

#### Description of Surface Sediments in the SEABEAM Survey Area in the Fram Strait

The reflection pattern is characterized by parallel, draped, more or less continuous reflectors. One distinct reflector at approximately 20 ms (two way travel time) can be seen on almost all profiles. On most of the profiles a transparent to semitransparent layer is bounded between this reflector and a distinct reflector at approximately 10 ms. Penetration in sediment-covered areas is generally 40 ms. The seafloor is gently undulating, except for areas that are effected by tectonic movements. The Molloy Fracture Zone develops from a steep and deep fracture zone without sediments on the northernmost profiles, to a gentle and sediment covered westward dipping flexure on the southernmost profiles. The northern extension of the Knipovitch Ridge develops from a sediment-covered partly faulted hill area in the north, to a steep slope without sediments in the south. Only the western part of the ridge is seen on the profiles from the southern area.

In both these tectonically active areas recent faults can be seen in the upper sediments. Gravity-driven sediment structures, probably triggered by tectonic movements are also observed at these locations.

#### **7.4. Sediment Sampling, Instrumentation and Station Work (GIK)**

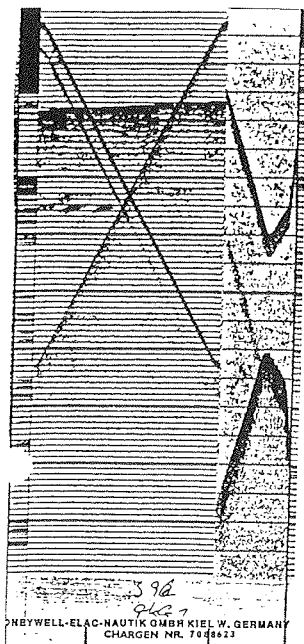
##### Instrumentation

One aim of the geological investigations was to obtain sediment samples with undisturbed surfaces and to get sediment cores as long as possible. For this purpose a giant box grab (GKG) developed by Thiel (Institut für Hydrobiologie und Fischereiwissenschaft, Hamburg) was used; manufactured by Wuttke (Henstedt-Ulzburg, size: 50 x 50 x 60 cm. A long box core (KAL) developed by Kögler (1963) was also used. It is a type 390 with a penetration weight of 3.5 t and a corebox segment sized 30 x 30 x 575 cm (manufactured by Hydrowerkstätten, Kiel-Hassee). Furthermore a combined gravity (SL) / piston (KOL) core type 446 was used which has a penetration weight of 2 t, a tube segment of 575 cm length and 120 mm diameter (manufactured by Hydrowerkstätten, Kiel-Hassee) (Fig. 56a-h).

EXTENSIONS

Marine Geological Sampling Instruments  
Depth and Traction Charts

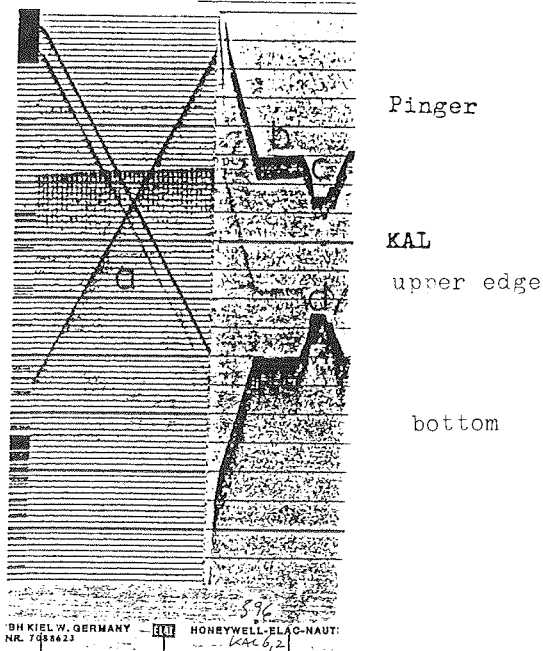
Fig.56a-h Successful attempts of GKG and KAL



396 GKG 1. attempt  
82.76 N 16.42 E  
WD 1380 m

notice: pinger 47m above instr.

- a) lowering to ground with a speed of 0.5m/sec
- b) traction relief
- c) maximum traction 3.63t
- d) oscillation of deep sea rope



396 KAL 6m 2. attempt  
82.80 N 16.03 E  
WD 1382 m

notice: pinger 41m above instr.

- a) lowering with minimum speed of 1.6m/sec
- b) stabilizing phase
- c) lowering to ground
- d) traction relief
- e) maximum traction 7.74t
- f) oscillation

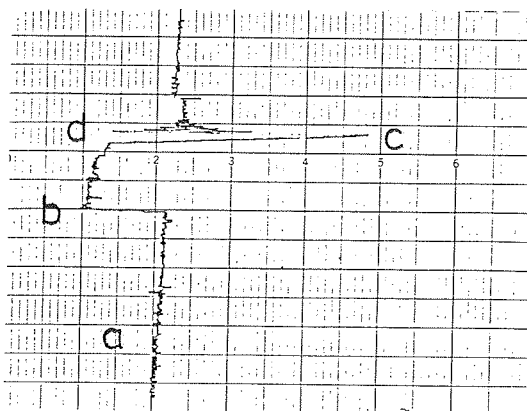


Fig. 56 a,b

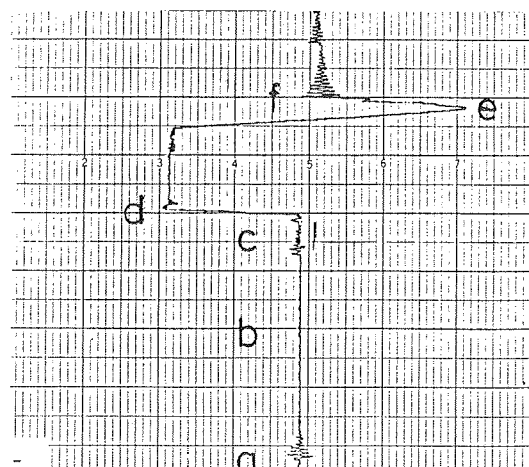
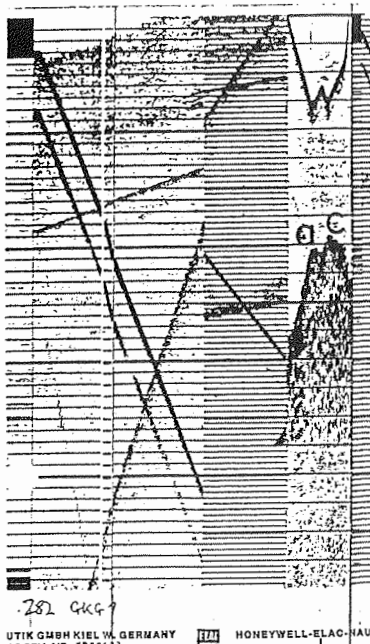


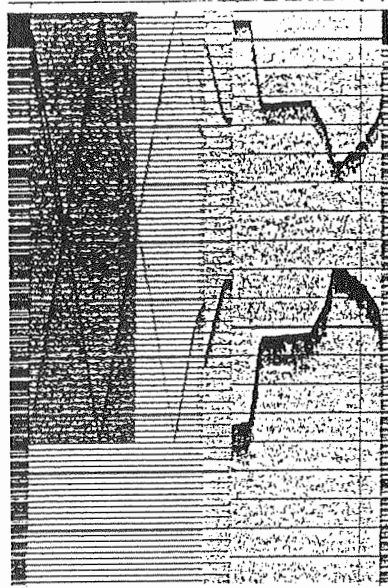
Fig.56 c,d

unsuccessful attempts of GKG and KAL



282 GKG 1.attempt  
81.60 N 31.55 E  
WD 1412 m

notice: twice touched ground  
a) 1st traction relief  
b) no traction increase  
c) 2nd traction relief  
d) maximum traction 3.45t



340 KAL 6m  
82.51 N 32.19 E  
WD 3716 m

notice: quenched and skipped  
a) KAL is lowered to ground  
with maximum speed of  
1m/sec, lowered to the  
ground, gets quenched  
and skips slowly towards  
wire b) lift up of the 3.5t  
penetration weight c) maximum  
traction 6.48t

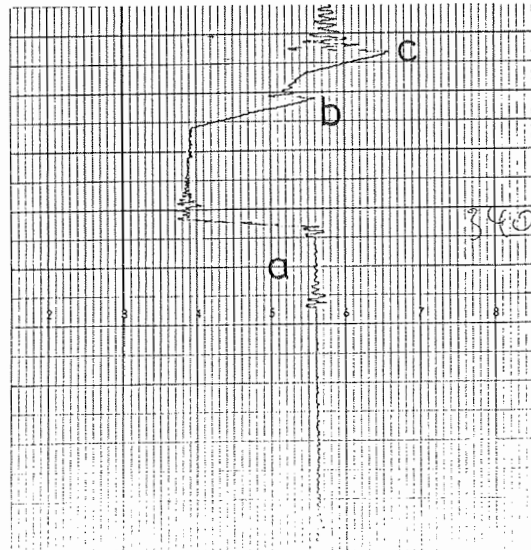
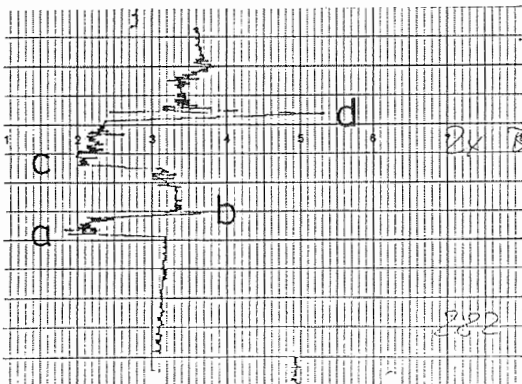
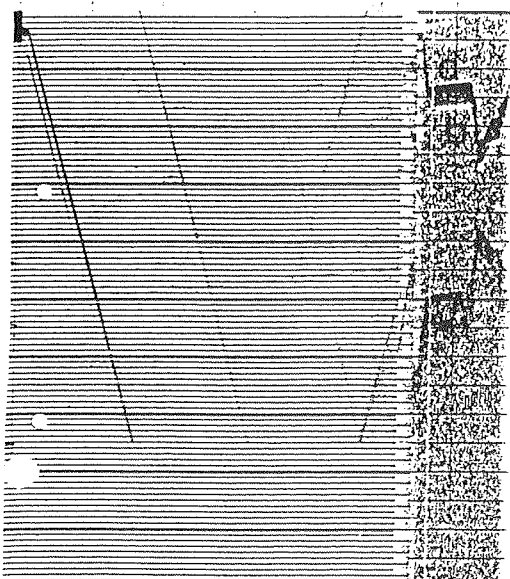


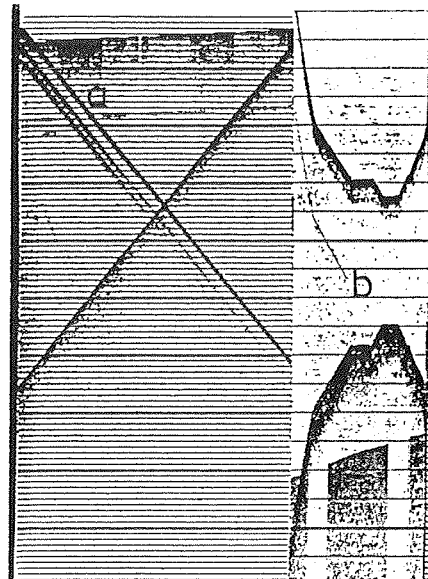
Fig. 56 e, f

successful attempts of SL and KOL



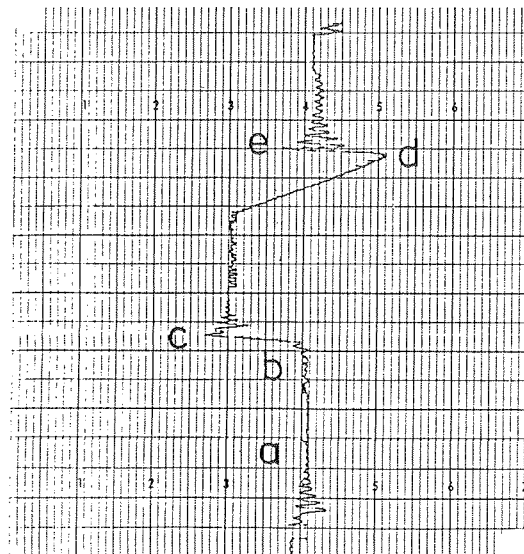
370 SL 6m 2.attempt  
85.93 N 22.73 E  
WD 5210 m

notice: pinger 41m above instr.  
a)stabilizing phase  
b)lowering to ground  
c)traction relief  
d)maximum traction 8.11t  
e)oscillation

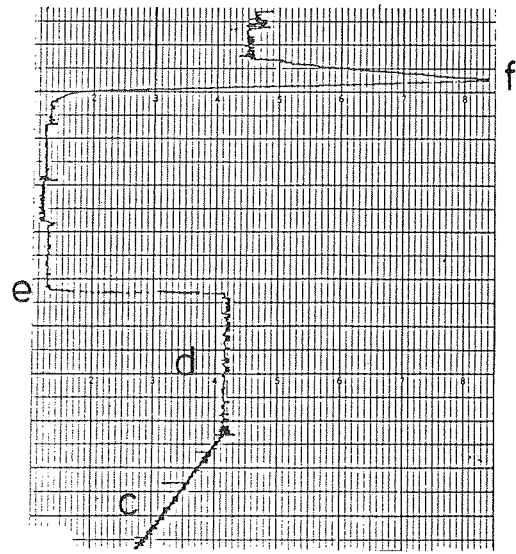


396 KOL 16m  
82.80 N 15.98 E  
WD 1385 m

notice: pinger 31m above instr.  
a)pinger, upper and lower  
edge of instrument  
b)fall of the instrument  
c)lowering with speed of 1.0m/s  
d)lowering to the ground with  
speed of 0.2m/sec  
e)traction relief(max.trac.6.01t

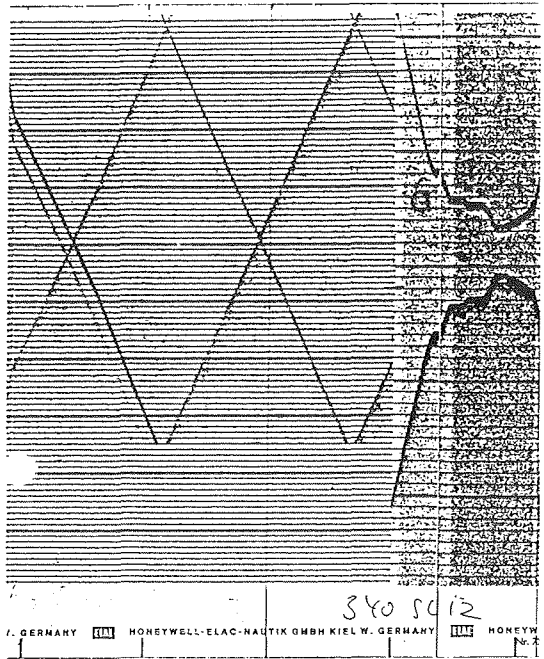


- 145 -



N 8.87

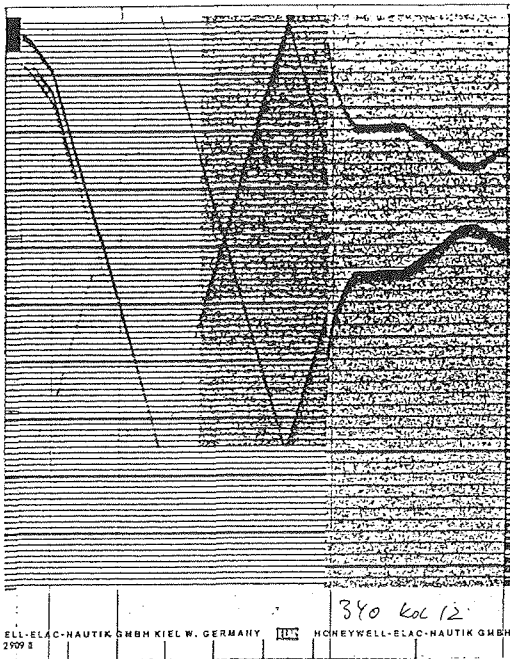
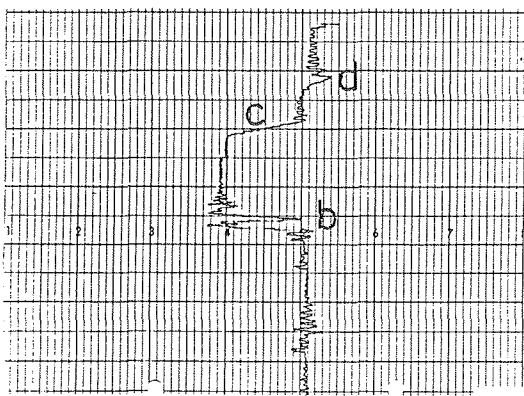
Fig.56 g,h  
unsuccessful attempts of SL and KOL



340 SL 12m  
82.55 N 32.08 E  
WD 3745 m

notice: skipped after 1m of penetration

- a) stepwise lowering to ground followed by stab. phase
- b) after relief new traction-peak appears
- c) straightening and heaving
- d) maximum traction 5.79t



340 KOL 12m  
82.53 N 32.16 E  
WD 3743 m

notice: quenched and caught  
into the wire

a)after relief new traction-  
peak appears

b)lifting up and pulling

c)maximum traction 6.83t

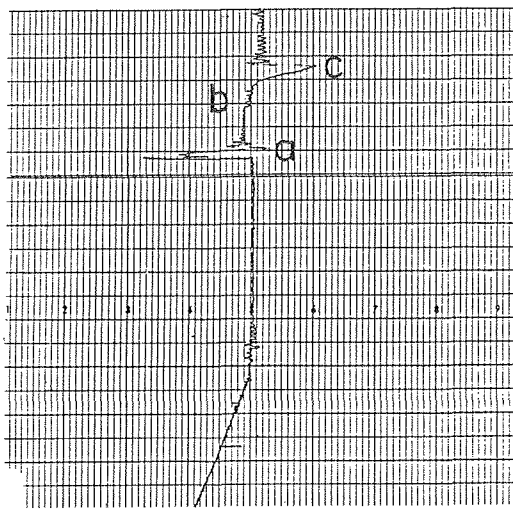


TABLE 11: Station Statistics

Inst.	Attempts all/succ. (no.)	max.trac- tion range (ton)	Score (m)	% Penetr./ Score of suc- cessful.sta. min/ max	Station time without pre- paration (min)
GKG	43	37	1.44- 6.61	14.79	100
KAL6	18	12	5.88-10.21	43.00	65 90 79
KAL12	5	3	6.23- 9.54	9.55	66 100 81
SL4	1	1	6.61	5.82	97
SL6	5	4	5.12- 8.11	14.17	56 100 74
SL12	3	1	5.90	3.60	65
KOL12	1	1	6.83	3.53	88
KOL16	2	2	6.01- 6.68	15.33	60 68 64
KOL18	2	2	6.31- 7.81	8.79	59 76 67
<hr/>		<hr/>		<hr/>	
	80	63		118.58	6625

For five of the six unsuccessful GKG-attempts the new instrument was used which had unsecured setscrews. The setcrews worked loose, allowing the triggerpin to move and therefore the weight was stuck.

The sixth attempt was unsuccessful because the giant box grab tipped over on a steep slope. This occurred because the center of mass of the GKG is near the point of suspension. Several general problems occurred during coring sediments of the eastern Arctic Basin. During the station the ship drifted. Therefore it was not possible to give a precise interpretation of the 3.5 KHz records which should have been used for preliminary assessments of the ocean floor properties. In the ice, the wire-angle could not be corrected which was the reason that one attempt to use a KAL was unsuccessful. On two further KAL attempts the core catcher did not close so the sediment core slipped out of box when the instrument arrived at the water surface.

The KAL sediment cores never broke off ideally at the deepest penetration depth. Only at Station 11/370 at the ridge crest where the basalts were found, no loss of the core material was involved. When the sampling instruments were freed from the ocean floor again registration of tensional force on the system showed oscillations of the cable. This gave a hint as to the possible shortening of the cable during traction relief.

For the 37 core sampling attempts, seven KAL boxes, seven overcoating tubes for SL and KOL and one tube sleeve were used.

#### 7.5 Surface Sediments and Sediment Surfaces (GIK)

Structure and composition of surface sediments are dependent on recent sedimentological, physical, chemical and biological interactions in the water column and at the sediment-water interface. The relationship of various sediments to oceanographic and biological processes is well documented. Most information relating to special features of surface sediments are discussed in detail elsewhere in this report. Here, onboard observations are summarized, providing a preliminary subdivision of surface sediments along bathymetric ranges and sedimentological provinces.

##### Sampling

Samples of surface sediment were recovered with large box corer (GKG) for geological and biological purposes. Sediments were undisturbed and well preserved in most cases. After removal of seawater from the sediment top, the surface was photographed, described and sampled.

##### Macroscopic Observations

All surface sediments were dark yellowish brown, except Station 11/269 which was greyish to dusky brown. Slightly variable silty, sandy clays and sandy, clayey silts were found on the continental slope and rise (Stations 11/269-287), while in the

silty, sandy clays and sandy, clayey silts were found on the continental slope and rise (Stations 11/269-287), while in the Nansen Basin and on the Nansen-Gakkel Ridge only silty to sandy clays were observed.

At Station 11/310, the clay was extremely muddy. At Stations 11/376 (on top of the Nansen-Gakkel Ridge) and 11/396 (Yermak Plateau) surface sediments were also composed of sandy silts. The sediment surface was always smooth and muddy, with high water content. No dropstones were visible on the sediment surfaces of the Svalbard/Nansen-Gakkel Ridge transect.

#### Carbonate Content

Onboard measurements, using the carbonate-bomb (after Müller and Gastner 1971), provided crude information on carbonate content of the surface sediments. In general contents are lower than 5% by weight. Maximum amounts were detected at Station 11/376 ( $\approx$ 8%) at the top of the Nansen-Gakkel Ridge crest and 10% on the Yermak-Plateau, Station 11/396.

#### Smear-slide observations

Results of the smear-slide analyses are summarized in Table 12. Main components of the surface sediments are feldspar, quartz, clay minerals and iron rich phases (amorphous and aggregate). Feldspar and quartz are common on the continental slope, rise and in Nansen Basin; feldspar is dominant on the Nansen-Gakkel Ridge and quartz decreases. Due to the volcanic origin of the Nansen-Gakkel Ridge, volcanic glass increases remarkably in contrast to the deep basin. Contents of heavy minerals, such as pyroxene and amphibole are significantly higher, and hydrothermal minerals (talc, zeolite?) are restricted to the Ridge area. In the Nansen Basin coccoliths are most abundant, iron rich coatings decrease and there is a slight increase in feldspar to the stations further north near the ridge area.

Biogenic carbonates with distinct origin, such as coccoliths, foraminifers or calcite spicules as well as idiomorphous calcite and calcite fragments with unknown origin have been observed in most sediments along the transect.

TABLE 12: Smear-Slide Investigations of GKG  
Surface Sediments: Preliminary Results

pos: area	Qu: quartz	Fs: feldspar
Cl: clay minerals	iC: idiom. calcite	Op: opaque minerals
Vg: volcan. glass	Fe: iron rich aggreg.	Co: coccoliths
Di: diatoms	Sp: sponge spicules	Bi: bioclasts
css: Svalbard continental shelf and slope		nb: Nansen Basin
ngr: Nansen-Gakkel Ridge		yer: Yermak Plateau

station	pos	Qu	Fs	Cl	iC	Op	Vg	Fe	Co	Di	Sp	Bi	remarks
<hr/>													
11/													
269	css	+	+	+	+	+		+		+	+		
276	css	+	?	+	+	+						+	
278	css	+	+	+		+	+	+	+	+	+	+	
280	css	++	+	+		+	+	+		+	+	+	
282	css	+	+	+		+	+	+				+	
285	css	+	+	+	+	+	+	+				+	
287	css	+	+	+	+	+		+			+	+	
296	css	+	?	+	+	+		+	+	+	+		mica
310	nb	+	+	+	+	+	-	++				+	
340	nb	+	+	+	+	+	?	-	++		+	+	mica
362	nb	+	++	+		+	+	-	+			+	tourm.
364	ngr	++	++	+		+	+	++	+			+	zeol.?
365	ngr	++	++	+	+	+	+	+	+			+	talc
371	ngr	+	++	+		+	+	+	-			+	v.min
372	ngr	+	++	+		+	+	+	+	+		+	zeol.?
376	ngr	++	++	+		+		+	+			+	zeol.?
396	yer	+	+	-	+	+	+	+	+	+	+	+	

++: abundant

+: common

-: rare

? : very few or questionable

## **7.6 Surface Sediment Layers: Composition and Structure (GIK, FG/UB, AGC/BIO)**

On ARK IV/3, 22 cores were taken by a large box corer ("Großkastengreifer", GKG), to be used for geological, geophysical and geochemical analyses of the recovered sediment. The average length of the cores was about 30-40 cm, and added up to a total length of 8.44 m.

### Sampling

After opening the core, a detailed description of the sediment column in terms of structure, texture and fossils was carried out. Color photographs and samples for X-ray radiographs were taken to provide reproducible information about the uppermost sediment layers. Continuous downcore sampling was done by long plastic tubes for analysis of geophysical properties, nutrients,  $\text{^{14}C}$ , pore water geochemistry, and biostratigraphy and sedimentology. Samples of the uppermost 15 cm were taken at selected locations for radionuclide analysis. Syringe samples (5 ml, 10 ml) were taken downcore in specific depth intervals for analyses of siliceous microfossils, palynomorphs and water content. Continuous reference box sampling and bulk sampling was carried out for analyses of microfossils and sediment petrography.

In addition, several locations were sampled for the following:

1. geoacoustic modeling: characterization of glacial/interglacial sediments to assist in determining downcore cycles of sedimentation in the central Arctic.
2. radiocarbon dating: accelerator C-14 dating to determine rates of sedimentation, and to help identify and characterize central Arctic surface sediments.

Subsamples from 6 GKG cores will be analysed for magnetic susceptibility, p-wave and attenuation. The subsamples will then be split, described, and analysed as follows: measurement of index properties, determination of foraminiferal abundances, and sampling at selected depths for approximately 30 accelerator C-14 analyses.

### Sediment Color

Using the Rock Color Chart (issued by the Geological Society of America), the sediment colors were described. They ranged mostly from pale yellowish brown to dark gray. The uppermost layer is usually of dark yellowish brown color with only rare variations. At the continental slope darker sediments (olive gray to dark gray) occurred at the base of the GKGs.

### Grain Size, Texture, and Composition

The grain size of the upper sediment layers ranges from clay to medium sand. However, definite sand layers are rare and restricted to turbidites and to foraminifer-rich horizons in the Nansen-Gakkel Ridge area. Most common are silty clays and sandy silty clays, the latter containing up to 25 % sand-sized particles

which are mostly of detrital origin in the continental shelf/slope/rise area, and of biogenic origin (foraminifers) in the ridge area. Dropstones were generally lacking beyond the shelf edge and mud clasts were common only on the Nansen-Gakkel Ridge. Furthermore, sediment sorting seems to be generally poor to medium within the clay-to-fine sand range beyond the shelf edge. Good sorting is only observed in areas of the abyssal plain not influenced by turbidites. A pure clay layer, 30 cm thick, was recovered in Core 11/362-15.

Bioturbation within the upper sediment column is rare to common in the shelf/slope area and on the ridge, but is nearly totally lacking on the continental rise and in the abyssal plain.

Only few investigations on sediment composition could be carried out onboard POLARSTERN. These preliminary investigations show that the composition of the uppermost 30-50 cm is very similar to that of the sediment surface (see Chapter 7.5). Other general observations may be summarized as follows: quartz is the main constituent in cores from the shelf/slope/rise area; quartz is replaced by feldspar, volcanic glass and heavy minerals plus iron-containing and iron-coated minerals on the Nansen-Gakkel Ridge; biogenic particles are included in the sand layers from the latter area whereas the sand-sized grains in near-shelf sediments are mostly detritic (quartz, feldspar, calcite).

#### Lithostratigraphy and Sedimentological Provinces

Five sedimentological provinces in the eastern Arctic Ocean can be distinguished from shipboard analyses of the uppermost sediment layers. Characteristics of this upper part of the sediment column are as follows (see Fig. 57 and Geoscientific Working Party (1988)).

##### a. The Shelf Edge (Station 11/269)

The only GKG taken from this area (water depth 200 m) consisted of a thin dark brownish top layer (2 cm) and a considerably thicker bottom unit displaying a variety of olive gray colors. A very high silt content dominates the grain size distribution in both sediment units.

##### b. The Continental Slope

(Stations 11/276, 278, 280, 282, 285, 287, 296, 310)  
In the GKGs from this area (water depth 500-3000 m) a dark brownish top unit is characteristic. It consists of several layers in the cores from the upper slope, but stratification generally decreases downslope. Its thickness is about 20 cm at 500-1000 m water depth and clearly increases from 9 cm to more than 35 cm with increasing water depth below 1400 m. This brownish unit consists of sandy clayey silts (60-80 % silt) and often shows darker laminae in the middle and lower part. Bioturbation was observed only occasionally.

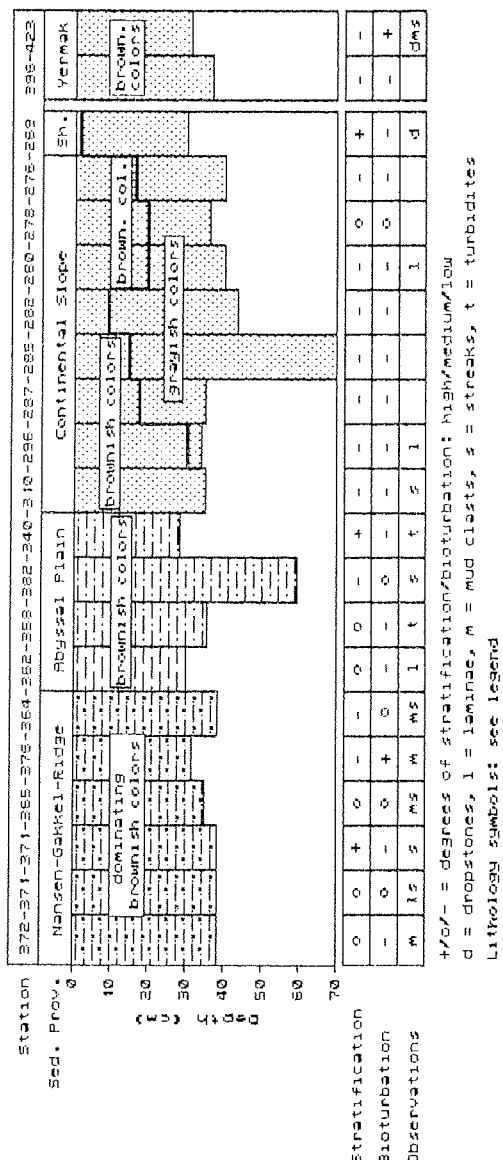


Fig. 57 Summary of GKG characteristics. For explanation of symbols see legend on Fig 58.

Below this unit, an often homogeneous olive gray unit with a rather sharp upper contact was present in cores from Stations 11/278-296. Silt content is about 60%. This unit was not observed in cores north of Station 11/296 due to increasing thickness of the upper brown layer. Both units are characterized by a downslope decrease in grain size. The sand content is below 3% in all cores from the continental slope north of Station 11/285.

c. The Continental Rise and Abyssal Plain

(Stations 11/340, 358, 362, 382)

Cores from this area consist of the above mentioned dark brown unit only, but are more stratified due to the presence of turbidites in cores from Stations 11/340 and 11/358. These turbidites show a fining-upward texture of sand to silty clay, sometimes laminated, with a sharp base truncating the sediment layer below. Non-turbiditic layers consist of silty clays, usually containing less than 5% sand particles. Bioturbation is generally poor. Core 362-15 (from Station 11/362) has typical abyssal-plain sediment, strongly dominated by clay with only slight color changes throughout the sediment column. Site 382 from the abyssal plain probably is protected from turbiditic influence by the Yermak Plateau. Therefore, stratification and color changes are limited throughout the core.

d. The Nansen-Gakkel Ridge

(Stations 11/364, 365, 371, 372, 376)

The 6 GKGS from this area consist mostly of dark brownish layers, with only rare olive gray intercalations. Stratification into distinguishable layers occurs frequently, possibly due to the influence of locally rough topography. Sediments from ridge sites can be classified as silty clays and sandy silty clays; sand layers often contain foraminiferas. Especially Core 11/372-7 (from station 11/372) shows a rather high content of planktonic foraminifers in sand layers. A thin sandy layer, 2 cm thickness at about 25-30 cm depth, is present in the 3 cores from Stations 11/371 and 372. Most cores from the ridge area show little to medium bioturbation. Horizontal streaks of grayish, brownish and reddish color are common, as well as mud clasts of different color.

e. The Yermak Plateau

(Stations 11/396, 423)

The two GKGS from the Yermak plateau are of dark brownish color, rather homogeneous, with little stratification, and consist of dominantly silty sediments. Core 11/423-6 (from station 11/423) appears to contain one thin turbidite layer. Darker brownish and grayish horizontal streaks are quite common.

Summarizing this short and preliminary description of the uppermost sediment layers of the eastern Arctic Ocean, the downslope decreasing grain size and stratification are rather usual features compared to other ocean basins. The uppermost sediments from the Nansen-Gakkel-Ridge appear to contain a well-structured record, including rather constant biogenic sedimentation and

influence of recent spreading activity and glacimarine conditions.

### 7.7 Long Sediment Cores: Composition and Structure (GIK, FG/UB, AGC/BIO)

One of the most exciting geoscientific problems of Arctic research is the paleoclimatic and paleoceanographic history of the northern polar deep-sea basins during the development of the glacial-interglacial cycles of the Quaternary. These developments can only be studied by means of long, large diameter sediment cores of high stratigraphic quality. Sediment coring was therefore high priority during ARK IV/3 (see Chapter 7.4). The location of the sediment cores can be found in the charts displaying the station locations (Fig. 2a, 36).

Only the long box cores (KALs) were opened on board POLARSTERN; the other cores will be opened at GIK following the cruise. After the KALs were opened, the sediment composition, grain size, sediment texture and colour were described in detail. Following core description, samples for radiographs and magnetostratigraphy were obtained and syringes for determination of water content were taken every 5 cm. Archive boxes were filled with sediment for a continuous downcore record. Then detailed sampling for biostratigraphy, isotope-stratigraphy, sediment-petrography and geochemistry (C-organic, C-carbonate, radioactive dating, trace and major elements, porewater analysis) was carried out. The rest of the material was placed in plastic sample bags (1 to 5 cm intervals). Piston cores and gravity cores were not opened on board. They were cut into 1 meter pieces, sealed and stored in wooden boxes. These cores will be opened in Kiel, where clean cutting of the liners is guaranteed. Detailed core descriptions are published by the Geoscientific Working Party (1988).

#### 7.7.1 Sediment Features and Composition of Long Box Cores (KAL) (GIK, AGC/BIO)

##### Sediment Colour

Surface sediments of the eastern Arctic Ocean are of dark yellowish brown to dark grey and black colour (Figs. 59 and 59). The contacts between brown and grey sediments are usually sharp. However transition zones are also common. The colours of these horizons may be olive brown to olive grey. Occasionally dark brown to black laminae, nodules or concretions (coal, Fe, Mn) occur in the upper yellowish brown units.

##### Sediment Texture and Grain Size

Grain size of the sediments usually ranges from silt to clay. However sand layers and lenses as well as sandy silt horizons are common. The sandy (sometimes gravelly) material preferentially occurs in the KALs from the continental slope and rise area. These layers are probably generated by turbidites or bottom currents and occur at Stations 11/282, 296, 340.

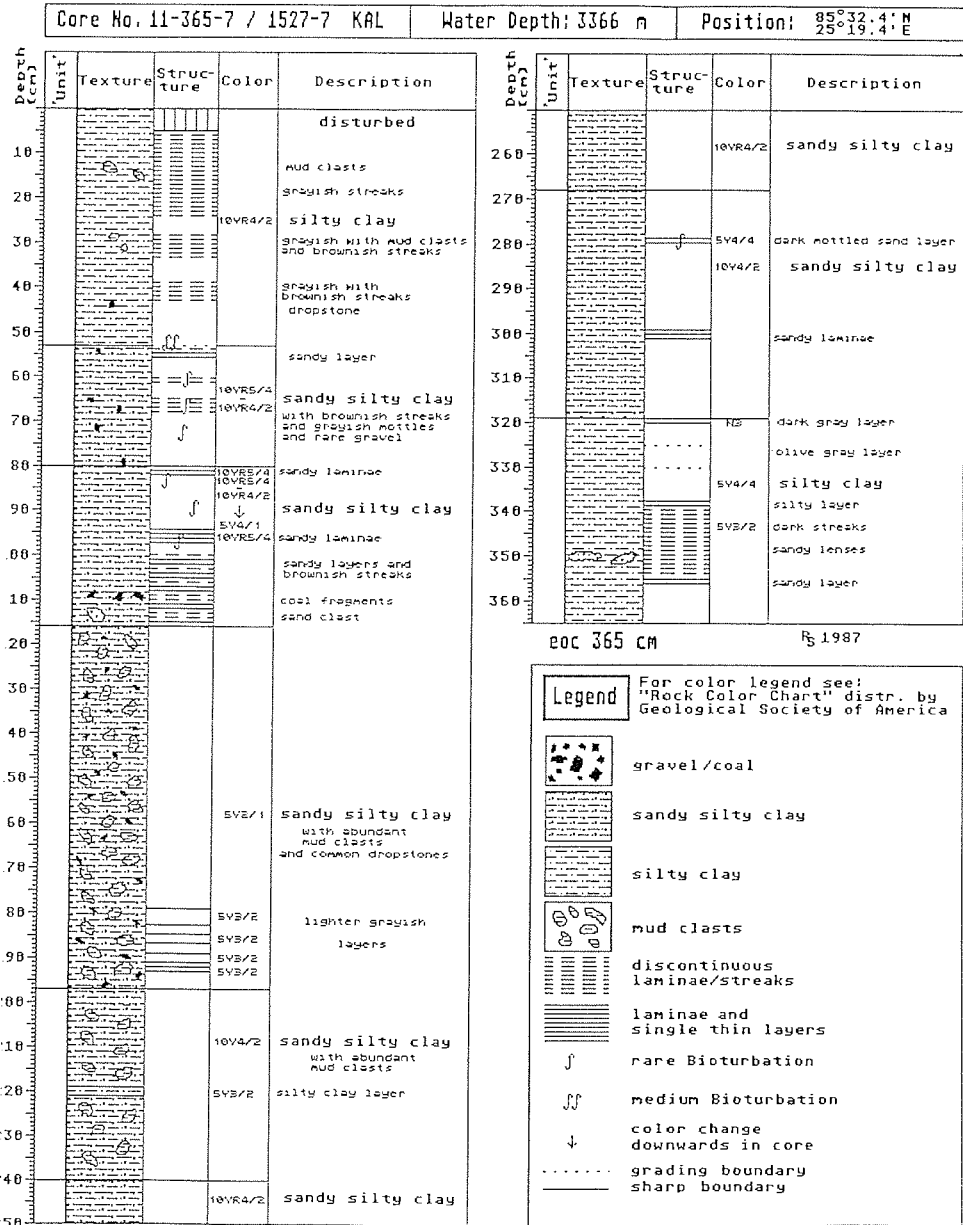


Fig. 58 Lithologic description of KAL 365. See Fig. 2 for station location.

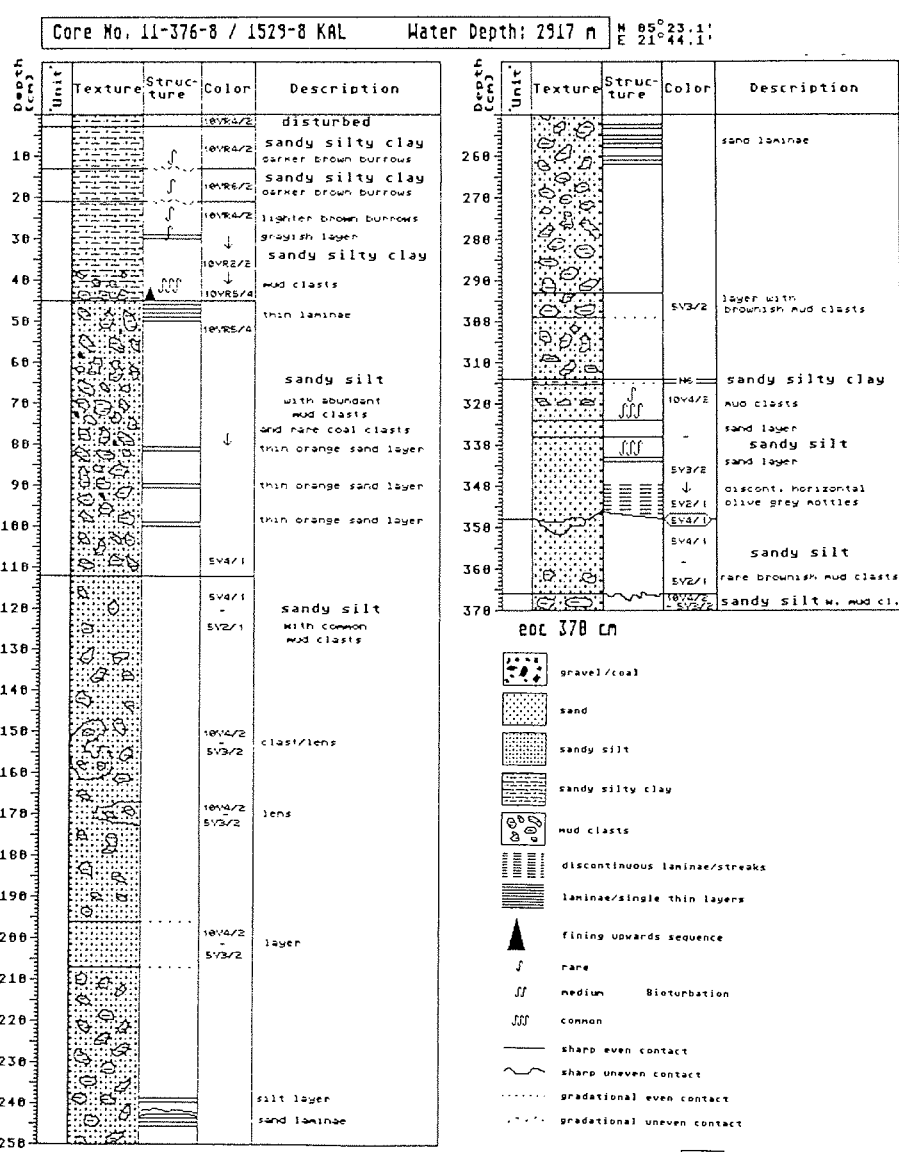


Fig.59 Lithologic description of KAL 376. See Fig. 2 for station location.

Few dropstones have been found in the sediments of the eastern Arctic Basin. However, mud clasts and pebbles occur, mainly within dark grey sediments (Figs. 58 and 59). The sediments of the Nansen-Gakkel Ridge area appear to have a higher sand content than the sediments of the abyssal plain area. Bioturbation is common in all sediments.

Station 11/370 contained coarse basalt fragments with hydrothermal minerals. The largest basaltic specimen was 15 cm in diameter.

#### Sediment Composition of Bulk Samples

Sediment composition of bulk samples was estimated by smear slide analysis. The carbonate content was determined gasometrically (Fig. 60). Only two KALs from the continental rise had a carbonate content higher than five percent. These higher values were measured mostly in sandy layers. In general, the mineralogical composition of all sediments appear to be uniform, consisting mainly of quartz plus feldspar (30-50%) and clay minerals (20-30%).

Carbonate content can reach almost 20% and consists of biogenic and/or detrital carbonate components. Heavy minerals (such as pyroxene and amphibole), volcanic glass (brown, green, yellowish-white) and hydrothermal alteration products of basalts (amorphous Fe-compounds, Mn-crusts, zeolites, talc, unidentified minerals) are common in the Nansen-Gakkel Ridge area (especially Station 11/370).

The yellowish brown surface sediments are characterized by amorphous Fe-compounds, which show pale yellow colours in transmitted light. Besides these isolated Fe-particles, Fe-coatings on mineral surfaces and around aggregates are very common. Black, spotty coatings ( $\text{MnO}_2$  ?,  $\text{FeS}_x\text{H}_2\text{O}$  ?) are also common.

The olive grey to dark grey sediments have a very similar mineralogical composition to the brown sediments. However the amorphous Fe-compounds are significantly reduced or absent. It appears that the opaque components increase in these sediments. Opaque materials were not identified microscopically but are believed to be coal, marine organic matter or Fe-sulphides. Mud clasts which occur preferentially in the dark grey units (Stations 11/285, 296, 310, 340, 364, 365, 372, 376, 396) show Fe-rich coatings or cements. The clasts are aggregates of clay to sand-sized minerals.

#### **7.7.2 Long Sediment Cores: Composition of the Sand Fraction of Cores 11/296, 340, and 372 (GIK)**

##### Methods of Investigation

Samples from three sediment cores were sieved and the sand-fraction extracted. Components were identified with the aid of a

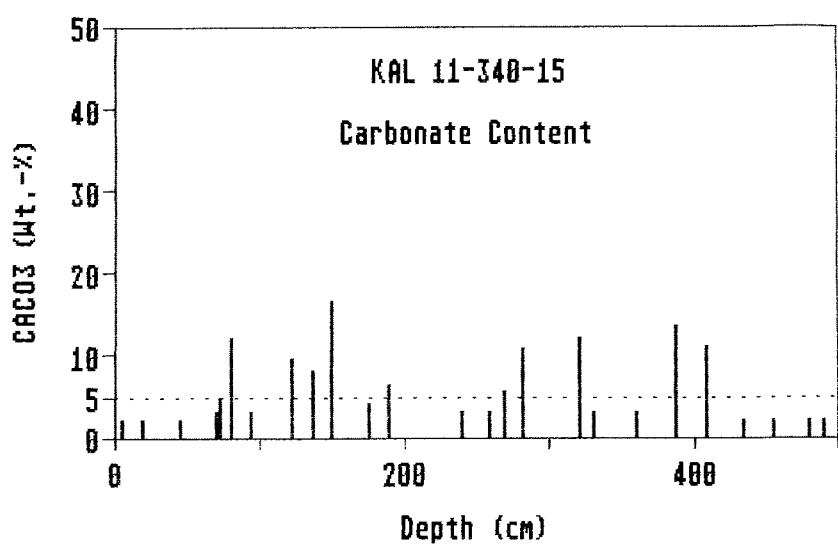
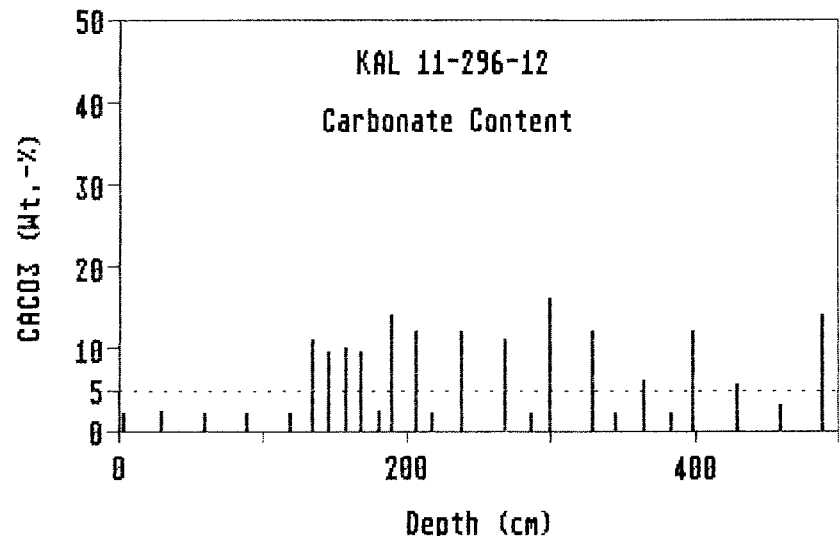


Fig. 60 Concentration of calcareous material in the bulk sediment of ARK IV/3 sediment cores 296 and 340. For station locations see Fig. 2.

binocular microscope and are listed according to estimated percentiles. The less abundant particles are listed as well (presence/absence) see Tables 13/1-3.

#### Components of the Sand Fraction

Quartz and feldspar are the most abundant components and often compose more than 90% of the sand fraction. Roundness, clarity and color were also described.

The group "rock fragments" combines metamorphic and magmatic leucocrate and melanocrate crystalline particles. Mica shists and phyllite shists also were distinguished. Pyroxene could be identified occasionally. Mica crystals (up to 1 mm in length) reach several percent in some samples.

Although dark grey quarzites are dominant, green and yellowish ones occur as well. Quarzites are also found in coarser sizes up to several centimeters in diameter.

Coal fragments with organic relict texture compose up to 10% of some samples and are occasionally more than 5mm in diameter.

Iron oxides and hydroxides are identified as fine-grained orange-colored particles. Iron crusts or oxidized pyrite are identified.

Detritic carbonate fragments (tested with HCl) are found in many samples but these were never more than a few percent of the whole.

Pyrite can be divided in two groups: shiny idiomorphic crystals, which are seldom oxidized, and frambooids, which were found in only one core (11/372).

Planktonic and benthic agglutinating and calcareous foraminifers are combined in this group. Mollusc shells, ostracods and sponge spicules are less abundant.

Dark red to black button-like disks approximately 1 mm in diameter were found in many samples. They are non-magnetic, are lighter than quartz and they can be burned. They may consist of resin and are called resin discs in this preliminary investigation.

#### Distribution of Coarse Components in Kastenlot Cores 11/296, 11/340 and 11/372

Core 11/296: In this core the diversity of components in the >63 um fraction is very low. The most common particles aside from quartz and feldspar are foraminifers, mica and rock fragments (Fig. 61 a-c). Some siltstones between 2 and 6mm in size were also found (Table 13/1). Except for minor variations in foraminifer abundance and rock fragments there is no change in the composition of the core down to 410cm depth. Between 410 and

COMPOSITION OF THE SANDFRACTION (particle-%)

CORE 11/296-12

Depth in cm	FELDSPAR QUARTZ QUARTZITE	CRYSTALLINE MICA	FORAMINIFERS	Rest	Components <1%
5-7	66 B-D	4	10	14	S
29-31	94 B-D	2	-	1	SFF
54-56	98 B-D	-	-	-	FC
79-81	97 B-C	-	-	-	CG
104-106	92 B-C	2	3	1	KP
119-121	95 B-C	-	2	-	O
149-151	97 A-C	-	-	-	KC
174-176	97 B-C	1	-	-	SFC
189-191	96 B-C	-	1	-	SKCG
214-216	98 B-C	-	2	-	CPIG
224-226	97 A-B	2	1	-	-
239-241	97 A-B	1	1	-	P
244-246	97 B-C	1	1	-	-
254-256	95 A-B	3	-	-	SF
269-271	96 B-C	1	1	-	KC
284-286	96 B-C	2	-	-	SF
314-316	98 A-B	1	-	-	F
324-326	98 A-C	2	-	-	GKF
339-341	95 B-C	5	-	-	GC
349-351	98 B-C	1	1	-	KDF
359-361	96 B-C	1	-	-	KF
374-376	95 A-B	1	2	1	S
384-386	92 A-B	4	5	1	K
404-406	95 B-C	4	1	-	CF
409-411	93 B-C	5	-	2	C
419-421	80 B-C	10	-	10	CG
424-426	69 B-C	1	-	30	KI
439-441	70 A-B	10	-	10	-
449-451	30 B-C	10	30	30	-
459-461	55 B-C	10	5	30	-
464-466	70 A-C	10	5	15	-
479-481	97 B-C	2	1	-	FKC

A=Glaucconite

G=Mica

O=Coal

C=Carbonate

I=Crystalline

R=Iron oxides

D=Siltstone

K=Resin disk

S=Sponge needles

F=Foraminifers

P=Pyrite

Letters behind quartz-% = Roundness (A=angular to F=rounded)

Table 13/1: Composition of the sand fraction (>0.063mm) in %. Core 11/296-12. See Fig. 2 for station location.

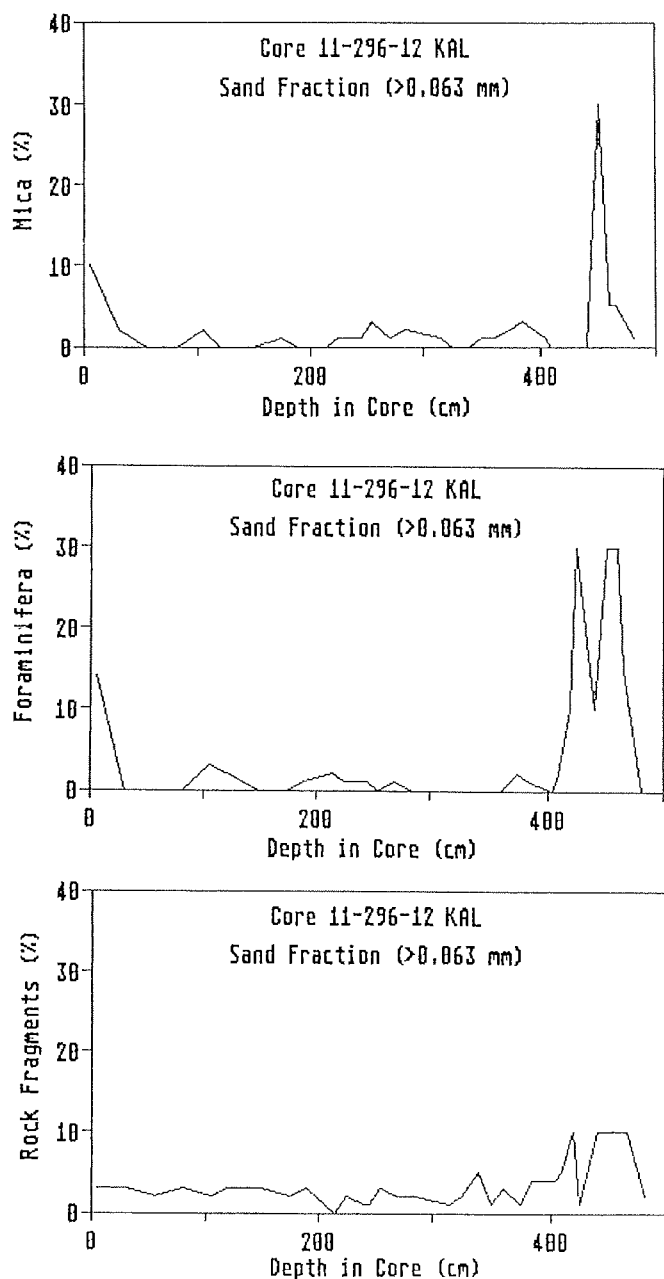


Fig. 61 a-c) Distribution of some major components of the sand fraction of core 11/296-12 of ARK IV/3.

460cm both foraminifers and rock fragments are abundant. Resin disks occur in the whole core but are more common below 330cm.

Core 11/340: Many different components could be distinguished in this core (Table 13/2). Gravel, composed mostly of siltstones, was found throughout the entire core (Fig. 62 a), especially in a 2cm thick gravel layer between 368 and 370cm. In this layer a 10cm-long siltstone with shell and coal fragments on its surface was found. A carbonate clast 3cm in diameter was found at 265cm depth. Coal fragments were very common in this core, reaching more than 20% at times and occurring in a rhythmic fashion between 70 and 150cm and between 250 and 410cm. Resin disks are also common in the same depths. Silt- and sandstones made up a large percentage of the 240cm level although the coarse fraction contained very little sand. Siltstones were most common between 350 and 400cm. Less than 2% carbonate detritus was observed, and iron oxides and rock fragments are spread throughout the core. There was a sharp mica peak between 390 and 420cm. Foraminifers were found at several depths but are more abundant between 250 and 320cm.

Core 11/372: The composition of this core shows good stratification (Table 13/3, Fig. 63 a-d). At the surface a peak in foraminifer abundance was found which continues to 50cm depth. Pyrite frambooids are very common and make up 15% of the layer between 70 and 140cm. They have a dark brown rim showing oxidation. Because they are formed in sulphidic facies they are probably transported and redeposited within the oxidizing sediment. Below 110cm (in the dark grey sediment) coal increases to 10%. Iron oxides occur only down to 140cm, where the abundance of rock fragments also decreases. Detrital carbonate made up only a small percent of the core, but was found throughout the core. One piece of amber (2mm in diameter) occurred at 250cm. Coarser material (>2mm) consisted of coal between 110 and 180cm and of siltstone and sandstone below 220cm. A siltstone 1cm in diameter and a quarzitic sandstone 3cm in length was found in the lower part of the core.

#### Comparison of the Sand Fraction

In Core 11/296 very little coal was found, quite a bit in 11/340 and a small amount again in 11/372. In those cores, where coal was identified, it seems to occur continuously through entire sequence. The resin discs correlate in 11/340 with the coal but in other cores the correlation is not as clear. In 11/296 there is hardly any coal but there are common resin discs, while in 11/372 coal frequently occurs and only one disk is found.

The coarser grains consisted mostly of coal or siltstone. Carbonate stones and quarzites were less abundant. Description of biogenic particles is presented in Chapter 7.8.

COMPOSITION OF THE SANDFRACTION (particle-%)

CORE 11/340-15

cm depth	QUARTZ QUARTZITE FELDSPAR	MICA	SILTSTONE SANDSTONE	COAL	FORAMI- nifers	Rest Compo- nents <1%
5	96	0	0	1	3	0 KIGRDA
20	93	0	3	0	1	3 CRA
30	99	0	0	1	0	3 GD
40	95	0	1	1	0	2 FIGR
55	98	0	0	2	0	2 F
60	96	0	0	2	0	1 FGCR
70	58	0	0	40	0	0 KFGCRD
80	89	0	0	10	0	1 FGCD
90	95	0	0	5	0	0 KFCRD
100	89	0	0	10	0	1 KFD
110	92	0	0	7	1	0 KIGCD
120	76	0	0	4	20	0 KIGRD
130	94	0	0	5	0	1 KFBG
140	70	0	0	15	15	0 K
150	70	0	0	30	0	0 K
160	93	0	2	0	0	0 FRDA
170	98	0	1	1	0	0 C
180	82	0	0	3	15	0 C
190	65	0	0	0	35	0 GROD
200	99	0	1	0	0	0 FCRO
210	99	0	0	1	0	0 CRD
220	98	0	1	0	0	1 ILCR
227	94	0	3	0	0	3 KIDRC
230	97	0	1	0	0	2 TRUC
240	40	0	60	0	0	0 GRO
250	50	0	0	48	0	2 KJ
260	15	0	0	0	85	0 DAD
270	79	0	0	20	1	0 CD
280	10	0	0	1	89	0 S
290	5	0	1	0	89	5 SG
300	85	0	0	15	0	0 KSGCA
310	88	0	0	10	1	0 KS5C
320	40	0	0	4	56	0 IRD
328	88	0	0	10	1	0 KDCAP
338	96	0	1	2	1	0 KIGARP
350	84	0	15	1	0	0 ECR
360	95	0	2	2	0	1 IP
369	77	0	20	2	0	1 ICAP
372	91	0	6	2	3	0 ICARP
378	77	0	1	10	12	0 KGAR
390	59	10	0	30	0	1 D
400	10	75	5	7	0	0 FK
410	15	17	0	68	1	1 S
420	94	0	0	4	2	0 RIARD
430	99	0	0	1	0	0 KFCRDP
440	99	0	1	1	0	0 FIA
450	98	0	0	2	0	0 SCARD
460	99	0	0	1	0	0 GCAD
470	96	0	1	3	0	0 ICAP
480	97	0	0	3	0	0 FICP
490	97	0	0	3	0	0 ICAP

(Letters as in core 11/296)

Table 13/2: Composition of the sand fraction (>0.063mm) in core 11/340-15. See Fig. 2 for station location.

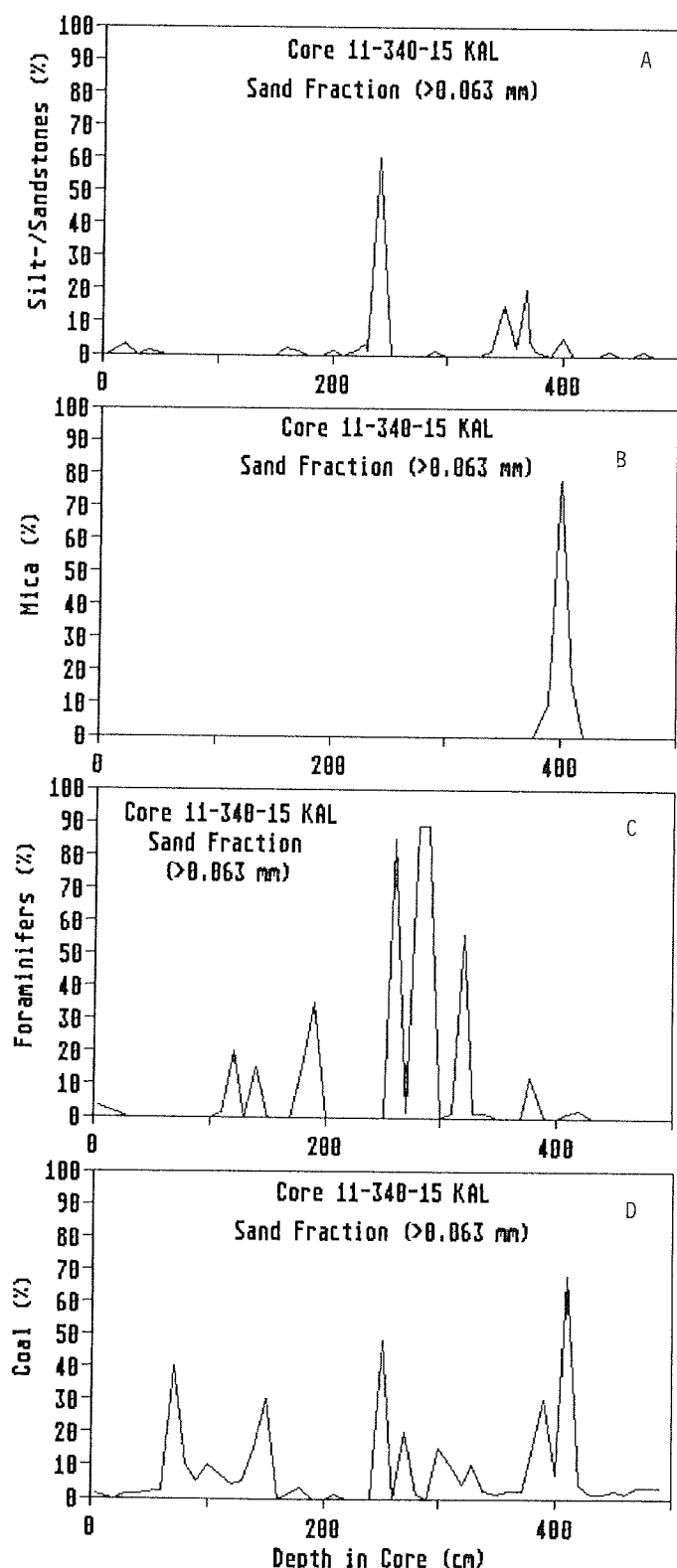


Fig.62/a-d Distribution of major components of the sand fraction of core 11/340 of ARK IV/3.

## Core 11-372-3

Depth (cm)	Quartz Quartzite Feldspar	Siltstone Sandstone	Coal	Pyrite	Forams	Compo- nents < 1%
1.5	C 40	0	1	0	59	SIRP
6.0	C 69	1	0	0	30	IRO
11.5	B-C 93	1	1	0	3	RPI
17.0	B-C 92	0	1	0	7	ICR
23.0	C 59	0	1	0	40	SFIGOD
28.0	B-C 83	0	1	0	15	SIG
33.5	B-C 79	0	1	0	20	IPD
39.0	B-C 60	0	0	0	40	ICROPD
45.0	B-C 83	2	0	0	15	ICROP
49.5	B 97	0	1	0	1	IGPD
53.5	B-C 99	0	0	0	0	FIGCO
60.0	B 99	0	0	0	0	FKIGCROPD
66.5	B-C 93	1	0	0	5	IGRP
71.5	B 86	0	3	1	10	IGRD
76.0	B 85	0	2	3	0	FGRC
81.5	B-C 79	2	2	10	0	IGC
87.5	B 93	4	0	0	0	FIGCR
92.0	B 93	2	0	2	0	FICR
100.0	B 90	0	0	8	0	ICROAD
106.5	B 85	0	0	15	0	IROD
114.5	B 85	1	3	6	0	ICR
121.5	B 83	3	4	8	0	ICR
127.0	B 86	6	2	3	0	IGCR
132.5	C-D 94	0	2	3	0	IGCRD
137.5	C 98	0	2	0	0	PIAD
145.5	C 98	1	1	0	0	PIGCA
151.5	B-C 99	0	1	0	0	PIGAD
157.5	B 98	0	1	0	0	PGCAD
162.5	B-C 97	0	2	1	0	IGAD
168.5	B-C 99	0	1	0	0	PIAD
173.5	B-C 99	0	1	0	0	PGD
177.5	B-C 99	1	0	0	0	PIG
185.5	B-C 99	0	1	0	0	IAD
191.5	C 98	1	1	0	0	PIC
197.0	B 99	0	1	0	0	PIGCD
202.0	B 94	0	3	0	0	GD
207.0	B 95	1	2	0	0	A
213.0	B 93	0	5	0	0	PGD
218.0	B 95	0	3	0	2	PIGCD
227.0	B 98	0	2	0	0	D
233.0	B 94	0	5	0	0	PGCD
237.5	B 97	1	2	0	0	PGC
241.0	B 95	0	3	0	0	PGD
CC	247.5B 90	0	10	0	0	IGD
CC	251.0B-C 90	1	7	0	0	FPIA

Table 13/3: Composition of the sand fraction (&gt;0.063mm) in core 11/372. See Fig. 2 for station location.

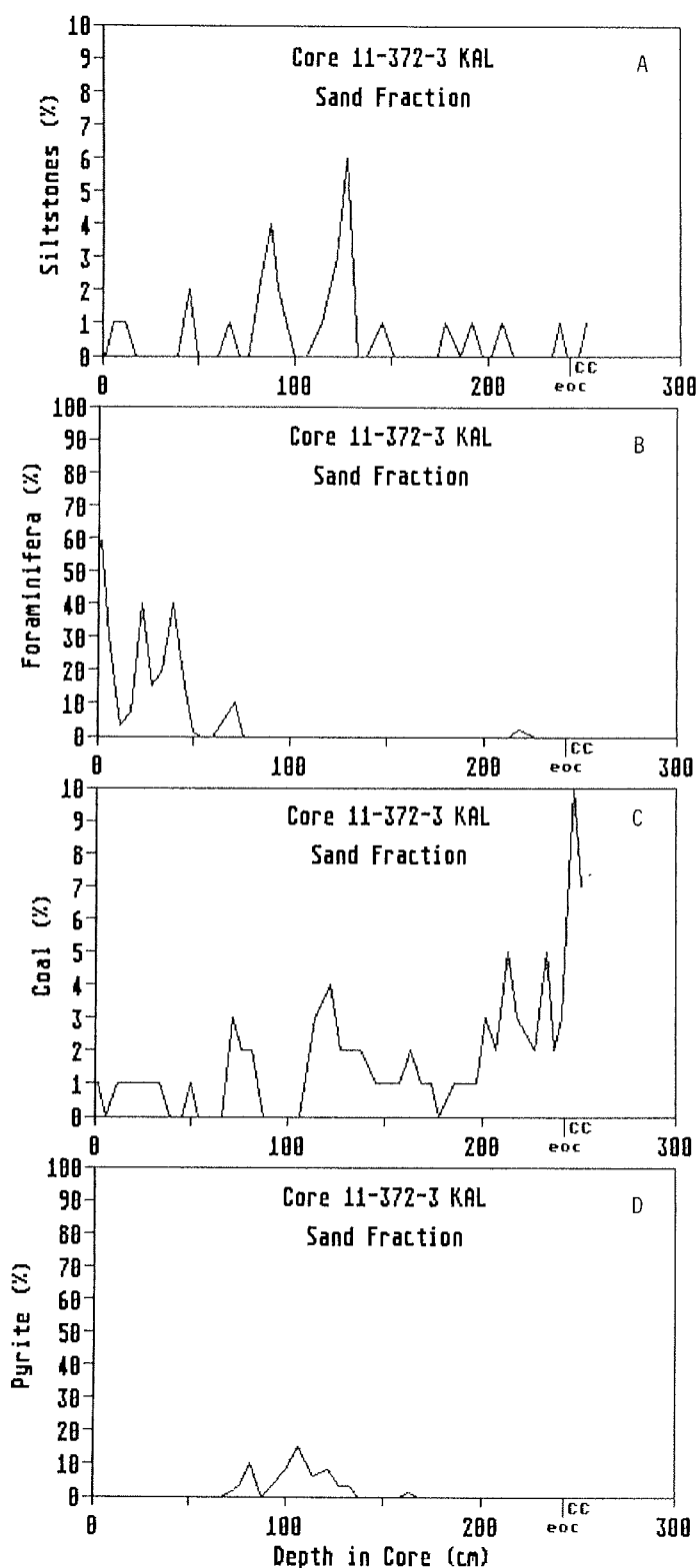


Fig.63/a-d Distribution of major components of core 11/372 of ARK IV/3.  
a) siltstone ; b) foraminifers ; c) coal fragments ;  
d) pyrite

### 7.7.3 Preliminary Discussion of KAL-sediments from the Eastern Arctic Ocean

The KAL-cores were described macroscopically and microscopically in great detail. Based on these descriptions, as well as on coarse fraction analysis and carbonate content measurements, an attempt was made to establish sediment types and regional sediment distribution patterns. One important aim was the correlation of the various sediment types occurring within the cores.

#### Sediment Types

The KAL-cores 11/282 and 285 derived from the continental slope contain predominantly dark grey silty sediments with sandy layers. Based on the mineralogical composition (mainly terrigenous quartz, feldspar and clay minerals) the sediments are recognized as being detritic in origin. Sediment structures indicate that these sediments were at least partly deposited by turbidity currents and/or downslope mass transport. Rapid deposition can possibly be inferred from the dark colour, reflecting less oxidizing or even reducing conditions because high sedimentation rates lead to less complete oxidation of organic matter in the surface sediments and therefore anoxic conditions are established very early. Lack of a (thin) oxic surface layer in the Cores 11/282 and 285 is probably due to loss during coring, because this oxic layer is present in both GKGs 11/282 and 285.

All other cores from the continental rise (Stations 11/296, 310, 340) as well as cores from the Nansen-Gakkel Ridge (Stations 11/362, 364, 365, 371, 372, 376) and from the Yermak-Plateau (11/396) show a characteristic rhythmical change in sediment colour downcore (Figs. 58 and 59). An uppermost brown horizon varies from 30 cm to 150 cm in thickness. The brown colour, which is probably due to amorphous Fe-oxide hydrate, indicates oxidizing conditions within this uppermost unit. With increasing core depth the colour changes from brown to olive grey over a transition zone, or dark grey to black. Both changes possible reflect a shift in redox potential, from oxidizing to less oxidizing or reducing conditions. It is uncertain what causes the dark colour. Based on microscopic analyses, the brown and black sediments have very similar mineralogical composition, but the brown colour is likely due to the Fe-oxide-hydrate content. These components are highly reduced or not abundant in the dark grey and black sediments. Furthermore, dark grey sediments appear to contain more opaque minerals. Thus, it is possible that an increase in iron sulphide content is responsible for the dark grey colour. However, it is also possible that the dark colour is due to finely dispersed coal or marine organic matter.  $MnO_2$  probably does not cause the dark colour as it was clearly found to be concentrated within the oxic layer, where it is stable.

Oxidizing and reducing conditions changed periodically in the sediment cores. It is possible that these changes reflect primary variations in oxygen content of bottom water. However, both a

higher organic production rate and faster sedimentation could also have led to the deposition of dark coloured sediments in the eastern Arctic Ocean.

Station 11/370, at the Nansen-Gakkel Ridge contained sediments ranging from sand- to pebble-size up to 15 cm in diameter composed of hydrothermally altered basalt. These basalts have Fe-rich crusts with some MnO<sub>2</sub>, and secondary mineralizations such as talc and zeolites. In general, sediments of the Nansen-Gakkel Ridge area contain hydrothermal and volcanic products mixed with hemipelagic "background-sediment".

#### Correlation of Sediment Cores

Correlation of sediment cores based on sediment colour alone is not possible, because sediment reworking and redeposition processes probably caused a more or less intensive mixing of the sediments. For example - although upper sediment units of cores 364 and 365 can probably be correlated as shown in Fig. 64, the middle and lower grey sediment units differ from each other. Correlation of both cores can be supported for the upper parts by the occurrence of stiff sandy horizons as well as coal fragments enriched in distinct layers.

Brownish layers at depths of 215 cm, 257 cm and 310 cm, within the grey sediments of Core 11/364 are interpreted to be intercalated reworked material and, therefore the grey horizons of Cores 11/364 and 365 are lithologically different. A further complication in correlating the cores is due to local variations in mineralogical and elemental input, in particular in sediments at or near to the Nansen-Gakkel Ridge. These sediments sometimes have large amounts of altered basalt fragments and/or secondary minerals like talc and zeolite. Furthermore, sediments of this area appear to have a high amorphous Fe-oxide-hydrate content and perhaps also a high MnO<sub>2</sub> content. Thus the surface sediments of the Nansen-Gakkel Ridge cannot directly be compared with those of the continental slope and the abyssal plain areas.

Diagenic remobilization and reprecipitation of Fe and Mn depends upon local Eh- and pH-conditions. This may cause significant changes in the primary metal content of the sediments resulting in colour changes during diagenesis.

Mud clasts observed in almost all sediment cores, could serve as a further lithostratigraphic tool. They occur often in the dark grey sediments. The clasts consist of aggregates of minerals of various grain sizes which have coatings, probably Fe-rich. It is not known where the aggregates formed nor how they were transported. However, they occur preferentially in sediments showing reworking features, perhaps indicating dependence upon local topography.

In summary, sediments of the eastern Arctic Ocean are hemipelagic muds showing changes in composition, texture and grain size due to variations in local input and diagenetic processes. Based on

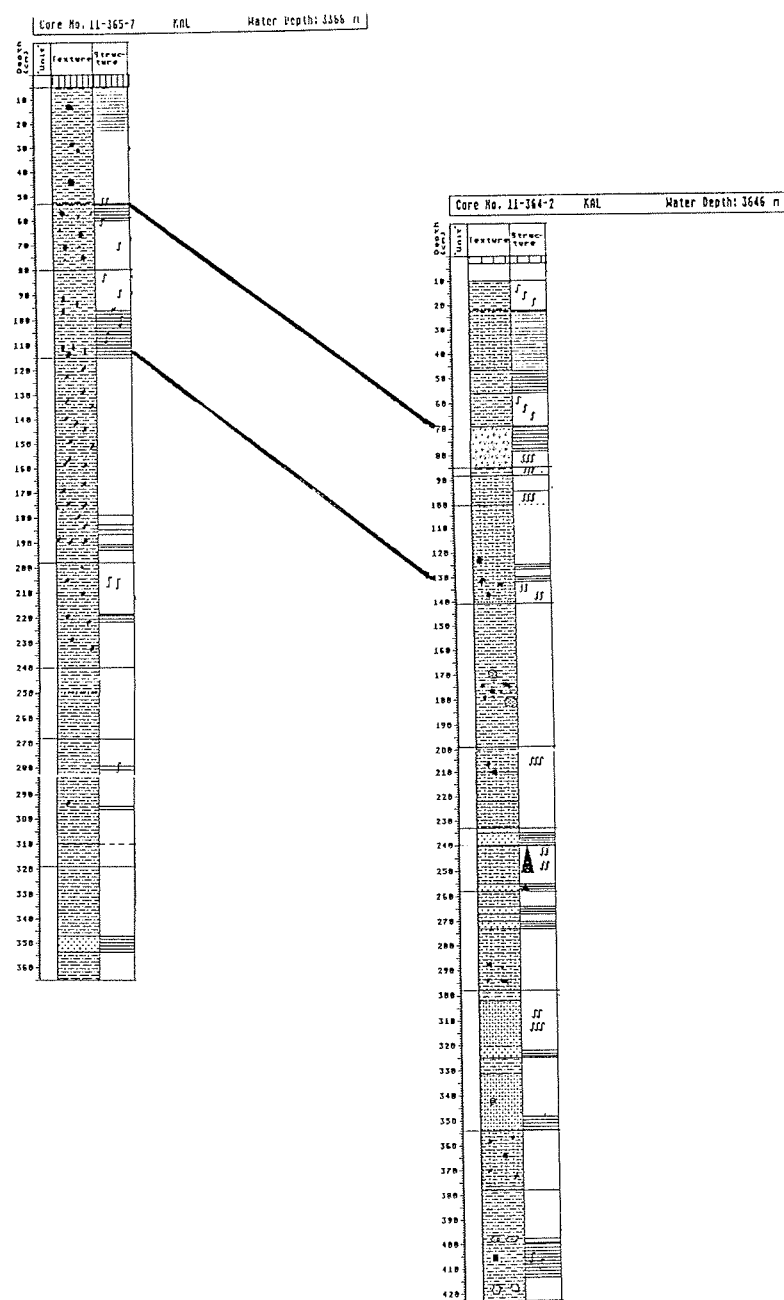


Fig.64 Lithostratigraphic correlation of cores 11/365 KAL and 11/364-2 KAL of ARK IV/3.

available descriptions and scarce lithological data, the cores can only be correlated within small regions such as the Nansen-Gakkel Ridge (Fig. 64).

## 7.8 Biostratigraphy of Quaternary Deposits (FG/UB, GIK, AGC/BIO)

### 7.8.1 Introduction

The history of sea ice formation and water circulation in the Arctic Ocean is of primary importance for understanding the magnitude and timing of Late Cenozoic climatic changes in the northern hemisphere. Knowledge of this climatic record is also needed to predict the results of continued atmospheric warming (the greenhouse effect) and changes in the volume of Arctic water mass outflow which supplies oxygen and nutrients to the global oceans. Biostratigraphic studies are a basic tool for interpreting the geological record of climatic change, as indicated by variations in microfossil composition, productivity and preservation state. The semi-isolated geographical setting of the Arctic Ocean also makes it a natural laboratory for study of evolution rates of marine biotas that have been able to adapt to the harsh polar environment.

Biostratigraphy and paleoecology of the Arctic Ocean has previously been studied mainly from sediment cores of the western basins and central ridges where sedimentation rates appear to be very slow (ca. 1 mm/1000 yrs.). These slow sedimentation rates prevented resolution of climatic changes with a time scale of less than ca. 20,000 yrs., e.g. the entire Flandrian warm interval plus the Weichselian glacial maximum. Previous studies also suffered from lack of knowledge about the precise relation between microfossil assemblages and water masses in the Arctic Ocean. The primary geologic objective of the ARK IV/3 cruise therefore was to obtain a detailed and accurate biostratigraphic record of long sediment cores from the eastern Arctic Ocean where much higher sedimentation rates of 1-4 cm/1000 yrs. have previously been found (Markussen et al. 1985). To accomplish this objective, a multidisciplinary biostratigraphic approach was planned, for which a wide spectrum of microfossils would be studied, including calcareous foraminifers and coccoliths, siliceous microplankton (radiolarians, silicoflagellates and diatoms) and organic-walled palynomorphs (pollen, spores, dinoflagellate cysts and acritarchs). The biostratigraphic value of each group is outlined in this report, after which some general conclusions and recommendations for future work are presented.

### 7.8.2 Abundance of Coccoliths in Sediments of the Eastern Arctic Ocean (FGUB)

#### Introduction

In Arctic marine sediments, coccoliths have been reported from the Alpha Ridge (Worsley & Herman 1980) and from cores of Vema and YMER-80 expeditions in the Fram Strait area (Gard 1986).

Abundance of coccoliths in these sediments is generally very low and seems to be restricted to thin layers within the sediment column. On the Alpha Ridge, oldest coccolith-bearing sediments recovered have a probable age of middle to late Pleistocene. The short YMER-80 cores cover the Holocene and the Late Pleistocene time interval. Gard (1986) determined species abundance in the Fram Strait region, but there is still no detailed study of the taxonomic composition of the coccolith flora in Arctic Ocean sediments. Species composition of coccoliths in sediments from the Fram Strait, however, are well known from previous studies of Baumann (unpublished data). The sediment cores from the ARK IV/3 cruise provide an opportunity to look at the northerly migration, distribution and composition of coccolithophorid floras in recent and older sediments.

#### Methods

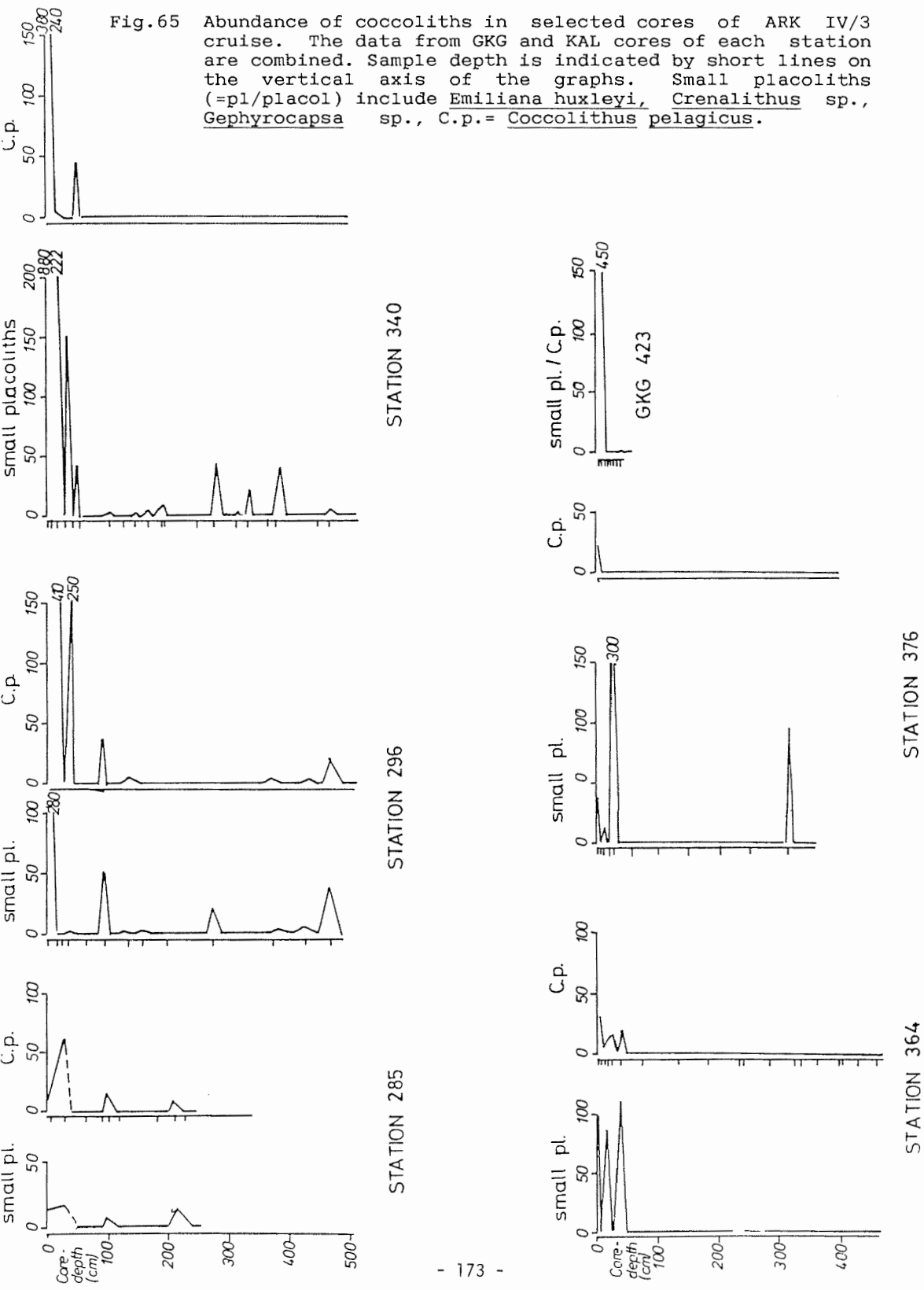
Smear-slides were investigated in all GKG box cores at sample intervals of 3 to 10 cm, and in all KAL long gravity box cores at sample intervals of 20 to 50 cm. For shipboard examination, a polarised light microscope with a magnification of  $\times 640$  was used. Samples containing coccoliths were then counted at a magnification of  $\times 1600$ . Due to the preparation procedure used for the smear-slides, the numbers obtained may vary by a factor of up to 3.

#### Preliminary Results

1. Shelf and slope cores (Stations 11/269-285) contained very low numbers of coccoliths (max. 60/mm<sup>2</sup>) in the surface layer (Fig. 65) and no coccoliths were found in deeper GKG samples. Sparse occurrences of coccoliths were found in some layers of the KAL cores, e.g. at Station 11/285 (Fig. 65).
2. Nansen Basin cores (Stations 11/296-358) contained high numbers of Coccolithus pelagicus (several hundred/mm<sup>2</sup>) in the surface lithofacies. Numbers declined in the lower part of the GKG. High abundances of small placoliths (Emiliana huxleyi, Crenalithus sp., Gephyrocapsa sp.) also occurred in the surface sediment layer. Small placoliths were also common (ca. 25-80/mm<sup>2</sup>) in some horizons of the KAL cores, e.g. at Station 11/340 (Fig. 65).
3. Nansen-Gakkel Ridge cores showed a lower increase of abundance of C. pelagicus in the upper part of some GKG cores. Large numbers of small placoliths prevail in the surface sediment. A conspicuous peak (up to 300/mm<sup>2</sup>) at depths of 23 to 38 cm of small placoliths has been observed. There is no apparent correlation between these peaks and the number of reworked specimens. Most samples from the KAL cores contained no coccoliths but a peak of small placoliths was found in one interval of KAL 11/376 (Fig. 65).

Compared to the coccolith abundance in Greenland Sea sediments, the numbers in the sediments of the eastern Arctic Ocean seem to

Fig. 65 Abundance of coccoliths in selected cores of ARK IV/3 cruise. The data from GKG and KAL cores of each station are combined. Sample depth is indicated by short lines on the vertical axis of the graphs. Small placoliths (=pl/placol) include Emiliana huxleyi, Crenalithus sp., Gephyrocapsa sp., C.p.= Coccolithus pelagicus.



be about one order of magnitude lower. The pattern of species composition found in Fram Strait, however, seems to extend into the eastern Arctic. *C. pelagicus* generally increases in abundance within the upper 5-10 cm of GKG samples and is indicative of a Holocene age. Among the small placoliths, *Emiliania huxleyi* appears to dominate over *Gephyrocapsa* species in the upper parts of the sediment column. Small placoliths prevail in deeper parts of the cores. Higher abundances of *Gephyrocapsa* found in some cores below 300 cm depth may indicate warmer stages, probably older than isotopic stage 3, assuming a normal sedimentation rate.

#### Future Work

Since smear-slide counts of coccoliths give only a rough outline of the coccolith flora, it is necessary to count and determine species with a SEM before final analyses are made. The following post-cruise studies are planned. -Examination of GKG surface samples from the the ARK IV/3 transects to determine the recent species composition by light microscopy (LM) and scanning electron microscopy (SEM).

- A study will be made of some selected cores for correlation of magneto- and nannofossil stratigraphies.

#### **7.8.3 Foraminiferal Content and Distribution in Eastern Arctic Sediments from selected KAL Cores: An Attempt at Stratigraphic Correlation**

##### Introduction

It was previously known that deep-sea Arctic sediment cores usually contain very low amounts of biogenic carbonate. Large volume sediment samples were therefore taken for detailed stable isotope studies in the little known Nansen Basin. During the ARK IV/3 cruise, an attempt was made to look for distinct markers in the poorly represented foraminiferal assemblage which might be able to document the history of glacial-interglacial cycles, similar to an oxygen isotope curve.

##### Methods

The following investigations were made on the coarse fraction (>63 um) of KAL cores 11/296, 11/340, 11/372: 1 -content of biogenic carbonate (bio-carbonate),  
2 - benthic/planktic ratio of foraminifers,  
3 - polar/subpolar ratio of planktic foraminifers,  
4 - morphotypes of *Neogloboquadrina pachyderma*.

Standard estimation charts were used to determine the content of the bio-carbonate. Raw faunal counts were done to calculate the planktic/benthic and polar/subpolar ratios.

The different morphotypes of *N. pachyderma* (Kennett 1968, 1970; Herb 1968) and distinctive Arctic Ocean forams e.g. "*N. parao-besa*" and "*N. occlusa*" (Herman 1974) were used for investigation

of variations in N. pachyderma. These species show trends from Subpolar to Arctic forms. The Arctic forms have a high trocho-spiral shape with low calcite encrustation and less distinct sutures. In subpolar areas they are more compact box-shaped. The typical Arctic species are only moderately encrusted, have visible sutures with more than 4 1/2 chambers in the last whorl and they show an elongated last chamber and aperture. "Optimum conditions" were identified using the combined results of studies 1 to 4 above: high numbers of subpolar morphotypes of N. pachyderma, together with high Subpolar ratios indicate positive conditions (see Fig. 66), while present-day conditions as found in the GKG samples are indicated by the arrow in Fig. 66. Reworked samples show a uniform grain size and contain broken individuals and foraminifer fragments. Indications of dissolution include holes in the foram tests and the presence of fragile tests even when these are heavily encrusted.

#### Preliminary Results

As expected, the amount of planktic foraminifers is low in the eastern Arctic Ocean. The foraminiferal assemblages are dominated by the left-coiling form of N. pachyderma (>95%). The subpolar faunal components are restricted to the right-coiling form of N. pachyderma, G. bulloides, G. quinqueloba and G. glutinata.

KAL core 11/296 generally contained low amounts of biocarbonate. Two maxima were found (Fig. 66): at 200-270 cm and as a distinct peak at 410-480 cm. The planktic/benthic ratio is variable. Two maxima of the Polar/Subpolar ratio are found at the same levels as bio-carbonate peaks. High positive "optimum conditions" are found at core depths of 220-320 cm and 420-480 cm. In one sample (464 cm) the faunal conditions appear to be more favorable than the present. Samples from 350 and 410 cm show a distinct fauna containing only very small, fragile individuals with a maximum diameter of about 100-125 um. Autochthonous sediment deposited during unfavorable environmental conditions is presumed because these fragile, translucent individuals are well preserved. This assemblage is thought to mark a glacial maximum period.

KAL core 11/340: the most conspicuous features in this core are three intervals that lack bio-carbonate (Fig. 66). Between the first two intervals at 200-250 and 345-370 cm, carbonate content shows the highest values, up to 95%. Another weak maximum occurs between 100 and 150 cm. In this interval, the subpolar faunal content reaches a maximum. This peak is also correlated with a high "optimum conditions" value, although the carbonate peak from 250-345 cm contained Subpolar species in only one sample, suggesting less favorable conditions. At 430 cm, a "glacial maximum" fauna was observed; below this event, from 450 cm to the base of the core, no bio-carbonate was found.

KAL core 11/372: the main feature of this core is the carbonate-free area below 190 cm. In the upper part, there is a carbonate maximum which is again combined with a higher content of subpolar

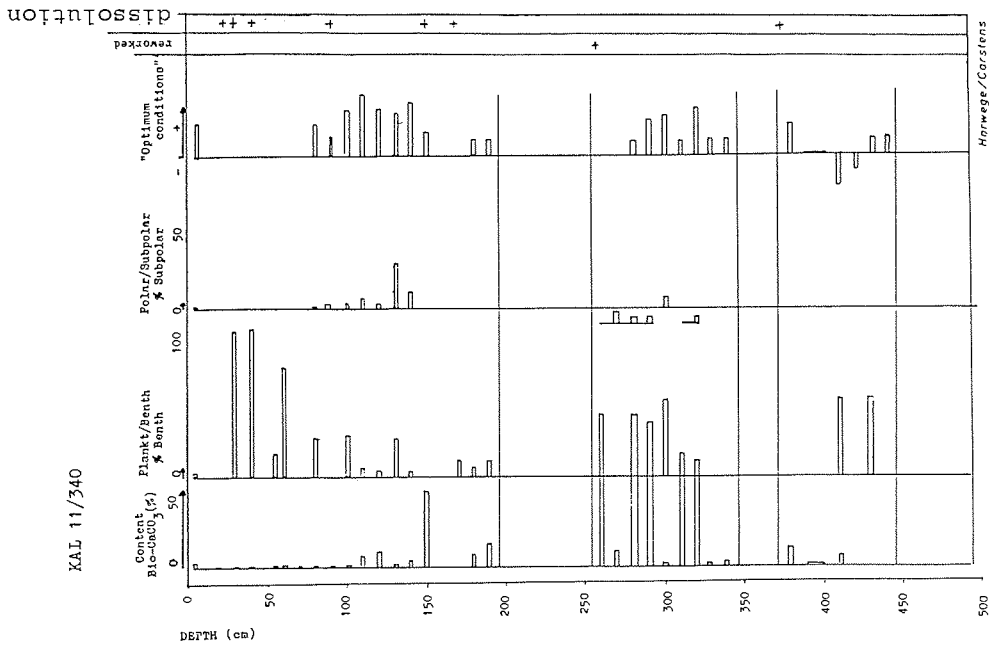
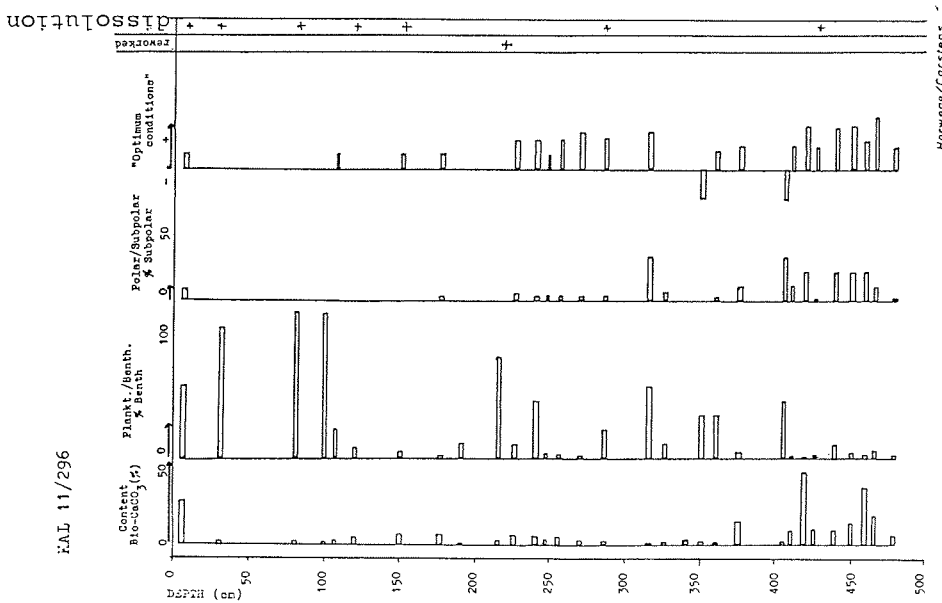


Fig. 66 Planktonic foraminiferal data for KAL Cores 11/340 (top) 11/296 (bottom). These graphs show the biocarbonate content (% coarse fraction  $>63\mu$ ), planktonic/benthic foraminifer ratios, polar/subpolar ratio of planktonic foraminifers (expressed as % subpolar forms) and the "optimum conditions" value where the arrow indicates present-day conditions.



species and high "optimum conditions" values. The carbonate-free interval contains coal debris, suggesting rapid influx of terrigenous sediment.

#### Future Work

These preliminary results must be supported by stable isotope measurements to ensure accurate reconstruction of past changes in deep and surface water masses in the Nansen Basin. To complete these investigations, it will also be necessary to obtain data from the Nansen Ridge to the Canada Basin.

#### **7.8.4 Palynomorphs (GIK, AGC/BIO)**

##### Introduction

Palynology has proved to be a primary stratigraphic tool for dating and paleoecological study of Cenozoic sediments in the circum-Arctic region, particularly in the Beaufort Sea area (Norris 1982) where intercalated deltaic and marine deposits often contain few calcareous fossils. In contrast, only one detailed study has been made of Upper Cenozoic palynomorphs in deep sea sediments of the Arctic Ocean (Mudie 1985; Aksu & Mudie 1985). Analysis of cores from the Alpha Ridge shows that dinocysts are useful biochronological markers, especially for sediment intervals lacking calcareous and siliceous microfossils. Quaternary pollen-spore assemblages are also unique indicators of Arctic paleowind direction (Burgeois et al. 1985) and they are possible tracers for fluvial input and provenance of ice-rafted clastic sediment (Mudie 1985).

The main objectives of palynological studies on cores from the ARK IV/3 cruise are:

1. to correlate palynomorph assemblages in surface sediments of the eastern Arctic Ocean with modern environmental conditions, e.g. water masses (temperature, salinity), ice cover, distance from continental margin;
2. to test the significance of palynomorphs as biostratigraphic tools in the eastern Arctic Basin;
3. to compare these data with palynostratigraphies of other cores from the Arctic region;
4. to interpret paleoceanographic and paleoclimatic conditions in the eastern Arctic basin during the Late Cenozoic period.

##### Methods

Shipboard studies were carried out on selected cores and lithofacies to obtain initial information about the concentration, preservation and distribution of palynomorphs. These data will be used to identify the most suitable cores for detailed post-cruise studies.

Surface sediment samples ( $8-10 \text{ cm}^3$ ) were taken from 20 GKG box cores, and samples ( $10 \text{ cm}^3$ ) of different lithologies were taken from 21 GKG and 13 KAL (long gravity box corer) cores

representing slope, basin and mid-ocean ridge environments at 20 stations (Table 14). Selected samples were examined on board as follows:

1. Sediment samples were disaggregated in 1 % Calgon solution.
2. The fractions 20 to 125  $\mu\text{m}$  and  $>125 \mu\text{m}$  were extracted by wet sieving.
3. The fraction  $>125 \mu\text{m}$  was dried in an oven at  $40^{\circ}\text{C}$ , stored in vials, and examined for foraminifers, pteropods and sponge spicules under a stereo microscope.
4. The fraction 20-125  $\mu\text{m}$  was treated with warm 10% HCl to remove carbonates and was then washed with distilled water until neutral.
5. The organic residues were then suspended with a Vortimixer to remove clay aggregates and, for coarse-grained lithologies, the fine organic sediment was separated from the denser clastics by swirling and decanting.
6. Strew slides were made of the organic residues which were mounted in glycerine gelatin.
7. The palynomorphs were examined with a light microscope at magnifications of  $\times 200$  to 1600, and estimates were made of the amounts of Quaternary dinocysts, pollen, spores and reworked pre-Quaternary palynomorphs.

The box cores GKG 11/269-12 to 340-14 and the gravity box cores KAL 11/282-8 to 362-21 were initially sampled every 5 to 10 cm with 10 cm<sup>3</sup> volume disposable syringes. Examination of selected samples showed that the palynomorph abundances were low. Furthermore, the core lithology was highly variable so that all lithofacies could not be represented with this sample spacing. All GKG cores from Stations 11/358 to 11/430 and all KAL cores from Stations 11/362 to 11/430 therefore were sampled with plastic liners which allow continuous sampling of at least 50-60 cm<sup>3</sup> volume at 1 cm intervals.

TABLE 14: Palynological samples taken from  
GKG and KAL cores for shipboard studies.

<u>Station #</u>	<u>GKG</u>	<u>KAL</u>
11/269	12	
276	9	
278	5	
	6	
280	11	
282	6	8
287	15	
296	11	12
310	10	13
340	13	15
	14	
358	19	
362	15	21
364	1	2
365	2	7
371	10	12
372	7	3
376	7	8
382	3	
396	3	6
423	6	
430	5	8

### Initial Results

1. GKG surface samples all contain moderate to large amounts of well-preserved Quaternary dinocysts and small amounts of pollen and spores (see Chapter 6.3 for details). Several new species of dinocysts and acritarchs appear to characterise areas of multi-year ice cover in the eastern Arctic Ocean. Small amounts of reworked Mesozoic/Paleozoic palynomorphs were found in the slope and basin cores but were rare/absent in surface samples from the mid-ocean ridge. Similar assemblages of pre-Quaternary sporomorphs and acritarchs were found in upper Quaternary sediments of YMER-80 cores (Robertsson 1984), suggesting that the source of the reworked palynomorphs in the eastern Nansen Basin is the Barents Shelf.

2. Continental margin cores. The surface yellow-brown and basal olive-gray lithofacies of the GKG cores all contained moderate amounts of well preserved Quaternary dinocysts and pollen-spore assemblages. The dinocyst assemblages are typical of recent marine sediments from Subarctic to circum-Arctic regions of the North Atlantic (Mudie & Short 1985; Harland 1983). In general, there are more indicators of low salinity surface water in the gray lithofacies, possibly denoting intervals of higher fluvial input. Similar increases in fluvial indicators are also found in the long core of olive gray mud (KAL 11/282-18) from 1436 m water depth (Fig. 67) where small peaks in Quaternary pollen-spore assemblages occur. These intervals also correspond to increased ratios of the Atlantic dinocyst indicator, Operculodinium centrocarpum, to the Subarctic indicator, Multispinula minuta. These features disappear below the laminated subfacies (180-195 cm) where they are replaced by reworked palynomorphs. In KAL Core 11/296-12, the palynofacies above the upper laminated gray clay (35-50 cm) is similar to that in the top 200 cm of Core 11/282-18, below which only reworked palynomorphs occur down to 365 cm core depth (Fig. 67). At this level, upper Quaternary palynomorphs reappear but the ratio of O. centrocarpum to M. minuta suggests a cooler (?) interstadial climate than the surface assemblages. More detailed sampling is required to determine whether this event occurs at isotopic stage 3 or the top of stage 5.

3. Nansen-Gakkel Ridge. Two long cores (KAL 11/364-2 and 376-8) were chosen for more detailed studies of this area because the amount of reworked palynomorphs was expected to be smaller on the midocean ridge than the slope and basin. Analyses of these cores, however, showed that samples from both cores are dominated by reworked palynomorphs (Fig. 68). Pollen are the major constituents of the reworked assemblage in contrast to the reworked slope assemblage which is dominated by trilete spores. The age of the reworked ridge palynomorphs appears to be Mesozoic and Paleogene, but at this time, a definite age can only be given for the dinocyst Isabelidinium sp. (sample KAL 11/364-2, 250 cm) which has a range from Albian to early Eocene (Wilson & Clowes 1980). The coarse fraction of this sample contains a few chalk fragments probably of late Cretaceous age.

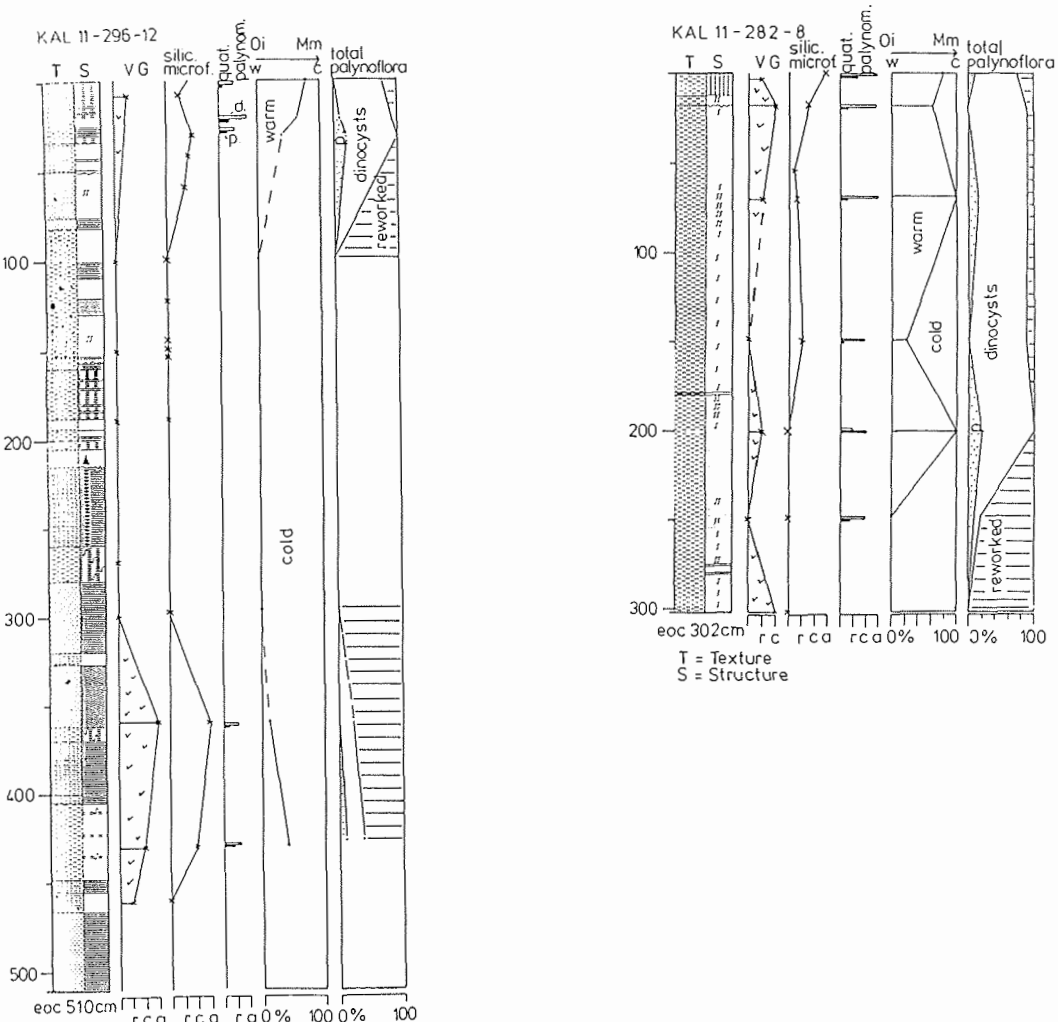


Fig. 67 Summary diagrams for cores 296 & 282, showing the relation between lithology and the distribution of palynomorphs, volcanic glass shards (VG) and siliceous microfossils (xx sponge spicules, ... diatoms; V radiolarians). Q = Quaternary; D = dinocysts; P = pollen and spores; Oc = Operculodinium centrocarpum; Mm = Multispinula minuta. Relative abundance symbols are: r = rare (<5); c = common (6-30); a = abundant (>30). Total palynoflora indicates the percentage abundances of Quaternary pollen-spores, dinocysts and reworked pre-Quaternary palynomorphs in each sample.

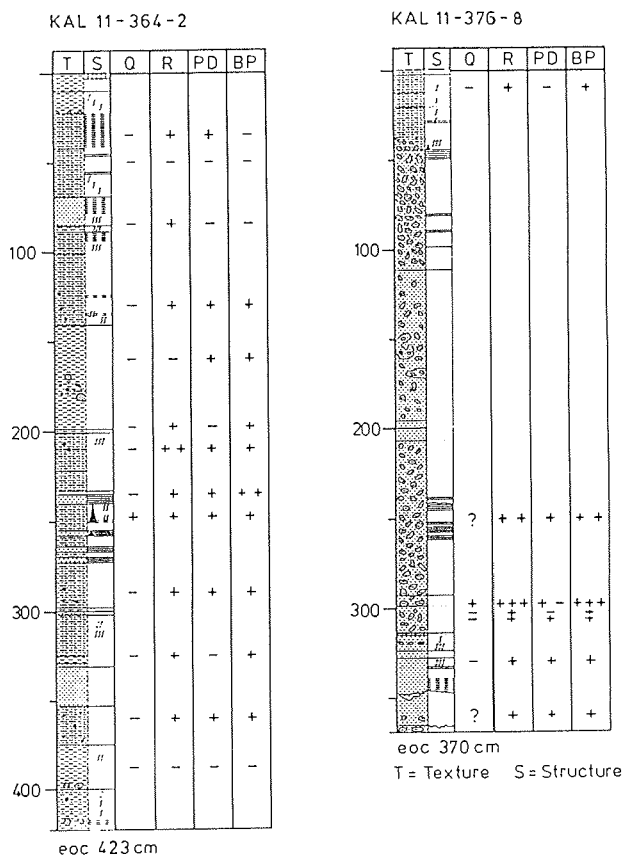


Fig. 68 Estimates of the percentages of Quaternary palynomorphs (Q), reworked pre-Quaternary palynomorphs (R), plant debris (PD) e.g. wood and leaf fragments, and black particles (BP) in KAL Cores 11/364 and 376. - = absent; + = rare; ++ = common; +++ = abundant.

The samples of Core 11/364-2 contain a slightly higher percentage of Mesozoic pollen than Core 11/376 which has a larger amount of older Tertiary pollen. The composition of reworked assemblages of Core 11/376-8 shows little variation downcore. Large bisaccate pollen grains form a major part of the assemblages and redeposition of Neogene sediments cannot be totally excluded because a specimen of *Opercudodinium longispinigerum* was found (Core 11/376-8, 300 cm) which has a last occurrence in the upper Pliocene of the North Atlantic (Mudie, unpublished data). Both cores from the ridge show a positive correlation between the amount of reworked palynomorphs, plant debris and black particles (coal clasts, manganese or iron sulphides). Further studies will be done on the black particles to determine their composition and possible value for indicating sediment provenance. It is notable that black coal is not present in cores from the western Arctic Ocean where totally different reworked assemblages are found which can be related to Paleozoic carbonates on Ellesmere Island and to Tertiary brown coals in the Sverdrup Basin/Mackenzie Delta (Mudie 1985).

Quaternary palynomorphs were only found in 2 samples (KAL 364-2, 250 cm; 376-8, 300 cm). The latter sample contains *Carya* and *Juglans* pollen which are indicators of warm temperate climates. Reworking is possible because these genera first appear in the Eocene but their excellent preservation and lack of visible thermal alteration suggest that they are young deposits. In the Labrador Sea-Baffin Bay region, the last occurrence of these species marks the Eemian interglacial stage (Mudie, unpublished data).

#### Future Work

1. All shipboard samples must be processed further using 52% HF to remove silicates and concentrate the palynomorphs so that accurate counts and assemblage compositions can be determined. Where necessary, oxidation may be used to digest coal particles and allow taxonomic identification of pre-Quaternary palynomorphs.
2. All samples from KAL Cores 11/269, 282, 340, 364 and 376 should be processed and analysed in order to complete and validate the initial shipboard interpretations.
3. Possible new Quaternary dinocysts and acritarchs will be studied using LM, SEM and fluorescence microscopy. These data will be published together with the surface sample data from the GKG cores in a joint paper to be written by Mudie and Matthiessen.
4. The shipboard studies clearly indicate that the Holocene dinoflagellate flora in the eastern Arctic Ocean is richer in species and more variable in assemblage composition than in the western and central Arctic Ocean. All GKG cores therefore merit full palynological study as they probably contain a detailed

record of ice fluctuations and meltwater events that may be correlatable with the classical sequence of Flandrian stages (from early Alleröd to the hypsithermal maximum and cooler late Atlanticum stages). Other long cores may also merit detailed study pending the results of magneto-, sedimentological and other biostratigraphic studies.

#### 7.8.5 Conclusions

1. The ARK IV/3 cruise has produced a unique set of new data on composition and surface distribution of calcareous and organic-walled microfossils in the Arctic Ocean. Smear-slide and water sample observations also indicate that siliceous microfossils (radiolarians, silicoflagellates, diatoms) are present in the surface sediments.
2. The outstanding value of this new data set is the systematic sample distribution along the entire cross-section of the eastern Arctic Ocean basin which also can be related precisely to detailed oceanographic and sea ice data. Large samples obtained from box cores also provide the first opportunity for study of all microfossil groups from the same core sample intervals.
3. Because of constraints on time and facilities available for shipboard studies, it is presently not possible to evaluate the full significance of this data set in relation to the Quaternary history of Arctic ice and ocean circulation. It is clear, however, that the coccolith and dinocyst abundances are much higher in the surface sediments of the eastern Arctic than on the Alpha and Lomonosov Ridges, while the opposite may be true for planktic foraminifers. It is also clear that pteropods are absent in most of the eastern Arctic sediments although they are always present in the youngest sediments (<0.4 Ma) in the western Arctic Ocean. These observations suggest that primary productivity is higher in the eastern Arctic, particularly in view of high sedimentation rates indicated by the lithostratigraphic data, while water/sediment chemistry appears to be less favorable for aragonite preservation.
4. In general, the low numbers of microfossils in the eastern Arctic sediments make detailed paleoecological studies time consuming and difficult, and the low diversity of high latitude assemblages constrains the magnitude of paleoclimatic signal that may accompany glacial-interglacial climatic changes. These factors, together with the high influx of clastic sediments (ice rafted and gravity flow deposits) containing reworked fossils mean that great effort is needed to interpret the true paleoclimatic signals of this region. On the other hand, the apparently rapid sedimentation rates (ca. 4 cm/1000 yrs.) are favorable for high resolution studies of Holocene paleoclimatic changes with time scales of a few thousand years, e.g. late glacial, hypsithermal and neoglacial stages. These high resolution data would provide the first proxy-climatic data from which climatic forecasting might be made of the Arctic Ocean response to future increases or decreases in global temperatures.

5. The number and diversity of Quaternary coccoliths and dinocysts in ARK IV/3 cores also appears to be large enough to permit detailed studies of selected cores in order to confirm tentative shipboard results and to allow definite correlation with floras from other parts of the Arctic Ocean. These studies, combined with new data on living and fossil planktonic foraminifers and post-cruise stable isotopic data, should permit accurate biostratigraphic dating of the ARK IV/3 cores which presently seem to have a maximum age of less than 300,000 yrs.

6. In order to confirm and understand the apparently large difference between the biostratigraphy of the eastern and western Arctic Ocean regions, however, it will be necessary to obtain a comparable suite of data across the Fram and Makarov Basins so that the apparently large differences in oceanography, water and sediment chemistry can be related to the microfossil assemblages and their paleoenvironments. Opportunity should also be sought to extend the sediment record for the eastern Arctic Ocean by drilling on the mid-ocean ridge, Yermak and Morris Jessup plateaus. This should provide a complete Neogene high resolution paleoclimatic record for analysis of the timing of onset of glacial conditions in the eastern Arctic Ocean and the evolution of the present low diversity polar floras and faunas.

## **7.9 Pore Water Content and Chemistry of Sediments**

### **7.9.1 Sediment Samples for Measurement of Water Content (IBG)**

Tubes (5 ml) were used for collecting sediment samples for measurements of water content. Samples were taken every fifth cm (every cm in some cases) from both GKG and KAL samples (Table 15). In total, 1105 samples were obtained. The tubes were sealed by a cap, packed in plastic bags or boxes, and brought to the cooling room (2-3 °C). Measurements carried out at IBG are contained in Geoscientific Working Party (1988). Tables 15 and 16 show water content for the two KAL cores portrayed in Figures 58 and 59.

TABLE 15:

ARK IV/3 RV POLARSTERN, 04.07 -03.09 1987

Water content (W.ct. %) in box gravity cores (Kastenlot).  
 Depths in cm.

Core no: 11-365

Depths:	W.ct. %.	Depths:	W.ct. %.
10	55,69	235	24,50
15	51,15	240	26,43
20	52,01	245	20,68
25	48,45	250	25,46
30	45,05	255	23,09
35	45,73	260	23,40
40	45,48	265	22,10
45	42,31	270	26,04
50	51,60	275	26,62
55	48,44	280	24,01
60	31,49	285	40,72
65	27,53	290	34,42
70	29,59	295	27,40
75	29,43	300	26,87
80	29,44	305	28,21
85	31,83	310	26,85
90	31,12	315	24,82
95	30,59	320	24,44
100	25,75	325	28,05
105	24,88	330	41,54
110	33,65	335	35,57
115	24,93	340	42,56
120	23,95	345	45,86
125	24,06	350	31,68
130	23,96	355	26,41
135	23,73	360	25,88 EOC
140	23,48		
145	23,92		
150	24,31		
155	23,98		
160	24,60		
165	25,06		
170	24,82		
175	24,99		
180	24,25		
185	25,14		
190	28,44		
195	26,13		
200	30,72		
205	38,91		
210	28,23		
215	27,16		
220	27,52		
225	29,87		
230	24,48		

TABLE 16 :

ARK IV/3 RV POLARSTERN, 04.07 -03.09 1987

Water content (W.ct. %) in box gravity cores (Kastenlot).  
 Depths in cm.

Core no: 11-376

Depths:	W.ct. %.	Depths:	W.ct. %.
10	45,25	235	26,49
15	41,91	240	23,68
20	44,89	245	20,18
25	42,96	250	19,57
30	38,66	255	22,73
35	44,89	260	21,82
40	39,21	265	23,04
45	29,17	270	22,87
50	26,51	275	22,58
55	26,65	280	23,11
60	29,33	285	24,23
65	26,70	290	22,33
70	25,82	295	22,51
75	28,31	300	21,47
80	27,54	305	39,27
85	28,16	310	17,53
90	28,26	315	37,01
95	27,86	320	25,39
<u>100</u>	<u>27,09</u>	325	24,49
105	27,26	330	26,16
110	26,57	335	25,05
115	26,97	340	24,71
120	27,27	345	24,72
125	26,16	350	23,30
130	27,52	355	23,74
135	26,90	360	22,91
140	28,11	365	28,66
145	27,96		
150	27,51		
155	27,44		
160	27,05		
165	26,35		
170	28,84		
175	26,52		
180	26,69		
185	26,44		
190	26,16		
195	27,28		
<u>200</u>	<u>28,80</u>		
205	30,14		
210	28,21		
215	27,21		
220	27,49		
225	28,94		
230	26,49		

### **7.9.2 Pore Water Chemistry (IfMK, FG/UB)**

During the last three years, investigations of pore water chemistry and diagenesis of deep sea sediments were carried out by the Sonderforschungsbereich 313 (GIK) in the Norwegian Sea. Pore water investigations on ARK IV/3 were undertaken to increase understanding of sediments and pore waters from purely Arctic environments. Sampling by the University of Bremen in Fram Strait and the Arctic Ocean is expected to provide information on climatic changes during glacial cycles through analysis of pore water composition and mineral transformations.

Sediment pore waters were sampled and measured onboard (see Table 17) from five different areas:

- Svalbard shelf
- Svalbard continental slope
- Nansen Basin and Nansen-Gakkel Ridge.
- Yermak Plateau
- Fram Strait

TABLE 17: Geochemical Sediment/Pore Water Parameters  
Sampled or Measured Onboard

Station	Tool	Area	Water Depth (m)	Nutrients	pH	Alka- linity	Fe/Mn	Organ. carbon	No. of samples
269	GKG	shelf	200	+	+	o	o	o	12
280	GKG	slope	884	+	+	o	o	o	12
287	GKG	"	2873	+	+	o	o	o	21
296	GKG	"	3003	+	+	o	o	o	12
296	KAL	"	3003	+	+	o	o	o	18
340	GKG	Nansen	3755	+	+	o	o	o	12
340	KAL	Basin	3720	+	+	o	o	o	18
358	GKG	"	4045	+	+	o	o	o	8
362	GKG	"	4037	+	+	o	o	o	12
364	GKG	"	3634	+	+	o	o	o	12
364	KAL	"	3646	+	+	o	o	o	16
371	GKG	Nansen	3698	+	+	o	o	o	12
371	KAL	Gakkel	3710	+	+	o	o	o	12
372	GKG	Ridge	3971	+	+	o	o	o	12
372	KAL	"	3977	+	+	o	o	o	12
376	GKG	"	2895	+	+	o	o	o	12
376	KAL	"	2920	+	+	o	o	o	11
396	GKG	Yermak	1375	+	+	o	o	o	12
423	GKG	Plat.	2270	+	+	o	o	o	12

+: onboard measurement o: lab measurements at IfMK

Nutrients = measurement of  $\text{NO}_3/\text{NO}_2$ ,  $\text{PO}_4$ ,  $\text{NH}_4$ ,  $\text{SiO}_4$ .

### Methods

Sediment samples selected from 15 GKGs and 11 KALs were extracted under *in situ* temperature in a freezing-room (+1°C). Pore water was extracted with up to 6 bars air pressure from sediments in a teflon squeezer. Measurement of NO<sub>3</sub>, NH<sub>4</sub>, PO<sub>4</sub>, SiO<sub>4</sub> and HCO<sub>3</sub> was done immediately onboard. A Hitachi spectrophotometer Type 100-20 was used for quantitative analysis of these nutrients. 10 cm diameter sediment cores were removed from the GKG with a plastic tube, including water above the top sediment layer. Sediment slices of 10 cm diameter were cut from KALs at selected layers downcore. If analysis could not be done immediately the samples were frozen. Special equipment (clean bench, teflon tools) as used for preparation of samples for determination of dissolved metals and measurement of alkalinity, which will be carried out IfMK.

### Preliminary Findings

Concentration profiles of nitrate and ammonia show regional variations. Most likely due to high carbon sedimentation rates, shelf sediments (Station 11/269, Fig. 69 and 70) become anoxic in the uppermost 20cm. The change to anoxic conditions is deeper in sediments from the continental slope (Stations 11/280, 287, 296) until a nearly constant depth position of about 1 m is reached in sediments from the Nansen Basin and the Nansen-Gakkel Ridge (Stations 11/340, 358, 364, 371, 376, see Fig. 71 and 72).

Increasing concentrations of phosphate (2.5 to 4.6 µM) were detected at stations down the continental slope, with maximum concentrations at Station 11/296 (12 µM). Stations further north in the Nansen Basin and along the Ridge have nearly constant concentrations at 1 µM.

Maximum silica concentrations are located at 3 cm sediment depth on the slope (80-150 µM). In all deep sea sediments only a slight increase is visible in the uppermost layers. Redox conditions in the boxcores in the uppermost 40-100 cm average high values of 200-500 mV and decrease with depth. Negative data have only been seen in KAL 11/396. If changes are observed, they correlate to stratification, but they do not occur in all cores (Fig 73).

### Future Work

Input from geological investigations on sedimentation rate and sediment composition will be available from participating scientists from GIK. Some data on biological activity already exist from onboard studies and flux rates may be available from the WHOI ice moored sediment trap (AEDB, see Chapter 5.3.3). This should provide detailed interpretations of processes near the sediment-water interface and diagenesis in the perennially ice covered, high Arctic environment.

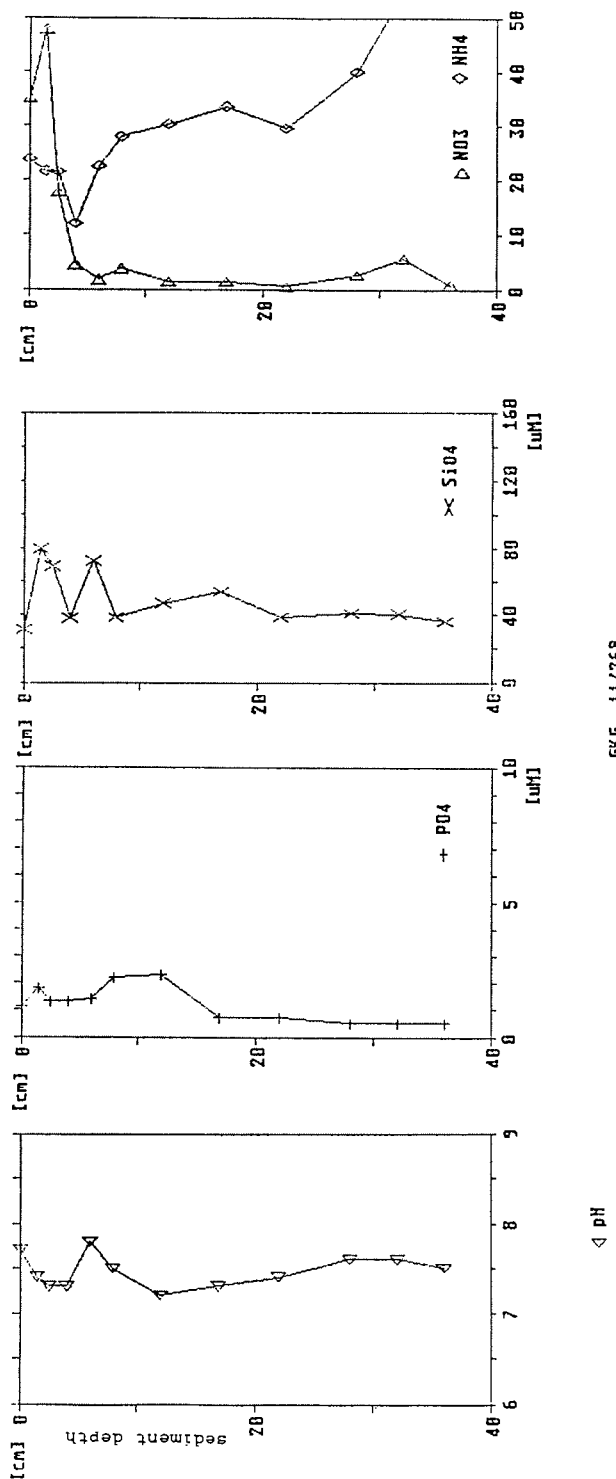


Fig. 69 Concentration of nutrients ( $\text{NO}_3^-$ ,  $\text{NH}_4^+$ ,  $\text{PO}_4^{3-}$ ,  $\text{SiO}_4^{4-}$ ) and pH values in porewaters from shelf sediments of the Svalbard area. Station 269, ARK IV/3. Nitrate values decrease to nearly zero in the uppermost 20 cm of the sediment column.

Fig. 70

Concentration of nutrients ( $\text{NO}_3^-$ ,  $\text{NH}_4^+$ ,  $\text{PO}_4^{2-}$ ,  $\text{SiO}_4^{4-}$ ) in pore-waters from sediments of the Svalbard continental slope. Station 296, ARK IV/3. Nitrate reflects nitrification/denitrification in the uppermost 20 cm of the sediment column. Ammonia values increase to 400  $\mu\text{M}$  at about 4m sediment depth. A phosphate maximum is reached for the entire transect in this station, at the base of the continental slope.

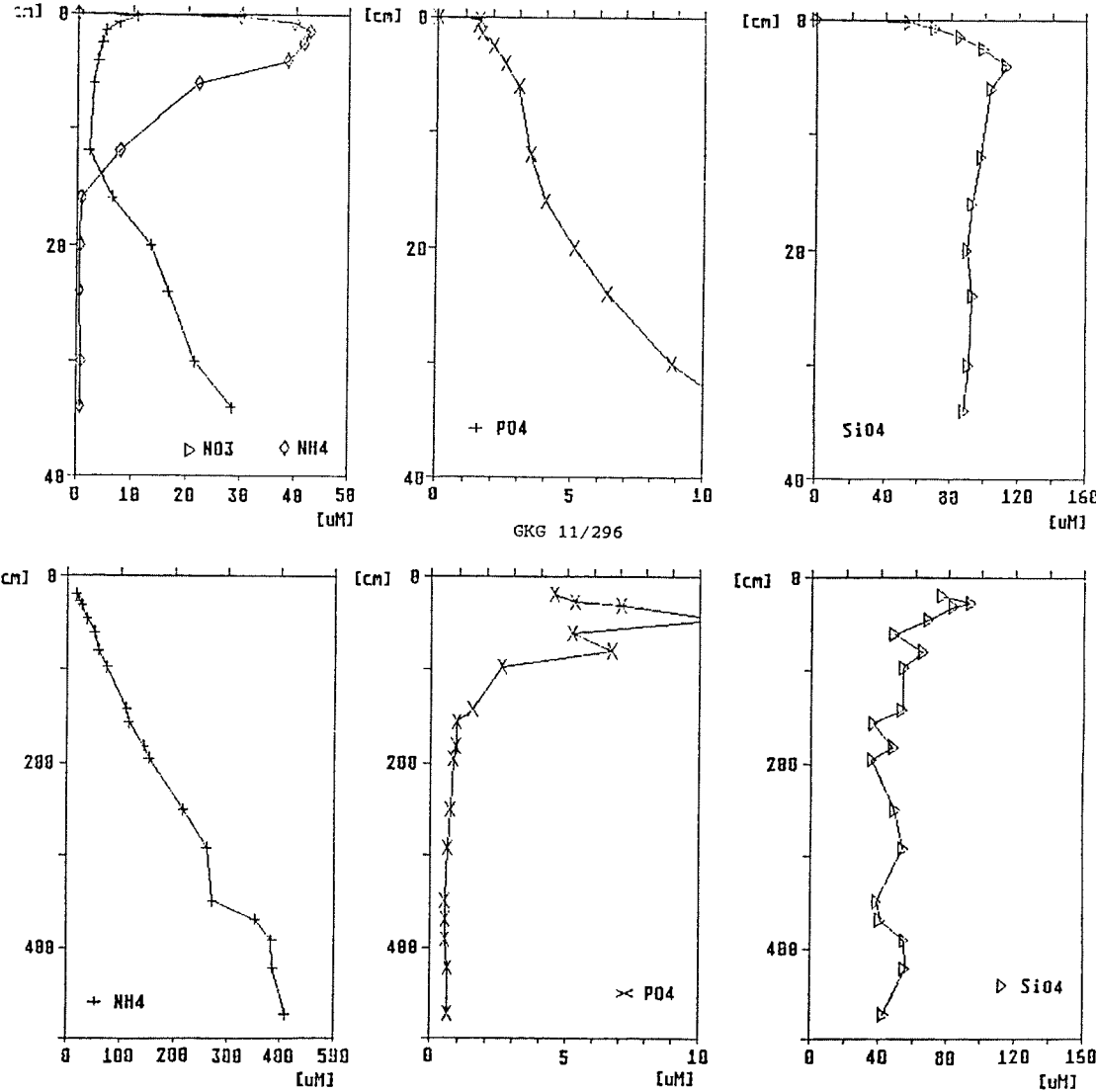
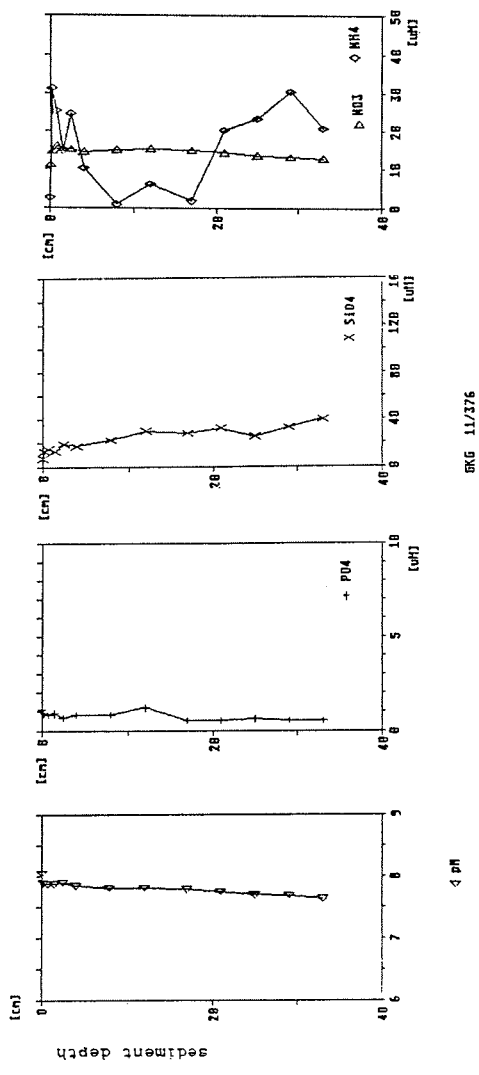
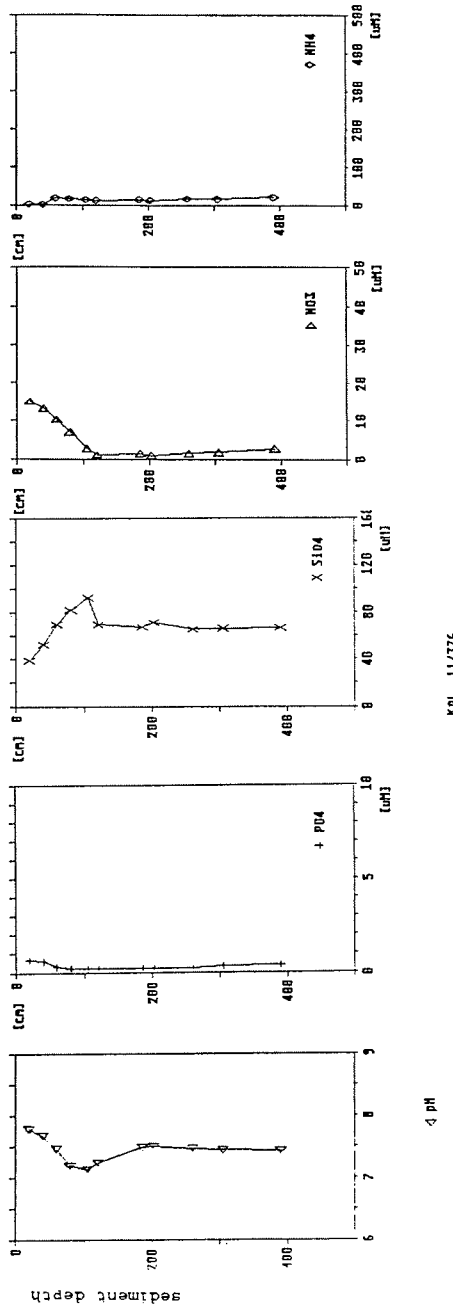
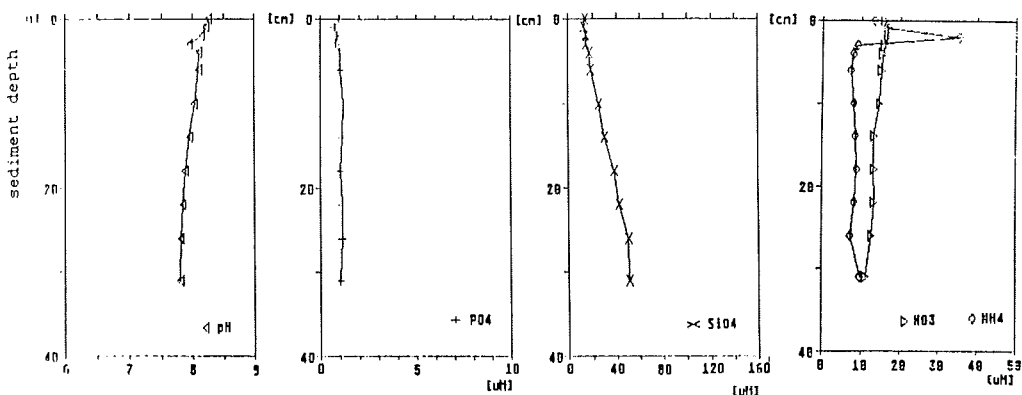


Fig. 7  
 Concentration of nutrients ( $\text{NO}_3$ ,  $\text{NH}_4$ ,  $\text{PO}_4$ ,  $\text{SiO}_4$ ) and pH values in porewaters from deep sea sediments of the Mansen Gakkel ridge, Station 376, ARK IV/3. Nitrate values slowly decrease in the uppermost 110 cm of the sediment column. Silica slowly increases with a maximum 100 cm down core. Compare pH minimum and  $\text{SiO}_4/\text{NO}_3$  content.

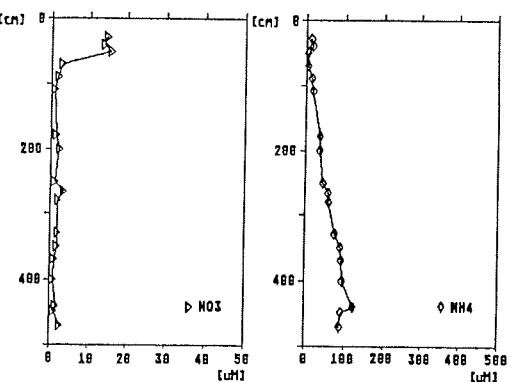
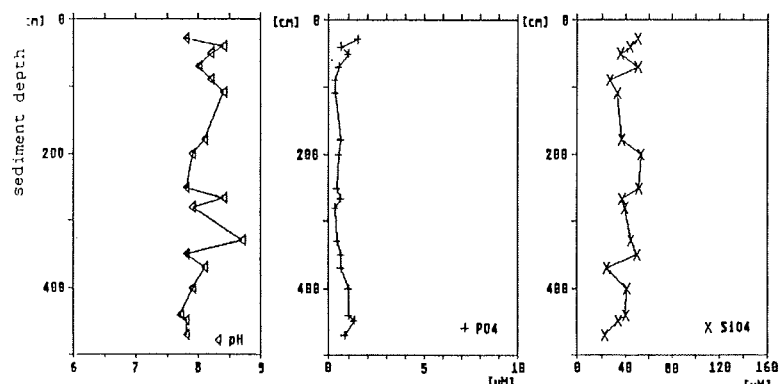


- 194 -





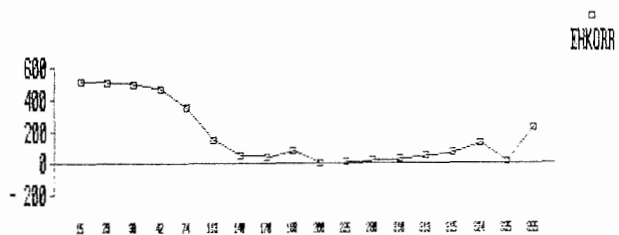
GKG 11/340



KAL 11/340

Fig. 72 Concentration of nutrients ( $\text{NO}_3^-$ ,  $\text{NH}_4^+$ ,  $\text{PO}_4^{4-}$ ,  $\text{SiO}_4^{4-}$ ) and pH values in porewaters from deep sea sediments of the Nansen Basin. Station 340, ARK IV/3. Silica starts at bottom water level in the surface layer and slowly increases down core up to about 50  $\mu\text{M}$  at 30 cm.

11376eh



11396eh

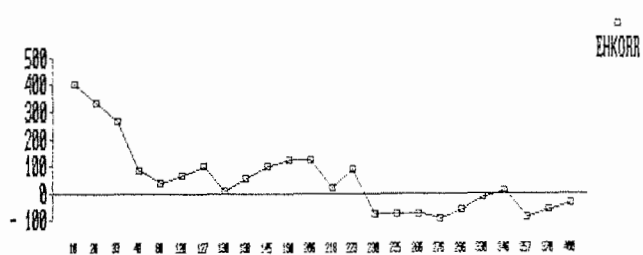


Fig.73 Profile of Eh-values of two cores following the stratigraphy of the cores.

Based on chemical-thermodynamical balances the species distributions and mineral stabilities of the chemical compositions of the pore solutions will be calculated by means of the computer program WATEQF (Plummer et al. 1976). Early diagenesis, dissolution processes and mineral transformations will be verified in Bremen by SEM and EMP investigations. Like the dependence on stratigraphy of the enrichment of iron compounds, these calculated saturation conditions are expected to show trends related to climatic changes during glaciations.

#### 7.10 Physical Properties: Thermal Conductivities (JSS, FG/UB)

The ability of a material to transport heat is reflected in its thermal conductivity. Therefore, sediment cores are expected to show a number of different values for thermal conductivity due to variable lithology and porosity. So-called instationary methods for determination of thermal conductivity are based on observation of the time variant temperature field created by either pulsed or constant heat sources (von Herzen & Maxwell 1959; Ratcliffe 1960; Villinger 1983).

##### Experimental Procedure

Two experimental approaches were planned for measuring thermal conductivity of sediment cores on ARK IV/3. The group from University of Bergen (JSS) used the steady state needle probe method. A Fenwal probe containing a thermistor and heating wire was used. The thermistor resistance was measured every 5 sec over a time period of 2 min. The values were measured on a Solartron 7151 computing multimeter interfaced to a HP-Integral personal computer. The resistances of the thermistor were converted to temperatures and thermal conductivities were calculated for every 5 sec interval using the equation:

$$K = V^2 * C * \ln(t_2/t_1) / (T(t_2) - T(t_1))$$

where:       $T$  is the temperature at two different times  $t_1$  and  $t_2$ ,  
 $V$  is the heating voltage, and  
 $C$  is a calibration constant.

The calibration constant was determined from measuring thermal conductivity in a mixture of 1% gelatine in water. An example of the computation is shown in Table 18. The first six readings done before heating were used to calculate temperature drift in the sediments.

The second experimental approach (FG/UB) involved a pulse probe method where seven needle probes of the type described before are heated at the same time for an interval of 5 sec. During the following observation interval of 95 sec the resistance was used to calculate temperature curves for each probe location. However, a defect relay in the dataquisition unit made regulation of the system and reading of the data impossible. Therefore this method had to be given up and the steady state method was used again.

TABLE 18: Example of the Computation of Conductivity

Station 11/376 Coring Type:KAL  
 Measurement # 36  
 Distance from top core 3.85 m

Time (sec)	R (Ohm)	Temp. (°C)	K (W/m/K)
-	2263.29	20.8032	
-	2263.26	20.8035	
-	2263.21	20.8041	
-	2263.19	20.8044	
-	2263.15	20.8049	
-	2263.11	20.8054	
-	2103.66	22.8225	
10	2085.90	23.0573	1.4513
15	2075.65	23.1940	1.4612
20	2068.46	23.2902	1.4724
25	2062.86	23.3654	1.4627
30	2058.29	23.4268	1.4618
35	2054.45	23.4785	1.4691
40	2051.10	23.5236	1.4572
45	2048.16	23.5632	1.4637
50	2045.54	23.5986	1.4685
55	2043.15	23.6308	1.4556
60	2040.96	23.6604	1.4498
65	2038.98	23.6871	1.4753
70	2037.10	23.7125	1.4380
75	2035.37	23.7358	1.4551
80	2033.76	23.7575	1.4629
85	2032.24	23.7781	1.4557
90	2030.80	23.7975	1.4489
95	2029.42	23.8161	1.4301
100	2028.15	23.8332	1.4756
105	2026.91	23.8499	1.4373
110	2025.75	23.8656	1.4661
115	2024.63	23.8807	1.4512
120	2023.54	23.8953	1.4277

Mean conductivity: 1.456 W/m/k

Drift: 0.07277 mK/s

On the gravity cores (SL), piston cores (KOL) and box cores (GKG) measurements of the thermal conductivity were done at 10 cm distance intervals. The measurements on the gravity box cores (KAL) were done at non regular intervals (10-20 cm) and are reported in Geoscientific Working Party (1988). Figure 74 shows examples of measurements from the two KAL cores shown in figures 58 and 59.

#### Preliminary Results

The average thermal conductivity and standard deviation for each core is shown in Table 19. The variation of thermal conductivity will be used in calculation of heat flow. Also efforts will be made to compare the conductivity/depth profiles with other physical properties (including magnetic susceptibility) as well as the lithostratigraphy.

ARKTIS IV/3/365  
KAL

ARKTIS IV/3/376  
KAL

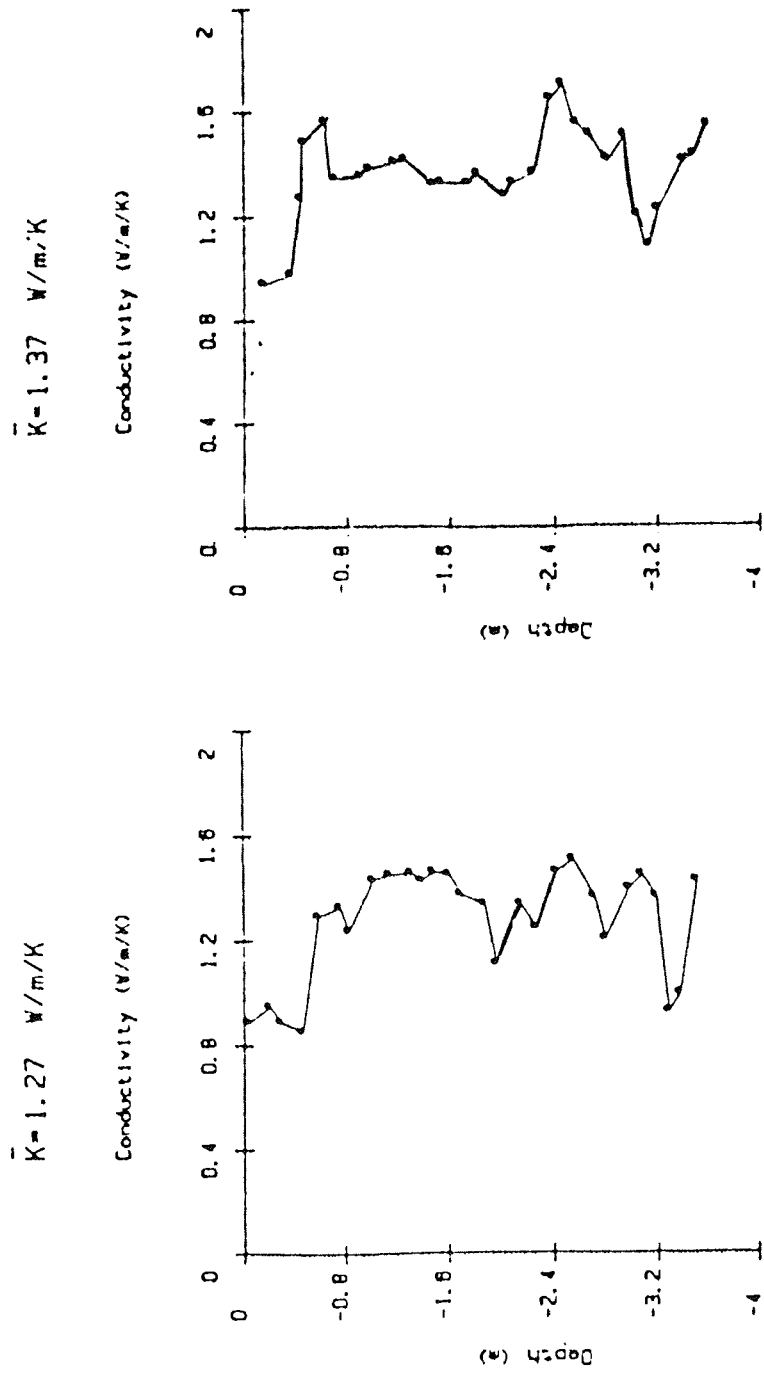


Fig. 74 Thermal conductivity for KAL 365 and 376. See Fig. 58 and 59 for detailed core descriptions and Fig. 2 for station location.

TABLE 19: Thermal Conductivities of Sediment Cores

Station	Lat. ( $^{\circ}$ N)	Long. ( $^{\circ}$ E)	Core type	k mean (W/m/K)
11/269	81 $^{\circ}$ 16.2'	31 $^{\circ}$ 26.2'	GKG	1.42 $\pm$ 0.07
11/276	81 $^{\circ}$ 29.7'	31 $^{\circ}$ 26.5'	GKG	0.93 $\pm$ 0.02
11/278	81 $^{\circ}$ 31.8'	31 $^{\circ}$ 34.6'	GKG	0.85 $\pm$ 0.01
11/280	81 $^{\circ}$ 34.5'	31 $^{\circ}$ 39.0'	GKG	0.92 $\pm$ 0.05
11/282	81 $^{\circ}$ 35.8'	31 $^{\circ}$ 31.5'	GKG	0.83 $\pm$ 0.01
11/282	81 $^{\circ}$ 35.8'	31 $^{\circ}$ 30.0'	KAL	0.93 $\pm$ 0.05
11/285	81 $^{\circ}$ 38.5'	31 $^{\circ}$ 26.1'	GKG	0.86 $\pm$ 0.02
11/285	81 $^{\circ}$ 38.2'	31 $^{\circ}$ 23.2'	KAL	0.94 $\pm$ 0.11
11/287	81 $^{\circ}$ 40.3'	30 $^{\circ}$ 40.3'	GKG	0.84 $\pm$ 0.02
11/296	81 $^{\circ}$ 47.5'	31 $^{\circ}$ 30.3'	GKG	0.86 $\pm$ 0.04
11/296	81 $^{\circ}$ 47.4'	31 $^{\circ}$ 30.1'	KAL	1.18 $\pm$ 0.27
11/310	82 $^{\circ}$ 01.4'	32 $^{\circ}$ 13.9'	GKG	0.86 $\pm$ 0.04
11/310	82 $^{\circ}$ 00.5'	32 $^{\circ}$ 19.9'	KAL	1.01 $\pm$ 0.19
11/340	82 $^{\circ}$ 57.0'	32 $^{\circ}$ 03.5'	GKG	1.09 $\pm$ 0.30
11/340	82 $^{\circ}$ 56.5'	32 $^{\circ}$ 05.0'	KAL	1.15 $\pm$ 0.15
11/340	82 $^{\circ}$ 56.4'	32 $^{\circ}$ 10.6'	KOL	1.13 $\pm$ 0.21
11/358	84 $^{\circ}$ 00.6'	30 $^{\circ}$ 19.0'	GKG	0.93 $\pm$ 0.07
11/362	85 $^{\circ}$ 04.6'	29 $^{\circ}$ 07.6'	GKG	0.85 $\pm$ 0.02
11/362	85 $^{\circ}$ 01.4'	28 $^{\circ}$ 08.4'	KAL	0.95 $\pm$ 0.06
11/362	85 $^{\circ}$ 03.5'	28 $^{\circ}$ 57.6'	SL	0.90 $\pm$ 0.07
11/364	85 $^{\circ}$ 21.5'	26 $^{\circ}$ 19.9'	GKG	0.89 $\pm$ 0.05
11/364	85 $^{\circ}$ 21.8'	26 $^{\circ}$ 12.9'	KAL	1.34 $\pm$ 0.25
11/365	85 $^{\circ}$ 30.8'	25 $^{\circ}$ 17.8'	GKG	1.12 $\pm$ 0.22
11/365	85 $^{\circ}$ 32.4'	25 $^{\circ}$ 19.4'	KAL	1.27 $\pm$ 0.21
11/370	85 $^{\circ}$ 54.4'	22 $^{\circ}$ 43.8'	SL	1.26 $\pm$ 0.20
11/370	85 $^{\circ}$ 55.9'	22 $^{\circ}$ 44.0'	SL	1.05 $\pm$ 0.20
11/371	86 $^{\circ}$ 08.1'	22 $^{\circ}$ 05.2'	GKG	0.92 $\pm$ 0.07
11/371	86 $^{\circ}$ 06.2'	22 $^{\circ}$ 01.5'	KAL	1.14 $\pm$ 0.19
11/371	86 $^{\circ}$ 08.5'	22 $^{\circ}$ 03.3'	KOL	1.43 $\pm$ 0.18
11/372	86 $^{\circ}$ 07.8'	23 $^{\circ}$ 09.5'	GKG	0.92 $\pm$ 0.04
11/372	86 $^{\circ}$ 08.0'	23 $^{\circ}$ 07.0'	KAL	1.24 $\pm$ 0.18
11/376	85 $^{\circ}$ 22.9'	21 $^{\circ}$ 42.5'	GKG	0.99 $\pm$ 0.02
11/376	85 $^{\circ}$ 23.1'	21 $^{\circ}$ 44.1'	KAL	1.37 $\pm$ 0.17
11/376	85 $^{\circ}$ 22.6'	21 $^{\circ}$ 21.8'	KOL	1.26 $\pm$ 0.16
11/376	85 $^{\circ}$ 22.1'	21 $^{\circ}$ 28.3'	SL	1.55 $\pm$ 0.32
11/382	83 $^{\circ}$ 24.6'	19 $^{\circ}$ 52.5'	GKG	0.85 $\pm$ 0.04
11/382	83 $^{\circ}$ 23.4'	19 $^{\circ}$ 42.4'	SL	1.00 $\pm$ 0.16
11/396	82 $^{\circ}$ 47.8'	16 $^{\circ}$ 03.3'	GKG	0.92 $\pm$ 0.04
11/396	82 $^{\circ}$ 47.9'	16 $^{\circ}$ 03.0'	KAL	1.12 $\pm$ 0.23
11/396	82 $^{\circ}$ 48.1'	15 $^{\circ}$ 59.1'	KOL	1.21 $\pm$ 0.26
11/412	82 $^{\circ}$ 01.9'	15 $^{\circ}$ 10.7'	SL	1.02 $\pm$ 0.12
11/423	81 $^{\circ}$ 19.6'	15 $^{\circ}$ 17.9'	GKG	0.95 $\pm$ 0.06

## 7.11 Physical Properties: Magnetic Susceptibility (FG/UB)

The magnetic susceptibility  $k$ , a material parameter relating a magnetic field  $H$  to the induced magnetization  $J$  is defined as:

$$J = k * H$$

Most rockforming minerals are diamagnetic ( $k \approx -10^{-6}$  SI) or paramagnetic ( $k \approx 10^{-6}$  SI). Magnetite is the only ferrimagnetic mineral which has a high magnetic susceptibility ( $k \approx 10^{-3}$  SI) and is present in small, variable concentrations in pelagic sediments. Therefore, a magnetic susceptibility log of marine sediment columns primarily reflects magnetite content.

Measurements onboard POLARSTERN were carried out with a Bartington Magnetic Susceptibility Meter using a core scanning sensor with an internal diameter of 135 mm. This sensor allowed measurements only on piston cores (KOL) and gravity cores (SL) ( $d = 120$  mm) but not on gravity box cores (KAL). Results obtained on short liners taken from the box corers (GKG) are not presented here.

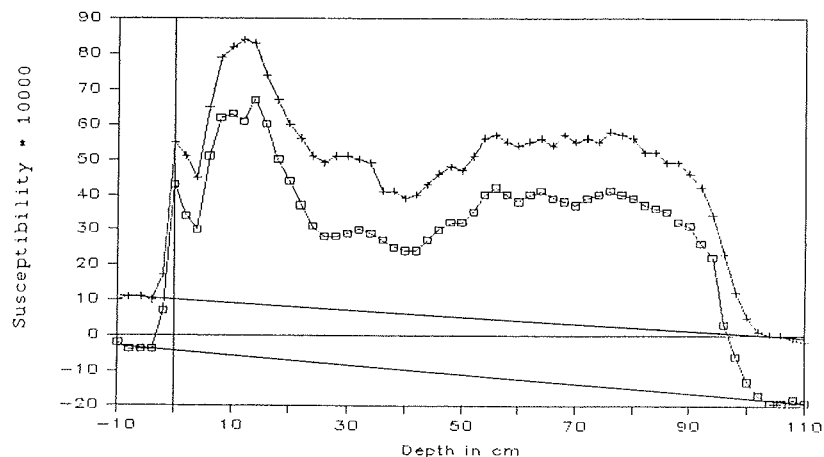
After testing for instrument drift and reproducibility, the following standard procedure was used for measurements. Cores were scanned from top to base and then back with a spacing of 2 cm. The profiles were extended 10 cm over both ends of the core to define the zero levels of the instrument and to calculate a linear drift which was subtracted from the data of both profiles (Figure 75). The average of the drift-corrected values is the final result. Where cores consisted of several segments, a continuous profile was obtained by adding the overlap of adjacent segments.

Susceptibility logs of all piston and gravity cores are presented in Fig. 76a and b. They can be divided roughly into three different groups. The first includes Cores KOL 11/340, SL 11/362 and SL 11/382 from near the southern and northern edges of the Barents Abyssal Plain together with two cores taken on the Yermak Plateau, KOL 11/396 and SL 11/412. These cores are characterized by comparatively low overall susceptibilities. There are no obvious correlations between the limited downhole variations in susceptibility.

The second group consists of three cores: KOL 11/371, KOL 11/376 and SL 11/376 from the top of the northern and southern ridge crest mountains of the Nansen-Gakkal Ridge. They show significantly higher susceptibility values. There is a sequence of high peaks which can be correlated in at least the two KL cores: section 1.70 m to 4.70 m in Core KOL 11/371 from the northern shoulder of the ridge and section 1.10 m to 3.30 m in Core KOL 11/376 taken on the southern shoulder of the ridge (Fig. 76a). In the third core, SL 11/376 taken at about the same site, the whole sequence of peaks (0-360 m) can be correlated to the first two meters of KOL 11/376. The difference in length most likely reflects different coring techniques.

KL 340  
0-92 cm

Raw - Data



Corrected Data

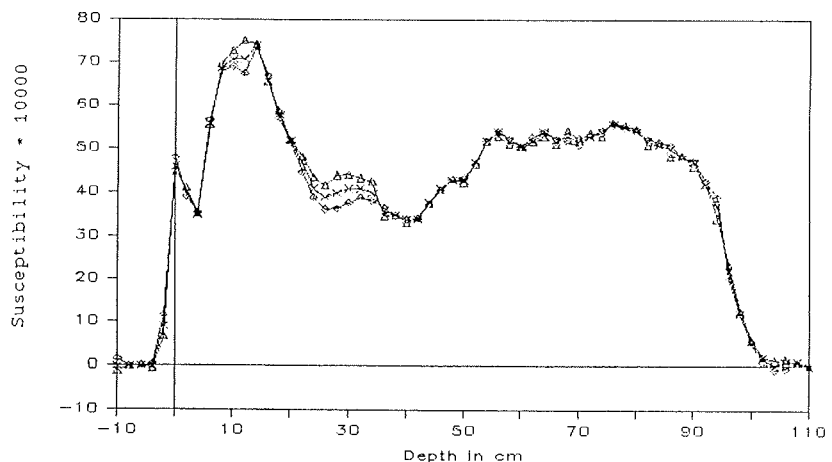


Fig.75 Measurements of magnetic susceptibility of sediment cores: Example of data aquisition and data reduction. For the two original susceptibility logs read downcore and upcore, an instrument drift is calculated from the zero-levels before and after the measurement (indicated by solid lines in the upper graph). The average of both drift-corrected sets of data is taken as the final result (% in lower graph).

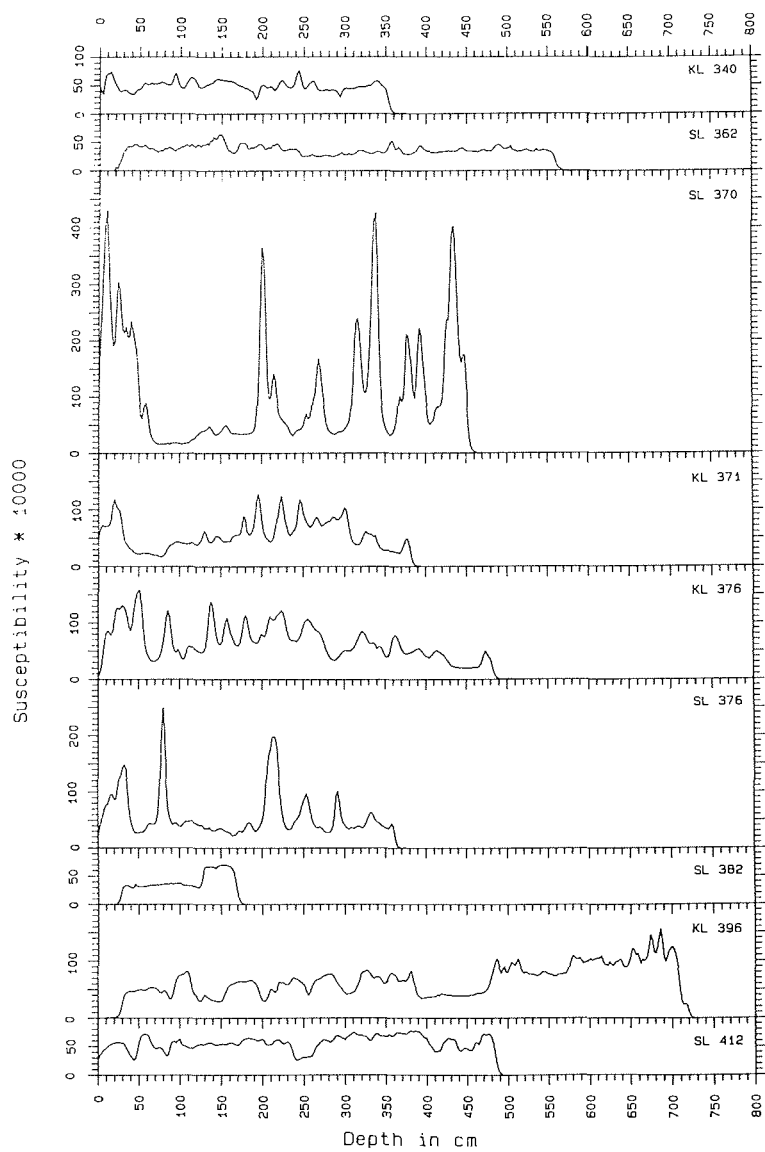


Fig. 76 a) Magnetic susceptibility versus depth of selected cores processed on ARK IV/3. For station locations see Krause et al. (in press)

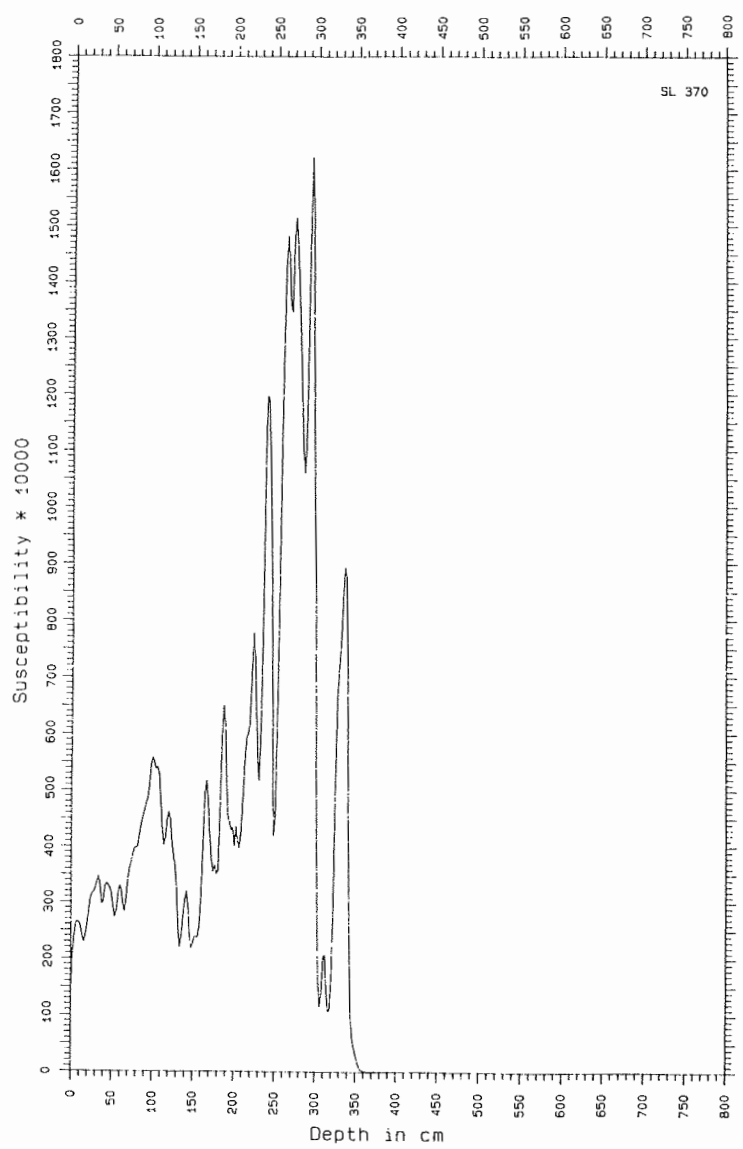


Fig.76 b)Magnetic susceptibility versus depth of core SL 11-370.

The third group includes the two cores taken in the rift valley of the Nansen-Gakkel Ridge. In part they show extremely high magnetic susceptibilities. The highest values of all ten cores analyzed were measured in the Core SL 11/370-20 (Fig. 76b) from the bottom of the rift valley. Core SL 11/370-12 (Fig. 76a) from the southern slope of the rift valley yielded intermediate amplitudes. Again there is a sequence of peaks which can be correlated. Ignoring the higher amplitudes, the series of peaks in the interval 1.70 m to 3.20 m in Core SL 11/370-20 (Fig. 76b) appears to be the same as in section 2.60 m to 4.50 m in Core SL 11/370-12 (Fig. 76a). Based on morphological comparison, the same sequence also appears to be present in the second group of cores taken from the shoulders of the Nansen-Gakkel Ridge.

There is clear evidence in the present data that the amplitude of magnetic susceptibility depends on distance to the Nansen-Gakkel Ridge axis. As susceptibility primarily reflects magnetite content of the sediments, this effect is most likely related to volcanic activity at the ridge. A series of prominent peaks observed in five of the logs is thought to indicate a specific lithological time sequence, which will be further investigated through sedimentologic and mineralogic studies.

#### 7.12 Magnetostratigraphy of the Sediment Section (FG/UB)

An extensive shipboard paleomagnetic sampling program was performed on all sedimentary sections recovered at 'Großkastengreifer (GKG)' and 'Kastenlot (KAL)' stations during POLARSTERN ARK IV/3. Vertically oriented specimens of about 7 cc were generally taken at intervals of 5 cm. In addition, 7 KAL sediment columns were continuously sampled with 2 x 2 cm plastic liners for shore-based paleomagnetic analyses with a new passthrough cryogenic magnetometer system.

Individual samples were measured onboard for their natural remanent magnetization (NRM) properties with a Molspin Spinner Magnetometer. Due to time constraints and the limited sensitivity of the magnetometer, detailed alternating field demagnetization treatment using a Schonstedt GSD-1 single axis demagnetizer was restricted to a small number of specimens. The bulk of detailed paleomagnetic analyses will be done onshore using facilities of the laboratory in Bremen.

NRM inclination logs for all KAL cores which retrieved 3 m or more of sediments are shown in Figure 77. Cores 11/282 and 11/296 were taken in about the middle and at the foot of the continental slope north of Svalbard, Cores 11/340 and 11/362 near the southern and northern end of the abyssal plain of the Nansen Basin, Core 11/364 on the outer flank, Cores 11/365 and 11/376 near the top of the southern ridge crest mountains of the Nansen-Gakkel Ridge, and Core 11/396 on the Yermak Plateau.

NRM of most marine sediments is known to have several components, including not only a primary remanence acquired shortly after deposition but also a viscous component of normal polarity from

Fig.77 Natural remanent magnetization inclination logs of large volume gravity cores ('KAL') having retrieved 3 m or more of sediments in the Eurasian Basin of the Arctic Ocean during POLARSTERN ARK IV/3.

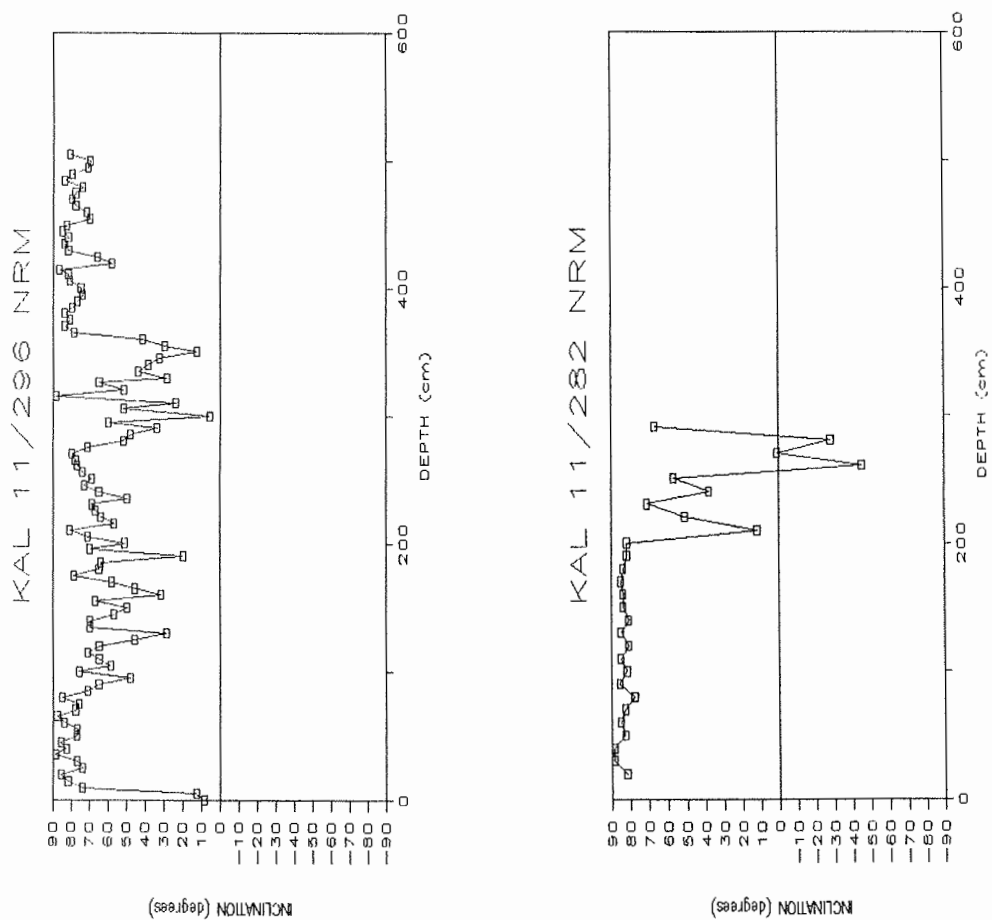


Fig.77 cont.

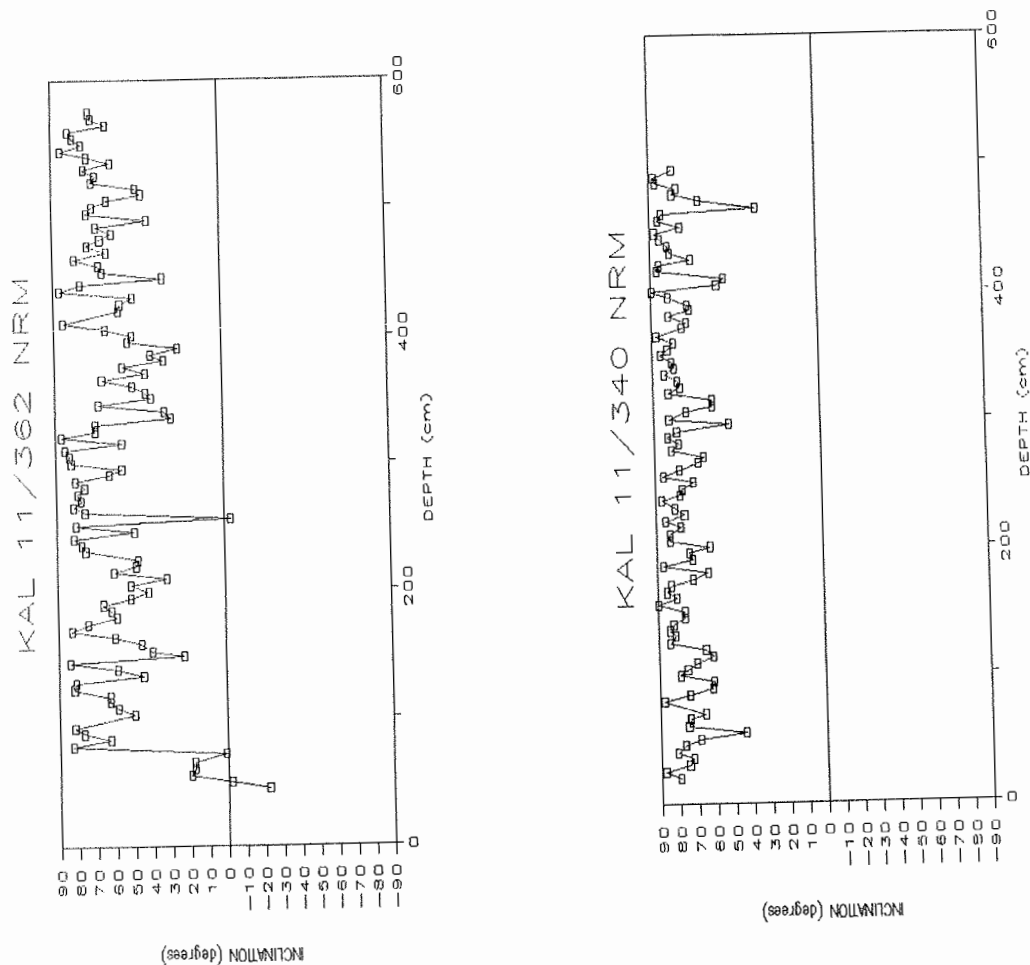


Fig. 77 cont.

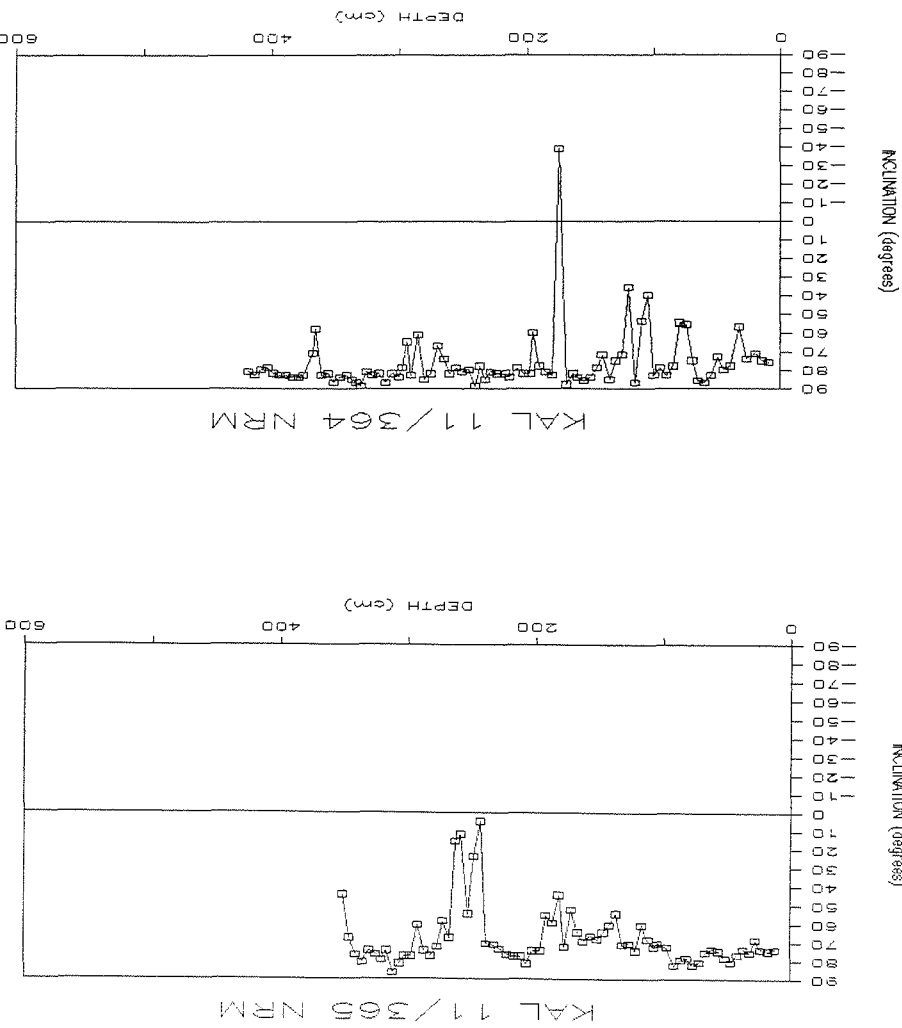
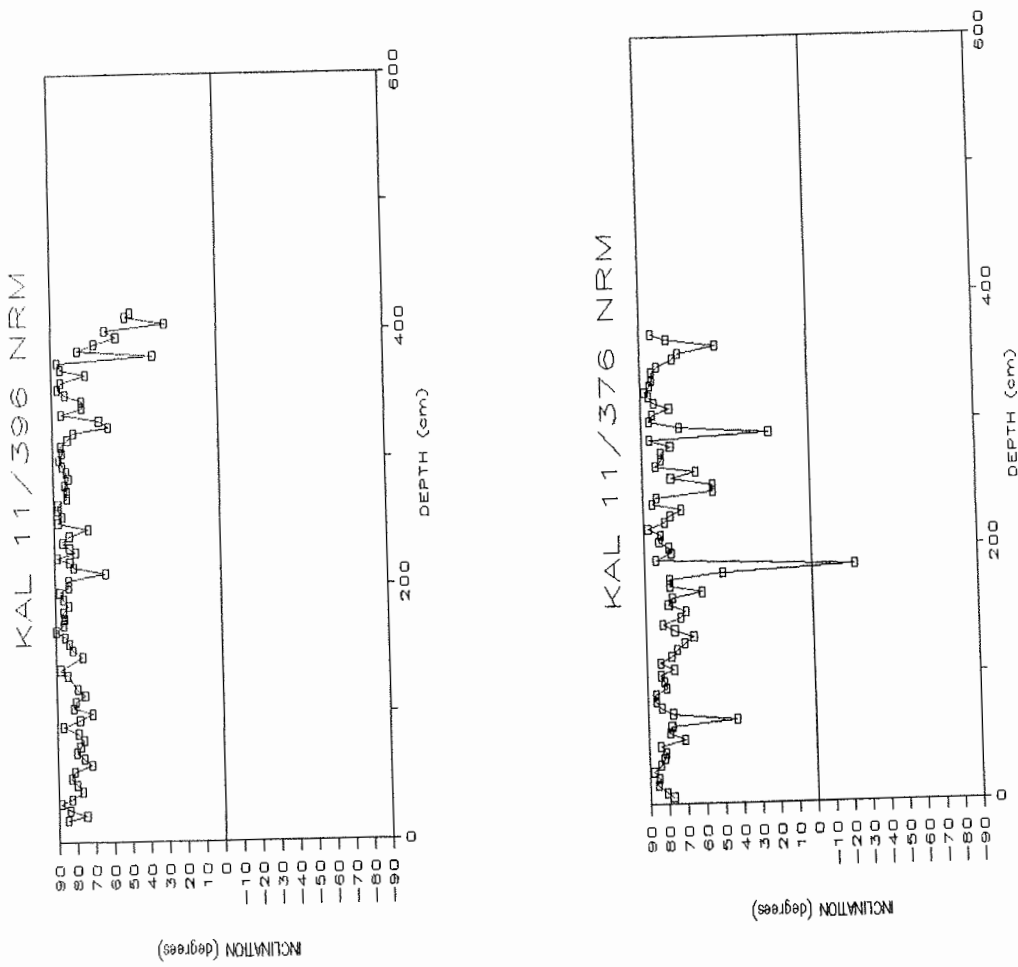


Fig. 77 cont.



in situ overprinting during the present normal geomagnetic Brunhes Epoch. Additional components frequently result from spurious magnetization processes during coring and sampling or subsequent handling of samples. Such secondary components can make up any fraction of total NRM intensity and therefore obscure primary remanent directions to various degrees. While viscous components will always cause a bias towards normal polarities (positive inclinations), directions of spurious components are mostly distributed at random. In general only a detailed demagnetization treatment will allow discrimination of secondary components and isolation of a primary characteristic remanent direction which then can be interpreted in terms of a magnetostratigraphic record.

The following magnetostratigraphic interpretation of the downhole NRM inclination pattern, therefore, is preliminary, tentative, in certain aspects even speculative, and represents but a first working hypothesis at best.

According to the also preliminary biostratigraphic information available, sedimentation rates at all sites are of the order of a couple of centimeters per thousand years. Therefore, these sediments should have accumulated exclusively during the last 0.73 m.y. of the normal geomagnetic Brunhes Epoch. In fact, none of the paleomagnetic logs contain a clearcut indication that the Brunhes/Matuyama boundary has been recovered. On these grounds a magnetostratigraphy is possible only on basis of the series of short polarity events that occur within the Brunhes Epoch. Although their number, exact timing and temporal extent are still a matter of controversial discussion at present, paleomagnetic work on core material from the Norwegian-Greenland Sea and the Fram Strait has shown that short polarity events are particularly useful for stratigraphic purposes in high latitudes (Bleil, in press).

In Core 11/282 the NRM inclination pattern suggests a first polarity event below about 2 m sub-bottom. The negative NRM inclinations found here have been confirmed with AF demagnetization of several samples. Correlated to the youngest established earth's magnetic field excursion, the Lake Mungo Event, the sediments at the base of Core 11/282 should have been deposited during oxygen isotope stage 3 and have an age of about 30,000 years.

Core 11/296 contains two zones of highly variable, overall unusually shallow inclinations (1 to 2 and 3 to 4 m sub-bottom). They are tentatively identified as recordings of the Lake Mungo and Laschamp Events, both previously observed within oxygen stage 3 (Lövlie et al. 1986). The nannofossil data (see Chapter 7.8) may suggest that at the base of the core the sediments have a late oxygen stage 5 age.

Both in Core 11/340 and Core 11/362 the NRM inclination logs are totally inconclusive with respect to magnetostratigraphic interpretation. While sediment magnetization in Core 11/340 may be

affected by a rather strong normal overprinting, Core 11/362 record shows clear indications of relatively strong sediment disturbance.

Core 11/364 and Core 11/365 sediments appear to contain a similar NRM paleomagnetic record which allows quite different identifications of a geomagnetic event series, however. Unfortunately, available biostratigraphic information offers no evidence to choose between higher or lower average sedimentation rate. The presently preferred interpretation recognizes (tentatively) the Lake Mungo Event at about 1.2 m in Core 11/364 (just above 2 m in Core 365), the Laschamp Event at about 2 m (2.5 m), the Blake Event at about 3 m (3.5 m) and the Biwa I Event at about 3.8 m sub-bottom. If correct, sediments near the base of Core 11/364 should be roughly 200,000 years old. This is perhaps a somewhat surprising result as the sediments near the Nansen Gakkel Ridge axis contain considerable amounts of volcanogenic material which has not been observed at the more distant sites.

Core 11/376 NRM inclination log yielded at least four, and possibly five, intervals with unusually shallow normal or reversed directions. Assuming a similar complete recording of geomagnetic events as postulated for Core 11/364 and identifying the lowermost zone of potential negative inclinations at about 3.6 m sub-bottom as the Biwa II Event, the sediments at the base of the core were deposited some 300,000 years ago. According to an alternative, equally plausible interpretation, they may be about 100,000 years younger.

In Core 11/396 from the Yermak Plateau, the NRM data show almost exclusively steep positive inclinations in the upper 3 m. Only in the deepest part is there a trend towards shallower inclinations. The core material, therefore, has either been deposited at a relatively high rate and is no more than about 300,000 years old at the base of the core, or, and more likely, the NRMs in the upper parts are dominated by a normal magnetic overprinting and the lowest section has been disturbed during the coring process.

## **8. BIOLOGICAL, OCEANOGRAPHIC, GEOPHYSICAL AND GEOLOGICAL PROPERTIES OF EASTERN ARCTIC DEEP-SEA BASINS SYNTHESIS AND SUMMARY OF ARK IV/3 SCIENTIFIC INVESTIGATIONS**

The previous Chapters contain detailed accounts of the scientific activities of POLARSTERN expedition ARK IV/3 which brought oceanographers, geoscientists and biologists into the central part of the eastern Arctic deep-sea basins, further north than any other research vessel ever had been. Scientific results on the preceding pages have been described in terms of rather independent investigations.

In the following chapters, we summarize major results and identify areas of interdisciplinary research which are especially promising for future investigations of the Eurasian Basin of the Arctic Ocean and its approaches. The summary is subdivided into chapters concerning ARK IV/3 investigations in the Eurasian Basin: 1) ice dynamics and influence, 2) oceanography, 3) the marine ecosystem, 4) geophysical properties, and 5) geologic history.

### **8.1 Ice Dynamics and Influence in the Eurasian Basin**

During ARK IV/3, scientific investigations of the dynamics, thermodynamics and material content of sea ice surveyed two of the four regions with distinct characteristics in the Nansen Basin: the basin marginal zone and the Siberian branch of the Transpolar drift (Fig. 7). The basin marginal zone is the nearshore region east of the Yermak Plateau, north of Svalbard and Franz Josef Land up to 83° N. The main ice stream of the Siberian branch of the Transpolar Drift occurs at about 84 - 86° N. In these two regions, sea ice looks quite different and probably has different source areas. Chemical analysis of surface waters conducted on the cruise (Chapter 5.4.) showed that in the southern region, surface water chemistry appears to reflect sea ice meltwater input. Prevailing undeformed, first year ice floes occur up to 83 - 84° N, while multiyear floes occur mostly north of 84° N. The thickness of the ice also varies, from an average of 1 to 2 m around 80 - 81° N to more than 3 m at 85 - 86° N. In the northern region, over the Nansen-Gakkel Ridge, the surface of the ice was rough, characterized by a lot of ridges. The compactness of the ice or sea ice concentration was quite irregular with a maximum of 9/10 around 82° N and at about 83 - 84° N, where, added to an increase in ice thickness, the ship's progress was slowed considerably. In general, sea ice conditions during the cruise were characteristic of the melting season. Many deep melt ponds and what appeared to be old snow covered much of the ice surface. Ice in the Fram Strait was found to be unusually extensive for this time of year.

Material accumulations affecting up to 10% of the ice surface were observed south of 83° N, but usually the amount was less

than 1%. Highest concentrations of dirty ice occur along the southern margin of the Nansen Basin from  $83^{\circ} 27' N$  to  $85^{\circ} 02' N$  and near the Nansen-Gakkel Ridge in the region of the Transpolar Drift  $85^{\circ} 40' N$  to  $86^{\circ} 10' N$ , here affecting greater than half of the ice surface.

Most of the nearshore ice (south of  $83^{\circ} N$ ) appeared younger, thinner and with lower ice concentrations when approaching the eastern slope of the Yermak Plateau. This change may be due to the strong influence of near surface warm and saline waters of Atlantic origin transported along the western coast of Svalbard by the West Spitsbergen Current. Most of the ice in the basin marginal zone will melt in the vicinity of the Yermak Plateau before reaching the Fram Strait.

The multiyear ice floes of the Siberian Branch of the Transpolar Drift stream, especially the oldest ones (3 years) probably originate on the Siberian shelves, in particular the Laptev Sea. In this northern region, the chemistry of the surface waters changed markedly with high alkalinity reflecting a river source (perhaps the Lena?) for surface waters of this branch of the Transpolar Drift stream (Chapter 5.4).

It is probable that the Laptev Sea and possibly the Lena River, are sources for extreme amount of material observed included in sea ice over the Nansen-Gakkel Ridge. Preliminary analysis of samples from dirty ice showed silt and clay-sized sediments with numerous wood fragments, moss leaves and moss spores which suggest a terrestrial origin. Most cores obtained from dirty ice locations appeared to sample multiyear ice. Greatest material accumulation at the surface was associated with regions where surface melting was extensive, and meltwater ponds covering 15-40% of the ice surface. Surface melting could concentrate material originally suspended in the ice, forming thick accumulations of material after several melting cycles. Because the majority of "dirty" ice is embedded in the Transpolar Drift, it is likely that it will be transported out of the Nansen Basin through the Fram Strait and be incorporated in the East Greenland Current.

Based on observations obtained during the cruise, the mean drift of sea ice can be estimated at about 3 km per day in the southwest direction; characteristic of the Transpolar Drift in this region. It is striking to note that one buoy (4996) drifted, with the same speed and direction, almost exactly over the 1895 path of Fram (Fig. 8). In addition, buoy drifts, including 3 buoys deployed one year ago 1000 km upstream, are extremely coherent. These observations indicate that mean ice motion is very stable over a long period of time in this area, and that ice motions are correlated over distances of up to 800 km.

Variability, in time and space, of sea-ice drift is the result of the combined effects of winds and currents. Most of the time, temporal variability is due to the winds, since they are fairly

uniform over this region of the Nansen Basin. The trajectory of the first buoy (buoy 5095 deployed on day 196) can be used to illustrate the effect of the wind on ice motion (Fig. 8). This buoy completed a loop in about 24 days as the wind direction changed  $360^{\circ}$ , from westerlies to northerlies, to southerlies and finally again to westerlies on day 220. Comparing trajectories of the other buoys to buoy 5095, we can detect some spatial variability due to the effect of oceanic currents. The loop described by buoy 5095 is much wider open than the ones described by the northern buoys, due to the mean southwest current typical of the Transpolar Drift. Similar differences occur also in the shape of a smaller curve described by all the buoys later on. This peculiar sea ice drift patterns appears common in summer in this area and it is worth noting that the Fram expedition nearly 100 years ago experienced the same phenomenon. Buoy drifts observed during the latter part of the ARK IV/3 cruise were more regular and similar to ice drift during the rest of the year.

## 8.2 Oceanography of the Eurasian Basin Water Column

A comprehensive programme was designed to describe the main features of the halocline, intermediate and deep circulation of the Nansen Basin in order to understand the role of the Basin in its relation to the Barents Sea shelf and the basins south of Fram Strait to the south and the Amundsen Basin to the north. For the first time in the Arctic Ocean a sampling programme with a carefully selected suite of natural and anthropogenic tracers was designed to describe how the fate and mixing history of the water masses are tied into the full-depth circulation of the Nansen Basin. Only a ship-borne expedition could carry out such a programme.

All sampling programmes were successfully completed. The goals of the cruise were fully met. Thus a first full-depth, basin-wide section in the Arctic Ocean is available with hydrographic, chemical and tracer data. Results from the expedition are already available. In addition to a thorough description of the mean state circulation around  $25^{\circ}$  E longitude across the Nansen Basin, unique features were revealed:

- a complicated regime on the Barents Sea slope with several well defined cores of boundary currents or shelf plumes that are fed either from the shelf or through Fram Strait from the Greenland-Norwegian Seas,
- a rather quiet deep basin interior with no measurable freons but with detectable levels of other halocarbons shows an age for the deep water masses of at least many decades,
- a frontal transition at  $83^{\circ}$  N from the southern half of the Basin that has characteristics of Fram Strait and Barents Sea sources at most depths to a northern half that more resembles the Central Arctic Ocean,

- a surface layer in the northern half of the section that is clearly marked through its total carbonate values as being fed by input from Siberian rivers. The absence of the shallow Arctic nutrient maximum found in the Canada Basin shows the Nansen Basin halocline to be dominated by regional sources.

### 8.3 The Arctic Marine Ecosystem

The Arctic Ocean water masses are habitats of highly specialized flora and fauna. Measured production rates of phytoplankton range from 1-30 mg organic carbon per cubic meter per day. In contrast, the maximal production of algae recovered from sea ice, both surface and the underside, was much higher. The true light conditions under the ice must be considered in comparing these measurements. These findings may be fundamental in understanding Arctic primary production.

Calanoid copepods belong to the primary herbivorous consumers and are important members of Arctic zooplankton. Typical Arctic species only appear north of 83-84°N. South of these latitudes, developing stages are dominant and females very rare. These southern populations show a clear Atlantic composition. During measurements on board, copepods only started egg production when given high food concentrations, raising questions about reproduction behavior.

Planktonic foraminifers were investigated as the next member of Arctic zooplankton. These single-celled forms show distinct faunal provinces all over the world ocean. Using these planktonic foraminifers it was possible to detect different water mass structures along the transect from the Svalbard margin to the Nansen-Gakkel Ridge. The water depth to maximum concentration rose to the north, paralleling the distribution of relatively warm water of Atlantic origin. Subpolar forms decreased northward, with a step between 83-84°N. Population densities were higher in the Arctic region than in the ice-covered region of Fram Strait (ARK III/2-3).

The polar cod as an ingestor of plankton is one of the intermediate members of the food chain, and is a food source for seabirds and seals. Capture technologies used on board encountered difficulties in attempting to fish in pack ice, but observations of population densities and the occurrence of one-year old forms were carried out. Future capture attempts based on our experience may be more successful.

The benthic system of the continental slope and the Nansen Basin is also dependent on input of nutrients from the Arctic euphotic zone. The existence of three different benthic assemblages depends on this fact. South of 83°N, the benthic assemblage reflects the influence of nutrient input from the relatively warm, sub-Atlantic water of the West Spitsbergen Current. As a result the assemblage, and in particular the benthic foraminifers, show exactly the same composition and structure as occurs

in the Norwegian Sea. Macrofaunas appear to show the same trend, but can only be sampled in a limited way by the giant box corer.

The analyses conducted by the biological shipboard party produced two major results (Fig. 78):

- 1) Productivity and population densities of plankton and benthos was higher than expected. The limited data analysis done on board already indicates important and new information on Arctic biota basic for future research in the Arctic.
- 2) The faunal border observed at 83-84° N occurred to various degrees in all biological investigations. The border reflects a boundary in the inflow of the warm water of Atlantic origin as detected by the oceanographers on board. Correlations can also be made with changes in sedimentary structures observed by the geologists.

#### 8.4 Geophysical Properties of the Eurasian Basin and Fram Strait

The sparse geologic and geophysical data available at present only allow a very preliminary outline of major trends in the plate tectonic evolution of the Arctic Ocean. In the Eurasian Basin, the most detailed information still comes from an aeromagnetic survey and the interpretation of the residual anomaly lineations (Fig. 79 and 80). With exception of studies in occasionally ice-free waters of the Yermak Plateau region (Sundvor et al. 1982) and the ice island investigation of Kristoffersen (1979, FRAM I) no other marine geophysical work has yet been performed or at least results have not been reported in the open literature.

In particular, prior to this cruise there were no seismic or even 3.5 kHz lines available over the Nansen-Gakkel Ridge and the adjacent abyssal plains of the Nansen and Fram Basins. Even the bathymetric charts published offer very limited detailed resolution only.

ARK IV/3 of POLARSTERN for the first time provided an opportunity to run a marine geophysical program as far north as about 86.2° N and across the Nansen-Gakkel Ridge crest. However, as very heavy ice conditions prevailed on most of the ship's track, it was impossible to use any towed equipment. Geophysical work, therefore, was restricted to the following methods:

- heat flow: in situ measurements of the thermal gradient in upper sedimentary layers at 22 stations (including one in Fram Strait);
- gravity: continuous record of a marine gravimeter system plus additional measurements at 26 stations on ice floes using a land gravimeter;
- acoustics: continuous records of the 20 kHz echosounder, 3.5 kHz sub-bottom profiler and SEABEAM system; - measurements on geologic core materials: thermal conductivity, magnetic susceptibility and remanent magnetic properties.

Biological/Paleontological shipboard scientific party  
Summary of Results  
Barents continental shelf and slope /Nansen Ridge transect

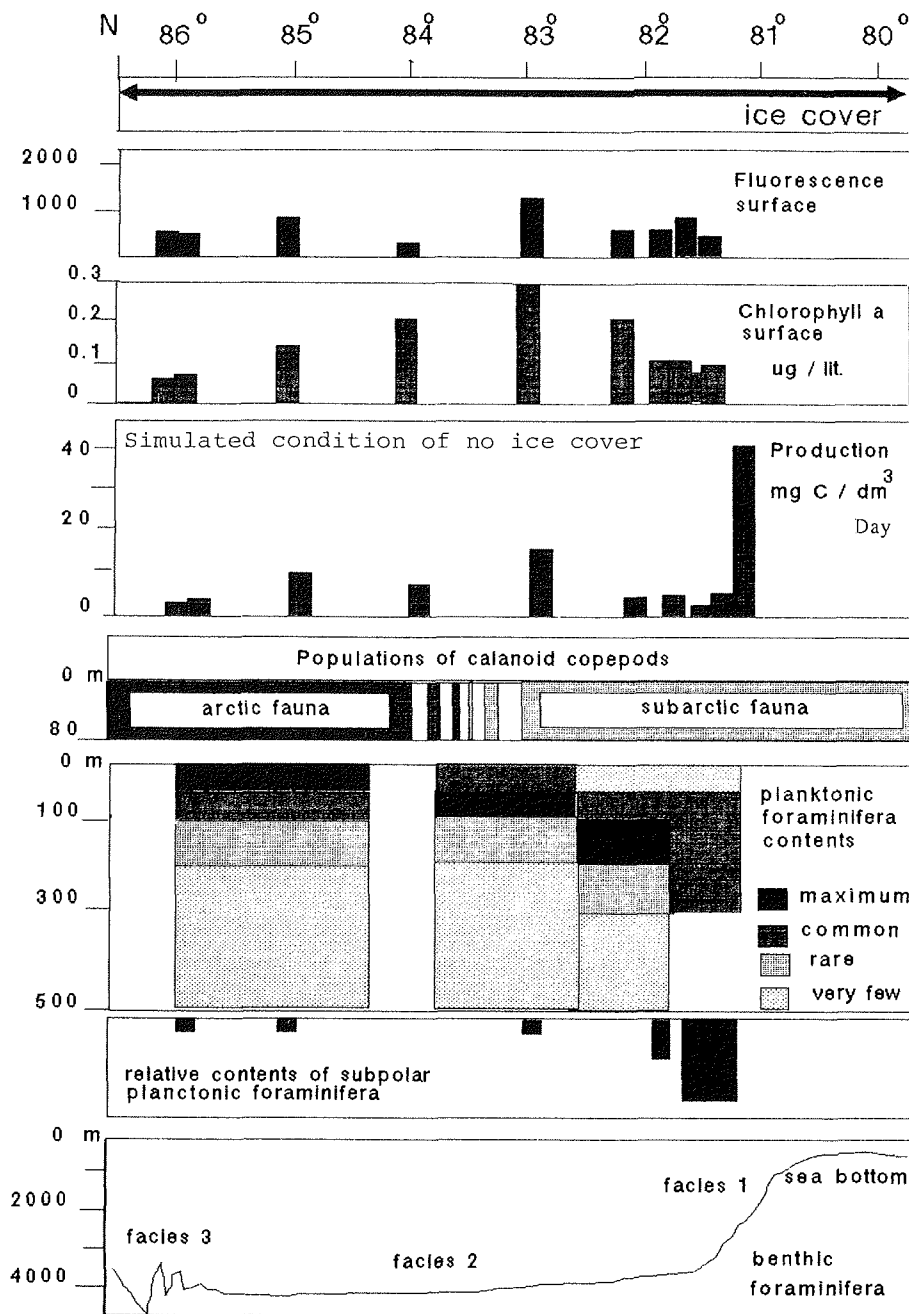


Fig.78 Selected parameters of the biological transect from the Barents Shelf to the Nansen - Gakkel Ridge.

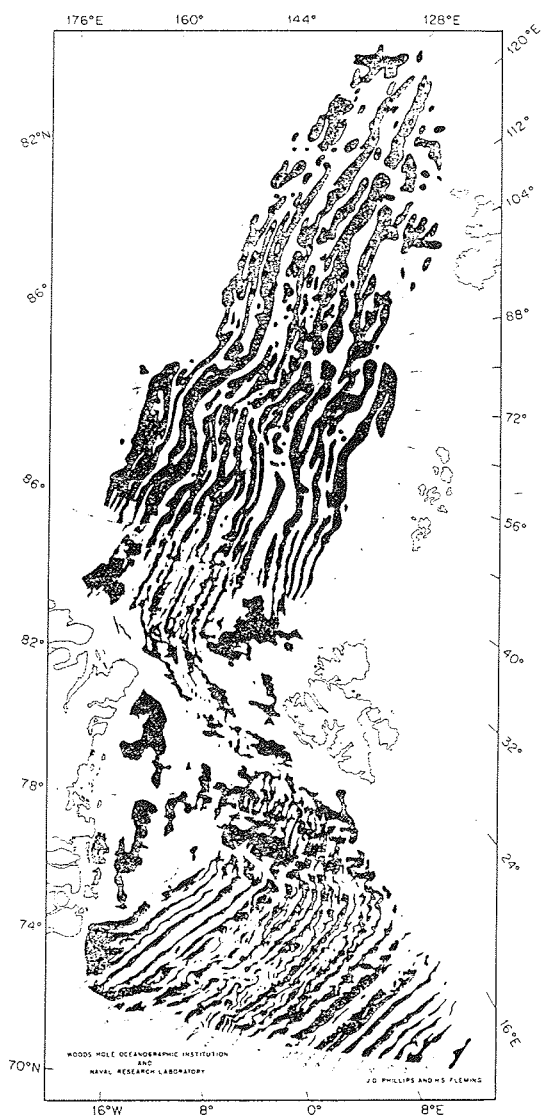


Fig.79 Residual marine magnetic anomaly lineations in the Eurasian Basin and the Norwegian - Greenland Sea (Vogt et al., 1981).

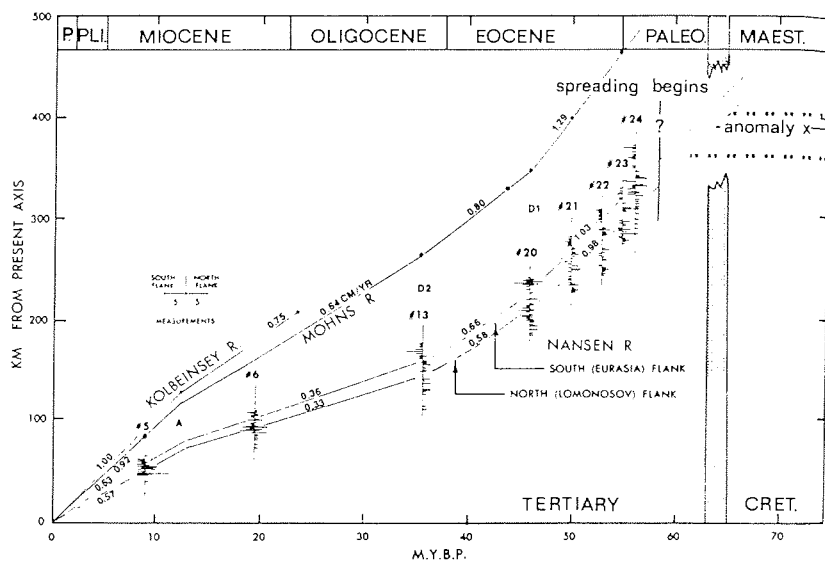


Fig.80 Age versus distance diagram including average spreading half-rates across the Kolbeinsey, Mohns, and Nansen - Gakkel Ridges (Vogt et al., 1981).

Preliminary results are discussed in detail in the respective chapters of this report. Although a number of interesting findings could already be documented, the geophysical data set needs to be thoroughly processed and supplemented by additional shore-based analyses before conclusions and an interpretation can be presented.

Successful measurements of the in situ thermal gradient in the upper sedimentary layers were carried out at 18 stations. At all these sites at least one, and sometimes several sediment cores were retrieved. Detailed shipboard thermal conductivity studies on these materials provide a reliable basis to calculate local heat flow from the in situ thermal gradient. It was most interesting to note that the two measurements in the Nansen-Gakkel rift valley indicate an extreme temperature regime. The heat flows observed are two to three times higher than values reported from the Knipovich Ridge (Sundvor, 1987). This may explain common hydrothermal features encountered in sediments and volcanic rocks retrieved from the Nansen-Gakkel rift valley.

Marine gravity measurements were recorded almost continuously both in digital and analog format. These measurements require not only standard processing but the data evaluation will also have to account for the high noise level and large disturbances introduced by the ship manoeuvering in heavy sea ice. This data reduction is expected to become a rather laborious time consuming task, and may require new data processing techniques. Gravimeter readings on ice floes will be used as tie points and should aid in deducing a reliable data set for the marine gravimeter profiles.

Both the gravity and heat flow results, the first ever obtained in the central Eurasian Basin, substantially contribute to understanding the plate tectonic evolution of this part of the Arctic Ocean which has a key position in the Tertiary and Quaternary relationship between Eurasian and North American land masses.

Shipboard studies of physical properties on sediment cores concentrated on measurements of thermal conductivity and various magnetic properties. Results obtained already reveal a number of most interesting features. For example a sequence of amplitude variations found in the core logs of magnetic susceptibility and remanent magnetic intensity can be traced over a wide area in the vicinity of the Nansen-Gakkel Ridge axis. It apparently also correlates with the downcore thermal conductivity pattern and lithostratigraphic findings. Additional shore-based work is planned to determine density, water content, acoustic velocities and several other parameters which are of critical importance in characterizing lithologic structures of the sediments and the paleoceanographic evolution they reflect.

Preliminary shipboard paleomagnetic measurements permitted establishment of tentative magnetostatigraphic frameworks for some of the sediment cores. Systematic shore-based analyses on a large

number of samples hopefully will result in detailed magnetostratigraphies which can be integrated with biostratigraphic and oxygen-isotope data into a high resolution chronostratigraphy.

### 8.5 Geological History of the Eurasian Basin and Fram Strait

The results of the geological investigations of this expedition have contributed considerably to our understanding of the volcanic and climatic-oceanographic history of the eastern Arctic Basin. The close coordination of the geological studies with a number of other polar research disciplines such as oceanography, meteorology and marine biology resulted in the possibility to relate recent patterns of sediment production and distribution to environmental parameters. The interdisciplinary cooperation of the various working groups during ARK IV/3 has thus been particularly beneficial for the geoscientists who applied both geophysical (see Chapter 8.4) and geological methods.

#### Morphology and Basement Geology

The Arctic Ocean and Fram Strait area is one of the last poorly surveyed and known regions of the world ocean. POLARSTERN is equipped with a SEABEAM echosounding system and has collected the first precisely positioned bathymetric data along the track lines of the expedition from the continental margin north of Svalbard across the crest and the well developed midocean ridge valley of the Nansen-Gakkel Ridge. Based on the morphology of the sea floor along the track lines it could easily be shown where the continental slope and foot north of Svalbard are bounded by the Barents Abyssal Plain. The abyssal plain is extraordinarily flat and is close to 4000 m deep. It is bounded to the north by the flanks of the Nansen-Gakkel Ridge whose deepest parts are slowly drowning in the turbidites of the abyssal plain. The crest of the Nansen-Gakkel Ridge is characterized a deeply incised, block-faulted midocean ridge valley. The northern rim was found to be considerably deeper than its southern counterpart. The track line back to the Fram Strait crossed the Yermak Plateau. To the northeast, the Plateau is bounded by an almost vertical wall rising abruptly from the abyssal plain.

An area to the south of the Molloy Deep in the central Fram Strait was mapped in detail with SEABEAM and 3.5 kHz profiling in an attempt to resolve in detail the position of the plate boundary separating the North American and Eurasian plates.

Sediment cores obtained in the Nansen-Gakkel Ridge area, provide insight into the geological evolution of this anomalous midocean ridge. The Nansen-Gakkel Ridge has the lowest spreading rate of any midocean ridge, and heat flow measurements on this cruise discovered that it has very high heat flow which is characteristic for active magmatism. Rock samples collected in the ridge valley consist of hydrothermally altered and tectonized basalts and will have to be evaluated in their significance later through detailed petrologic studies. However, they are the first sample

of well preserved basement rocks from the entire Arctic Ocean; highly weathered basalts had previously only been recovered from the flanks of Alpha Ridge during the Canadian CESAR expedition (Van Wagoner & Robinson 1985). The sediment cores themselves contain considerable quantities of hydrothermal sediment components (mostly Fe-oxides) documenting hydrothermal precipitation for the past 200-300,000 years of this youngest part of the Arctic Ocean. Accounts of magnetic susceptibility (related to the sediment concentrations of magnetite) show that in general the contributions of magnetite to the sediment decrease with increasing distance from the ridge crest. Downcore variations in magnetic susceptibility in individual cores point to important temporal changes of the ridge processes generating this mineral.

#### Sediment Distributions and Modern Depositional Environment

Sediment distributions have been mapped along the entire track line by means of a 3.5 kHz system; they seem to be closely related to the morphology of the seafloor. The Barents Abyssal Plain is characterized by strongly reflecting layered sediments; repeated attempts to core these layered sediments have failed and it remains unknown what is hidden below the upper few decimeters of soft terrigenous muds which were contained in the box cores.

Numerous box cores along the entire track line permit description of the surface sediment composition. Deposits covering the continental slope and foot north of Svalbard consist of strongly stratified brownish carbonate-poor terrigenous sandy clayey silts. The clearly expressed stratification decreases downslope, and lower parts of the core sections often display a characteristic dark brown lamination. This zone is underlain by often homogenous olive gray silts and clays. The upper brown layer increases systematically in thickness with increasing water depth and distance from the continental shelf.

The sedimentary facies and distributions of biogenic sediment components in these surface layers reflect the depositional environment, largely conditioned by the overlying water masses. To our surprise coarse, ice-rafted terrigenous debris is virtually missing in surface sediments as well as downcore in sediment cores. The sea ice and ice bergs above the Nansen Basin obviously never contained or deposited coarse material. The dominant share of ice-rafted sediment input appears to have consisted of clays and silts, much like sediment components found in the modern pack ice.

Surface sediments are carbonate poor in the area immediately north of Svalbard, as was previously described by Markussen (1986). Both carbonate content and preservation of calcareous fossils improve with increasing distance from the shelf region. Well preserved planktonic foraminiferal faunas are found in sediment from the central midocean ridge valley of the Nansen-Gakkel-Ridge, which is over 5 km deep. The position of the calcite lysocline and compensation depth in the entire Arctic

Ocean has to be studied in detail and with care; it is one of the major unsolved problems of Arctic sedimentology.

The distribution of benthic and planktonic organic remains in surface sediments reflect a clear response to the major boundary between Atlantic and Arctic water masses close to 83° N. In the area of the continental margin north of Svalbard and of the Nansen-Gakkel Ridge fossil assemblages are influenced by reworking and lateral transport. Organic-walled fossil assemblages contain Arctic floras, but they are diluted by long distance-transported pollen. The proportion of reworked organic-walled fossil assemblages is always higher in the subsurface sediments than in the Holocene surface deposits.

#### History of Quaternary Depositional Environment

The sediment cores which have been taken along the transect from the continental margin north of Svalbard to the Nansen-Gakkel Ridge provide a unique opportunity to carry out detailed investigations of variations in the late Quaternary depositional environment. Magneto- and biostratigraphic data seem to suggest that most of the cores have been deposited at rates of approximately 4 cm/1000 years, offering much better possibilities for high stratigraphic resolution than central Arctic cores (Clark et al. 1980). In particular, these cores will provide sample material for high resolution studies of the late glacial, hypsithermal and neoglacial stages. Stratigraphic data seem to suggest that the oldest parts of the 5-7 m long sediment cores have ages of approximately 300,000 years at maximum; coccoliths, planktonic foraminifers and dinocysts were the most useful biostratigraphic tools. The magnetostratigraphic resolution has been refined through the observation of a number of short events within the Brunhes Epoch.

Lithostratigraphy of cores not affected by turbidite sedimentation, points to important temporal variations of the depositional environment. The virtual complete lack of coarse dropstones, the large amounts of coal clasts in certain horizons, and the strange clay clast facies are surprising features of the lithology of these cores which we do not yet understand. Sediment compositions in cores from the southern and northern flank of the Nansen-Gakkel ridge, separated from each other by a rift valley more than 2 km deeper than the adjacent ridge crest, are surprisingly similar. It is presently believed that most major variations in sediment composition and stratigraphy are related to major changes in the nature of the ice cover.

Many sections of the cores are composed of relatively fine-grained sediment components much like the silt and clay fraction observed in pack ice (see Chapter 8.1). Today, in the vicinity of the Nansen-Gakkel Ridge, sediment on the ice surface was observed to form cohesive mudballs which may sink intact to the sea floor. Major sections of the stratigraphic record in some cores consist of similar mud clasts.

Well defined intervals of some sediment cores obtained in the Nansen-Gakkel Ridge area contain sand layers indicating both a source for sand in the basin interior, and a means for concentrating the sand into distinct layers.

A detailed picture of the variability and nature of Quaternary deposition can only be developed once stratigraphic problems have been solved, but there is no question that the history of changes of the pack ice-covered central Arctic can be now studied in considerable detail.

## 9. REFERENCES

- Aagaard, K., L. K. Coachman and E. Carmack (1981) On the halocline of the Arctic Ocean. Deep-Sea Res., 28, 529-545.
- Aagaard, K., J. H. Swift and E. C. Carmack (1985) Thermohaline circulation in the Arctic mediterranean seas. J.Geophys.Res., 90, C3, 4833-4846.
- Aksu, A. E. & P. J. Mudie (1985) Magnetostratigraphy and palynology demonstrate at least 4 million years of Arctic Ocean sedimentation. Nature, 318, 280-283.
- Anderson, G. C. (1971) Oxygen Analysis, Marine Technician's Handbook, Scripps Institution of Oceanography Reference No. 71-8, Sea Grant Publication No. 9.
- Anderson, L. G., & D. Dyrsen (1981) Chemical constituents of the Arctic Ocean in the Svalbard area. Oceanol.Acta, 4, 305-311.
- Anderson, L. G., D. Dyrsen and E. P. Jones (1987) An assessment of the transport of atmospheric CO<sub>2</sub> into the Arctic Ocean. submitted.
- Anderson, L. & A. Graneli (1982) A compact automated titration system applied to high-precision determination of calcium in seawater. J.Autom.Chem., 4, 75-82.
- Atlas E. L., J. C. Callaway, R. D. Tomlinson, L. I. Gordon, L. Barstow and P. K. Park (1971) A Practical Manual for Use of the Technicon Auto-Analyzer in Sea Water Nutrient Analysis; Revised. Oregon State University Technical Report 215, Reference No. 71-22.
- Augstein, E., G. Hempel, J. Schwarz, J. Thiede, W. Weigel (1984) Die Expedition ARKTIS II des FS "POLARSTERN". Ber.Polarforsch., 20. Alfred-Wegener-Institut für Polar-forschung. 192 pp.
- Bartz, R., J. R. V. Zaneveld and H. Pak (1976) A transmissometer for profiling and moored observations in water. SPIE 160 Ocean Optics V.
- Be, A. W. (1960) Some observations on arctic planktonic foraminifera. Contributions of the Cushman Foundation for Foraminiferal Research, 11, 2, 64-68.
- Bleil, U. (1987) Quaternary high latitude magnetostratigraphy. Polar Research (in press).
- Böggild, O. B. (1904) On the bottom deposits of the North Polar Sea. Norweg. Polar Exped. 1893-1896. Sci.Res, 5, 1-52.

- Bonani, G., H. J. Hofmann, E. Morenzoni, M. Nessi, M. Suter and W. Wölfli (1986) The ETH/SIN Dating Facility: A Status Report. *Radiocarbon*, 28, 246-255.
- Boström, K. & J. Thiede (1984) YMER-80 Swedish Arctic Expedition. *Medd. Stockh. Univ. Geol. Inst.*, 260, 1-123.
- Brewer, P. G., D. W. Spencer, P. E. Biscaye, A. Hanley, P. L. Sachs, C. L. Smith, S. Kadar, J. Fredericks (1976) The distribution of particulate matter in the Atlantic Ocean. *Earth Planet. Sci. Lett.*, 32, 393-402.
- Bullister, J. L. & R. F. Weiss (1983) Anthropogenic chlorofluoromethanes in the Greenland and Norwegian seas. *Science*, 221, 265-268.
- Burgeois, J. C., R. M. Koerner, and B. T. Alt (1985) Airborne pollen: a unique air mass tracer, its influx to the Canadian high arctic. *Ann. Glaciol.*, 7, 109-116.
- Burreson, B. J., R. E. Moore and P. Roller (1975) ??? *Tetrahedron Lett.*, 7, 473-476.
- Carpenter J.H. (1965) The Chesapeake Bay Institute technique for Winkler dissolved oxygen method. *Limnol. Oceanogr.*, 10, 141-143.
- Clark, D. L., R. R. Whitman, K. A. Morgan and S. D. Mackay (1980) Stratigraphy and glacial marine sediments of the Amerasian Basin. *Geol. Soc. Amer.*, 181, 57 pp.
- Clark, D.L. & A. Hanson (1983) Central Arctic Ocean sediment texture: Key to ice transport mechanisms. In Molnia, B.F. ed. *Glacial-Marine Sedimentation*, Plenum Press, 301-330.
- Coachman, L. K. & C. A. Barnes (1962) Surface water in the Eurasian Basin of the Arctic Ocean. *Arctic*, 15, 251-277.
- Cochran J. K., H. D. Livingston, D. J. Hirschberg and L. D. Suprenant (1987) Natural and anthropogenic radionuclide distributions in the Northwest Atlantic Ocean. *Earth Planet. Sci. Lett.*, in press.
- Colony, R. & A. S. Thorndike (1984) An estimate of the mean field of Arctic sea-ice motion. *J. Geophys. Res.*, 89(C6), 10623-10629.
- Damuth, J. E. (1978) Echo Character of the Norwegian-Greenland Sea: Relationship to Quaternary sedimentation. *Mar. Geol.*, 28, 1-36.
- Damuth, J. E. (1980) Use of High-Frequency (3.5-12 kHz) Echograms in the Study of Near-Bottom Sedimentation Processes in the Deep Sea: A Review. *Mar. Geol.*, 38, 51-75.

- Dehlinger, P. (1978) Marine Gravity. Elsevier, Amsterdam.
- Drewry, D. (1986) Glacial Geologic Processes. Edward Arnold. 276 pp.
- Ekman, V. W. (1905) On the influence of the earth's rotation on ocean currents. *Ark.F.Mat., Astron.och.Fysik*, 2, 11, 1-53.
- Eckstaller, A., H. Miller and H. Lange (1984) Anschluß an absolute Schwerewerte. *Ber.Polarforsch.*, 19, 98-99.
- Feden, R. H., P. R. Vogt and H. S. Fleming (1979) Magnetic and bathymetric evidence for the "Yermak" hot spot northwest of Svalbard in the Arctic Basin. *Earth Planet.Sci.Lett.*, 44, 18-38.
- Gard, G. (1986) Calcareous nannofossil biostratigraphy of late Quaternary Arctic sediments. *Boreas*, 15, 217-229.
- Gascard, J.C., P.F. Jeannin (1986) ARCTEMIZ 86. Cruise report, Int. Rept., LODYC, University of Paris.
- Geoscientific Working Party (1988) GEODATA: ARK IV/3 expedition of the PFVS POLARSTERN - The central eastern Arctic Basin, Summer 1987. Berichte 21, GIK/CAU.
- Gordienko, P. A. (1958) Arctic Ice Drift. Proc. Conf. on Arctic Sea Ice, National Academy of Sciences, National Research Council, Publ. 598, 210-220, 1359.
- Greenland Sea Project. An International Plan of the Arctic Ocean Sciences Board, Alfred Wegener Institute for Polar and Marine Research, Bremerhaven, April 1987 and AOSB, Ocean Studies Board, National Academy of Sciences, Washington, D.C.
- Harland, R. (1983) Distribution maps of recent dinoflagellate cysts in bottom sediments from the North Atlantic and adjacent seas. *Paleontology*, 26, 321-387.
- Heinze, C., P. Schlosser, K. P. Koltermann and J. Meincke (1987) A tracer study of the deep water renewal in the European Polar Seas. Submitted to Deep-Sea Res.
- Herb, R. (1968) Recent planktonic foraminifera from sediments of the Drake Passage, Southern Atlantic Ocean. *Eclog. geol. Helv.*, 61:2, 467-480.
- Herman, Y. (1974) Arctic ocean sediments, microfauna and climatic record in the Late Cenozoic time. In: Herman, Y. (ed.): *Geology of Arctic Seas*, Springer Verlag, New York, pp. 283-348.

- Herzen von R. & A. E. Maxwell (1959) The measurements of thermal conductivity of deep sea sediments by a needle probe method. *J.Geophys.Res.*, 64, 1557-1563.
- Honjo, S., S. J. Manganini, A. Karowe, and B. L. Woodward (1987) Particle Fluxes, Northeastern Nordic Seas: 1983-1986, Techn. Rep. WHOI-87-17. 84 pp.
- Horner, R.A. (1985) History of ice algal investigations. In: Horner, R.A. ed. *Sea Ice Biota*; CRC Press Inc., Boca Raton, Fla. pp. 1-19.
- Jackson, H.R., G. L. Johnson, E. Sundvor and A. H. Myhre (1984) The Yermak Plateau: formed at a triple junction. *J.Geophys.Res.*, 89, 3223-3232.
- Jackson, H. R., P. J. Mudie and S. M. Blasco (eds.) (1985) Initial geological report on CESAR - The Canadian Expedition to Study the Alpha Ridge, Arctic Ocean. *Geol.Surv. Canada Pap.*, 84-22, 177 pp.
- Johansson, O. & M. Wedborg (1982) On the Evaluation of Potentiometric titrations of Seawater with hydrochloric acid, *Oceanol.Acta*, 5, 209-218.
- Johnson, K. M., A. E. King and J. M. Sieburth (1985) Coulometric TCO<sub>2</sub> Analysis for Marine Studies, An Introduction *Mar. Chem.*, 16, 61-82.
- Jones, E. P. & L. G. Anderson (1986) On the origin of the properties of the Arctic Ocean halocline, *J.Geophys.Res.*, 91, 10759-10767.
- Kennett, J. P. (1968) Latitudinal variation in G. pachyderma in surface sediments of the Pacific Ocean. *Micropaleontology*, 14:3, 305-308.
- Kennett, J. P. (1970) Comparison of G. pachyderma in Arctic and Antarctic areas. *Contrib.Cush.Found.Foram.Research*, 21:2, 47-49.
- Kiär, H. (1904) Thalamophora of the bottom deposits and the mud from the ice surface. *Nor.Polar.Exped. 1893-1896, Sci. Res.*, 5, 58-62.
- Kögler, F. C. (1963) Das Kastenlot, Meyniana 13. Kiel 1963.
- Koltermann, K. P. (1985) New evidence for a deep boundary current of polar origin through Fram Strait. ICES, C.M.1985/C:38, Copenhagen.
- Koltermann, K. P. (1987) Die Tiefenzirkulation der Grönland-See als Folge des thermohalinen Systems des Europäischen Nordmeers. Diss, Univ. Hamburg. 287 pp.

Krause, G., J. Meincke, and J. Thiede (1988) ARK IV Fahrtbericht.  
Berichte zur Polarforschung. AWI.

Kristoffersen, Y. (1979) Fram-I. Ekspedisjonsrapport.  
Nor.Polar.Inst., Oslo, 88 pp.

Kromer, B., C. Pfleiderer, P. Schlosser, I. Levin, K. O. Münnich,  
G. Bonani, M. Suter and W. Wölfli (1987) AMS  $^{14}\text{C}$  measurement  
of small volume oceanic water samples: Experimental proce-  
dures and comparison with low-level counting technique.  
Nuclear Instruments and Methods, in press.

Lange, M.A. (1987) Basic properties of Antarctic sea ice as  
revealed by textural analysis on ice cores. Submitted to:  
Symposium on Ice-Core analysis, Bern, Switzerland, 1987.

Livingston, H. D. (1987) The use of Cs and Sr isotopes as tracers  
in the Arctic mediterranean seas. Phil.Trans.Roy.Soc., Lon-  
don, submitted.

Loosli, H. H. (1983) A dating method with  $^{39}\text{Ar}$ . Earth Planet.  
Sci. Lett. 63, 51-62.

Lövlie, R., B. Markussen, H. P. Sejrup and J. Thiede (1986)  
Magnetostratigraphy in three Arctic Ocean sediment cores;  
arguments for geomagnetic excursions within oxygen-isotope  
stage 2-3. Phys.Earth Planet.Inter., 43, 173-184.

Lynch, M.C.F. & D.J. Kay (1981) Performance of a mass spectro-  
meter for determining low tritium levels from  $^3\text{He}/^4\text{He}$  meas-  
urements. In: Methods of Low-Level Counting and Spectrom-  
etry, IAEA-SM-252/47, IAEA, Vienna, 511-523.

Markussen, B., R. Zahn & J. Thiede (1985) Late Quaternary  
sedimentation in the eastern Arctic Basin: stratigraphy and  
depositional environment. Palaeogeogr., Palaeoclimat.,  
Palaeoecol., 50, 271-284.

Markussen, B. (1986) Late Quaternary sedimentation and paleo-  
ceanography in the eastern Arctic Ocean. -dr. scient.-  
thesis, mat.-nat. fak., Univ. Oslo, 175 pp.

McCave, I. N. (1975) Vertical Flux of particles in the ocean.  
Deep-Sea Res., 22, 491-502.

Melling, H. & E. L. Lewis (1982) Shelf drainage flows in the  
Beaufort Sea and their effect on the Arctic Ocean. Deep-Sea  
Res., 29, 967-985.

Minster, J.B. & T.H. Jordan (1980) Present-day plate motions.  
Summary. Centre National de la Recherche Scientifique,  
Paris, pp.109-124.

Mudie, P. J. (1985) Palynology of the CESAR cores, Alpha Ridge.  
Geol.Surv. of Canada Pap., 84-22, 149-174.

- Mudie, P. J. & S. J. Short (1985) Marine palynology of Baffin Bay. In: J.T. Andrews (ed.) Quaternary Environments of Baffin Island, West Greenland and Baffin Bay. Allen & Unwin Pub.; p. 263-308.
- Müller, G. & Gastner (1971) The "Carbonate Bomb", a simple device for the determination of carbonate content in sediments, soils and other materials. N.Jb.Mineral., 10, 466-469..
- Nansen, F. (1902-1906) "The Norwegian North Polar Expedition 1893-1896". Scientific Results. vol I-VI. Oslo.
- Norris, G. (1982) Spore-pollen evidence for early Oligocene high-latitude cool climatic episode in Northern Canada. Nature, 297, 387-388.
- Östlund, H. G., Z. Top and V. E. Lee (1982) Isotope dating of waters at Fram III. Geophys.Res.Lett., 9, 1117-1119.
- Östlund, H.G., G. Possnert and J.H. Swift (1987) Ventilation rate of the deep Arctic Ocean from Carbon 14 data. J.Geophys.Res., 92:C4, 3769-3777.
- Perkin, R. G. & E. L. Lewis (1984) Mixing in the West Spitsbergen Current. J.Phys.Oceanogr. 14, 131-132.
- Perry, R. K., H. S. Fleming, J. R. Weber, Y. Kristoffersen, J. K. Hall, A. Grantz, G. L. Johnson, N. Z. Cherkis, B. Larsen (1986) Bathymetry of the Arctic Ocean. Naval Research Laboratory - Acoustics Division. printed by the Geological Society of America.
- Peterson, W. H. & C. G. H. Rooth (1976) Formation and exchange of deep water in the Greenland and Norwegian seas. Deep-Sea Res., 23, 273-283.
- Plummer, L. N., B. F. Jones and A. H. Truesdell (1976) WATEQF- a fortran IV version of WATEQ, a computer for calculating chemical equilibrium of natural waters. U.S.Geol.Surv., Water Res.Invest., 76-13, 61 pp., Washington, D.C.
- Ratcliffe, E. H. (1960) The thermal conductivities of ocean sediments. J.Geophys.Res., 65, 1535-1541.
- Redfield, A. C., B. H. Ketchum and F. A. Richards (1963) The influence of organisms on the composition of seawater, in The Sea, vol. 2, edited by M. N. Hill, pp 26-77, John Wiley, New York.
- Robertsson, A.-M. (1984) Clay mineralogy, diatoms and palynomorphs from the Arctic Ocean and the Barents Sea. Svenskhemmet Voksenäsen Norges Nationalgave. Report on Sediments and Climate in the Arctic, p. 31-54.

- Schlosser, P. (1985) Ozeanographische Anwendungen von Spurenstoffmessungen im Mittelmeerausstrom und im Europäischen Nordmeer. PhD Thesis, University of Heidelberg.
- Schlosser, P., C. Pfleiderer, B. Kromer, I. Levin, K. O. Münnich, G. Bonani, M. Suter and W. Wölfli (1987) Measurement of small volume oceanic  $^{14}\text{C}$  samples by Accelerator Mass Spectrometry. Radiocarbon, 29, 347-352.
- Schoch, H. and K. O. Münnich (1981) Routine performance of a new multi-counter system for high-precision  $^{14}\text{C}$  dating. In: Methods of Low-Level Counting and Spectrometry, IAEA, Vienna, 361-370.
- Slater, J. E. (ed.) (1969) The Arctic Basin. Arctic Inst.N.Am. Washington, D.C., 337 pp.
- Smethie, W. D. Jr., D. W. Chipman, J. H. Swift, K. P. Koltermann (1987) Chlorofluoromethanes in the Arctic Mediterranean Seas: Evidence for Formation of Bottom Water in the Eurasian Basin and Deep Water Exchange through Fram Strait, in press J.Geophys.Res.
- Smethie, W. M., Jr., H. G. Östlund and H. H. Loosli (1986). Ventilation of the deep Greenland and Norwegian seas: evidence from krypton-85, tritium, carbon-14 and argon-39. Deep-Sea Res., 33, 675-703.
- Smethie, W. M., Jr. & G. Mathieu (1986) Measurement of Kr-85 in the ocean. Mar.Chem., 18, 17-34.
- Sundvor, E. (1987) Heat flow measurements on the western Svalbard margin. Int. Rep., Seismol. Obsv., Univ. Bergen.
- Sundvor, E., A. M. Myhre, A. Austegard, K. Haugland, O. Eldholm, and A. Gidskehaug, (1982) Marine geophysical survey on the Yermak Plateau. Seismol.Obs., Univ. Bergen, Sci. Rep. 7: 29 pp.
- Sweeney, J.F., J.R. Weber, and S.M. Blasco (1982) Continental ridges in the Arctic Ocean: LOREX constraints. In: G.L. Johnson and J.F. Sweeney (eds), Structure of the Arctic. Tectonophysics, 89:217-237.
- Swift, J. H. & K. P. Koltermann (1987) On the origin of the Norwegian Sea Deep Water. Submitted to J.Geophys.Res.
- Thiede, J., D. Clark and Y. Herman (in press) Late Mesozoic and Cenozoic paleoceanography of northern polar oceans. Chapter 25 in Arctic Ocean, DNAG.
- Thiede, J., S. Pfirman, H.-W. Schenke and W. Reil (in prep.) Bathymetry of Molloy Deep (Fram Strait between Svalbard and Greenland).

- Untersteiner, N. and A. S. Thorndike (1982) The Arctic Data Buoy Program. *Polar Record*, 21, 127-135.
- Untersteiner, N. (1986) Glaciology - A primer on ice. *Oceanus*, 29, 18-23.
- Van Wagoner, N. A. & P. T. Robinson (1985) Petrology and geochemistry of a CESAR bedrock sample: Implications for the origin of Alpha Ridge. *Geol. Surv. Canada Pap.*, 84:22, 47-57.
- Villinger, H. (1983) In-situ Bestimmung der Wärmeleitfähigkeit in Bohrungen. Dissertation, Berlin.
- Vinje, T. (1982) The drift pattern of sea-ice in the Arctic with particular reference to the Atlantic approach. In: *The Arctic Ocean, the Hydrographic environment and the fate of pollutants*, Louis Rey ed. Comite Arctique International, Monaco, 83-96.
- Vinje, T. (1987) Morphology and dynamics of the Barents Sea ice fields. *POAC-87 Proceedings*, University of Alaska, Fairbanks. In press.
- Vogt, P. R. (1986) Seafloor topography, sediments, and paleoenvironments. p. 237-410, in B.G. Hurdle: *The Nordic Seas*. Springer Verlag, New York, 777 pp.
- Vogt, P. R., R. K. Perry, R. H. Feden, H. S. Fleming, and N. Z. Cherkis (1981) The Greenland - Norwegian Sea and Iceland environment: Geology and geophysics. In: Nairn, A.E.M., M. Churkin, Jr. and F. G. Stehli, *The ocean basins and margins Vol. 5: The Arctic Ocean*. Plenum Press, New York, 493-598.
- Vogt, P. R., P. T. Taylor, L. Kovacs, and G. L. Johnson (1979) Detailed aeromagnetic investigation of the Arctic Basin. *J. Geophys. Res.*, 84, 1071-1089.
- Wallace, D. W. R. & R. M. Moore (1985) Vertical profiles of CC13F (F-11) and CC12F2 (F-12) in the Central Arctic Ocean Basin. *J. Geophys. Res.*, 90, 1155-1166.
- Wallace, D. W. R., R. M. Moore and E. P. Jones (1987) Ventilation of the Arctic Ocean cold halocline: Rates of diapycnal and isopycnal transport, oxygen utilization and primary production inferred using chlorofluoromethane distributions. *Deep-Sea Res.* (in press).
- Weiss, W., W. Roether and G. Bader (1976) Determination of blanks in low-level tritium measurement. *Int. J. Appl. Radiat. Isotopes*, 27, 217-225.
- Wilson, G. T. & Clowes (1980) A concise catalogue of organic-walled fossil dinoflagellate genera. New Zealand *Geol. Surv. Rep.*, 92, 199 pp.

Worsley, T. R. & Y. Herman (1980) Episodic ice-free Arctic Ocean in Pliocene and Pleistocene time: calcareous nannofossil evidence. *Science*, 210, 323-325.

## 10. ALPHABETICAL LIST OF SCIENTIFIC PARTICIPANTS

Altenbach, A.	(GIK)	Mühlhan, N.	(GIK)
Anderson, L.	(UGÖ)	Mumm, N.	(IPÖ)
Baumann, M.	(FG/UB)	Muus, D.	(SIO)
Bieser, J.	(UTü)	Nowaczyk, N.	(FG/UB)
Bleil, U.	(FG/UB)	Osborne, J.	(UW)
Bohrmann, H.	(GIK)	Pagels, U.	(GIK)
Bönisch, G.	(IUPH)	Pfirman, S.	(GIK)
Botz, R.	(GIK)	Richez, C.	(LODYC)
Buessler, K.	(WHOI)	Richter, B.	(SWA)
Carstens, J.	(FG/UB)	Rodriguez, J.	(PHYBE)
Gascard, J.-C.	(LODYC)	Schlosser, P.	(IUPH)
Haake, F.-W.	(GIK)	Sobiesiak, M.	(FG/UB)
Heidland, K.	(AWI)	Sonnabend, H.	(SWA)
Hirschberg, D.	(NYSB)	Spielhagen, R.	(GIK)
Horwege, S.	(GIK)	Steen, E.	(GIK)
Jones, E. P.	(BIO)	Stute, U.	(RWTH)
Koerner, T.	(IfMK)	Sundvor, E.	(JSS)
Koltermann, P.	(DHI)	Swift, J.	(SIO)
Krishfield, R.	(WHOI)	Thiede, Jörn	(GIK)
Kromer, B.	(IUPH)	Thomsen, L.	(IfMK)
Krysell, M.	(UGÖ)	Torp, J.-E.	(JSS)
Kubisch, M.	(GIK)	Vassmyr, S.	(IBG)
Lüthje, H.	(DHI)	Wallace, D.	(BIO)
Marian, P.	(IUPH)	Weber, W.	(FG/UB)
Masten, D.	(SIO)	Westerlund, S.	(UGÖ)
Matthießen, J.	(GIK)	Wollenburg, I.	(GIK)
McKeown, P.	(APL/UW)	Zemlyak, F.	(BIO)
Mudie, P.	(AGC/BIO)		

## 11. LIST OF ACRONYMS USED IN THE TEXT

ADCP	Acoustic Doppler Current Profiler (part of the AEDB)
AEDB	Arctic Environmental Drifting Buoy, deployed by WHOI
AIDJEX	Arctic Ice Dynamics Joint EXperiment
ALS	Autonomous Listening Stations (LODYC)
AMS	Accelerator Mass Spectrometry
APL/UW	Applied Physics Laboratory, University of Washington
ARCTEMIZ	ARCtic Ocean and European MIZ (MIZ = Marginal Ice Zone)
ARK IV/3	Leg 3 of the PFVS POLARSTERN's 1987 Arctic cruise
AWI	Alfred-Wegener-Institut für Polar- und Meeresforschung, Bremerhaven
AGC	Atlantic Geoscience Center
BIO	Bedford Institute of Oceanography
CAU	Christian-Albrechts-Universität, Kiel
CESAR	Canadian Expedition to Study the Alpha Ridge
CHN	Carbon-Hydrogen-Nitrogen
CFM	ChloroFluoroMethane
CTD	Conductivity-temperature-depth profiler
DHI	Deutsches Hydrographisches Institut
DVM	Digital voltmeter
ERS1	European Research Satellite 1
FG/UB	Fachbereich 5 - Geowissenschaften, Universität Bremen
GIK	Geologisch-Paläontologisches Institut und Museum Christian-Albrechts-Universität, Kiel
GKG	GroßKastenGreifer - large box grab (50x50x60 cm)
GPS	Global Positioning System
GSDW	Greenland Sea Deep Water
HSW	Helikopter Service, Wasserthal
IBG	Institutt for Biologi og Geologi, Universitetet i Tromsö
IfMK	Institut für Meereskunde, Christian-Albrechts-Universi- tät, Kiel
INDAS	Integrated Navigation and Data Acquisition System
IPÖ	Institut für Polarökologie, Christian-Albrechts- Universität, Kiel
IUPH	Institut für UmweltPhysik, Universität Heidelberg
JSS	JordSkjelvstaSjonen, Realfagbygg, Bergen-Universitet
LODYC	Laboratoire d' Oceanographie DYnamique et de Climatolo- gie, Paris
LOREX	LOmonosov Ridge EXperiment
LVS	Large Volume Sampling
KAL	KAstenLot - long box core (30x30cm x ≤18m)
KOL	KolbenLot - piston core (12cm diameter x ≤18m)
LM	Light Microscope
MEDOC	MEDiterranee OCcidentale
MODE	Mid Ocean Dynamics Experiment
MIT	Massachusetts Institute of Technology
MIZEX	Marginal Ice Zone EXperiment
NBIS	Neil Brown Instrument Systems (maker of the DHI CTD)
NBS	Single (Narrow) Beam echo Sounder
NO	tracer defined by Nitrogen and Oxygen concentrations in seawater
NOAA	U.S. National Oceanic and Atmospheric Administration

NRM	Natural Remnant Magnetism
NSDW	Norwegian Sea Deep Water
NSF	U.S. National Science Foundation
NYSB	Marine Science Research Center, State University of New York, Stony Brook
ONR	U.S. Office of Naval Research
PHYBE	PHYSIKALISCHES Institut, BErn
POLYMODE	POLY M.O.D.E
PU	Princeton University
RWTH	Rheinisch-Westfälische Technische Hochschule, Aachen
S	Salinity
SEABEAM	Multibeam bathymetric swath survey system
SEM	Scanning Electron Microscope
SIO	Scripps Institute of Oceanography, Oceanographic Data Facility, La Jolla, CA 92093
SL	SchwereLot - gravity core (12cm diameter ≤18m)
SOFAR	SOund Fixing And Ranging
SOFARGOS	SOFAR and ARGOS
SPM	Suspended Particulate Matter
SWA	SeeWetterAmt, Hamburg
T	Temperature
TEM	Transmission Electron Microscope
TOURBILLON	Case study of an open ocean eddy in the northeastern Atlantic (Tourbillon means eddy in french)
TRAPOLEX	TRANSPOlar EXPedition -- 1991?
UTÜ	Geologisch-Paläontologisches Institut, Universität Tübingen
UGÖ	Department of Analytical and Marine Chemistry CTH/GU, University of Göteborg
WHOI	Woods Hole Oceanographic Institution
XBT	eXpendable BathyThermograph
XCP	eXpendable Current Profiler
YU	York University, Centre for Research in Experimental Space Science, Ontario

## Folgende Hefte der Reihe „Berichte zur Polarforschung“ sind bisher erschienen:

Verkaufspreis/DM

* <b>Sonderheft Nr. 1/1981</b> – „Die Antarktis und ihr Lebensraum“ Eine Einführung für Besucher – Herausgegeben im Auftrag von SCAR		
<b>Heft Nr. 1/1982</b> – „Die Filchner-Schelfeis-Expedition 1980/1981“ zusammengestellt von Heinz Kohnen	11,50	
<b>Heft Nr. 2/1982</b> – „Deutsche Antarktis-Expedition 1980/1981 mit FS „Meteor“ First International BIOMASS Experiment (FIBEX) – Liste der Zooplankton- und Mikronektonnetzfänge zusammengestellt von Norbert Klages	10,—	
<b>Heft Nr. 3/1982</b> – „Digitale und analoge Krill-Echolot-Rohdatenerfassung an Bord des Forschungsschiffes „Meteor“ (im Rahmen von FIBEX 1980/81, Fahrtabschnitt ANT III), von Bodo Morgenstern	19,50	
<b>Heft Nr. 4/1982</b> – „Filchner-Schelfeis-Expedition 1980/81“ Liste der Planktonfänge und Lichtstärkemessungen zusammengestellt von Gerd Hubold und H. Eberhard Drescher	12,50	
* <b>Heft Nr. 5/1982</b> – „Joint Biological Expedition on RRS ‘John Biscoe’, February 1982“ by G. Hempel and R. B. Heywood		
* <b>Heft Nr. 6/1982</b> – „Antarktis-Expedition 1981/1982 (Unternehmen ‚Eiswarte‘)“ zusammengestellt von Gode Gravenhorst		
<b>Heft Nr. 7/1982</b> – „Marin-Biologisches Begleitprogramm zur Standorterkundung 1979/80 mit MS „Polar-sirkel“ (Pre-Site Survey)“ – Stationslisten der Mikronekton- und Zooplanktonfänge sowie der Bodenfischerei zusammengestellt von R. Schneppenheim	13,—	
<b>Heft Nr. 8/1983</b> – „The Post-Fibex Data Interpretation Workshop“ by D. L. Cram and J.-C. Freytag with the collaboration of J. W. Schmidt, M. Mall, R. Kresse, T. Schwinghammer	10,—	
<b>Heft Nr. 9/1983</b> – „Distribution of some groups of zooplankton in the inner Weddell Sea in summer 1979/80“ by I. Hempel, G. Hubold, B. Kaczmaruk, R. Keller, R. Weigmann-Haass	15,—	
<b>Heft Nr. 10/1983</b> – „Fluor im antarktischen Ökosystem“ – DFG-Symposium November 1982 zusammengestellt von Dieter Adelung	23,—	
<b>Heft Nr. 11/1983</b> – „Joint Biological Expedition on RRS ‘John Biscoe’, February 1982 (II)“ Data of micronecton and zooplankton hauls, by Uwe Piatkowski	16,—	
<b>Heft Nr. 12/1983</b> – „Das biologische Programm der ANTARKTIS-I-Expedition 1983 mit FS „Polarstern“ Stationslisten der Plankton-, Benthos- und Grundsleppnetzfänge und Liste der Probennahme an Robben und Vögeln, von H. E. Drescher, G. Hubold, U. Piatkowski, J. Plötz und J. Voß	14,—	
* <b>Heft Nr. 13/1983</b> – „Die Antarktis-Expedition von MS „Polarbjörn“ 1982/83“ (Sommercampagne zur Atka-Bucht und zu den Kraul-Bergen), zusammengestellt von Heinz Kohnen		
* <b>Sonderheft Nr. 2/1983</b> – „Die erste Antarktis-Expedition von FS „Polarstern“ (Kapstadt, 20. Januar 1983 – Rio de Janeiro, 25. März 1983)“, Bericht des Fahrtleiters Prof. Dr. Gotthilf Hempel		
* <b>Sonderheft Nr. 3/1983</b> – „Sicherheit und Überleben bei Polarexpeditionen“ zusammengestellt von Heinz Kohnen		
<b>Heft Nr. 14/1983</b> – „Die erste Antarktis-Expedition (ANTARKTIS I) von FS „Polarstern“ 1982/83“ herausgegeben von Gotthilf Hempel	40,—	
<b>Sonderheft Nr. 4/1983</b> – „On the Biology of Krill <i>Euphausia superba</i> “ – Proceedings of the Seminar and Report of the Krill Ecology Group, Bremerhaven 12.–16. May 1983, edited by S. B. Schnack	75,—	
<b>Heft Nr. 15/1983</b> – „German Antarctic Expedition 1980/81 with FRV ‘Walther Herwig’ and RV ‘Meteor’“ – First International BIOMASS Experiment (FIBEX) – Data of micronecton and zooplankton hauls by Uwe Piatkowski and Norbert Klages	22,50	
<b>Sonderheft Nr. 5/1984</b> – „The observatories of the Georg-von-Neumayer-Station“, by Ernst Augstein	8,—	
<b>Heft Nr. 16/1984</b> – „FIBEX cruise zooplankton data“ by U. Piatkowski, I. Hempel and S. Rakusa-Suszczewski	19,—	
<b>Heft Nr. 17/1984</b> – „Fahrtbericht (cruise report) der „Polarstern“-Reise ARKTIS I, 1983“ von E. Augstein, G. Hempel und J. Thiede	29,—	
<b>Heft Nr. 18/1984</b> – „Die Expedition ANTARKTIS II mit FS „Polarstern“ 1983/84“, Bericht von den Fahrtabschnitten 1, 2 und 3, herausgegeben von D. Fütterer	25,—	
<b>Heft Nr. 19/1984</b> – „Die Expedition ANTARKTIS II, mit FS „Polarstern“ 1983/84“, Bericht vom Fahrtabschnitt 4, Punta Arenas–Kapstadt (ANT-II/4), herausgegeben von H. Kohnen	41,—	
<b>Heft Nr. 20/1984</b> – „Die Expedition ARKTIS II des FS „Polarstern“ 1984, mit Beiträgen des FS „Valdivia“ und des Forschungsflugzeuges „Falcon 20“ zum Marginal Ice Zone Experiment 1984 (MIZEX)“ von E. Augstein, G. Hempel, J. Schwarz, J. Thiede und W. Weigel	42,—	